HARDWARE SIMULATION OF FUEL CELL / GAS TURBINE HYBRIDS

A Dissertation
Presented to
The Academic Faculty

By

Thomas Paul Smith

In Partial Fulfillment
Of the Requirements for the Degree
Doctor of Philosophy in the
School of Mechanical Engineering

Georgia Institute of Technology

May 2007

HARDWARE SIMULATION OF FUEL CELL / GAS TURBINE HYBRIDS

Approved by:

Dr. William J. Wepfer, Co-Advisor
Woodruff School of
Mechanical Engineering
Georgia Institute of Technology

Dr. Samuel Graham
Woodruff School of
Mechanical Engineering
Georgia Institute of Technology

Dr. Comas Haynes, Co-Advisor
Center for Innovative Fuel Cell
and Battery Technologies
Georgia Tech Research Institute

Dr. Christiaan Paredis
Woodruff School of
Mechanical Engineering
Georgia Institute of Technology

Dr. David Tucker
National Energy Technology Laboratory
U.S. Department of Energy

Dr. Meilin Liu
School of Materials Science
and Engineering
Georgia Institute of Technology

Date Approved: April 6, 2007

Essentially, all models are wrong, but some are useful. -George E. P. Box (1987)

To my parents, Carlen and Floyd Smith

ACKNOWLEDGEMENTS

Many individuals and organizations played significant roles in making the completion of this dissertation possible.

First, I express my gratitude to NETL and the NASA Glenn Research Center for funding this work.

Second, I would like to thank several individuals at the National Energy Technology Laboratory (NETL), U.S. Department of Energy in Morgantown, WV. Dr. David Tucker offered considerable assistance and guidance with this dissertation and with life in general. Eric Liese developed the numerical fuel cell model that was used for this project. Larry Lawson offered valuable insights into operation and controls integration. David Ruehl played a crucial role in the execution of experimental tests and in the maintenance of the HyPer facility.

I wish to also acknowledge John Auckland, a mentor for my master's work. His guidance with system operation provided me with many of the tools that I brought to the current project.

A special thanks to my advisors from Georgia Tech. To Dr. William J. Wepfer for his valuable practical guidance and encouragement. And to Dr. Comas Haynes for providing research insights and feedback and for showing me that one can be virtuous and successful.

Recognition is also due to those who helped me through the writing process. I thank Dr. Jeffrey A. Donnell of Georgia Tech for his assistance with writing and editing this dissertation. I thank Cynthia Morgan for helping edit the dissertation and offering emotional support.

Finally, I also thank my mother and father for providing me with the foundation for who I am and all my achievements. I believe in myself because they believed in me first.

TABLE OF CONTENTS

LIST OF TABLES

LIST OF FIGURES

NOMENCLATURE

Abbreviations

AC	alternating current
ADC	analog-to-digital converter
APU	axillary power unit
DAC	digital-to-analog converter
DC	direct current
DOE	U.S. Department of Energy
EGT	exhaust gas temperature
GAP	Graphical Application Program
GT	gas turbine
HILS	hardware-in-the-loop simulation
HyPer	Hybrid Performance Project
LHV	lower heating value
NETL	National Energy Technology Laboratory
PEMFC	proton exchange membrane fuel cell
PEN	positive/electrolyte/negative
SOFC	solid oxide fuel cell
SWPC	Siemens-Westinghouse Power Corporation
TPB	triple phase boundary
1-D	1-dimensional

English Symbols

A	area, m^2
c_p	specific heat capacity, kJ/(K·kg)
C_p	heat capacity, kJ/K
E	potential of EMF, V
$E°$	standard potential, V
E_a	electrode activation term, kJ/mol
D	diffusivity term, m/s
F	Faraday's constant, 96,485 C

$\bar{g}_f$	Gibbs free energy of formation, J/mol
h_{HT}	convection heat transfer coefficient, W/(m^2·K)
h	specific enthalpy, kJ/kg
$\dot{H}$	enthalpy rate, kJ
i	current density, A/m^2
I	current, A
i_o	exchange current density, A/m^2
k	electrode reaction rate pre-exponential coefficient, 1/(Ω·m^2)
m	mass, kg
$\dot{m}$	mass flow rate, kg/s
$\dot{n}$	molar flow rate, mol/s
p	partial pressure, kPa
P	pressure, kPa
$P°$	standard pressure, 100 kPa
$\dot{Q}$	heat rate, kW
r	area specific resistance, Ω·m^2
R_u	universal gas constant, 8.314 J/(mol·K)
t	time, s
T	temperature, K or °C
U_F	fuel utilization
V	voltage, V
$\forbar$	volume, L
$\dot{W}$	power, kW
x	mole fraction
z	number of participating electrons

Greek Symbols

α	transfer coefficient
Γ	heat capacity scalar
η_{act}	Activation polarization, V
η_{conc}	Concentration polarization, V
η_{ohmic}	Ohmic polarization, V
η_S	efficiency, isentropic
η_{TH}	efficiency, thermal
λ	anode recycle level
τ	thickness, m

Subscripts

add,dyn	dynamic additive (for temperature)
add,ss	steady-state additive (for temperature)
air	cathode air, bulk property
an	anode
atm	atmospheric pressure
ave	average
bulk	bulk property
C1	C1 precombustor parameter
ca	cathode
cell	electrolyte, electrodes and interconnect
CH4	methane
eff	effective value for pressure correction
fuel	fuel parameter
gen	generation parameter
H2	hydrogen, bulk parameter
H2O	water (steam), bulk parameter
HT	heat transfer parameter
in	inlet parameter
inter	interconnect
LHV	lower heating value
Nernst	Nernst potential
O2	oxygen, bulk parameter
out	outlet parameter
pass	per pass fuel parameter
PEN	electrolyte and electrode property
ref	reformer parameter
rxn	cell reaction
stack	stack property
sys	model subsystem property
TPB	triple phase boundary

SUMMARY

Hybrid solid oxide fuel cell / gas turbine (SOFC/GT) systems offer high efficiency power generation, but face numerous integration and operability challenges. This dissertation addresses the application of hardware-in-the-loop simulation (HILS) to explore the performance of a solid oxide fuel cell stack and gas turbine when combined into a hybrid system. Specifically, this project entailed developing and demonstrating a methodology for coupling a numerical SOFC subsystem model with a gas turbine that has been modified with supplemental process flow and control paths to mimic a hybrid system. This HILS approach was implemented with the U.S. Department of Energy Hybrid Performance Project (HyPer) located at the National Energy Technology Laboratory. By utilizing HILS the facility provides a cost effective and capable platform for characterizing the response of hybrid systems to dynamic variations in operating conditions.

HILS of a hybrid system was accomplished by first interfacing a numerical model with operating gas turbine hardware. The real-time SOFC stack model responds to operating turbine flow conditions in order to predict the level of thermal effluent from the SOFC stack. This simulated level of heating then dynamically sets the turbine's "firing" rate to reflect the stack output heat rate. Second, a high-speed computer system with data acquisition capabilities was integrated with the existing controls and sensors of the turbine facility. In the future, this will allow for the utilization of high-fidelity fuel cell

models that infer cell performance parameters while still computing the simulation in real-time. Once the integration of the numeric and the hardware simulation components was completed, HILS experiments were conducted to evaluate hybrid system performance. The testing identified non-intuitive transient responses arising from the large thermal capacitance of the stack that are inherent to hybrid systems. Furthermore, the tests demonstrated the capabilities of HILS as a research tool for investigating the dynamic behavior of SOFC/GT hybrid power generation systems.

CHAPTER 1: INTRODUCTION

Today's power demands and environmental concerns are stimulating the advancement of new power generation technologies. Near the forefront of such developments are fuel cells, which generate electricity directly through electrochemical reactions. Advancing this technology a step further in the pursuit of highly efficient and clean power generation is the fuel cell and gas turbine hybrid system. The integration of these two distinct power conversion technologies into one system produces performance projections of 60% or more efficiency (net AC electrical / LHV of natural gas fuel) (Veyo, 2002) while lowering pollutant levels such as nitrogen oxides (NO_X) and sulfur oxides (SO_X). The plausibility of this high efficiency projection was recently demonstrated by the world's first solid oxide fuel cell (SOFC) and gas turbine (GT) hybrid system in proof-of-concept trials, conducted between 2000 and 2003 at the National Fuel Cell Research Center in Irvine, California. Designed and built by Siemens-Westinghouse Power Corporation (SWPC), the 220 kW hybrid system, shown in Figure 1.1, achieved 53% efficiency (Litzinger, 2005). The outcome of that project highlights the hybrid fuel cell's potential to answer the growing call for clean and efficient power generation technologies.

While the SWPC 220 kW hybrid displayed desirable efficiency performance, there existed operational and control challenges that limited the operability of this system (Veyo, 2003). Before SOFC/GT hybrid systems can be deployed beyond the research

Figure 1.1: The SWPC 220 kW Hybrid System

environment, these challenges must be addressed. The two distinct power systems—SOFC and GT—have disparate time scales and physical operating condition requirements. This means that the principles common to a simple gas turbine cycle do not directly apply to the complexities of the hybrid system. Often feedback mechanisms between the two devices may lead to undesirable amplification or cancellation of responses to changes in conditions, and these effects are often not intuitive. This makes it necessary to study the interaction of the two power conversion devices in order to facilitate the development of reliable control strategies for the integrated system.

1.1: Fuel Cell/Gas Turbine Hybrid Power System

The U.S. DOE Office of Fossil Energy has identified fuel cell/gas turbine hybrids as an essential component in achieving high overall efficiency and superior environmental performance as part of the FutureGen program (Williams, 2006). FutureGen is an industrial consortium formed by a presidential initiative to produce a nearly emission-free power plant. This coal fueled plant will produce electricity and hydrogen, while capturing carbon dioxide for later sequestration.

Thus far, the SOFC/GT hybrid cycle has been in large part designed and analyzed through conceptual studies. The primary advantage that has been identified in SOFC/GT systems is higher efficiency in the conversion of chemically stored energy to electrical power. Furthermore, limited small-scale demonstrations fueled with natural gas, such as the SWPC 220 kW, have proven the viability of integrating a fuel cell and a gas turbine into a system. Figure 1.2 graphically depicts the projected efficiency advantage that SOFC/GT hybrids have over several currently dominant and proposed power generation technologies.

For power needs between 1 and 100 MW, SOFC/GT hybrids are projected to be more efficient than competing technologies such as turbines and internal combustion engines. For smaller-scale power needs, stand-alone fuel cell systems and microturbines are a better fit due to the complexity of operating hybrids. On the larger scale, nuclear or coal-fired steam turbine plants are the standard for large-scale central power generation. However, the efficacy of the central power generation we use today is under scrutiny, and a distributed power system may be a viable alternative for reducing distribution losses, addressing grid congestion where new lines cannot be built, and more importantly,

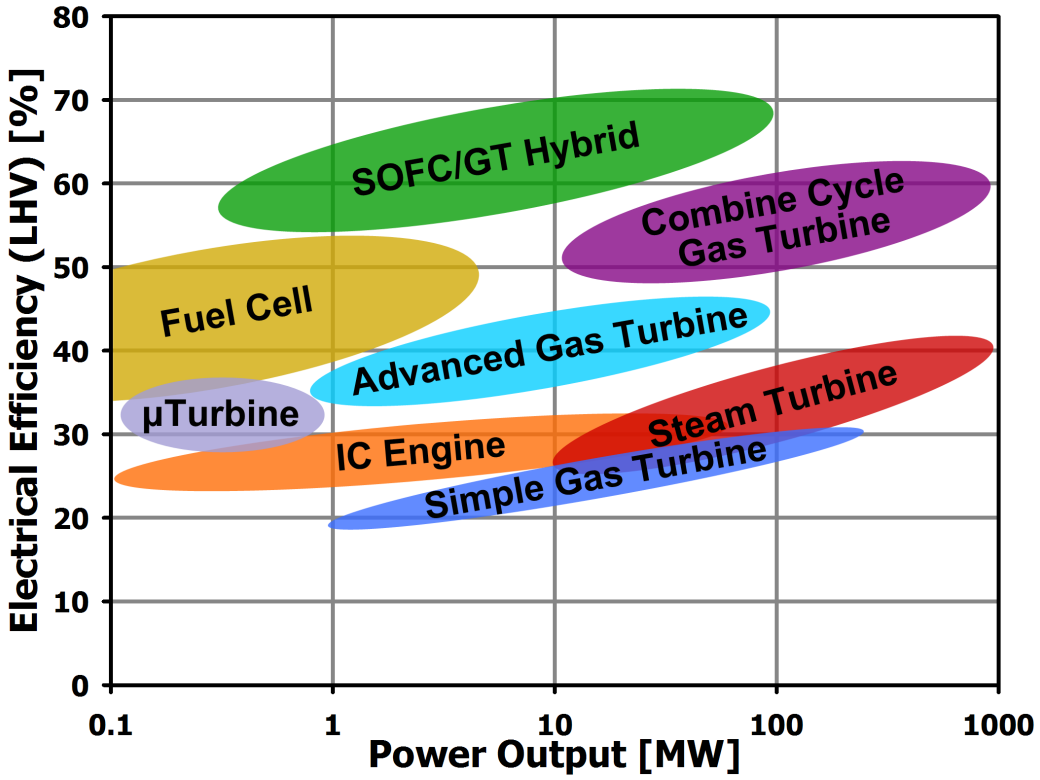

Figure 1.2: Electrical Power Generation Technologies

addressing energy security, which has become a national concern in recent years. Since they are modular, SOFC/GT hybrids fit well into a distributed power generation model.

SOFC/GT hybrids have the added advantage of being environmentally sound compared to standard technologies because they allow for cleaner conversion of a variety of fuels. Even when utilizing fossil fuels, hybrids emit lower levels of controlled pollutants. With lower operating temperatures than flames, fuel cells do not promote the formation of nitrous oxides as in traditional combustion-driven power generation. Sulfur oxides are also eliminated since sulfur is removed from the fuel before it is used in the cell. While carbon dioxide is not a controlled byproduct, political concerns over global warming indicate that it may be in the future. The high conversion efficiency of a hybrid system results in lower levels of carbon dioxide per kW-hr of electrical production.

SOFC/GT hybrids also exhibit fuel versatility. In the first stages of commercialization, natural gas will be the most commonly utilized fuel source because it is readily available, and the high temperature of the solid oxide fuel cell facilitates reformation of the fuel, which converts the methane rich natural gas into a hydrogen rich gas. If energy generation from coal becomes more desirable, SOFC/GT hybrids will present a clean alternative to conventional combustion because they fit well with a gasification scheme which allows for the removal of pollutant precursors before utilization. Additionally, the implementation of carbon sequestration strategies is simplified with SOFC since the carbon dioxide byproduct can remain separate from the process airflow, avoiding otherwise costly dilution in the air exhaust. Lastly, since fuel cells ultimately oxidize hydrogen, the implementation of the proposed hydrogen economy is aligned with any deployment of SOFC/GT hybrids.

1.2: Research Gap Facing Hybrid Development

While the benefits of SOFC/GT hybrid systems are clear, if such systems are to be realized in stationary power generation, several developmental challenges must be addressed. As with traditional power generation technologies, the design and construction of hybrid power generation facilities require a substantial investment leading to a substantial monetary risk. And as with any new technology, there is additional uncertainty since hybrid technology has not yet been proven. This poses a challenge to the adoption of the SOFC/GT hybrid by the relatively fiscally conservative utility industry, meaning that the feasibility and reliability of the technology must be established

early in the design phase to in order to attract research funds for refining and enhancing the technology and to encourage investment in its implementation.

Component matching and controls development are of particular importance in the early phases of development of the SOFC/GT hybrid. These tasks are complicated by the non-intuitive interactions of the two systems when integrated, and these interactions have not been adequately explored. Currently, in the field of hybrid development it is widely accepted that, "The effects of transient events on hybrid systems, as dynamic interdependencies resulting from the integration of these two power generation technologies are not well understood." (Taccani, 2006) The two systems have drastically different physical time scales, particularly in their thermal responses. The turbine will respond within seconds to any changes in thermal conditions, whereas a fuel cell stack has thermal time constants on the order of hours. When integrating these two systems together this has the potential to lead to unstable feedback loops that will challenge system developers. Furthermore, since fuel cell experts are usually not familiar with the operation of gas turbines, and gas turbine experts lack an understanding of fuel cells, it is often difficult for engineers from either field to accurately predict the responses of the hybrid system. This requires that a means be developed for researchers to identify and specifically address these non-intuitive interactions at the early stages of hybrid commercialization.

Component matching must be established before construction of the systems and will have a far reaching effect on the operability, efficiency, and profitability of the constructed systems. Component matching entails designing, sizing and selecting the individual pieces of a system so that they operate in harmony when integrated. The

criteria for doing so are “based on the matching of components and its physical characteristics in design[,] off-design, steady-state and transient operation” (Hildebrandt, 2005). This means there may be competing objectives and numerous conditions that must be considered when designing a system. For example, when designing the most efficient system during steady-state operation, other factors may be overlooked. Such a system may not be feasible in real world operation since it may not be capable of handling difficult but required transients such as startup and shutdown. Therefore a whole system approach must be taken when designing hybrid systems. It is not sufficient to take an existing turbine “off the shelf” and an atmospheric fuel cell stack and expect them integrate simply. This was the approach for the SWPC 220 kW hybrid system, and its trial operation showed that, while the SOFC/GT hybrid concept is feasible, such a design approach is not practical for widespread commercialization.

Control methods must be developed before hybrid plants can be operated in the field. The control system must ensure safe operation while achieving high performance. Today's extensive digital control systems allow for complex and powerful schemes that manage the operation to obtain optimal performance from power generation systems. This will often lead to a complex control system with numerous sensors, actuators and user interfaces. These systems have to be designed, programmed and tested, often under pressing time constraints. This requires that the control engineers have a knowledge of the unique characteristics of a SOFC/GT hybrid. As mentioned, these hybrid systems have numerous intrinsic feedback mechanisms and widely varying response time scales that will challenge controls design. However, at this time extensive investigations into the hybrid's dynamic response to transients has not been performed. Also it is expected

that counterintuitive integration issues exist that cannot be currently accounted for in controls design. For example, an unexpected negative outcome observed in the operation of the SWPC 220 kW was the surging of the compressor arising from overmodulating the stack bypass valve. Furthermore, with today's safety requirements, exhaustive testing of the control system prior to applying it to a real plant is essential. Because of the importance of developing sound control methods and selecting and integrating the proper components in the preliminary design phase, a feasible means of developing and validating system designs without constructing final operating facilities is required.

To establish operability and to garner industry buy-in, SOFC/GT hybrids must be studied in a manner that allows for prolific data generation without excessive costs or risks to the hardware and human safety. Adequate initial design will also address investors' interest in preventing costly failures during the design, building and operation of the system. The accuracy and applicability of the research methods must also be ensured. Current research strategies must be scrutinized and evaluated against these criteria.

1.3: Weaknesses of Current Hybrid Research

Thus far, the SOFC/GT hybrid development has primarily been through system studies and computational modeling. Thermodynamic analysis of steady-state performance has been key in discriminating between various fuel cell and turbine cycles (Calise, 2006; Massardo, 2000; Stiller, 2005). However, these studies do not address transients that the systems will experience. Recent advancements in dynamic modeling have made progress towards simulating hybrid system transients, but still face significant

challenges in capturing the physical phenomena (Ferrari, 2005; Roberts, 2006). Particularly difficult is numerically simulating pressure transients and losses of the compressed airflow. Furthermore, validating the hybrid model has been limited because the number of physical systems for the generating operational data has been few. While the operation of the SWPC 220 kW system was an important step in demonstrating the feasibility of the SOFC/GT hybrid cycle and garnering insights into hybrid operation, it was only a conservative step towards system realization. The system's demonstration was limited to achieving and maintaining steady operation. This precluded the experimental testing necessary for developing the requisite understanding for the design of the next generation hybrid power generation systems.

1.3.1: SOFC Stack Component Challenges

The use of fuel cell stacks for research purposes in the early development phases of SOFC/GT hybrids has severe limitations. At their current early developmental stage, SOFC stacks are extremely costly, well into the millions of dollars, and are not readily available. Moreover, they can easily be damaged in conducting the type of testing that is required to aid in hybrid development. For example, establishing an operating envelope for stack operation parameters, such as inlet air temperature range, requires that a stack be operated at extreme conditions. Beyond normal operation, hybrid systems will have to be tested for unexpected and extreme events, such as electrical load trips or compressor surges. It is precisely these types of test conditions, necessary to study fuel cell stack responses, that carry a high risk of sacrificing an actual stack. Therefore, using real fuel cell stacks is not practical for producing a thorough range of experimentation.

1.3.2: Turbomachinery Component Challenges

While gas turbine engines are a widely utilized technology, both in the aerospace and stationary power generation industries, this second major component requires substantial research advancement to facilitate integration into a SOFC/GT hybrid system. The critical component to both a stand-alone turbine engine or a hybrid system is the compressor and its ability to maintain stable flow during a transient event. A flow instability can initiate a compressor surge which may lead to an engine shutdown or damage to the other components. Even with today's widespread understanding of compressor performance there remains "a dearth of high-speed centrifugal compressor instability initiation information addressing transient operation" (Oakes, 2004). Therefore, the compressor remains an area of uncertainty in hybrid design that must be addressed before commercialization.

Furthermore, turbomachinery design offers challenges to both computer modeling and hardware development in hybrid systems. This is because engineers have successfully designed and applied gas turbine technology beyond the scientific knowledge of the processes taking place, particularity in calculating the details of three-dimensional, time variant flow (Cumpsty, 2004). Additionally, Al-Hamdan (2006) indicated that optimizing gas turbine cycles by mathematically solving the complex aerothermodynamic analysis for only steady-state operation is challenging and that modeling transients would be more difficult. These turbomachinery numerical simulation challenges, especially surges initiated during transient operation, would only be compounded by the additional components in a hybrid model.

Building and field-testing turbomachinery specifically for hybrid cycles offers its owns challenges, with special emphasis upon cost. Designing a new gas turbine engine is prohibitively expensive. Today's compressors have complex fin or blade designs to avoid surges and are tailored to specific turbine engines. The desired characteristics for a hybrid's compressor will be different than those for a stand-alone turbine engine, primarily due to the large compressed air volume following the compressor, and therefore are not well understood. Initially, fuel cell companies tried to integrate exiting turbine engines into their fuel cell stacks, as with the SWPC 220 kW. However, this approach gave rise to many operational challenges and even prematurely ended later SWPC hybrid projects when the turbomachinery did not perform as necessary (Veyo, 2003).

1.3.3: Hybrid System Challenges

In SOFC/GT hybrids not only is the performance of individual components of concern, but an understanding of the response of the system as a whole is essential. Engineers must anticipate how a failure in one component will affect the others and how the entire system will respond. Moreover, control systems must be designed to ensure that the proper action is taken by safety controls in response to an incident, such as a load trip, a power outage or a broken turbine. Designing for undesired conditions is important to establish the survivability of other system components and to protect the safety of personnel. However, it is difficult to evaluate the robustness and effectiveness of control methods. Testing with an actual hybrid hardware system is prohibitively expensive, time-intensive and hazardous. With real systems, the reproduction of many failure methods is difficult or impractical. Difficulties also exist with numerical models since inclusion of all the factors is challenging and modeling extreme conditions introduces

discontinuity or creates numerical singularity, making simulations unstable. Moreover, data for model verification is limited.

1.3.3.1: Operability Considerations

Most analyses of SOFC/GT hybrid system design studies have been narrowly focused on achieving maximum efficiency. However during normal system operation, optimal conditions rarely exist and ambient conditions and external parameters are ever changing. Engineers must also integrate system startup, shutdown, and partial load operation into hybrid design. Often the most *effective* system is not necessarily the most *efficient* system; i.e., operability is a significant factor in designing optimal hybrid systems. Numerous reports have identified SOFC/GT hybrid systems as highly efficient power generation systems (Layne, 2000; Leeper, 1999, Winkler, 2006). However, there is a limited accounting for necessary support components that will lower efficiency of hybrid systems. For example the inclusion of a stack air bypass valve, which lowers system efficiency, provides a critical control over airflow to the fuel cell. However, the effectiveness of different control configurations cannot easily be explored on a hybrid system without modifications. The cost of such testing is prohibitive, and the large thermal heat capacitance of a SOFC stack limits the practical testing conditions.

1.3.4: Summary of the Gaps in Current Research Methods

While past and ongoing studies have proven the SOFC/GT hybrid concept, they have not employed adequate research methodology for establishing the feasibility and reliability of the system. There are too few physical systems to generate sufficient operating data for the validation of paper studies and simulation analyses. Construction of more real systems is not the solution. Fuel cell stacks are simply too expensive to

build for testing purposes. Moreover, they cannot be operated at extremes due to the risk of destroying the system and introducing too much unpredictability into the grid or power plant. Lastly, while thermodynamic analysis and computational modeling has provided crucial initial insights and guidance, their effectiveness is not sufficient as hybrids move closer to commercialization. The difficulty in capturing the pressurized flow physics and the lack of understanding of non-intuitive phenomenological characteristics requires that systems including physical components be built.

1.4: Addressing Hybrids Research Needs

The research concerns and gaps outlined above must be addressed with a new strategy for evaluating hybrid systems—one that reconciles the shortcomings and advantages of numerical models and hardware systems. A means to thoroughly test and validate the developmental steps must be developed at a reasonable cost. This new strategy must specifically address the real obstacles to establishing the feasibility and reliability of SOFC/GT hybrids. The research approach should be able to assess system performance under various operating conditions. Additionally, it should possess the capability to evaluate novel control methods, such as flow bypass valving, and then test the effectiveness of control methods applied to them during operation. Most importantly, the new research path should accurately identify non-intuitive interactions between the SOFC stack and the GT that are not being sufficiently addressed by current means.

1.4.1: Facility for Developing Hybrids

Developing a new understanding of the interaction between the two systems requires a research platform to conduct tests. Since the high cost of fuel cell stacks

prohibits the construction of an actual hybrid system, engineers have been drawing upon computer simulations to explore fuel cells and hybrid cycles. As of yet though, important operating and performance parameters, especially in the area of dynamic interactions, are not sufficiently understood to be captured in numerical simulation. Consequently, developing a facility that draws upon interfacing both hardware-based and numerical simulations is a key compromise. Hardware-in-the-loop simulations (HILS), which had not been applied to hybrid power generation systems prior to the development of the facility utilized in this study, are a necessary and effective means for generating essential information on the interaction of the two systems. The Hybrid Performance Project (HyPer) is a system designed and built specifically for this purpose (Tucker, 2002). Located at the U.S. Department of Energy (DOE) National Energy Technology Laboratory (NETL) in Morgantown, WV, it is a unique platform for performing the hybrid testing and characterization necessary for further refinements of the SOFC/GT system.

1.4.2: Applying HILS to Hybrids

HILS is a technique to investigate a complex dynamic system by separating it into numerical and physical components and then coupling the two simulations. In the automotive industry HILS is a popular means to test electronic control units (Maclay, 1997). Instead of being connected to real equipment, the controllers are evaluated by connecting them to a real-time computer simulation based on a mathematical model that replaces an actual engine or vehicle component.

The application of HILS to a real gas turbine paired with a model fuel cell stack has great potential for generating the necessary insights for further hybrid development.

The goal in using HILS here is to show physical interactions, some of which are not so apparent, and to quantify them so these hybrid systems can be better understood. This information then can be used to develop controls and to assist in design. HILS is an advantageous method for researching SOFC/GT hybrid systems. Fuel cells are expensive and their availability is very limited, however they can be readily modeled, and thermal models are sufficient to be useful for testing purposes. Gas turbine hardware is more readily available and is relatively inexpensive, making the integration of a turbine with a fuel cell numerical model a solid compromise.

To this point HILS has not readily been applied to power generation systems, so the method for doing so must be developed. The HyPer hardware (gas turbine, pressure vessels, combustor, etc.) was designed specifically to be the physical component of a HILS simulation. However, the numerical simulation portion and the means to interface with the hardware had to be developed. This entailed that a real-time computer simulation, albeit a simple model, operate on the original HyPer controller while it is coupled with the physical system. Toward that goal, this dissertation research addresses the needed numerical simulation portion of the HyPer facility and therefore propagates the implementation of a complete HILS investigation of a SOFC/GT hybrid.

1.4.2.1: Dedicated Simulation Computation System

Once the physical hardware and the means for conducting HILS with the original HyPer control platform have been developed a more robust and higher-fidelity numerical component is desired. In order to generate more meaningful fuel cell model data when conducting a HyPer HILS a numerical simulation of higher-fidelity is required. A principal goal of increasing the fidelity is to capture spatial temperature gradients. This

will characterize the internal thermal stresses in the ceramic cells and the survivability of a stack when integrated into a hybrid.

Transitioning to higher-fidelity models greatly increases the complexity and computational loading of the fuel cell models that must be run in real-time. And given that "running complex simulation models in real-time requires large amounts of processing power" (Maclay, 1997), the computation capabilities of HyPer must be augmented. Therefore, a powerful computational system dedicated to and specializing in real-time simulation was supplemented to HyPer to run in parallel with the original control platform. This computer significantly increases the simulation capabilities of HyPer, allowing it to further advance its investigation of hybrids.

1.5: Solution Approach

This dissertation focuses on developing and demonstrating a methodology for conducting SOFC/GT hybrid HILSs on the HyPer facility. This work entailed several steps:

- Developing a socket program that interfaces a SOFC subsystem computational model with real-time HyPer measurements
- Implementing the HILS approach with a bulk subsystem model on the existing HyPer control platform
- Establishing a high-speed computational hardware platform for executing SOFC subsystem models
- Interfacing this computational system with the HyPer hardware

- Conducting HILS transient studies of stack load changes to demonstrate HyPer functionality

Correspondingly, the initial HILS experiments were used to evaluate hybrid system transient responses and gain preliminary insights regarding SOFC/GT hybrid operation.

1.6: Delineation of Contribution to HyPer Project

The extensive path to creating a platform for conducting HILSs of SOFC/GT hybrids began over five years ago with the conception of HyPer. Since then NETL has invested hundreds of thousands of dollars in its design, construction and operation. Numerous NETL personnel have contributed and are essential to its progress. This dissertation depends upon, and is integral with, that work. The methodology developed and described in this dissertation is for the connection of a numerical simulation with the exiting hardware. This is an essential step that had not been addressed before this dissertation effort. Previously, HyPer conducted only hardware testing, but with the implementation of the HILS methodology, HyPer is a capable and valuable dynamic simulator of SOFC/GT hybrids.

To that effect, this dissertation research is a contribution to, and a portion of, a larger project. It is only through the collaboration with NETL personnel that it was accomplished. Furthermore, portions of the methodology presented in this dissertation are based on their efforts. The inclusion of these efforts provides a more complete explanation of conducting HILSs with HyPer, and speaks to the interdependent relationship this dissertation effort has with NETL's hybrid research effort. In particular, included in this dissertation are these items drawn from their work:

- Dr. David Tucker is HyPer's project lead. He oversaw the design and construction of the facility and now directs the research. The details concerning the HyPer hardware and its operation are taken from project documentation he developed.
- Eric Liese developed the bulk numerical model of a single SOFC cell in the Simulink environment.
- Larry Lawson is responsible for HyPer controls and programmed the AtlasPC controller that executed the bulk model for HILS.
- Dave Ruehl is the HyPer facility operator. In addition to his maintenance of the facility, he assisted in installing the dedicate simulation computer system.

In conjunction with those endeavors, I was responsible for several specific components of integrating a numerical model with the HyPer hardware. The following undertakings constitute this dissertation effort:

- Designed the approach and outlined the specification for the numerical substructure.
- Programmed the Simulink interface that connects the SOFC subsystem model with the hardware system. This includes the other modeled components of the fuel cell subsystem.
- Aided in developing the approach utilized for the bulk-parameter fuel cell model.

- Evaluated performance of the bulk-parameter fuel cell model to verify the programming and to provide limited validation of the approach before its use in HILS.
- Developed the steps to initiate fuel cell model control of HyPer's combustor to conduct a HILS.
- Established the need for, selected and installed the high-speed computational system dedicated to simulation execution.
- Created the user interface and Simulink program to conduct HILS on the high-speed computer system.
- Envisioned and performed HILS experiments with HyPer to investigate SOFC/GT hybrids. This experimental process included the following: devising HILS experiments relevant to hybrid operation based on previous operation observations; creating HyPer test plans; conducting the testing with the HyPer team; analyzing the experimental data; and interpreting the HILS results.
- Developed SOFC/GT hybrid operational insights and recommendations based on the transients observed in HyPer HILS testing.

The success of the implementation and testing of HILS is due to the combined efforts of the HyPer team. The research components relevant to this dissertation have been completed as planned, and, more importantly, the HyPer facility is now equipped to run HILS on a SOFC/GT hybrid.

1.7: Significance of Work

This dissertation effort expanded the capabilities of the HyPer platform in conducting HILS of SOFC/GT hybrids. The observations obtained in conducting HyPer HILS experimentation will provide a deeper understanding of the transient behavior of direct SOFC/GT hybrids. In time this will assist in the commercialization of these highly efficient electrical power generation systems.

As detailed in this dissertation, several key advances have been accomplished in the implementation and utilization of HILS with HyPer. First, the methodology for integrating a numerical fuel cell model with the gas turbine hardware was developed and implemented. This allowed the application of HILS to a SOFC/GT hybrid to be demonstrated by several experimental tests. Second, a powerful and stand-alone computational system was integrated with the existing HyPer control platforms. This expands the facility's capabilities in incorporating higher fidelity SOFC models that will improve the simulation performance and provide greater insight into hybrid systems. Lastly the results from the experimental HILS tests were evaluated to glean new insights into the operation of hybrid systems. These results show the existence of non-intuitive system responses that arise from integrating the large thermal capacitance of the fuel cell stack with the gas turbine. It is results such as these that call for more detailed HILS studies to aid in designing hybrid systems and the controls that go with them.

This dissertation effort focused on a natural gas fueled, direct-fired fuel cell / gas turbine hybrid configuration. Future HyPer research will address the utilization of coal syngas to fuel the system. Current and future HyPer research efforts will provide an important tool to aid in hybrid development. This tool will move hybrids closer to

commercialization by addressing the development challenges that must be overcome before widespread hybrid adoption occurs. The construction and utilization of SOFC/GT hybrid systems will lead to more environmentally friendly power generation.

This dissertation's specific contribution—an innovative application of HILS to hybrid systems—will enhance the DOE HyPer's capability in researching hybrid cycles by increasing its ability to simulate SOFC performance. Enabling HILSs of hybrids and interfacing a computational platform with the turbine will facilitate high quality HILSs of hybrid systems that will provide insight into the operation and performance of SOFC stacks when matched with gas turbines. Additionally, the HyPer facility will provide a platform for developing and testing control strategies of hybrid systems. In the long term, this work will promote the advancement and implementation of the first generation SOFC/GT hybrids for electrical power generation and demonstrate the application of HILSs to advanced energy systems.

CHAPTER 2: BACKGROUND

In this research effort, HILS is being applied to a direct fired SOFC/GT hybrid system. This hybrid concept, diagrammed in Figure 2.1, combines a SOFC stack and a microturbine in a synergistic manner such that the by-product of one is utilized by the other. The high temperature fuel cell needs a primary air mover to supply oxygen for the chemical reaction as well as airflow for cooling. For its operation, the gas turbine requires pressurized high temperature air to expand across the turbine, which drives the compressor. By arranging the two power generators together in a hybrid system, the fuel cell's byproduct heat supplies the energy required by the turbine, largely replacing fuel combustion. This in turn powers the compressor which supplies air to the fuel cell stack.

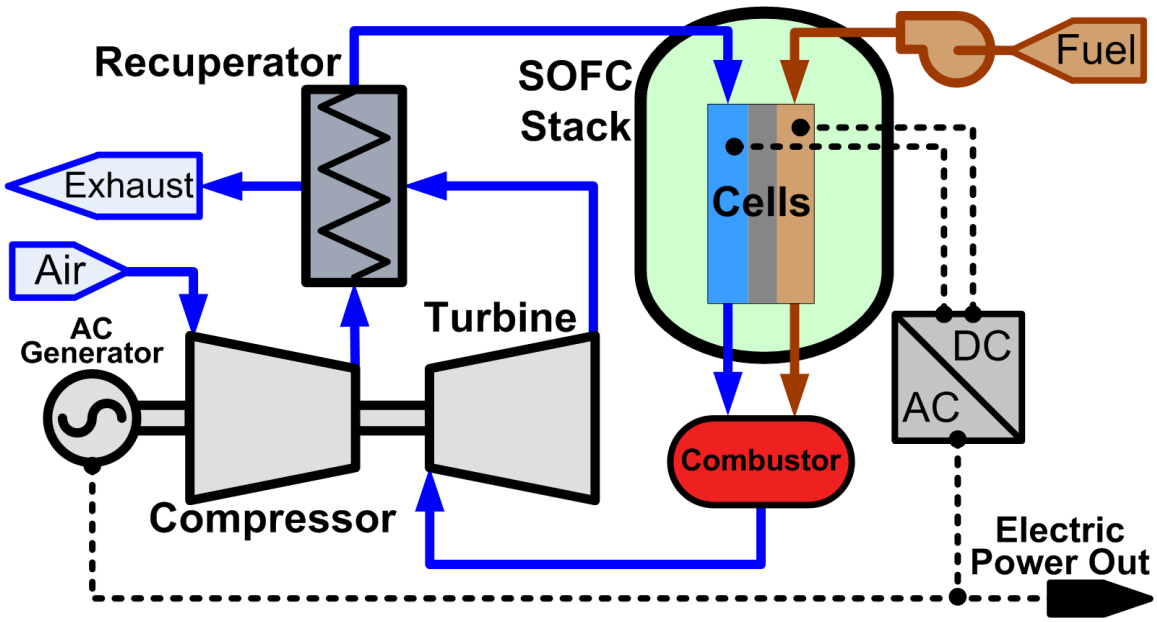

Figure 2.1: Representative Direct Fired Fuel Cell / Gas Turbine Hybrid System

In addition, the pressurization of the fuel cell enhances the electrochemical reactions so that the power density of the stack is increased. Furthermore, energy not required to drive the compressor drives an AC electric generator for added power output.

Numerous descriptions of SOFC/GT hybrid systems have been presented in the literature (Haynes, 2000; Litzinger, 2005; Massardo, 2002) Here, the unique characteristics of the major components relevant to this research effort are outlined.

2.1: Solid Oxide Fuel Cells

As stand-alone power generation systems, SOFCs have demonstrated promising, but limited, operation (George, 2000). In general, a fuel cell is an electrochemical device that converts chemical energy to electrical energy directly and continuously as long as reactants (fuel and air) are supplied. This energy conversion device is similar to a battery in that the power is electrochemically produced. However, like an engine, a fuel cell will conceptually provide continuous operation as long as it is constantly supplied with reactants—fuel and air. The electrochemical reaction most commonly found in fuel cells employs hydrogen fuel as the reducing agent and oxygen from the air as the oxidant. The overall reaction is split into two half reaction that occur on each side of the electrolyte, as shown in Figure 2.2. To complete the overall reaction oxygen ions, O^{-2}, migrate across the electrolyte and electrons are force to an external circuit. This leads to the net exothermic reaction:

$$H_2 + 1/2\ O_2 \rightarrow H_2O + \text{Electricty} + \text{Heat} \qquad [2.1]$$

As this reaction proceeds, electrical power is produced as well as byproduct heat from electrochemical losses.

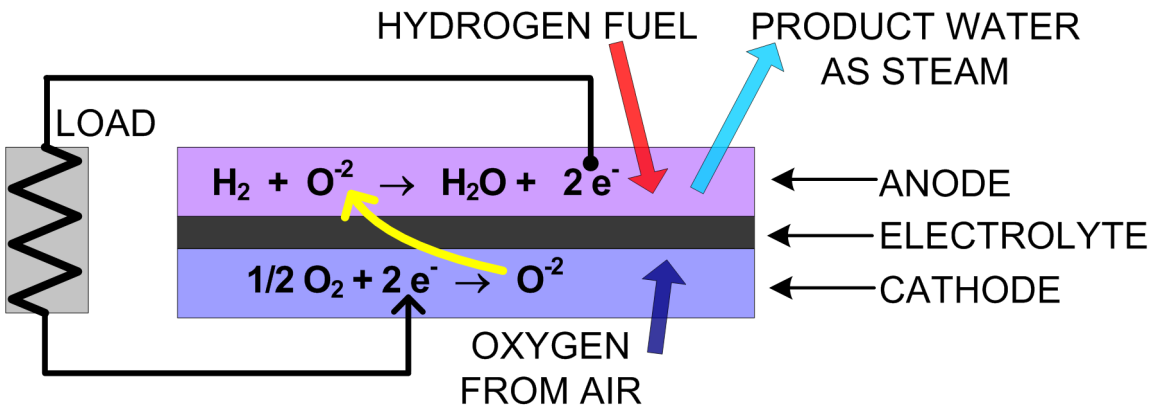

Figure 2.2: Representative Solid Oxide Fuel Cell with Half Reactions

While there are several common types of fuel cells, of interest here are solid oxide fuel cells that operate between 700 - 1000 °C. The basic components of a single cell are shown in Figure 2.2. A large number of cells are assembled into a stack to achieve the desired power output. In this ceramic based electrolyte cell, the high temperature is necessary for the reaction to proceed without accruing large electrochemical losses. In the cell, approximately 50 % of the chemical energy is converted to electrical energy, with the remaining energy manifested as heat which must be removed, usually via excess air. With the high cell temperature, the thermal effluent captured in the airflow is of a sufficient quality to drive a turbine. It is this characteristic of the SOFC that promotes its integration with turbomachinery to form a hybrid system.

Inside a solid oxide fuel cell the reactants are separated by a positive electrode / electrolyte / negative electrode (PEN) structure, which is composed of a ceramic electrolyte between the two electrodes, as shown in Figure 2.2. In contrast to the electrodes, the electrolyte is nonporous to ensure the fuel and air remain separated, and most importantly at elevated temperatures it is an anionic conductor. The electrolyte allows for the transport of oxygen ions, O^{-2}, in the case of a solid oxide fuel cell, but

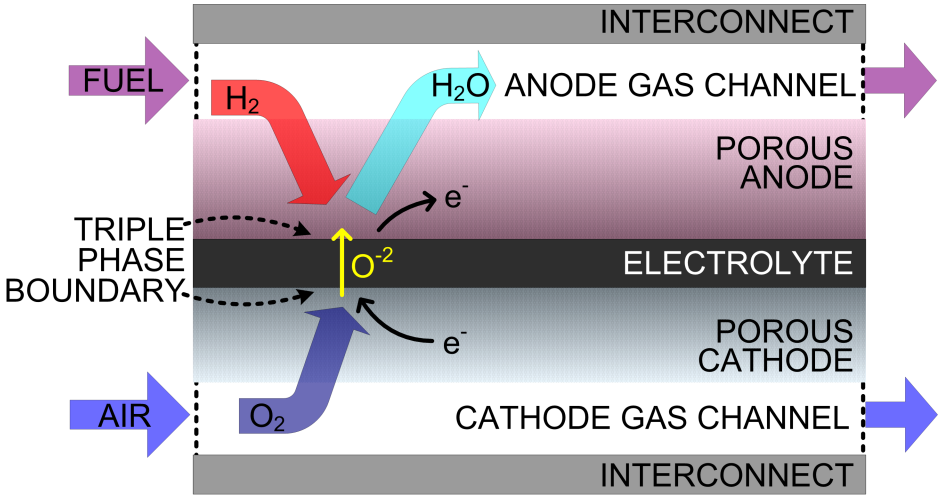

Figure 2.3: Representative Planar Solid Oxide Fuel Cell

prevents electronic current flow across the electrolyte. The electrons must then travel by an external circuit, and hence produce the desired electrical prower. The electrolyte is typically composed of zirconia (ZrO_2) doped with 8% to 10% yttria (Y_2O_3) for stabilization. The dopant creates oxygen ion deficiencies in the zirconia crystal structure. At temperatures above 600 °C the ions and deficiencies can interchange positions with sufficient frequency so that the ceramic becomes ionically conductive.

Attached to each side of the gas impermeable electrolyte is an electrode. Each electrode is porous to allow the gas reactants to diffuse to the reaction location at the electrolyte/electrode interface, as diagrammed in Figure 2.3. During the reaction, oxygen and hydrogen are consumed at the triple phase boundary (TPB) and must flow from the reactant stream, through the electrode, and to the electrolyte. The TPB is a site where the gas phase, the electrode and electrolyte material are each present. Conversely, the steam product must be transferred away from the TPB. Additionally, the electrodes must be electronically conductive to collect, or distribute, the electrons from, or to, the reaction sites. The electrode in the fuel compartment is designated as the anode and produces a

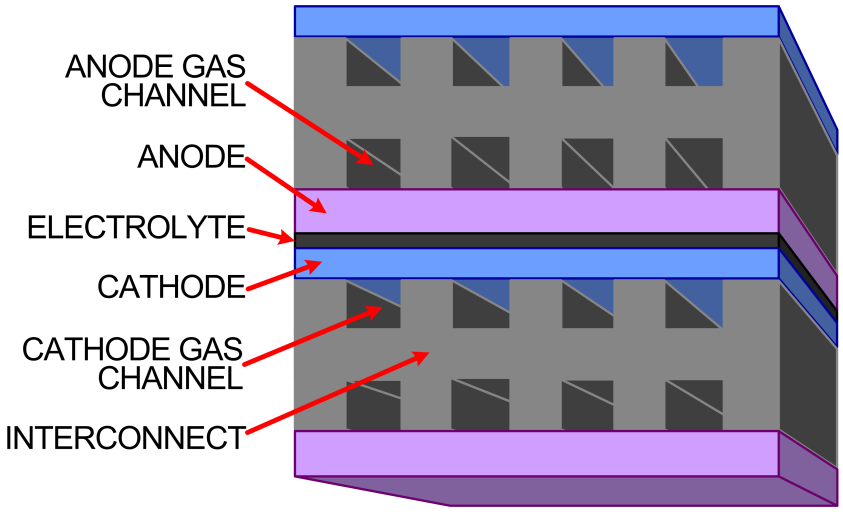

Figure 2.4: Representative Planar Solid Oxide Fuel Cell

negative charge via the oxidation of the fuel. The common anode material is a ceramic-metal cermet of nickel and zirconia (Ni/ZrO_2). Its counterpart on the air side of the electrolyte is the positive-polarity cathode, also called the air electrode. It is composed of lanthanum manganite commonly doped with strontium ($La_{0.8}Sr_{0.2}MnO_3$ or LSM).

To generate a substantial level of power the single cells must be bundled together into a stack. An interconnect is then used to connect a cathode of one cell to the anode of the next one, as diagram in Figure 2.4 This results in an electrical series configuration, so that summing each cell's voltage is the stack voltage and each cell carries the same current. A second function of the interconnect is to keep the gaseous reactants separate and to direct their flow by the cells. A grooved design creating reactant stream flow channels is often used to accomplish this. The interconnect material varies amongst fuel cell manufacturers, but stainless steel is typical. The interconnects add a substantial amount of mass and thermal capacitance to the stack. Therefore, they are an important factor in the thermal response of a stack.

2.1.1: Cell Performance

A fuel cell's potential is generated at the electrolyte/electrode interfaces by the electrochemical half cell reactions. These interfaces are commonly referred to as the triple-phase boundary because gaseous reactants are in close contact to both the electrolyte and electrode material. For a solid oxide fuel cell the half cell reactions are

$$\text{Anode:} \quad H_2 + O^{-2} \rightarrow H_2O + 2e^- \quad \text{(oxidation)} \qquad [2.2]$$

$$\text{Cathode:} \quad 1/2\ O_2 + 2e^- \rightarrow O^{-2} \quad \text{(reduction)} \qquad [2.3]$$

Water is formed at the anode, and electrons are produced at the anode while being consumed at the cathode. Figure 2.2 displays these cell reactions graphically and illustrates the oxygen ion transfer across the electrolyte. Additionally, the electron flow through an external load is denoted on the figure. The current drawn from a cell is proportional to the rate of reactant consumption.

The performance of a solid oxide fuel cell is governed by the cell potential resulting from the operating conditions such as current density, reactant concentration, and cell temperature. Cell voltage is nominally between 0.6 to 0.8 volts per cell during operation.

The a cell's performance is mathematical represented by calculating the ideal voltage and the electrochemical losses. The ideal voltage, E_{Nerst}, is governed by the molar change in Gibbs energy of the cell's reaction and is represented by the thermodynamic Nernst equation:

$$E_{Nernst} = \frac{-\Delta \bar{g}_f}{2F} = E^o + \frac{R_u T}{2F} \ln\left(\frac{x_{H2}\sqrt{x_{O2}}}{x_{H2O}}\right) + \frac{R_u T}{4F} \ln\left(\frac{P}{P^o}\right) \qquad [2.4]$$

In Equation 2.4, $E°$ is the temperature dependent standard potential. From the equation,

it can be seen that temperature, pressure and species concentration have an impact on cell performance.

The cell's operating voltage is then found by accounting for the cell polarizations and subtracting them from the Nernst voltage,

$$V_{cell} = E_{Nernst} - \eta_{conc} - \eta_{act} - \eta_{ohmic} \quad [2.5]$$

Equation 2.5 shows the three polarizations, or loss terms, associated with an electrochemical reaction. Activation losses, η_{act}, are associated with the reaction kinetics. Ohmic losses, η_{ohmic} arise from the resistance to current flow in the cell. While the more familiar electrical resistance is present in the electrodes, the bulk of the ohmic loses are from the flow of ions in the electrolyte. Concentration losses, η_{conc}, are from the limiting mass transfer of species through the porous electrodes. The magnitude of all the loss terms is dependent upon current density of the cell, increasing as more current is drawn from the cell. The mathematical representation used to calculate these loss terms varies based on governing assumptions and complexity of the evaluation.

As mentioned, the operating voltage results from subtracting the losses from the Nernst potential. This is shown in Figure 2.5 on a representative voltage-current density (V-i) curve for a typical solid oxide fuel cell. It shows the regions where each polarization is dominant and the resulting power curve which is the product of the current and the voltage. In operating a fuel cell stack, the power curve maximum is of concern in not only determining the stack's electrical output, but also in the operability. Increasing the current demand beyond this peak “starves” the cell of electroactive reactants and could result in cell damage.

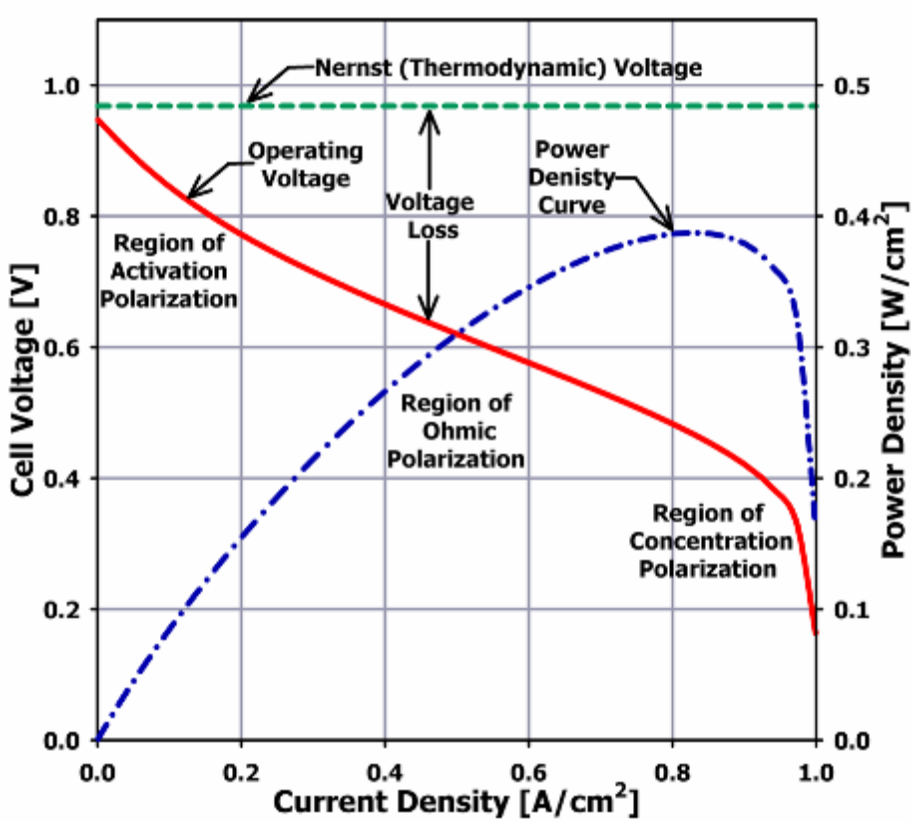

Figure 2.5: Representative Fuel Cell Voltage and Power Curve

2.1.2: Fuel Cell Stack and System Performance

To build a stand-alone power generation system several key supporting components are integrated with the stack. At a minimum a fuel supply, air supply and power conditioning system, and control system must be included. The fuel supply system delivers the required hydrogen to the anode. Fuel reforming equipment is typically required to convert the hydrocarbon fuel. Additionally species harmful to the cell, such as sulfur, must be removed from the fuel. Often a fuel pump is required, especially if the stack is operated above atmospheric pressure. In operating the stack, an important fuel parameter is the fuel utilization, U_F. Fuel utilization is the percentage of the inlet fuel that is reacted as it passes through the cell. Operating at high fuel utilization

will decrease a cell's voltage, because of the decease in Nernst potentials and increased concentration polarizations. Furthermore, possible damage may occur to the cell's anode if all the fuel in the anode volume is utilized, as its nickel content could be oxidized. However operating at a low fuel utilization will result in an excessive level of unreacted fuel passing through the stack. This will lead to a low overall electrical efficiency. Often any unutilized fuel that passes through the stack is oxidized in the stack air exhaust to create heat for inlet air preheating.

Today's common cells deliver on the order of 100 W of electrical power, therefore they must be "stacked" to build a generator of useful size. Building stacks from the cell unit creates several significant design challenges. With high temperature cells a primary concern is the reliability of seals used to keep the reactants separate. A second challenge is designing manifolding that properly and evenly delivers the reactants to the cell and provides a path for the exhaust streams. Uneven reactant supply can lead to hot-spot or fuel deficient areas in the stack that will degrade the cells and lower stack performance. Furthermore, the flow resistance inherent in the cells and manifolds, especially on the higher-flow air side, must be kept low so that high parasitic loses are not incurred in reactant delivery. An additional critical stack component is the electrical power leads that collect the current from the stack. They must be able to withstand the high temperature surrounding the cells and they must conduct high currents.

In SOFC stacks, thermal management has a large impact on performance and reliability. The cathode airflow, as well as supplying oxygen, provides the majority of the thermal management. Heat is removed by excess airflow normally supplied at more than five times what is required stoichiometricly for the electrochemical reaction. The

ratio of the air supply rate divided by the stoichiometric rate is commonly called the "number of stoichs". In operating stacks delivering the targeted number of stoichs of airflow is a key factor in maintaining the desired cell temperatures. If operating temperatures are too low the ohmic losses rise, decreasing cell performance. However, if the temperature is too high the cells degrade and crack. Airflow delivery is normally accomplished with an air blower driven by an eclectic motor. The power required for this motor is a significant parasitic loss lowering the generation system's net power output and efficiency.

The power conditioning system connects the fuel cell generator and the electrical grid. Since a fuel cell delivers DC electrical power, inverters are required to convert it to the 60 hz AC power used by the U.S. grid. A power conditioning system will also protect the stack from grid disturbances, such as power surges. Last, a control system, such as a programmable logic controller, monitors the system during operation.

2.2: Gas Turbine Basics

The other major component of the hybrid system is a gas turbine. As stand-alone systems, these engines have been used in aerospace and electrical power generation applications for several decades. For electrical generation, turbines produce the torque to drive an AC generator. This mechanical power is captured by expanding pressurized high-temperature gas across a turbine in what is known as the Brayton cycle. At the front of the engine, a rotating compressor generates the needed compressed gas, which is normally air. Next, heat is imparted to the process airflow at a constant pressure. The heat is normally generated by the combustion of natural gas or liquid fuel. This energetic

gas then goes to the turbine, which drives the compressor via a shaft and produces a net power output to the shaft load. In this simple Brayton cycle, the process air moves directly from the compressor to the combustion chamber and on to the turbine, as shown in Figure 2.6(a).

2.2.1: Turbine Engine Configurations

For stationary power generation, there are several different turbine engine configurations. The simplest is a single spool turbine system for delivering shaft power, as depicted in Figure 2.6. In this configuration, the turbine, compressor, and electrical

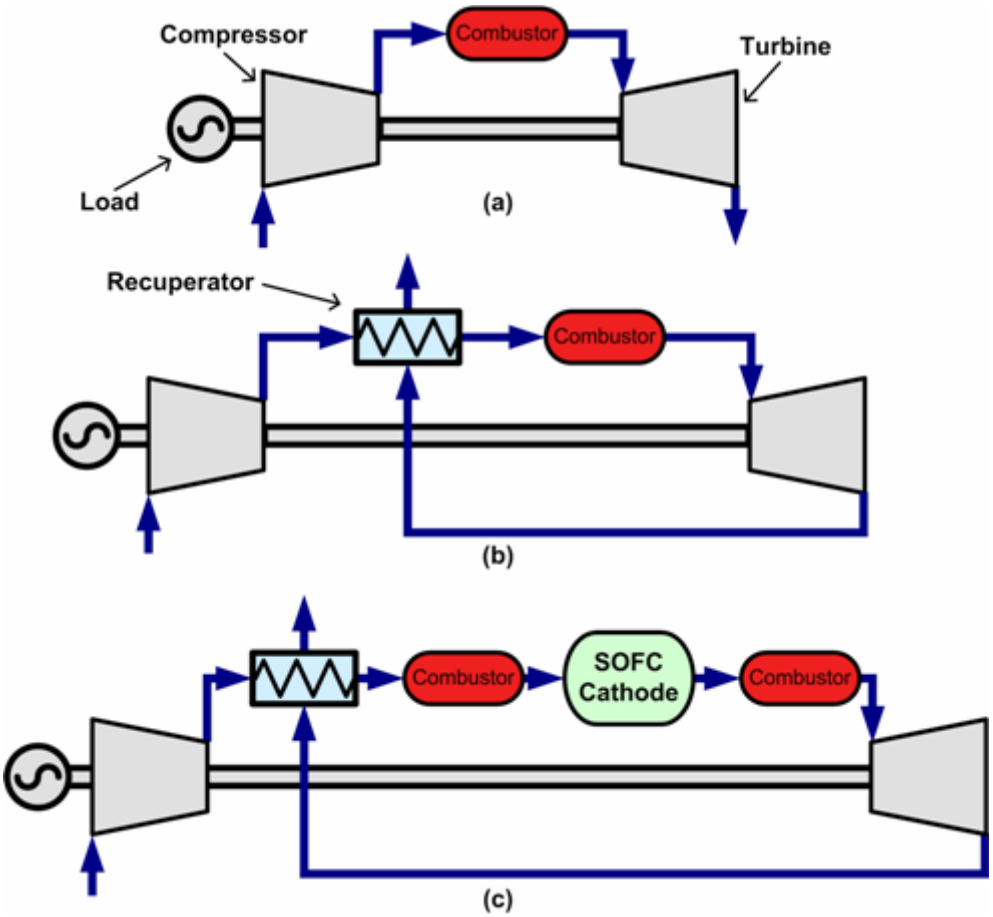

Figure 2.6: Airflow Path: (a) Simple GT, (b) Recuperative GT, (c) Direct SOFC/GT Hybrid

load generator all operate at the same rotational speed. Because of this, large gas turbines must be operated at a constant rotational speed to facilitate a direct connection of the generator with the 60 Hz U.S. power grid. This constant speed requirement has design implications for large SOFC/GT hybrids, since it prohibits control of the process airflow via the turbine's electrical loading. Therefore, other airflow control modes are required for hybrids, since SOFC operation requires modulation of airflow rate for temperature control.

For smaller systems the engine may be designed to operate in a variable speed mode for control, since a "power electronics" module can be used to rectify the output electricity frequency to 60 Hz. The speed can then be adjusted via the generator loading which leads to modulation of the process airflow.

A duel-shaft design may also be used in gas turbines. In this configuration the load is driven by a power turbine separate from the gasifier turbine driving the compressor. The duel-shaft turbine improves off-design performance, but does not allow for the manipulation of the airflow by varying the load.

Other design considerations are compressor intercoolers and recuperators. Intercoolers are used to lower the power requirement of the compressor. In a recuperated cycle a heat exchanger is used to lower the specific fuel consumption rate and is discussed below.

2.2.2: Compressor Characteristics and Surge

In evaluating gas turbine performance, the component of primary concern is the compressor. The purpose of a compressor is to increase the pressure of the process gas at the required flow rate while consuming a minimum of the turbine's power. By its nature,

it is a relatively unstable device in that it moves airflow against an unfavorable pressure gradient. It does this by converting mechanical work to velocity and pressure through aerodynamic lift and/or centrifugal force.

The common method to convey the operating characteristics of a compressor is by use of a compressor map, which defines points of steady-state aerodynamic performance (Oakes, 2004). A representative compressor map is shown in Figure 2.7, which plots pressure ratio versus mass flow for various constant rotational speed lines. The pressure ratio is defined as the exit pressure divided by the inlet pressure. The map utilizes corrected variables that account for changes in inlet air temperature and pressure. Also shown on the compressor maps are isentropic efficiency, η_S, islands that indicate the energy conversion effectiveness of a compressor. A map for a certain compressor design

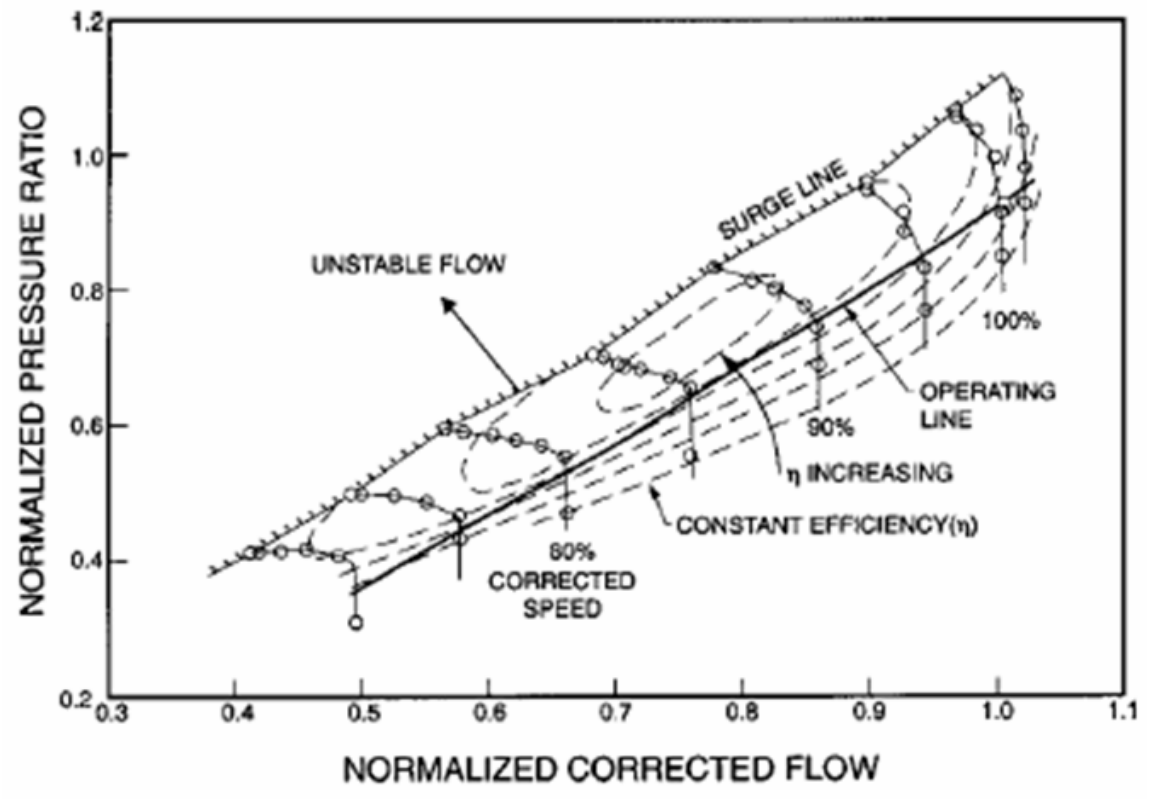

Figure 2.7: Generalized Compressor Map (Oakes, 2004)

is normally produced empirically by compressor manufacturers. In recent years, computer programs have been utilized to predict maps based on aerodynamic analysis.

For a given speed, the point of operation lies between the choke (throttle) limit (at high mass flows) and the surge line. The choke limit is where a speed line approaches vertical, indicating that a maximum mass flow is reached even though the pressure ratio is reduced.

On the other side of a speed line, as the pressure ratio increases and mass flow decreases, the surge line indicates a critical operating limit. The region of operation to the upper left of the surge line in Figure 2.7 indicates unstable operating conditions normally leading to an undesirable compressor surge. Surge is a swift breakdown of the stable compressor flow. This leads to a flow reversal so that it briefly goes backwards through the compressor from high to low pressure. Surge arises as the adverse pressure gradient across the compressor rises above what can be aerodynamically supported by the compressor blades and resulting mass flow. Often a compressor will quickly reestablish positive flow only to surge again leading to a cycle that can repeat multiple times in a second. This leads to a dynamic phenomenon consisting of large-amplitude low-frequency oscillations of flow rate and dangerous pressure pulsations (Taccani, 2006). In an operating gas turbine, occurrence of surge is readily evident to those nearby due to the loud bangs generated. The relative distance of an operating point from the surge limit is commonly called the surge margin.

During operation a sufficient surge margin must be maintained, otherwise costly engine damage may result. In a compressor surge large amplitude pressure waves and vibrations are generated in the system. This induces large mechanical loads on the

engine structure and may lead to broken or damaged compressor blades. This aversion to surge is ever more important when a compressor is integrated with a SOFC in a hybrid. The high temperature ceramic material is brittle and susceptible to vibration and pressure wave damage. Hildebrandt (2005) stated that "reverse flow and surge itself have to be avoided under every circumstance in order to protect the compressor and the downstream fuel cell."

Furthermore, transient operation exacerbates surge avoidance concerns. Transients arise from changes in turbine speed, loading, or in response to changing ambient conditions. During transients, operating points on the compressor maps can deviate significantly from the predicted steady-state performance, reducing the surge margin (Oakes, 2004).

2.2.3: Recuperated Gas Turbines

In a modified Brayton cycle with heat recovery (Figure 2.6(b)), compressed air is preheated before combustion in a recuperator by capturing heat from the turbine exhaust. The recuperating heat exchanger used must withstand the pressure differential between pressurized compressor discharge and near atmospheric pressure turbine exhaust. The recuperator does increase the system weight and expense of the engine, therefore recuperative cycle turbines are not suitable for aerospace propulsion. However, the heat reuse reduces the specific fuel consumption and makes recuperated cycles attractive for stationary applications where efficiency is a leading design factor. Furthermore, heat recovery is pivotal to hybrid systems due to the requisite air preheating before it enters the fuel cell stack.

An important factor to consider with recuperated systems is the significant increase in compressed volume and flow path between the compressor outlet and the turbine inlet. For the simple cycle, the volume is on the order of 0.02 m^3 while it is an order of a magnitude larger for recuperated systems (Greitzer, 1976). The use of a recuperative system also increases the flow impedance significantly, leading to higher pressure losses in the system. The effects of the increased pressure losses are apparent even on steady-steady system analysis. In comparing a recuperated system to a simple cycle, important competing factors are indicated in optimizing efficiency. In a simple cycle, efficiency increases with the pressure ratio; however, in a recuperative cycle pressure losses rise with pressure ratio and become much more dominant, resulting in a maximum efficiency at a pressure ratio of 7 to 9 (McDonald, 1996).

A larger compressed volume has a noticeable effect on compressor performance and surge. The increased volume raises the susceptibility of the compressor to surge because more energy is stored in the larger pressurized volume (Ng, 2004). The increased flow impedance also reduces the surge margin since system mass flow will be lowered for a given pressure head from the compressor. The effect on surge probability from a larger volume is even more pronounced during a transient, due to a volume packing effect where fluid density is responding to pressure and temperature changes. This is of particular concern during a deceleration, where mass flow rate reduction is faster than pressure ratio drop-off due to the large storage of pressurized air.

2.3: SOFC/GT Hybrids

As mentioned in the Introduction, this research effort focuses on the integrated cycle that combines a high temperature fuel cell and turbomachinery into a hybrid power generation system. While there are numerous plausible system configurations for a fuel cell / gas turbine hybrid, this dissertation focuses on direct hybrid cycles, in which the fuel cell is placed between the compressor and turbine and is operated at an elevated pressure (see Figure 2.1). Furthermore, the turbine of interest is a single-shaft design. It is also desirable to investigate constant speed turbine operation, so that it is applicable to larger scale hybrid systems.

2.3.1: Advantage of Hybrid Power Generation Systems

A SOFC/GT hybrid system has the potential to achieve high efficiency electrical power generation. The value of this potential has led the U.S. DOE to express their support of hybrid systems by declaring them the "most exciting innovation in power in the next 10 years" (Hamilton, 1999). The efficiency gains are achieved through combining the unique characteristics of fuel cells and gas turbines. The pressurization of the cells improves their overall performance. The turbine's principal role in the hybrid system, though, is analogous to a turbocharger in a diesel engine. The turbine pressurizes the fuel cell stack and provides the necessary airflow. In an operational SOFC/GT hybrid system, typically 80% of the electrical power is produced by the fuel cell stack with the remaining power supplied by the gas turbine's generator. The total power generation capacity is projected to range from 200 kW to 100 MW.

The overall system efficiency will be higher than that of operating either the SOFC or the GT alone. In a stand-alone fuel cell stack, supplying the required airflow

consumes a large portion of the gross power generated. When a GT is integrated with the SOFC, though, the fuel cell's byproduct heat is partially recovered to supply the stack's airflow through the turbomachinery. This significantly reduces parasitic losses since the need for an externally-powered air blower is removed, and results in higher net output of the fuel cell power. Furthermore, the turbine can often generate an additional 10 to 20 % of electrical power, further increasing system efficiency.

The thermodynamic gains also have the potential to improve the financial attractiveness of fuel cell stacks. Fuel cell stacks are, and will remain for some time, an expensive component. In a direct hybrid cycle the fuel cell stack is pressurized, which increases stack power output and efficiency. This leads to more effective utilization of this expensive component. This may lower the per kW capital cost of a stack when it is integrated with a gas turbine. Furthermore, higher efficiency directly reduces the fuel usage of a system, lowering the operating cost. This will decrease the time required to recover the higher initial capital cost for a hybrid system.

2.3.2: Challenges Facing Hybrid Power Generation Systems

While actual trials have indicated the feasibility of hybrid cycles, certain obstacles must be addressed before they can be commercialized (Litzinger, 2005, Veyo 2003). With the SWPC 220 kW trials, several key factors were observed to have a significant influence on the performance of the system. The most noteworthy of these factors are related to airflow management. Fuel cells are very sensitive to airflow because it is the primary means of heat removal, and operating temperature largely determines the performance and longevity of the cells. With the air being supplied by the microturbine, it is more difficult to regulate the airflow rate than it would be with an independently

controlled, electric motor-driven air blower, as one would have in a stand-alone stack. Furthermore the thermal timescales for the stack are on the order of tens of minutes to hours due to the large thermal capacitance of the stack, whereas the microturbine responds to thermal changes on the order of seconds. This leads to a significant feedback loop between the stack and turbomachinery that may amplify or cancel desired changes implemented via external controls. Conversely, the turbine is also dependent upon the stack. For example, reducing the stack loading and fuel supply will reduce the amount of thermal energy available to the turbine. This may limit the ability of the turbine to supply the stack's airflow.

The compressor performance is also significantly influenced in a hybrid configuration. With the introduction of the stack's cathode volume into the airflow path (Figure 2.6(c)), the pressurized volume is increased to approximately 2 m^3 (Tucker, 2005a). This is two orders of magnitude greater compressed volume than a simple turbine cycle. Furthermore, the transient behavior from a fuel cell stack load change becomes more severe due to the delay of mass flow change for a large plenum volume (Hildebrandt, 2005). These factors would greatly increase the likelihood of a compressor surge occurring during operation (Tucker, 2005b). As previously mentioned, these surge events can generate large pressure fluctuations in the system. This is of chief concern to the development of SOFC/GT hybrids, since the ceramic cells, as well as the turbomachinery, may be damaged by a surge event.

A significant challenge to hybrid development is simply the marrying of these two distinct systems into one. The SOFC and GT operate on distinctly different time scales, have several competing operating factors, and the resulting system performance is not

intuitive. The current design approach has been to find existing turbine hardware that fits most of the fuel cell operating requirements. However, the SWPC 220 kW Hybrid clearly showed the need for air flow capacity matching between SOFC and GT (Veyo, 2003). Furthermore, being able to modulate the airflow rate to meet the SOFC needs while maintaining turbine performance needs to be considered. Other desirable design factors are:

- A high modulation combustor that handles high temperature inlet air. Current turbine combustors use cooler inlet air to protect the combustor and have a narrow turndown range.
- A turbine system that has air-bearings or insurance against oil leakage. Most turbine systems use oil lubrication to protect the rotating equipment. The oil may leak to the process air and degrade the cathode surface to the fuel cell stack and may destroy the stack.
- A turbine system that can be motored (such as by a starter motor) for extended periods to facilitate SOFC startup and shutdown.
- A SOFC stack suited for pressurized operation. Pressurization has been shown to exacerbate uneven distribution of reactants, which will degrade stack performance.

To be successful, it may be necessary to design the fuel cell and turbine system from the ground up as an integrated system from the start; however, this is a costly endeavor. Furthermore, turbine designers do not understand the special requirements of a fuel cell stack. Likewise, fuel cell designers do not appreciate the challenges in creating

reliable turbomachinery. This highlights the strong effort that is required to commercialize SOFC/GT hybrids.

2.4: Previous SOFC/GT Hybrid Analysis and Development

SOFC/GT systems have primarily been explored through steady state thermodynamic analyses and by dynamic numerical models. These types of analysis have been explored extensively since the 1980's. In the last several years, the groundwork established by these studies has been demonstrated in several operating prototype hybrid systems.

2.4.1: Hybrid Modeling Efforts

Hybrid system numerical simulation research is conducted by developing and then integrating fuel cell and balance-of-plant component models. Literature examples of developed numerical models are numerous. A overview of SOFC modeling approaches and the use of these models in simulated SOFC/GT hybrid system was presented by Bove (2006), which stated that zero-dimensional fuel cell models are primarily used in system analysis. The analysis of hybrid systems through modeling has shed light on the complexity and nonintuitive nature of hybrid cycles. For example, steady-state modeling efforts have shown that when integrating the GT and SOFC, operating the fuel cell at lower stack efficiencies may lead to higher overall cycle efficiency (Haynes, 2000). More recent studies have detailed the development of transient simulation codes (Magistri, 2006). Numerical simulation work is also being conducted on testing control methods for hybrids. Stiller (2006) has investigated part-load performance of a hybrid system based on SWPC tubular design, utilizing a 2-D fuel cell model, and a variable

speed turbine. Wachter (2006) evaluated hybrid controls utilizing a linearized state-space model of a hybrid system using bulk component models. Hildebrandt's (2005) modeling efforts highlighted the importance of compressor characteristics in evaluating hybrid system control.

A significant area of need is the validation of numerical hybrid simulation against operating systems. Work by Yi (2003) validated steady-state component models against SWPC 220 kW hybrid operational data. Likewise, SWPC 220 kW was utilized by Roberts (2006) to validate dynamic models developed in Simulink.

In contrast to the numerical models, hardware-based simulation with externally fired gas turbines has been shown effective in test hybrid concepts. Work at HyPer, the DOE facility associated with this dissertation, has characterized the control of air flow through the use of bypass flows (Tucker, 2005a). At a similar facility in Italy, work by the Thermochemical Power Group has evaluated a novel means for rotational speed control of the turbine by acting on a valve that bypasses heat exchangers (Traverso, 2005). A second group from Italy is developing a gas turbine and air plenum experimental test facility to validate fuel cell/gas turbine dynamic simulations (Taccani, 2006).

2.4.2: Operated Hybrid Systems

Toward the development and testing of hybrid hardware, the world's first SOFC/GT hybrid was built by SWPC and started operation in 2000. This 220 kW hybrid system is described in the next section. Since the completion of the 220 kW trials, SWPC has designed and built a SOFC/GT hybrid system known as the PH300 for demonstration in Europe (Litzinger, 2005). The PH300 had 1704 tubular cells, 552 more that the

220 kW hybrid system, and an 100 kW microturbine manufactured in Europe. However this system faced numerous turbine integration issues and only operated on a limited basis.

In parallel, GE Energy and Rolls-Royce Fuel Cell Systems have active programs pursuing the commercialization of SOFC/GT hybrid systems. GE Energy SOFC stack design is based on a circular planar cell design. The Rolls-Royce approach is based on a segmented cell design that integrates a series of micro-cells on a single ceramic backing. Additionally, FuelCell Energy has developed and demonstrated an indirect molten carbonate fuel cell / gas turbine (Roberts, 2006). The molten carbonate fuel cell is a distinctly different fuel cell technology that operates at approximately 600 °C. In the indirect hybrid cycle, the fuel cell is placed after the turbine exhaust and is operated at atmospheric pressure. High-temperature heat exchangers are utilized to transfer the heat from the stack exhaust to the turbine inlet air.

2.5: Siemens-Westinghouse Power Corporation 220 kW Hybrid

As mentioned in the Introduction, the SWPC 220 kW hybrid (see Figure 1.1) was a proof-of-concept demonstration of a fuel cell / turbine hybrid system. The testing consisted of four different operational periods and was conducted between June 2000 and January 2003. Designed and manufactured by the Siemens Westinghouse Power Corporation (SWPC), the 220 kW system was operated through a partnership between Southern California Edison and the National Fuel Cell Research Center on the campus of the University of California, Irvine. In nearly 3,200 hours of operation, a wealth of technical data and engineering experience on SOFC/GT hybrids was garnered. While the

unit was never connected to the electrical grid (the electrical power generated was dissipated onsite) it did archive a projected 53 % efficiency (AC electrical power / lower heating value of fuel) and generated approximately 500 MWh of electricity (Veyo, 2003). Most importantly, it demonstrated the feasibility of a SOFC/GT system and furthermore showed that several challenges must be resolved before commercialization.

2.5.1: Experience in Hybrid Operation

While at the University of California, Irvine for my master's degree I participated in the operation of the SWPC 220 kW Hybrid. My role in this proof-of-concept trial was to assist John Auckland, the site operator contracted by Southern California Edison and the National Fuel Cell Research Center, and the SWPC personnel with the operation of the 220 kW hybrid system. I was involved in the day-to-day system operation and maintenance, as well as startups and shutdowns. In addition, I compiled and archived the data acquired by the control system and recorded by the operators.

From this fortunate level of involvement I gained a wealth of hands-on knowledge pertaining to the characteristics inherent to hybrid power generation systems. This included monitoring the system during operation, allowing for the observation of long term cell temperature transients as the system responded to changes in ambient conditions or user set parameters. This unique experience provides a solid background for evaluating simulations of SOFC/GT hybrids to ensure the observed results are applicable to these systems. Furthermore, the operational experiences assisted in identifying dynamic interactions inherit to SOFC/GT hybrids to test with HILS on the HyPer facility.

2.5.2: SWPC 220 kW Hybrid Stack Description

As is presented in Figure 2.8 the 220 kW Hybrid system (also referred to as the PH200) integrated two major components: the tubular solid oxide fuel cell stack in a pressure vessel and a microturbine. Siemens-Westinghouse designed and manufactured the solid oxide stack using their unique tubular cell design. The tubular cell design eliminates seals that are inherent to planar cells. These seals are difficult to maintain at the cell operating temperatures. The stack is essentially a modified 100 kW atmospheric stack, composed of 1152 cells. The fuel cell generator was adapted so that it is vertically housed in a pressure vessel allowing it to be integrated into the hybrid cycle. Solid oxide fuel cells show an increase in power density and efficiency with an increase in operating pressure, but as operating pressure increases the fabrication costs rise. Balancing these factors and the microturbine integration led to an operating pressure of approximately 3

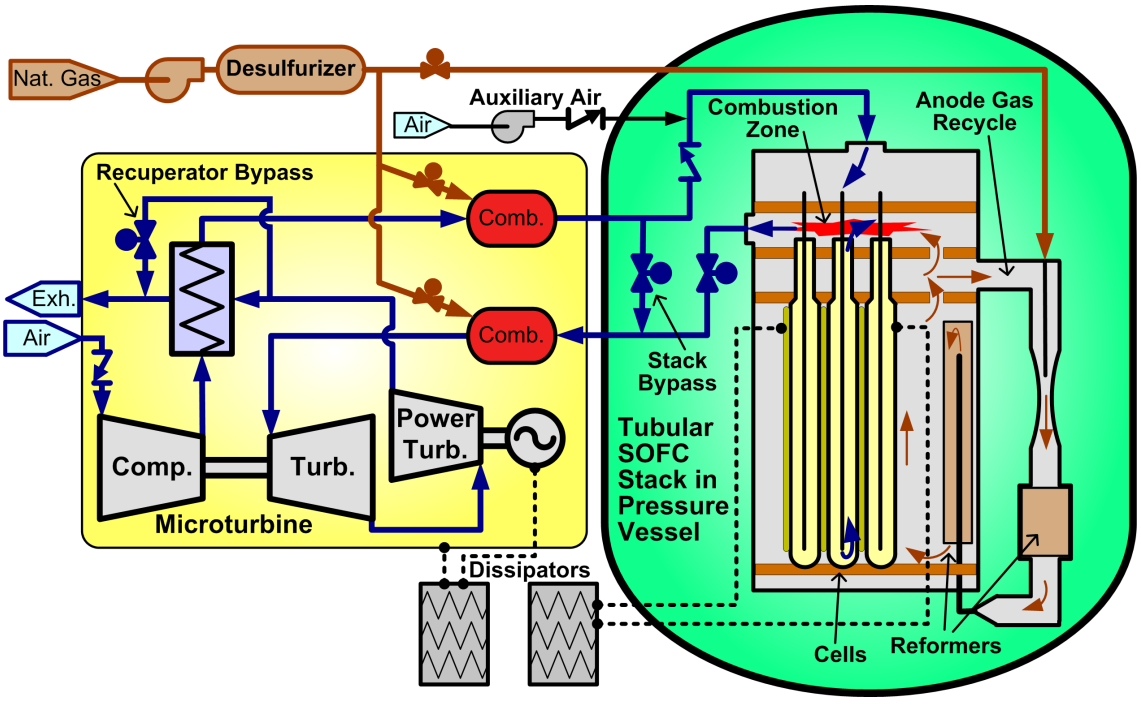

Figure 2.8: SWPC 220 kW Hybrid System Flow Diagram

atmospheres. At this level, the maximum fuel cell power production rises to 180 kW of DC electrical power. At this level of loading, the electricity produced is at about 750 amps and 240 volts.

The SWPC tubular stack design incorporates several key items to supply the required air and fuel to the cells. On the cathode side, air was injected to the inside of each cell through alumina air supply pipes. During operation the air enters the stack near 500 °C and is further heated in the air pipe before reaching the bottom of the cell. A portion of this heating is done as the air supply pipe passes through a stack combustion zone where utilized cell fuel is oxidized. At full load, the stack was supplied 5 to 6 times the airflow required for the reaction alone. This was approximately 0.5 kg/s of airflow and it exited the stack at approximately 800 °C. The stack air supply also had a stack bypass valve which allowed for around 20 % of the airflow to be directed around the tubular stack. During operation of the system, this butterfly valve was used to manage the airflow to the stack.

On the fuel side, desulfurized pipeline natural gas was supplied to the stack and reformed into hydrogen rich gas by internal reformers. To support the endothermic reforming, the fuel supply system creates a circulating flow mixing fresh and depleted fuel. The anode-off gas contains byproduct water (steam) and heat from the electrochemical reaction. The natural gas is injected into the fuel stream at the neck of a nozzle creating a venturi pump that drives the recirculation. The mixed fuel is then sent through prereformer and reformer plate modules that are inserted between cell rows. By integrating reforming modules amongst the cells, the heat for reforming comes directly from the cells, therefore the reformer modules act as a heat sink for the stack. Leaving

the bottom of the reformer plates, the hydrogen rich fuel mixture flows along the anode surface of the cells from bottom to top and into the depleted fuel reclaim zone.

At the top of the stack the anode-off gas stream is split with about 15 % exiting the stack through the combustion zone while the bulk of it is recirculated. The utilized fuel is then oxidized above the cells in a combustion zone as it mixes with the stack air exhaust. In order to maintain the desired voltage and to protect the anode surface the fuel utilization is targeted at 82 %.

2.5.3: SWPC 220 kW Hybrid Turbine Description

The second major component, the microturbine, was supplied by Ingersoll-Rand and is a modified stand-alone product originally rated at 75 kW. The microturbine system is a recuperated two-shaft configuration comprised of a radial compressor shafted with a high-pressure radial turbine, and a low-pressure radial turbine connected to an AC generator. In this configuration, the power turbine (low-pressure) can operate at a lower rotational speed than the compressor and gasifier turbine (high-pressure). When coupled with the SOFC stack, the turbine produced an additional 30 kW of electric power. In the 220 kW system, the compressor supplied approximately 0.65 kg/s of airflow at a pressure ratio just above 3.

The turbine housing also contains many of the balance of plant items such as the recuperator and combustors. The combustors in the system are used for stack heating during system start-up and maintaining operation during partial loads when the stack does not produce sufficient waste heat to power the turbine portion of the cycle. The recuperator is an air-to-air heat exchanger that captures heat from the turbine exhaust to

preheat the compressor discharge air before it enters the fuel cell stack. For this unit the effectiveness is estimated to be 90 %.

2.5.4: Insights from SWPC 220 kW System

During the operation of the hybrid several key factors were observed to have a significant influence on the performance of the system. The predominant factor affecting operation is airflow mass flow rate. Process air is the principal thermal energy carrier that removes heat from the stack, thereby establishing the stack temperature. If the airflow supply rate decreases, the stack temperature will rise. This outcome may take several hours to be fully realized, though, since the thermal mass stored in the stack and vessel is large. Furthermore, the pressurization of the vessel and the performance of the turbomachinery are also affected by the airflow.

The primary airflow mover is the compressor and its rotational speed governs the airflow supply rate. The SWPC 220 kW used a dual-shaft configuration that does not allow the rotational speed of the gasifier turbine to be controlled directly. While the duel-shaft design does offer some advantage by simplifying the power generator and associated gearing, it complicates the airflow control in this system. Furthermore, the turbine was originally designed for a higher air mass flow rate than what was required for the SWPC SOFC stack. A stack bypass valve allowed for around 20 % of the airflow to be directed around the tubular stack. This configuration did prove itself to be an effective means to modulate the stack airflow. However, any level of bypass lowers the turbine inlet temperature and increases the compressor work load. These effects of bypassing air lower the overall efficiency of a hybrid system, but significantly increase its operability.

In the stack, the overall cell temperature and resulting performance is greatly influenced by the airflow rate. Furthermore, the SWPC tubular cells operate with an axial temperature profile, which is responsive to the airflow rate changes. The extent of the temperature bow has a strong effect on stack performance. Specifically, a "flatter" bow will result in a higher percentage of the cell's active surface area being in the optimal temperature range. A reduction in the axial temperature gradient is accomplished through increasing the airflow.

Ambient temperature also affects compressor performance resulting in an airflow decrease as the surrounding temperature rises. This because the density of the air entering the compressor decreases. Compressor performance is acutely sensitive to inlet air temperature, so much so that the diurnal variations are significant. Therefore, a hybrid system's SOFC stack that is operating at elevated temperature during the day may over cool at night without any operational setpoint changes. From a system analysis standpoint, when accounting for the daily swings in ambient conditions and the large thermal mass of the vessel, one quickly concludes that the hybrid system is in a continuous dynamic as it responds to the external conditions.

Secondary to inlet temperature, turbomachinery performance is sensitive to ambient pressure and humidity, as they also affect the density of air (Brooks, 2000; Walsh, 2004). As pressure decreases, air density decreases. Pressure is dependent upon site elevation in that pressure decreases as altitude increases. Pressure is also affected by barometric pressure, which is a product of weather systems and is therefore variable at a given site. As relative humidity increases the density of the humid air decreases, since water vapor is less dense than dry air. This is because the molecular weight of water is

less than that of dry air. Therefore, hybrid developers and operators must be cognizant of the influence of ambient conditions due to their affect on air density, and in turn, compressor behavior. This governs system airflow, which is a primary factor in both fuel cell stack and overall system performance.

2.6: Hardware-in-the-Loop Simulation

As discussed above, research into SOFC/GT has primarily been conducted with numerical analysis and limited application of trial systems. These past research efforts highlight the need for a new strategy. In general, there are three methods that have traditionally been utilized for analyzing dynamic systems and for predicting their responses to external parameters. For simple, often idealized systems, there are analytical methods that offer insights into the underlining phenomena governing a system's behavior. More complex and nonlinear systems necessitate the use of numerical methods to approximate a physical system. However, as the complexity of a system under study increases, the uncertainties associated with the knowledge underlying these mathematical approaches reduce the accuracy of the analysis, or the behavior may be impossible to model computationally (Darby, 1999). Often then, a prototype or physical simulation for experimental testing is required for analyzing a complex system. This hardware based approach can be impractical and expensive for large systems, such as advanced power generation plants. Therefore, a means is desired that can exploit the benefits of both mathematical and hardware simulations, while avoiding their shortcomings (Kyrychko, 2006). A concept to address this need is hardware-in-loop simulation.

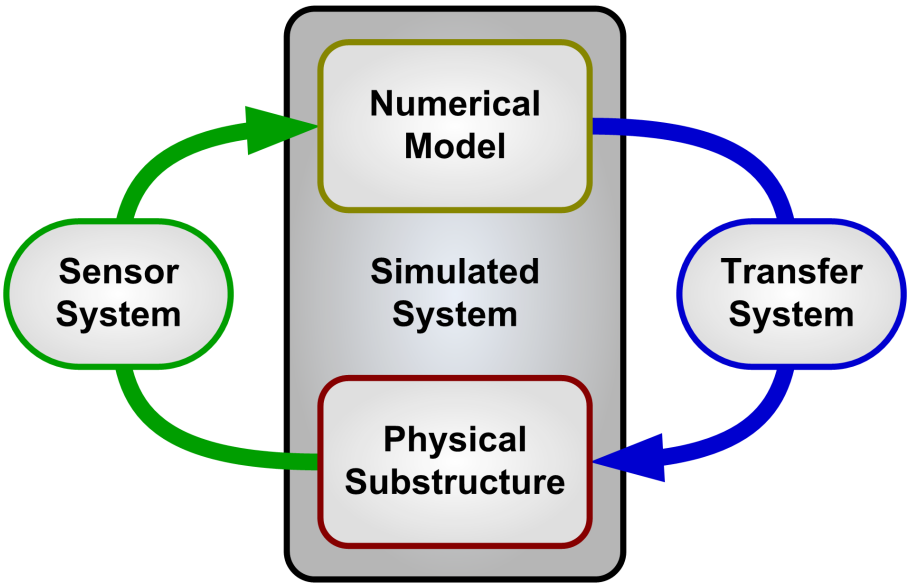

Figure 2.9: HILS Concept

"HILS is a technique that combines and interfaces real and virtual components into an operational configuration to simulate and test the dynamic behavior of complex systems" (Cravotta, 2005). This method, also called real-time dynamic substructuring, consists of dividing the simulation of the complex system under study into two parts: a physical component and a numerical model, as illustrated in Figure 2.9. During a simulation the two subsystems interact in real-time creating a realistic representation of a system's time-dependent nonlinear behavior. The simulation's substructures are coupled by transfer and sensor systems that communicate between the physical and virtual components. The sensor system consists of instrumentation to measure physical conditions and convert them to numerical inputs. The transfer system, in turn, interprets numerical outputs and transforms them to physical phenomena by using actuators, heat sources, or other controlled devices.

As depicted in Figure 2.10, HILS is a compromise between numerical models and physical systems. Numerical simulations, because they are safe, fast, and cost effective,

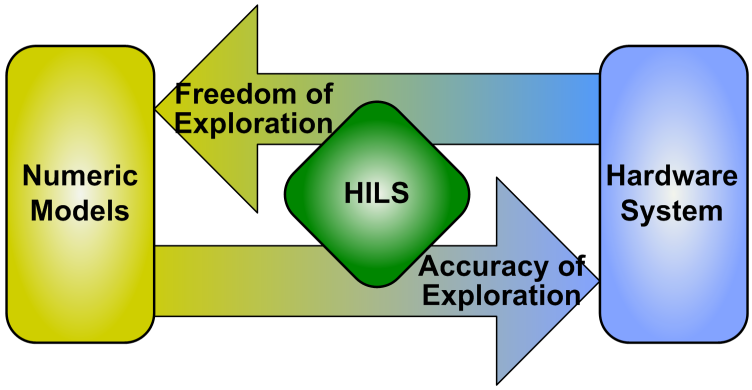

Figure 2.10: HILS Design Value

offer the advantage of flexibility that allows for the exploration of a large design domain. The disadvantage is that they may produce low accuracy results and not reflect reality. Three factors contribute to diminishing the accuracy of numerical simulation: the limits in the understanding of the governing physical phenomena, the formulation of the mathematical abstractions used to model the phenomena, and the errors inherit to the numerical methods used to solve the equations. In contrast, hardware-based simulations capture the physical phenomena precisely, but are expensive, time-intensive, may require operating in domains dangerous to personnel and equipment, and limit research flexibility. Hybridization of numerical model with a physical substructure into a single simulation system offers an advantageous compromise, allowing for increased freedom of exploration to observe dynamics, while maintaining the level of accuracy. HILS can therefore be an effective tool to reduce experimental and design costs in developing new products, such as SOFC/GT hybrids.

2.6.1: Examples of HILS

HILS has been used extensively by the automobile industry and has proven itself to be a cost-effective tool for controls development and testing (Kohl, 2005). The

aerospace industry has been using this technique ever since software became a "safety-critical aspect of flight control" (Maclay, 1997). The application of HILS to advanced energy systems has been limited, but it has the potential to provide an effective, timely, and safe testing method for power systems. Developers and researchers have documented where they have begun to apply HILS to energy devices. For example, Palma (2005) outlines the methodology for HILS with the Modelica environment, and Monti (2005) details several HILS case studies and the associated interfacing issues. Related research from the automotive industry has offered insight into the implementation of HILS with proton exchange membrane fuel cells (PEMFC), which share some characteristics with SOFCs. Salem (2005) applied a numerical PEMFC to a physical electrical motor. The work also outlined the basic elements for a HILS system. Ungethum (2005) developed a PEMFC model in Modelica that was integrated into Simulink, compiled with MATLAB Real-Time Workshop, and executed on a dSPACE processor DS1005 board. Furthermore, Lemes (2006) used a dynamic PEMFC model with HILS to implement a controls development test bench. In other research Zhang (2005) utilized HILS in the development of a gas turbine engine for marine applications. Mansoor (2003) applied HILS to investigate changing the control strategy before implementation in an existing pumped storage hydro power station operating six 300 MW synchronous water turbines.

Several companies service the HILS market, especially for the automotive industry. dSPACE Inc. initially focused on automotive control system development and has expanded to offer hardware systems and simulation software products. Opal-RT Technologies provides software, hardware, and related services for real-time simulation.

Applied Dynamics International (ADI) develops software and hardware tools for the automotive, aerospace, and defense industries to test control systems. To a lesser extent, National Instruments, with its Labview product line, has entered the HILS market.

2.6.2: Real-time Models

The coupling with the hardware substructure in a HILS system requires dynamic numerical models that execute in real-time. In general, real-time simulation can be defined as simulation in which changes in the variables (pressure, flow, temperature, etc.) proceed on the same time-scale as in the physical world (Mansoor, 2003). To fulfill the real-time requirement each numerical integration step must be computed within a hard-time limit that is less than the simulated time step. The time required for a computer processor to compute the next time step during a simulation is referred to as the turnaround time. Additionally in HILS, during each time step the model must read measured values from the physical system and return control parameters. Therefore, in a real-time model the turnaround time, including handling of input/output signals, must be less than the simulation's sampling time.

Four traits of real-time modeling are fixed-time step, deterministic computing time, numerical stability, and high computing speed. The fixed-time step prohibits the use of a shorter step length when more accuracy is required, as in off-line simulation. In order to provide a deterministic computing time, the models formulation should avoid iterative solution algorithms, when possible. This may require symbolically eliminating nonlinear sets of equations in establishing the mathematical approach. However, if it is not possible to avoid implicit equations, the real-time requirements can still be fulfilled if the number of iterations is moderate (Ungethum, 2005). Numerically unstable models

cannot be applied to HILSs. Instabilities arise from numerical discontinuities or stiff differential equations. They lead to rapid variation in the solution and may halt execution of the model. High computing speed is achieved by keeping the mathematical description of the modeled subsystem as simple as possible. This may require formulating the model with low fidelity or a bulk parameter approach. A second approach in dealing with computation speed is to increase processing power, thereby reducing the computation time per integration time step. This means that in a HILS facility, upgrading the computational hardware can permit higher fidelity models, while ensuring real-time numerical simulation.

2.6.3: Design of HILS System

Conducting a HILS requires tying together physical components, computational hardware, and software into a single simulation platform. The basic conceptual layout of a HILS system is shown in Figure 2.11. Identified are the three primary components of a simulation platform: a host computer which serves as the user interface, a target computer that executes the real-time numerical simulation, and a physical structure to capture real phenomena. The host and target system may be a single computer system, but this approach limits functionality since the numerical simulation and host's operating system compete for processor time. Furthermore, in conducting more complex simulation, multiple target processors can be used for parallel computation. The host and target systems are connected by high speed communication links, while input/output devices interface the virtual and real sub-simulations. The details of each simulation platform piece are outlined below.

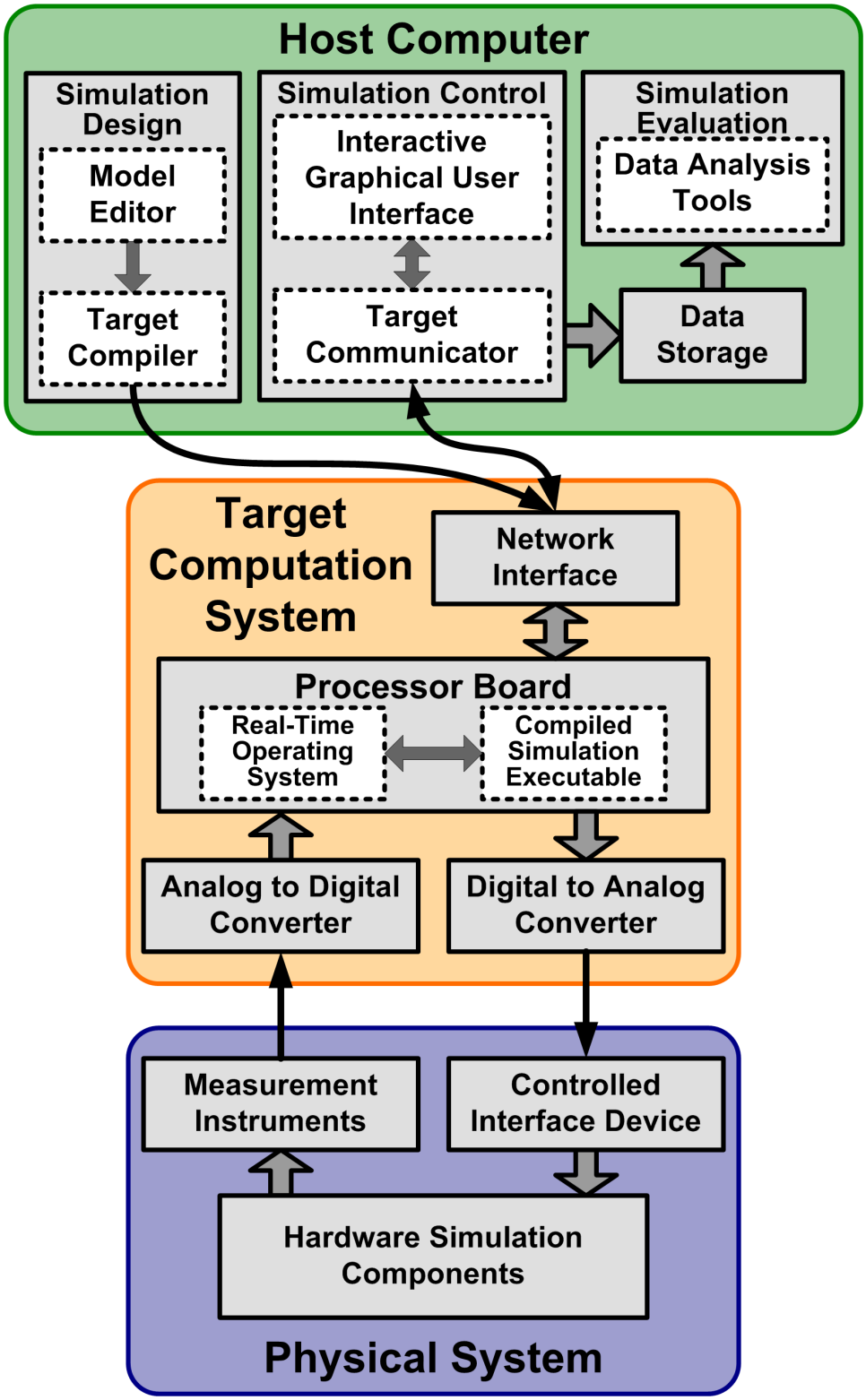

Figure 2.11: HILS System Components

The host computer is normally a PC workstation with a Windows or Linux operating system. Its primary function is to serve as the user interface for the creation, the execution, and the post analysis of a simulation experiment. For designing the numerical simulation, a model editing environment is used, such as C programing language or Mathworks MATLAB/Simulink package. Once the model is created, the host computer compiles it specially for the target's processor and uploads the compiled simulation program onto the target system. In the Mathworks environment this is done with the Real-Time Workshop, which generates and compiles C code based on a Simulink model. To manage a simulation through the host computer, the user also designs a graphical user interface to control the execution of a model. The interface program communicates with the target's simulation to initiate, stop, update input parameters on, and display live outputs from the numerical simulation. dSPACE's ControlDesk is an example of a software package for simulation management. Communication is accomplished by connected network boards on the host and target computers. The connection is normally done by a dedicated scheme, such as fiber optic cable, but may be done on a local area network. During an experiment, the host computer receives and records data streamed from the target. Post simulation, the host computer has data analysis tools to retrieve and interpret the results.

The target computer is dedicated to computation of the numerical model. At its core is a processor board that is designed for high-speed computing. It is loaded with a real-time operating system to ensure the execution of simulation programs in real-time. Supporting the processor board on the target computer are the network board, mentioned above, and input/output boards that relay signals between the real and virtual subsystems.

An analog-to-digital converter (ADC) acquires and discretizes the continuous signals from the physical structure and sends them to the processor for utilization in the numerical simulation. For HILS, ADC boards often have multiple channels, fast sample times, and supporting signal conditioning, such as a signal noise filter. Coupling the numerical predictions with the physical structure is a digital-to-analog converter (DAC) for signal output.

The physical system includes the real simulation components and the devices that interface with the target computer input/output board. The hardware composing the simulation's physical substructure can vary greatly depending on the research or testing being conducted. Examples include an electronic system, such as an embedded controller, or a mechanical system, such as an automotive suspension component. Controlled interface devices transmit actions to the physical system as directed by signals from the target's DAC board. These transfer systems could be but are not limited to actuators, electrical loads, heat sources. When conducting high frequency simulation, care must be taken to avoid time delays in the transfer system that may affect the dynamics under study. On the sensor side, instrumentation (thermocouples, pressure transducers, etc.) is used to measure physical parameters and generate the signal for the ADC. A concern here is systematic and random measurement errors in the sensor system that could lower the accuracy of a simulation.

2.6.4: Application of HILS to Hybrids

In order to realize the benefits of HILS, its proper application to the system under scrutiny is essential. Specifically with hybrid systems, it is prudent to utilize numerical simulation for the fuel cell components since turbomachinery is readily accessible while

fuel cells are expensive, not readily available, have a large thermal capacitance, and are susceptible to damage. Furthermore, the thermal phenomena are more readily captured by numerical simulation. However, the dynamic characteristics of the fluid mechanics, such as compressor surges, are complex and highly nonlinear; therefore, physical equipment is more effective in capturing fluid flow phenomena.

While the benefits of applying HILS to hybrid systems are apparent, there exist challenges that must be addressed. Most significant among them is designing the numerical models and utilizing sufficiently powerful computational hardware to ensure real-time numerical simulation. Moreover, in designing the HILS system, the interfacing methodology between the physical and numerical components must be developed correctly.

2.7: Hybrids HILS Research Methodology

SOFC/GT hybrid systems offer the promise of high efficiency power generation. At this time however commercialization is limited by challenges to fuel cell stacks, gas turbines and in particular, their integration into a hybrid cycle. While past research has identified and begun to address these challenges; to continue advancing SOFC/GT hybrid development, a more effective and accurate investigation platform is required. Applying HILS to a hybrid system provides a solution. This dissertation effort offers a methodology for conducting HILS of hybrid cycles and details the initial results obtained.

CHAPTER 3: METHODOLOGY

Researching SOFC/GT hybrid power generation systems through HILS entails interfacing a real-time SOFC stack computational model with operating gas turbine hardware. This dissertation is concerned with the development of a methodology for integrating a fuel cell subsystem model with the existing HyPer gas turbine facility. During a HILS, the numerical model will respond to operating turbine flow measurements to predict a SOFC stack's thermal effluent. The simulated level of heating will then dynamically control HyPer's combustor firing rate, reflecting the heating from a SOFC stack.

Described in this chapter are the elements composing the HyPer facility and the design approach to conduct HILSs of a SOFC/GT. First, a description is provided of the HyPer facility and its operation. Then, the bulk-parameter fuel cell model's formulation is outlined. This numerical model is utilized for generating the HILS experimental results presented in this dissertation. Next, the method for coupling the numerical model and the hardware simulations is detailed. Last, this chapter addresses the implementation of a high-speed computer system capable of interfacing the existing HyPer control platforms, which will accommodate the utilization of higher fidelity numerical models. The development of this approach arose from a thorough literature review, work with the HyPer facility and NETL personnel, and operational experience with the SWPC 220 kW hybrid system.

Once the numeric and hardware simulation components were integrated as described in this chapter, a set of tests representative of normal hybrid operating conditions were conducted to evaluate the performance of the HyPer HILS methodology. The results of these experimental simulations are discussed in Chapter 4.

3.1: Description of the NETL HyPer Facility

As mentioned, the physical substructure for conducting HILSs of SOFC/GT hybrid power systems is the HyPer facility located at NETL in Morgantown, WV. The HyPer facility was design as a hardware simulator emulating systems in the range of 300 kW to 900 kW (Tucker, 2005a). The project was commissioned to investigate the steady-state and dynamic operation of direct fired SOFC/GT hybrid cycles. As opposed to focusing on simulating highly efficient hybrid cycles, HyPer is devoted to developing greater understanding of the unique transient phenomena inherent to SOFC/GT hybrids and improving the operational functionality of these systems. The hardware is comprised of a modified microturbine, high performance primary surface recuperators, pressure vessels that represent the volumes and flow impedances of a fuel cell subsystem, an external natural gas combustor, and the associated integration piping. The turbomachinery is a 120 kW Garrett Series 85 consisting of a single-shaft, direct-coupled turbine; a two-stage radial compressor; and a gear-driven generator. The test facility is located inside a high bay building at NETL. Figure 3.1 is an overhead photograph of the facility showing the scale of the hardware. Additionally, Figure 3.2 focuses on the air plenum that replicates the large compressed air volume in the stack's cathode of a SOFC/GT hybrid.

Figure 3.1: HyPer Facility

Figure 3.2: Air Plenum and Heat Exchanger

3.1.1: HyPer Hardware

The HyPer facility was designed to be a versatile and accessible research platform for investigating SOFC/GT hybrids. The design is far less compact than a commercial system to accommodate instrumentation essential for system characterization and process modifications. The primary concern in designing HyPer was to incorporate an existing turbine engine with air plenums, heat exchangers, and an external combustor. The systems would have to safely withstand moderately high temperatures and pressures. A second goal in its design was to minimize the pressure losses in the primary process air flow path. With this in mind, the primary process airflow loop does not have any control or check valves. The air plenum physically simulates a SOFC's cathode volume and was sized to be on the order of a 250 kW tubular SOFC stack (Tucker, 2005a). Additionally, the natural gas combustor was designed for control by a fuel cell model to simulate the stack thermal dynamics.

3.1.1.1: System Process Flow and Components

Figure 3.3 is a computer rendering of the design with all the major components identified. It also has the primary flow loop denoted with dark outlined arrows, while the bypass flows are indicated with the light outlined arrows. A process flow diagram of the facility is shown in Figure 3.4 with the primary flow loop highlighted. The process itself begins with ambient air being drawn in down a vertical pipe by the compressor (C-100). The inlet air is from within the building bay. Compressed to a pressure ratio near 4, the air is discharged into a compressor plenum with two exit ports. The primary port is an annulus extraction T-pipe that connects the compressor to the two heat exchangers for recuperating the turbine exhaust heat. The second port is used for bypassing or bleeding

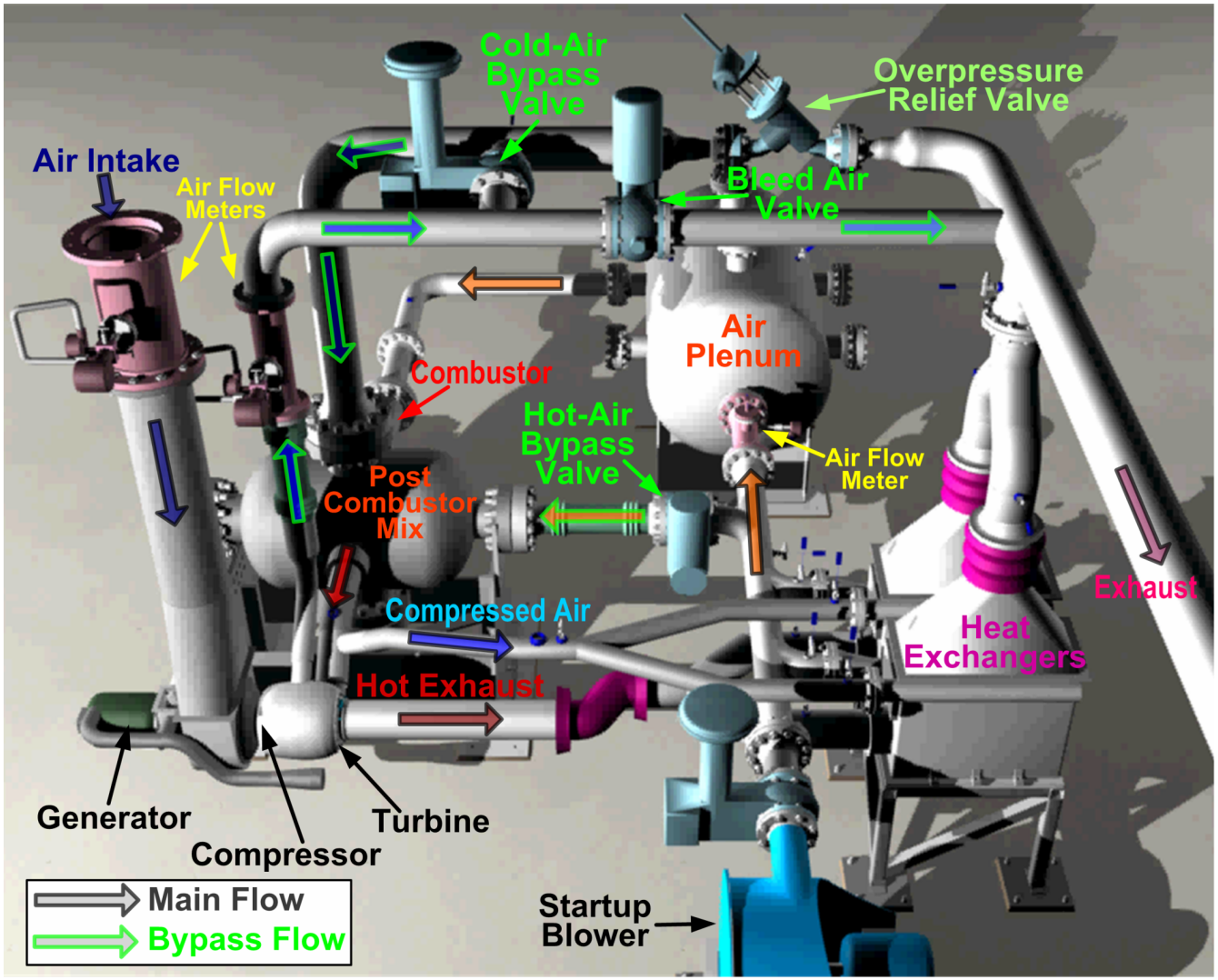

Figure 3.3: HyPer Facility Components

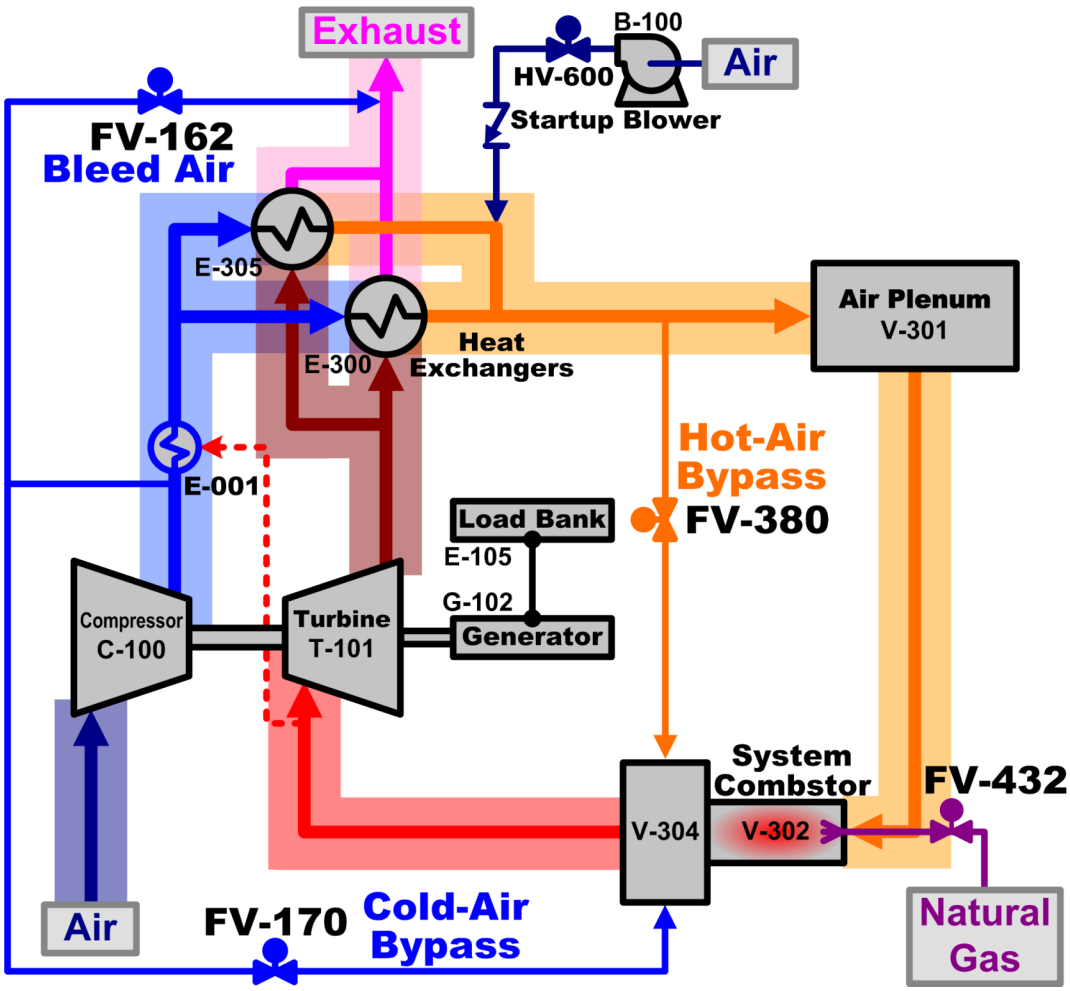

Figure 3.4: HyPer Process Flow Diagram

airflow. Leaving the compressor the main flow enters the pressurized, cold side of the heat exchangers (E-300 and E-305) where it is preheated by the hot turbine exhaust. The primary flow then passes through the air plenum (V-301), which simulates a fuel cell's cathode volume. Upon leaving the air plenum, the process airflow passes through a natural gas combustor (V-302) that supplies the thermal input to the system. The combustor fires into a second pressure vessel denoted as the post-combustor mix (V-304). The post-combustor plenum also allows for the reincorporation of the bypass flows. The energetic combustion effluent then re-enters the turbine engine via a stab pipe that routes it through the compressor discharge extraction T-pipe. It is then expanded through the turbine (T-101) producing power to drive the compressor and electrical generator. The hot turbine exhaust then passes through the hot side of the heat exchangers, where waste heat is recovered. Last, the process air is exhausted to the outside atmosphere via a muffled, vertical stack pipe.

In addition to the primary flow loop, the facility has been designed with three parallel air flow loops with control valves: a hot-air bypass (FV-380), a cold-air bypass (FV-170), and a compressor bleed (FV-162). The hot-air bypass extracts the airflow at the heat exchangers' cold-side exit and re-injects it into the post-combustor. This circumvents the air plenum and combustor. The cold-air bypass utilizes the secondary port in the compressor discharge plenum to divert a portion of the flow to the post-combustor. The bleed air also extracts air with the compressor's secondary port and directs it to the atmosphere via the exhaust stack. The system can operate with all three valves fully closed, thereby allowing no bypassed flow. While all three valves can open fully, there are operational limits that may prohibit high levels of bypassing or bleeding.

These bypasses were designed into the HyPer facility to investigate novel control methods. They promise the benefits of lowering the probability of a compressor surge and allowing for the management of the stack airflow in a SOFC/GT hybrid.

3.1.1.2: Garrett Gas Turbine

Originally developed in the 1950's by Garrett Turbine Engine Company, the GTC85 axillary power unit (APU) gas turbine was designed to provide mechanical and pneumatic power. Its typical application was on aircraft for starting larger main-propulsion turbine engines and to provide electrical power. The engine consists of three sections: a compressor, a turbine, and an accessory section that includes a electrical generator. The turbine and compressor are directly coupled on a single shaft with a nominal rotation speed of 40,500 rpm. The engine produces electrical power via a gear driven generator. This model of turbine was used by military aircraft for onboard power generation and to supply compressed air for main engine starting. It originally operated on jet fuel. For the HyPer project, the Series 85 turbine with a 120 kW electrical generator accessory was purchased on the secondary market. NETL then mounted it on an adjustable stand, removed the jet fuel combustor, and modified the engine with an extraction T-pipe for integration with the HyPer facility. The engine is shown integrated with the HyPer facility in Figure 3.5.

3.1.1.2.1: Compressor

The two-stage centrifugal compressor supplies the compressed process air for the system. In the depiction in Figure 3.6, the compressor air inlet is the rectangular item located on the top of the engine. The two-stages combine to nominally deliver about 2.0 kg/s of airflow at a pressure ratio of approximately 4. The compressor discharge

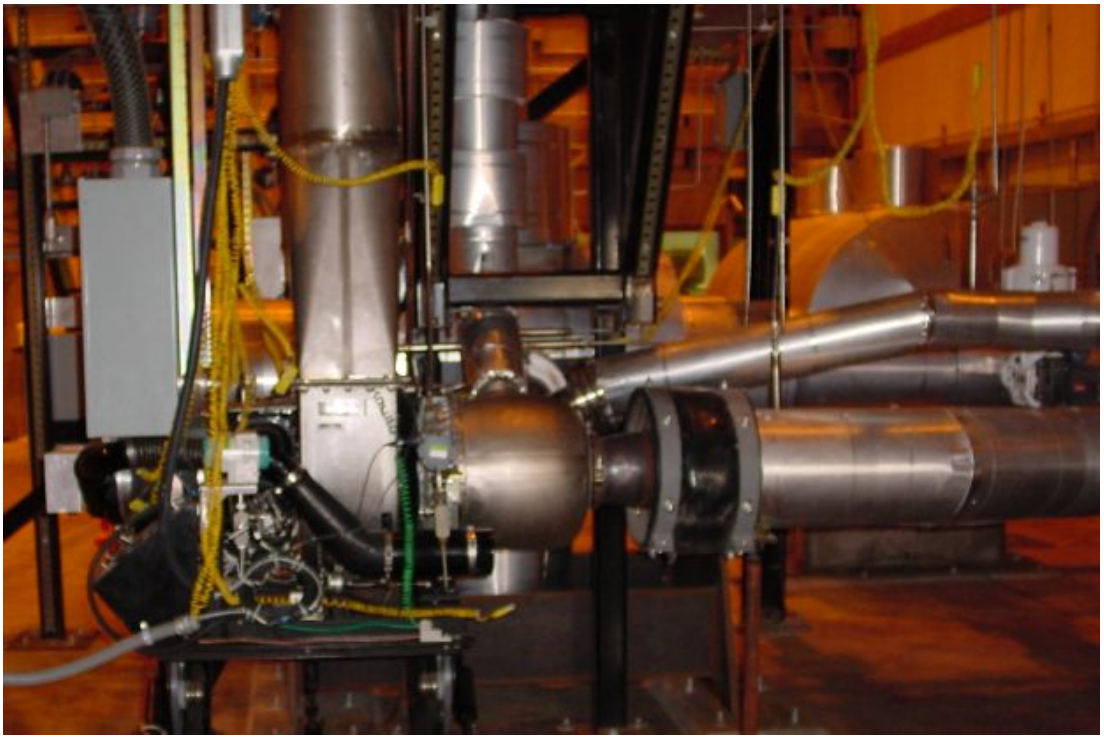

Figure 3.5: Garrett Series 85 APU Engine Installed in HyPer

temperature is typically 200 °C. The two radial outward-flow impellers are mounted on a common shaft. Item 4 in Figure 3.7 is the first stage compressor impeller and Item 7 is the second stage impeller.

The compressor discharges into a plenum assembly that encases the turbine section. There are two extraction ports for the compressed air, as shown in Figure 3.8. The primary compressor discharge flow is connected to the HyPer piping via an extraction T-pipe (E-001) that is composed of a concentric pipe that encircles the turbine inlet stab pipe. Originally, this port was the location for the engine's combustor can. The second port was designed to deliver compressed bleed air for pneumatic power. In its HyPer configuration this port feeds the system's bleed air and cold-air bypass.

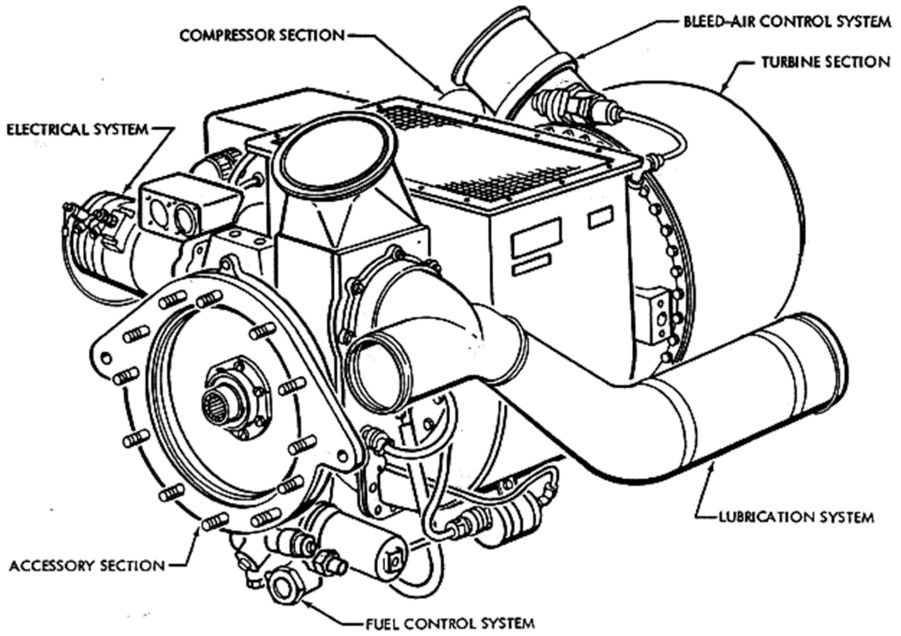

Figure 3.6: Garrett Series 85 APU (Garrett, 1982)

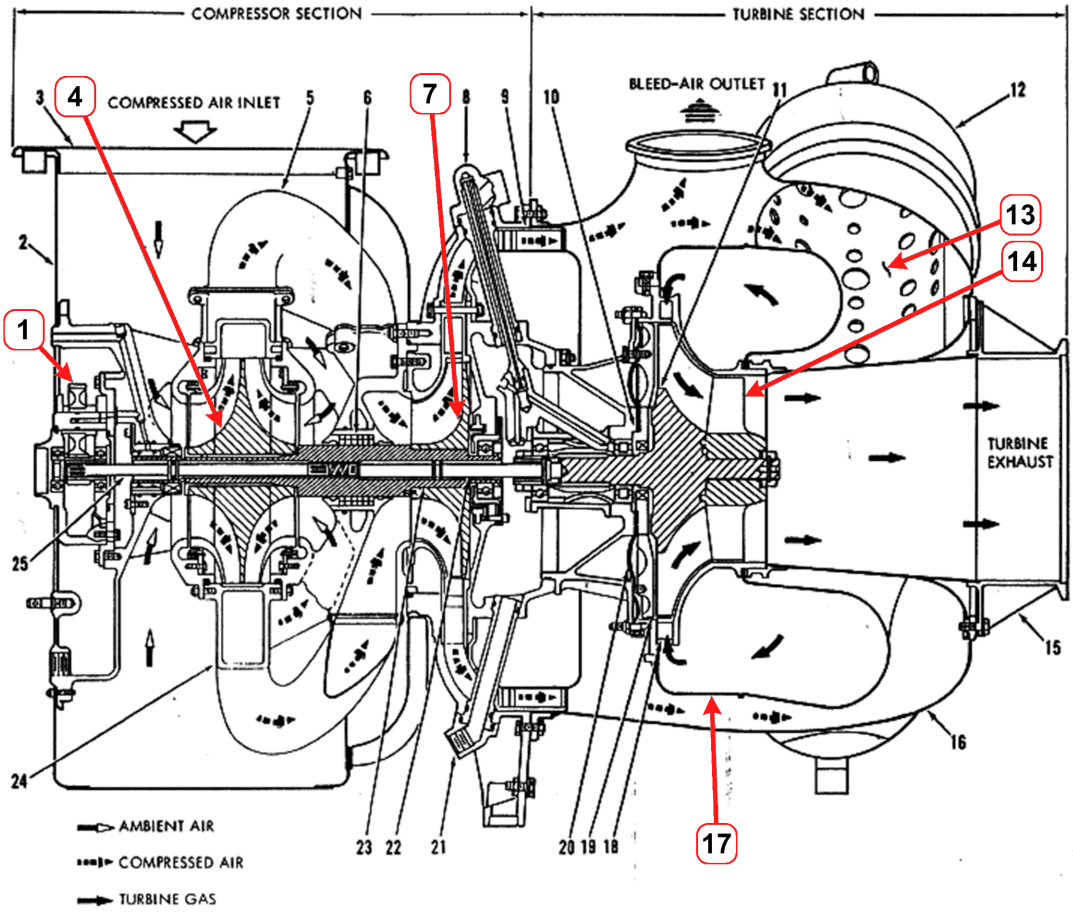

Figure 3.7: Garrett Series 85 APU Air Flow (Garrett, 1982)

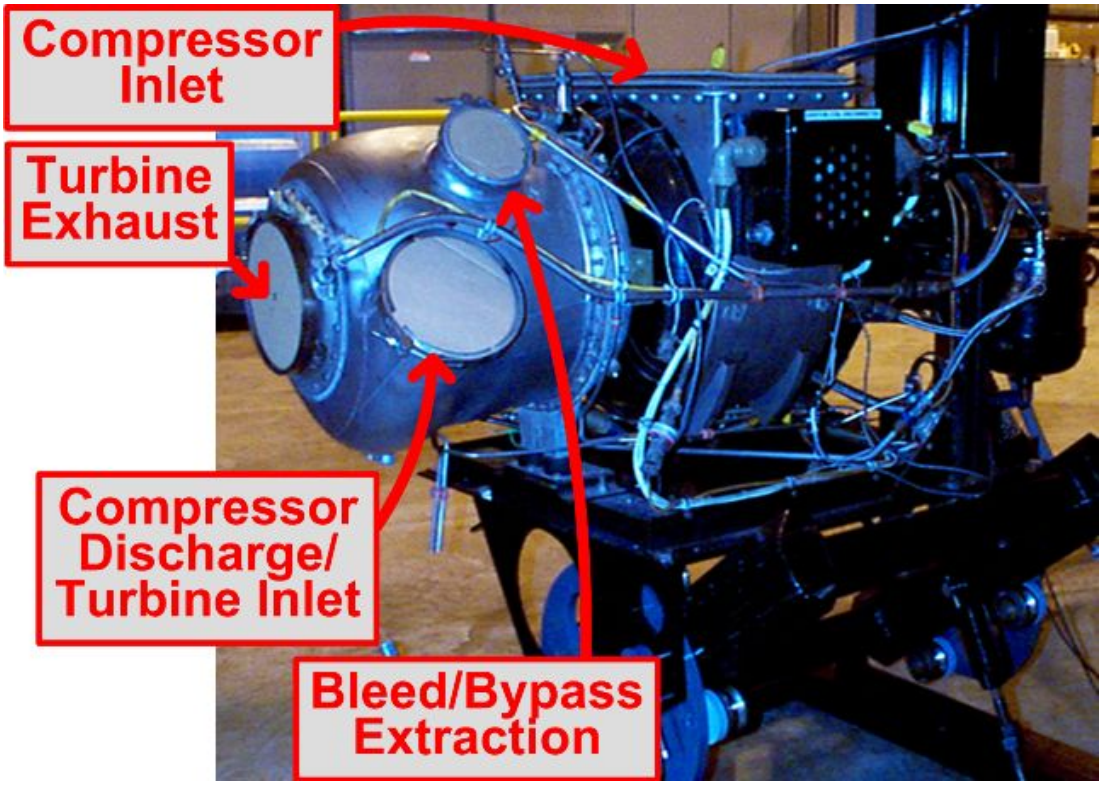

Figure 3.8: Garrett Series 85 APU Airflow Connection Ports

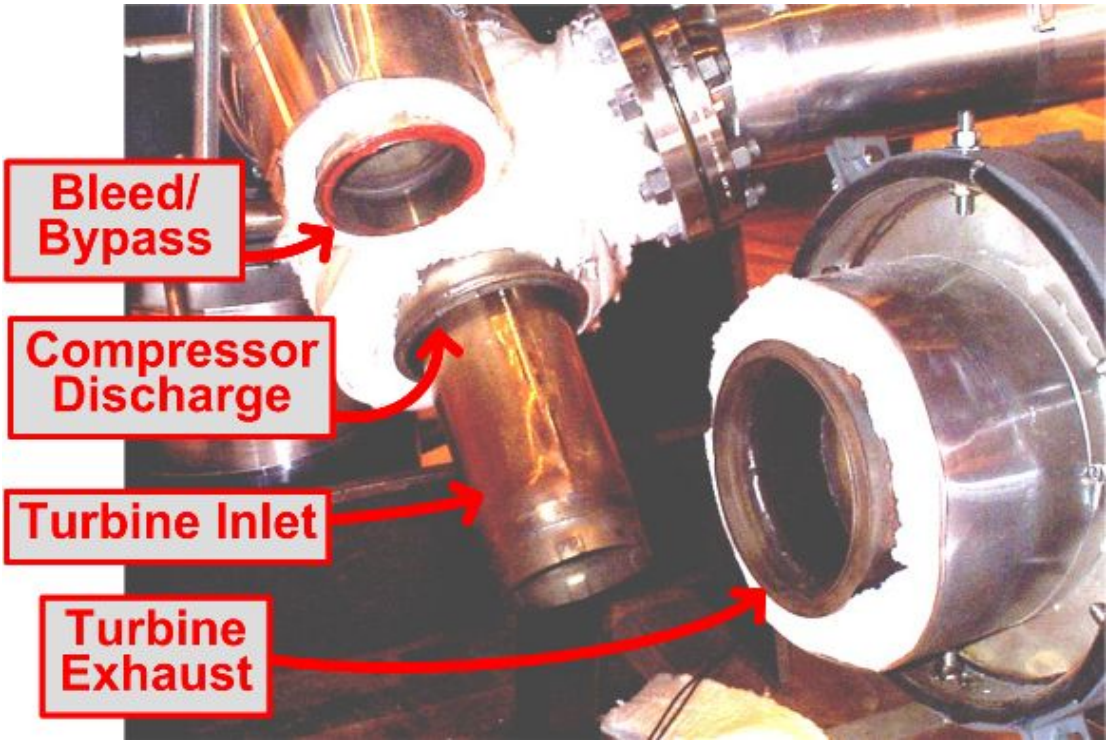

Figure 3.9: System Piping Connections to Garrett Engine

3.1.1.2.2: Turbine

The turbine section supplies power to drive the compressor and generator. Its primary component is a radial inward-flow turbine wheel, Item 14 in Figure 3.7. The wheel is directly coupled to the compressor on a common shaft so that the compressor and turbine rotate at the same speed. The compressor discharge plenum encases the turbine housing. This configuration prevents the turbine intake scroll, Item 17 in Figure 3.7, from overheating. In the original engine configuration, the turbine scroll received compressed heated air from the combustor can. In HyPer, the turbine inlet utilizes a stab pipe, that transfers the inlet air from the system's piping, through the extraction T-pipe, and to the turbine scroll. After expanding through the turbine, the process air is transferred back to the system's piping through the turbine exhaust port at the end of the engine, as shown in Figure 3.8. Important manufacturer's limitations on the turbine are the maximum rotation speed and the turbine exhaust temperature. The maximum wheel speed is 44,500 rpm. The turbine discharge air is limited to exhaust gas temperature (EGT) of 636 °C to protect the metal components.

3.1.1.2.3: Accessory Section and Electrical Generator

The accessory section powered the supporting engine hardware in the original configuration. Item 1 in Figure 3.7 is a planetary gear that is coupled to the compressor shaft. In its original design, the planetary gear drove the fuel pump, cooling fan, and oil pump. Additionally, the starter motor was coupled to the planetary gear. The fuel pump and starter motor have been removed as part of the turbine modification for the HyPer project. The oil pump, which supplies lubrication oil to the engine, and cooling fan have been retained for the current configuration. The planetary gear is also coupled to a hub

gear, which drives the output shaft. Its gearing ratio of 6.75 rotates the output shaft at 6,000 rpm clockwise when the turbine is at a nominal speed. The output shaft is connected to an AC electric generator that can produce power up to 120 kW. The generator outputs 3-phase 400 Hz electrical power at 120 volts.

3.1.1.2.4: Compressor Extraction T-Pipe and Turbine Inlet Stab Pipe

The most significant modification to the turbine for its integration into the HyPer facility was the replacement of the combustor can (Item 13 in Figure 3.7) with a connection pipe assembly (E-001) composed of a compressor discharge extraction T-pipe and turbine inlet stab pipe. The T-pipe and stab pipe assembly connects the engine to the rest of the system's piping to transfer process airflow in and out of the engine. A labeled photograph of the connection piping is shown in Figure 3.9, and a CAD drawing comparing the connection assembly with the original combustor can is shown in Figure 3.10.

The turbine was originally designed to operate on jet fuel that was injected into a combustor can that was inserted into the compressor's discharge port. The combustor can also directed the process airflow radially inward from the surrounding compressor discharge plenum into the turbine scroll, as diagrammed in Figure 3.10. Additionally, in the Series 85 engine, the turbine scroll is protected from overheating by the compressor discharge air flowing over it, an aspect of the original design that had to be retained in any modifications for the HyPer integration. Therefore, a connection pipe assembly was designed and built to extract the compressed air from the engine concentrically around the hot turbine inlet airflow. In this design, the extraction T-pipe is connected to the primary compressor discharge port and the stab pipe is inserted into the turbine scroll

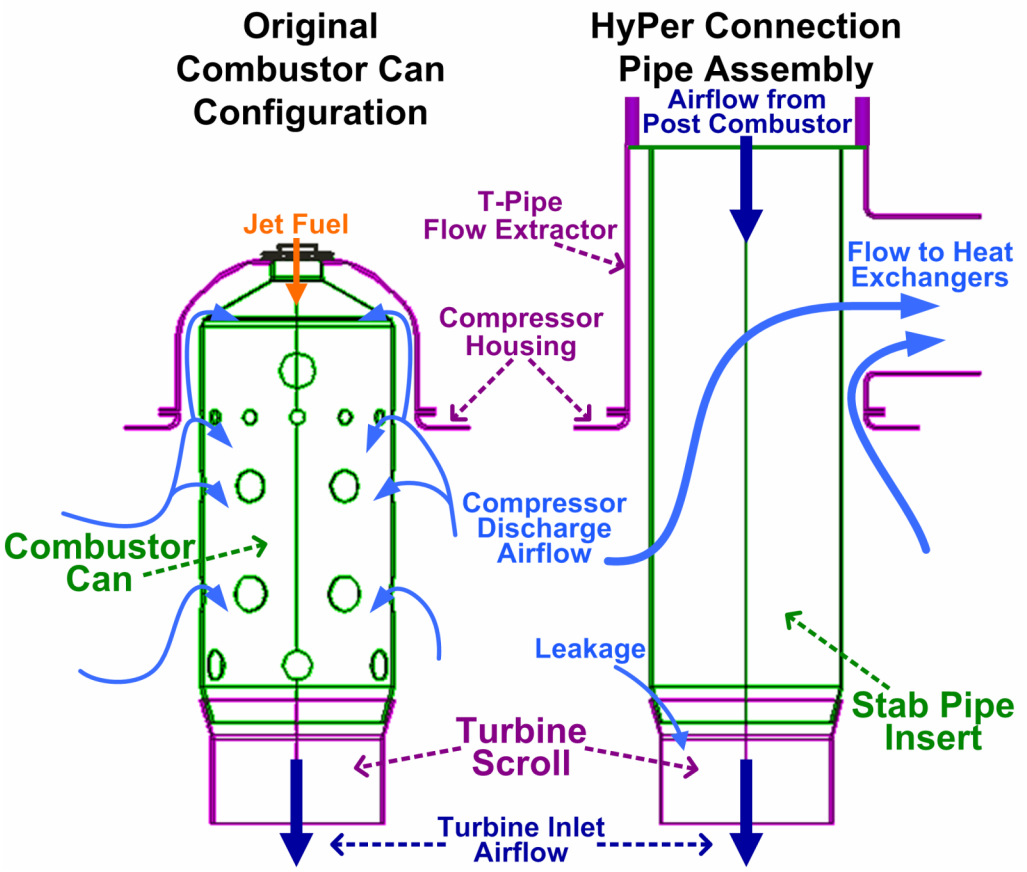

Figure 3.10: Compressor Air Modification

inlet. As diagrammed in Figure 3.10, the T-pipe extracts compressed air from the compressor plenum in the annulus around the stab pipe, and the turbine inlet stab pipe directs hot gases from the post combustor mix (V-304) into the turbine scroll. Then with the removal of the combustor can, as well as the original fuel system, the engine can be joined to rest of HyPer piping by the connection assembly.

While the connection assembly allows for the integration of the engine with external piping, it does give rise to factors that reduce system performance. In order to facilitate assembly, the stab pipe is just pressed into the receiving socket on the turbine scroll. This results in a loose fitting connection between the stab pipe and the turbine

scroll. During operation, this allows air to flow directly from the high pressure compressor discharge to the turbine, short-circuiting the rest of the system. This process air leakage is shown on Figure 3.10. The estimate is that the stab pipe leakage flow is between 10 to 20 % of the compressor discharge flow on a mass basis. While the short-circuited flow is not available to the rest of the system, its compression by the compressor still consumes turbine work output. Additionally, since the assembly is essentially a counter-flow, concentric heat exchanger, there is heat transfered from the turbine inlet air to the compressor discharge. The heat and flow transfers both lower the turbine inlet temperature, thereby lowering the turbine performance. The magnitude of temperature drop is unknown since the air temperature at the turbine scroll cannot be measured due to the design of the engine, but it is estimated to be approximately 100 °C. However, the stab pipe leakage does lower the overall pressure loss between the compressor discharge and the turbine inlet, which may aid system performance, especially during startup.

3.1.1.3: Recuperating Heat Exchangers

Two heat exchangers, denoted by E-300 and E-305 in Figure 3.4, are used to recuperate heat from the turbine exhaust and impart it to the compressor discharge air. The two counter-flow heat exchangers are primary surface recuperators (PSR33) manufactured by Solar Turbine. The two exchangers are connected in parallel to accommodate the full range of compressor flow. During operation the heat exchangers usually take about 10 minutes to reach a new steady condition after a transient.

The primary heat transfer surfaces are made from 300 series stainless steel. At the pressurized cold-side inlet, the air maximum temperature is 540 °C and the maximum pressure is 480 kPaa (absolute). On the hot side, which receives the expanded turbine

exhaust the maximum inlet air temperature is 620 °C and the maximum pressure is 108 kPaa. The manufacturer's effectiveness is 89 % and the flow pressure losses are 2.5 % and 3 % on the cold and hot sides, respectively.

3.1.1.4: System Pressure Vessels and Piping

Pressure vessels and associated process air piping are used to provide the physical simulation of representative fuel cell air components. During the operation of HyPer, the vessels handle hot airflow and are pressurized to approximately 350 kPaa. The air plenum (V-301) simulates the cathode flow volume and associated manifolding of a solid oxide fuel cell. The post-combustion vessel (V-304) provides for the volume used to combust the anode-off gas in a SOFC stack. The system's piping transfers the process airflow through the primary flow loop and the bypasses. The vessels and piping primarily represent the flow impedance that would exist in a fuel cell stack of a hybrid system. Additionally, the volumes physically replicate the residence time of pressure transients associated with the compressed air volume of a hybrid system. The vessels were designed to facilitate changes in the volumes to accommodate other fuel cell designs.

For the primary process airflow and the three bypasses, the pipes have a 15.2 cm diameter and are covered with 5 cm of microtherm insulation. The pipes are A312-TP316 stainless steel that is sized according to ASME/ANSI Schedule 40S for 6 inch (15.2 cm) diameter piping. Included at critical points in the piping are expansion joints that allow for thermal expansion as the piping and vessel warm during operation.

3.1.1.4.1: Air Plenum

The air plenum (V-301) represents the cathode volume of a fuel cell stack. It is located between the recuperators and combustor in the main process air flow. The

volume of the air plenum is 1,974 L (approximately 2 m^3). The air plenum was sized to be on the order of cathode volume for a 250 kW tubular SOFC stack. The plenum is cylindrical in shape with the inlet airflow entering axially and the outlet airflow exiting radially. The walls of the plenum are made from stainless steel and are covered in microtherm insulation. The maximum operating temperature of the inlet airflow is 427 °C and the pressure is limited to 385 kPaa.

3.1.1.4.2: Post Combustor Mix

The post combustor is located between the system's combustor and the turbine inlet. It is located such that the natural gas combustor fires directly into the side of the cylindrical vessel radially. The hot gas exits directly across the vessel on its way to the turbine. The vessel also allows for the reincorporation of the hot-air bypass and cold-air bypass flows. The hot-air bypass flow enters along the cylinder's axis on a side, and the cold-air bypass enters the vessel's top radially. The cold volume of the post combustor (V-304) is 780 L (0.78m^3) and is increased to 790 L under maximum operating temperature. The vessel is fabricated from 2.54 cm Incaloy 800AT, and is designed to operate at temperatures as high as 927 ºC at a pressure of 385 kPaa. The thick metal walls of the post combustor add a large thermal capacitance to the system. Since it is located just before the turbine inlet, the absorption or release of heat from this vessel's wall will have a noticeable effect on the turbine inlet air temperature. During operation the post combustor metal temperature takes on the order of an hour to come to a steady thermal condition after a transient.

3.1.1.5: Combustor

During operation of the HyPer system, a natural gas diffusion flame burner (V-302) is used to provide the thermal energy to drive the turbine. When conducting a HILS, the combustor's firing level is controlled by a real-time fuel cell model to simulate the thermal characteristics of the effluent from a SOFC stack subsystem. The combustor is situated in a 19.4 cm inside diameter schedule 80 Incaloy 800AT pipe welded directly to the inlet nozzle of the post combustor. The process air-cooled combustor can was designed specifically for natural gas fuel and for the airflow rates expected from the air plenum. The volume of the combustor is 22 L. A plasma igniter is used to light the flame during the startup of the system.

3.1.1.5.1: Fuel Control Valve

The fuel flow, and therefore the thermal output of the combustor, is manipulated by a high-speed electromechanical control valve (FV 432). The valve is manufactured by the Woodward Governor Company and is designated as the Woodward Swift Gas Metering System. It is designed to give accurate, fast and reliable fuel flow metering for turbine engines up to 2 MW in size. The Swift valve consists of a sonic flow metering section and a contoured valve needle which is positioned by a stepper motor capable of implementing fast natural gas flow changes. The sonic valve provides choked flow conditions so that the fuel flow rate is independent of the downstream pressure. This allows for precise gas flow metering without an additional flow meter. The valve is designed to maintain choked flow for outlet to inlet pressure ratios up to 0.85. This pressure ratio is typically less than 0.5 in HyPer. For a 90 % to 10 % open actuation the valve has a slew rate of 150 ms. A Woodward AtlasPC control system, described in

Section 3.1.3.3, is used to set the position of the Swift valve needle at an update rate of 5 ms. During normal operation of HyPer, the valve demand is set by a feedback control algorithm to target the turbine rotational speed setpoint. In HyPer the natural gas is supplied to the Swift valve by a 2.54 cm fuel line at 650 kPag.

3.1.1.6: Bypass Valves

To minimize pressure losses through the system, no valving was placed in the main pressure loop between the compressor and the turbine. However, flow control is critical in the management of cathode airflow rate in fuel cell stacks and the avoidance of compressor surge in turbomachinery. Therefore, HyPer was designed with three valved bypasses to test novel control methods in SOFC/GT hybrids. This allows the effectiveness of airflow bypasses to be evaluated. As mentioned, in HyPer three bypasses are designated as bleed air, cold-air bypass, and hot-air bypass. The locations of the three valves are indicated in Figure 3.3. The system can operate with all valves fully closed, allowing no level of bypassed flow. The characterization of the three bypass valves with a 45 kW electrical turbine loading applied was presented in Tucker (2006a). This article presented the percentage of the compressor flow that was bypassed by each valve separately as a function of the valve's position.

3.1.1.6.1: Bleed Air

Compressor discharge air is diverted directly to the system exhaust using the bleed-air bypass valve (FV-162), as highlighted in Figure 3.11. The bleed air is extracted from the compressor discharge plenum through the secondary port in the plenum housing. Bleeding compressed air to the atmosphere is effective in increasing the mass flow through the compressor without raising the pressure ratio. It has traditionally been

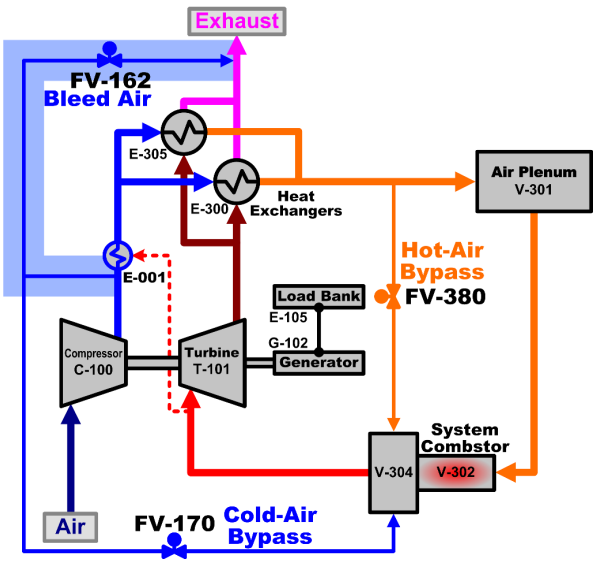

Figure 3.11: Bleed Air Flow Path

used by turbine designers as a surge avoidance measure. Compressor bleed provides an additional source of load to the turbine, while maintaining the mass flow through the turbine, the fuel cell simulator and the heat exchangers.

The bleed-air valve, a Valtek ShearStream, is a segmented ball control valve. It has a 15.4 cm inside diameter and has a full range slew rate of about 1.5 s. The valve is actuated by onsite compressed plant air. The associated piping has a 15.2 cm diameter. In HyPer, at a valve position of 15 % open the maximum bleed level is reached, which corresponds to approximately 8% of the compressor flow. This level is determined by the turbine exhaust gas temperature limit. Since a high level of bleed air loads the turbine, the turbine inlet temperature must increase, thereby overheating the equipment. The valve is set to fail open in case of the loss of plant air or site power, and its stem position (0-100 % closed) is indicated by the ZC-162 tag.

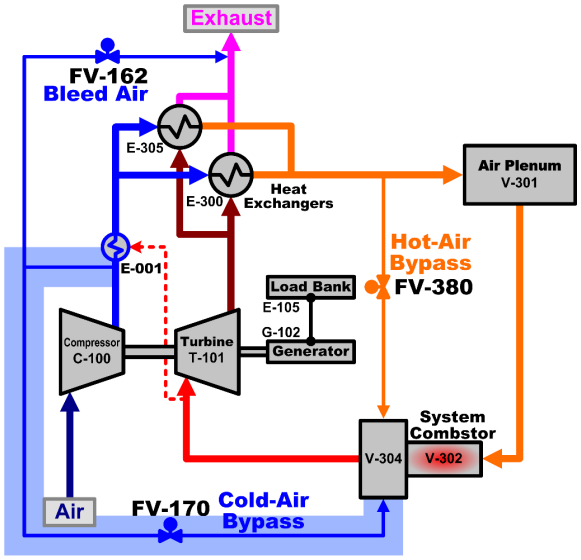

Figure 3.12: Cold-Air Bypass Flow Path

3.1.1.6.2: Cold-Air Bypass

The use of the cold-air bypass valve (FV-170) allows compressor discharge to be directed into the turbine inlet, bypassing the heat exchangers, air plenum and combustor. The flow path is indicated in Figure 3.12. It shares piping with the bleed air to extract the air from the compressor plenum, but the two flows separate at the valving located above the engine. FV-170 is a Fisher V150 Vee-Ball control valve. Like FV-162, it is also air actuated and has a 15.4 cm inside diameter valve with a similar full range slew rate. During operation, the bypass valve can be fully opened, diverting 68 % of the compressor's discharge flow. It is set to fail closed and the indicated position is given by tag ZC-170 (0-100 % open).

3.1.1.6.3: Hot-Air Bypass

The hot-air bypass valve (FV-380) is used to bypass air around the air plenum and system combustor. In a hybrid system, the use of a hot-air bypass is expected to control the air flow to the stack while reducing the impact to the turbomachinery. As

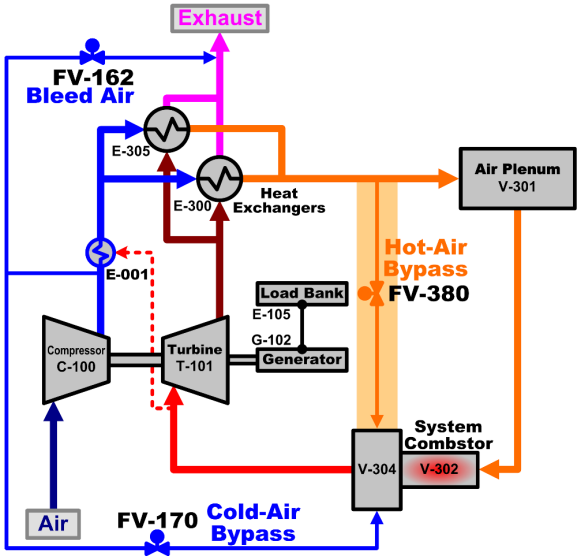

Figure 3.13: Hot-Air Bypass Flow Path

indicated in Figure 3.13, heated airflow is extracted after the cold-side exit of the recuperators and diverted to the post combustor. This air-actuated valve is a 15.4 cm inside diameter Valteck MaxFlo 3 eccentric rotary plug control valve. The valve is designed for pressure operation at temperatures in excess of 400ºC, and has a full range slew rate of about 2 s. Its associated piping has a 15.2 cm diameter. In HyPer, when FV-380 is fully open, 54 % compressor discharge flow is diverted. It is set to fail closed, and the indicated position tag is ZC-380 (0-100 % open).

3.1.1.7: Electrical Load Bank

With the turbine's AC generator the HyPer system produces up to 120 kW of electrical power that must be dissipated. Transferring the power to the electrical grid is not suitable for this experimental setting, so a variable load resistor bank is employed to dissipate the power. The resistor bank converts the electricity to heat that is then exhausted to the environment, with the aid of a cooling fan. The AC generator is regulated to 120 V, so the generator's power output is dictated by the amperage. To

control the power from the generator, the level of resistance is adjusted to pull the desired amperage, and therefore power, from the generator.

The original load bank used with HyPer had a dissipative capacity of 75 kW, adjustable in 15 kW steps. This load bank has been replaced with a new unit having 96 kW of resistive dissipation (real power) that is continuously variable. Additionally, the new load bank has reactive loading that can be used with the resistor bank to dissipate up to 120 kW of apparent power. With the installation of the continuously variable load bank, turbine rotational speed control via feedback to the electrical loading was implemented. This allows for constant speed operation during HILS, where the combustor is being controlled by the fuel cell model.

3.1.1.8: Startup Blower

In its original configuration the turbine engine had an electric starter motor to spin up the turbine. For integration into the HyPer system, this starter motor was removed. Instead, an external blower (B-100) is used to spin up the turbine. Furthermore, the blower is used to purge the system before startup to ensure that any residual combustible gas is removed from the system. The blower injects airflow into the system air piping after the recuperator's cold-side exit. The blower is isolated from the system during operation by closing a block valve (HV-600) and a check valve prevents backwards flow from the system to the blower.

3.1.1.9: Rupture Pin Valve

To ensure safe operation of HyPer, a rupture pin valve is used to prevent over pressurization of the piping and vessels. The overpressure release valve and associated piping, shared with the cold-bypass, will release pressurized process air from the system

through the post combustor vessel and to the exhaust stack pipe. The critical component of this valve is the rupture pin that will fail at a specified compression load and allow the valve to open. In HyPer, this pin is specified to fail at a system pressure of 365 kPag. The valve may also be triggered open via an electrical signal or will fail open due to loss of site electrical power. Additionally, the release valve will be electronically triggered to vent the system if a turbine overspeed is sensed, where its rotational speed increases beyond 44,550 rpm (110 % nominal speed).

3.1.1.10: Site Support

There are several onsite supporting items, such as fuel and compressed air, that support the operation of the HyPer facility. First, the HyPer equipment is housed in a high bay building that is climate controlled. This aids in maintaining more uniform ambient conditions for conducting HyPer tests. The building also provides a separated control room that protects the operators from the high noise levels generated by the turbine engine. The building also has a muffled, vertical stack pipe that rises above the building's roof to exhaust the turbine's effluent. In the building's bay there are also combustible gas sensors to warn against the the accumulation of such gases.

3.1.1.10.1: Natural Gas Supply

The combustor's fuel is supplied to HyPer by the building's natural gas header at a pressure of 2,500 kPag. A natural gas compressor on the NETL campus is used to pressurize the fuel. It is supplied to the compressor by a mix of pipeline gas and an onsite well. This will lead to variability in the heating value of the fuel combusted in HyPer. Tracking of the natural gas fuel has shown that it may range from 800 to 900 kJ/mol in lower heating value. The fuel is then regulated down to 650 kPag before it

is metered by the Swift fuel valve. Additionally, HV-408 and HV-430 are motored ball valves that are used by the control system to automatically isolate the fuel supply from the combustor when there is no flame present.

3.1.1.10.2: Plant Air

The building's plant air is supplied to the HyPer at 690 kPag. This compressed air is use to actuate the bypass valves. It also serves to cool the UV flame detector and plasma igniter used in the system's combustor.

3.1.2: Instrumentation and Operating Parameters

The HyPer facility has over 100 process variables measured and recorded at varying rates. The bulk of the variables are temperatures and pressures measured throughout the system. Other important parameters are airflow rates, fuel flow rate, and turbine rotational speed. The various measurement devices are connected to one or more of the HyPer control platforms, described in Section 3.1.3, for data acquisition during HyPer testing. The sample rate of the recorded data is determined by the control platform. The majority of the instrumentation is connected to the APACS platform with a 0.4 s sample rate.

This section describes the sensors used to collect measured data that are relevant to HyPer's HILS testing. The process flow diagram in Figure 3.14 identifies the location of the various measurements. In HyPer, all instruments are identified by letter and numerical tags. In the diagram, TE denotes a thermocouple, PT is a pressure transducer, FE is a flow element, ST is used for rotational speed measurement, and JI is for electrical power. Appendix B discusses error associated with the airflow and air temperature measurements.

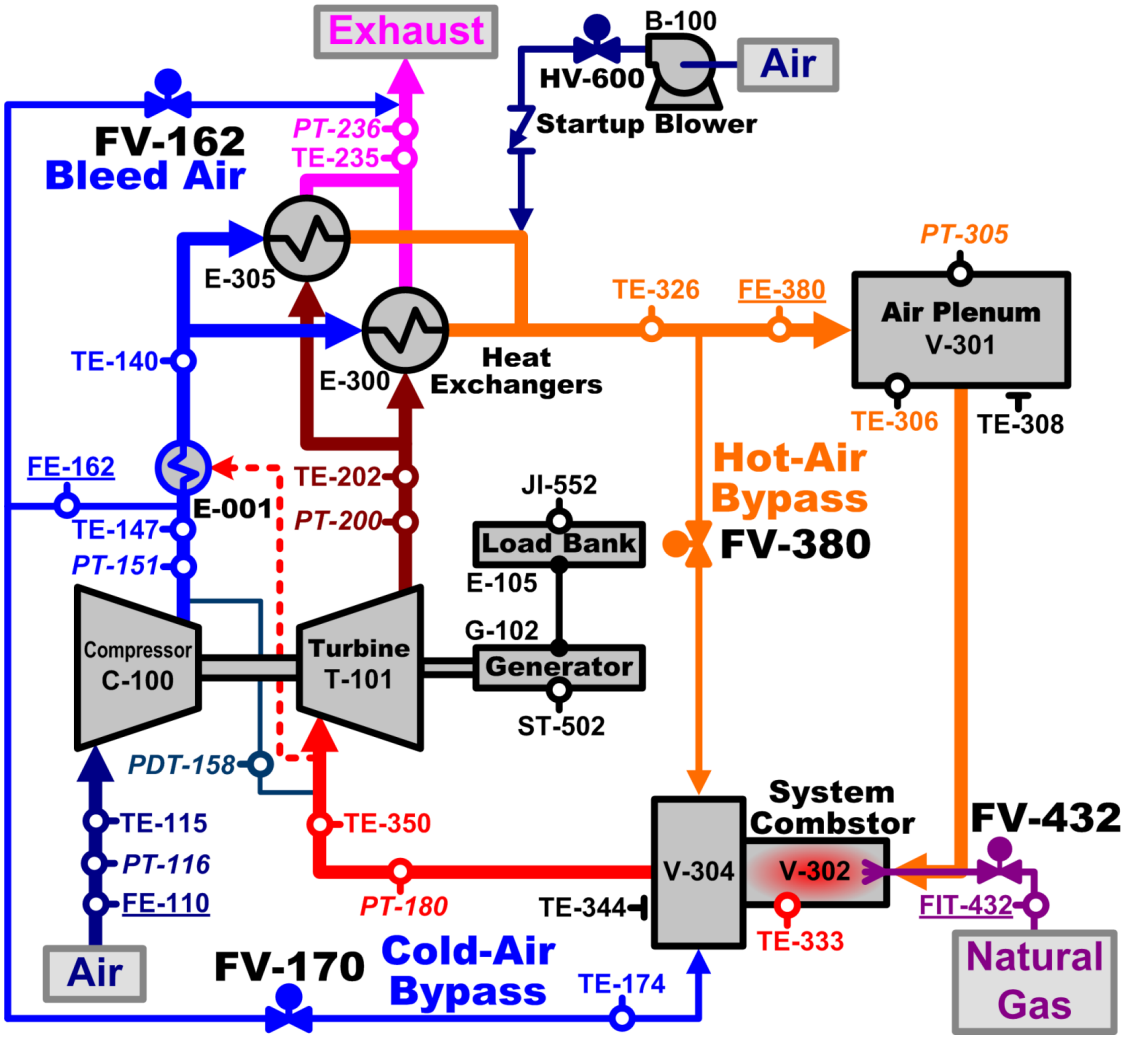

Figure 3.14: HyPer Instrumentation

3.1.2.1: Air Flow Measurement

The mass flow rate of the process air is a critical parameter to the performance of turbomachinery, fuel cells and hybrids. In HyPer, airflow is measured at three locations: the compressor inlet (FE-110), the secondary compressor discharge port for bypass flow (FE-162), and at the inlet to the air plenum (FE-380).

3.1.2.1.1: Compressor Inlet Mass Flow

Compressor inlet airflow is measured using a Dieterich Standard Mass ProBar annubar flow element (FE-110). It dynamically calculates the compensated mass flow by measuring the static pressure, temperature, and the differential between the stagnation and static pressures. The sensor is inserted into the flow through a single pipe penetration. As seen in Figure 3.3, in HyPer the inlet air is measured as it flows down to the compressor. The inlet pipe has a 30.5 cm inner diameter. Also, to ensure fully developed flow, the inlet pipe extends 3.1 m upstream and 2.4 m downstream of FE-110. It is scaled to measure flows of 0-3 kg/s, and typical compressor inlet airflow during operation is 1.8 kg/s.

3.1.2.1.2: Bypass Mass Flow

Compressor bleed or cold-air bypass airflow is measured using an annubar flow meter (FE-162) similar to FE-110. It is situated in a 15.2 cm inside diameter pipe that leads from the secondary compressor discharge port up to the the bleed and cold-air bypass valves. Since it measures the flow upstream to the valves, the level of each bypass cannot be distinguished if both the bleed and the cold-air valves are open at the same time. FE-162 is scaled to measure flows of 0-1.5 kg/s

3.1.2.1.3: Plenum Mass Flow

Inlet air mass flow to the air plenum is measured using an annubar flow meter (FE-380) similar to FE-110. It is located after the extraction point for the hot-air bypass flow. The pipe to this meter has a 15.2 cm inner diameter, and the meter empties directly into the pressure vessel. For a system startup, before the ignition of the combustor, positive flow must be measured by FE-380 for several seconds to ensure the system is purged of any combustible gas. During a HILS, this mass flow is used in the fuel cell numerical simulation. It is scaled to measure flows of 0-3 kg/s.

3.1.2.2: System Temperatures and Pressures

Temperatures and pressures are measured throughout the process flow to capture the thermodynamic conditions in the system. Type K thermocouples are inserted into the airflow to measure temperatures. For pressure measurements, impulse lines (6.35 mm stainless steel tubes) are used to transfer the static pressure to electronic pressure transducers mounted throughout the system. The location, tag labels and typical operating values of several measurement points are described below.

3.1.2.2.1: Ambient Conditions

The ambient conditions in the high-bay building are recorded so that their affect on the system's performance can be monitored. The temperature is tagged as TE-005 and is typically 25 °C, since the high-bay room is climate controlled. The ambient absolute pressure of the facility bay is measured using PT-003. Typically, it is slightly below 101.3 kPaa (absolute) or atmospheric pressure. PT-003 is also used to convert the gauge pressures measured in the system to absolute pressures for thermodynamic calculations.

3.1.2.2.2: Compressor Inlet Conditions

The compressor's inlet pressure and temperature have an affect on its performance. TE-115 measures the temperature at the inlet of the compressor scroll. An additional compressor inlet temperature reading is TE-112, which is integral to the FE-110 flow meter. The inlet compressor pressure is identified by PT-116 and is scaled from 40-120 kPaa.

3.1.2.2.3: Compressor Discharge Conditions

The compressor outlet temperature is measured using TE-147. The heat of compression typically raises this temperature to 200 °C during operation. The compressor discharge pressure is captured by PT-151. It is scaled to 0-400 kPag (gauge) and is typically 250 kPag when operating. This corresponds to a compressor pressure ratio of 3.5.

3.1.2.2.4: Recuperator Cold-Side Inlet Conditions

The temperature of the airflow before it enters the two heat exchangers is given by TE-140. This temperature is typically 30°C warmer than TE-147. It gives an indication to the level of heat imparted to the compressor outlet flow as it passes over the turbine inlet stab pipe.

3.1.2.2.5: Air Plenum Conditions

The process air conditions entering HyPer's air plenum correspond with those entering a fuel cell stack in an actual hybrid system. Therefore, when conducting a HILS the airflow conditions here are monitored closely. The inlet airflow is measured by TE-326. A normal operating temperature here is 400 °C, but can vary significantly depending on operating conditions. PT-305 is the plenum air pressure measurement, and

is scaled to 0-400 kPag. It is typically 20 kPag less than PT-151, which is due to the flow's pressure loss as it passes through the recuperators. During HILS TE-326 and PT-305 are used in the fuel cell numerical simulation. Additionally, the temperature of the vessel's metal wall is measured by TE-308.

3.1.2.2.6: Combustor Exit Temperatures

The thermocouple TE-333 is located at the entrance to the post combustor mix, close to the combustion flame. This air temperature reading is unreliable, since the combustor effluent has not mixed fully. A more important temperature reading is the post combustor skin temperature, TE-344. The large thermal capacitance of the metal vessel's walls leads to a slow thermal response. Therefore, TE-344 is monitored to establish when a near steady-state operation has been achieved during HyPer testing. A typical reading for the post combustor skin is 700 °C but the temperature can range between 500-800 °C during heated operation.

3.1.2.2.7: Turbine Inlet Conditions

The turbine inlet temperature, measured by TE-350, is taken before the stab pipe leakage and heat exchange. Turbine inlet pressure is measured with PT-180 and is scaled to 0-400 kPag. Typical turbine inlet conditions are 700 °C and 210 kPag.

3.1.2.2.8: Turbine Exhaust Conditions

TE-202 measures the turbine exhaust gas temperature (EGT) and typically ranges from 450-500 °C. The original APU control system incorporated a turbine EGT limit to protect the engine materials from overheating. The EGT limiting strategy has been transfered to HyPer and is set at 590 ºC. If this limit is reached the fuel demand is

reduced until TE-202 returns below the EGT limit. PT-200 is turbine exit pressure, which is normally about 10 kPag, and the instrument is scaled to 0-20 kPag.

3.1.2.2.9: Recuperator Hot-Side Exit Conditions

The process air conditions of the rucuperator's hot-side exhaust are captured by TE-235 and PT-236. This airflow is normally exhausted to the atmosphere at 300 °C.

3.1.2.2.10: Compressor to Turbine Differential Pressures

An additional pressure reading of significance is the differential pressure between the compressor discharge and the turbine inlet. This differential represents the flow pressure loss in the compressed portion of the HyPer system. It is measured by PDT-158, which is scaled to 0-70 kPad (differential). This reading ranges from 10-50 kPad, depending on the level of bypassed flow being utilized, which corresponds to 4-14 % of the compressor discharge pressure.

3.1.2.3: Natural Gas Fuel Conditions

To ensure the Swift valve is supplying natural gas at the desired rate a Coriolis mass flow meter is used. The fuel mass flow meter is tagged as FIT-432. Typical fuel flow measurements for HyPer are in the range of 10 g/s to 20 g/s, depending on the load placed on the turbine. Additionally, the fuel flow conditions at the inlet to the Swift valve are measured by TE-422 for temperature and PT-436 for pressure.

3.1.2.4: Turbine Rotational Speed

Rotational speed is measured by an optical sensor (ST-502) which picks up laser light reflected from a rotating target on the end of the generator shaft and transmits the pulse train to a frequency input of the control system. The optical sensor provides a

1,200 Hz signal at the nominal 40,500 rpm turbine speed. The dynamic range of the speed variable is 1,000 to 50,000 rpm.

3.1.2.5: Flame Indicator

An ultraviolet sensor (BE-405) is used to detect the natural gas flame. If the flame should extinguish during operation, the control system will automatically close HV-408 and HV-430 to stop the natural gas flow. Plant air is used to cool the detector when the combustor is firing.

3.1.2.6: Electrical Power

Electrical power produced by the AC generator is tagged as JI-552. It is calculated from the measured voltages and currents on all three phases of the generated power. The generator can produce between 0-120 kW.

3.1.3: Control Platforms

The HyPer facility combines multiple controllers with varying degrees of flexibility to create a control system that is functional for the experimental setting and that is safe. The focus on flexibility in designing the control system has been essential toward testing novel hybrid control strategies. Initially, the facility was supported by three controllers: QUADLOG, APACS , and AtlasPC. The QUADLAG controller maintains the safety interlocks that ensure the avoidance of potentially hazardous conditions. The APACS platform implements the standard device controls and the operational interlocks that guard the equipment integrity. The AtlasPC controller handles the fuel supply Swift valve and is used for implementing novel control investigations. To

expand the computational power of HyPer's controls, a dSPACE system was added as a fourth platform, as part of this dissertation work and will be described in Section 3.4.

3.1.3.1: QUADLOG

A QUADLOG system is the supervisory safety controller for HyPer. This programmable logic controller was manufactured by Siemens Moore Process Automation and was designed specifically for critical applications, such as emergency shutdown systems. In HyPer it provides protection for system equipment through a series of safety interlocks. For example, it insures that the appropriate system purge is completed during startup by monitoring positive flow on FE-380 for 10 seconds. Once this requirement is satisfied, the QUADLOG issues a permissive command to allow natural gas fuel flow and combustor ignition. During operation, QUADLAG monitors the ultraviolet flame detector for loss of flame and will shut off fuel flow if detected. Additionally, this platform monitors for a turbine over speed. If observed, it releases the rupture pin valve to vent the turbine inlet gases to the stack pipe.

3.1.3.2: APACS

An APACS platform, also manufactured by Siemens Moore Process Automation, serves as the main process controller and data acquisition platform for HyPer. APACS's architecture is based on modularity to allow for easy expansion of the system. It is built with control modules for executing programmed logic, input/output modules for interfacing with field signals and controlled devices, and communications modules networking with other computers.

For HyPer, the APACS system handles the majority of process controls and operator commands, such as setting the position of the bypass valves and electrical

Figure 3.15: HyPer Control Room

dissipater load. It communicates with a host PC, which runs a graphical user interface tailored for HyPer. The graphical interface continuously updates and presents process conditions. It also handles operator initiated commands, such as adjusting a bypass valve position. APACS is also responsible for monitoring the operational interlocks that are used to protect the equipment. These interlocks are set by the equipment's operating envelope. Figure 3.15 is a photo of the HyPer control room showing the APACS host PC running the graphical user interface.

Furthermore, the APACS system acquires and stores the bulk of the process variables for HyPer. The data is continuously recored at a sample rate of 0.4 s. A Windows based PC acts as the user interface with the APACS system. Thia allows the

operator to graphically monitor the HyPer process variable and issue commands during operation. After operation the computer is used to retrieve the acquired data.

3.1.3.3: AtlasPC

Manufactured by the Woodward Governor Company, the AtlasPC is designed primarily to serve as a basic fuel controller for turbine engines, as it does in the HyPer facility. The AtlasPC is built around a modest 266MHz Pentium CPU with 64MB RAM. It also has an onboard analog input/output module and network communication cards. Essential to its function of providing system control is the real-time VxWorks operating system. This operating system ensures deterministic update times of the controller outputs at a high rate, up to 20 Hz (5 ms).

The AtlasPC also makes use of Woodward's Graphical Application Program (GAP) to interface with engineering personnel on a host computer. The GAP is a picture-to-code programming tool that utilizes function blocks to express the control algorithm. Each function block performs a specific task at a set update rate. The GAP program has the capability to include MATLAB/Simulink models that have been compiled with Real-Time Workshop. With the inclusion of Simulink code, the GAP environment allows for the creation of powerful and flexible control programs. This permits the testing of novel control approaches and accommodates the fuel cell numerical models for the HILS approach on HyPer.

The AtlasPC records process variables into a data log into a onboard memory buffer. The log buffers data for approximately 30 minutes before it must be stopped and retrieved or it is overwritten. It is utilized to acquire high speed data on a selected subset of the process variables at a sample rate of 80 ms.

The AtlasPC controls the Swift valve (FV-432) that meters natural gas to the combustor. In HyPer, the demanded position to the fuel valve from the AtlasPC is updated at the 5 ms interval. The primary control approach is turbine rotational speed control via a feedback loop to set the fuel flow. In normal operation, the fuel valve's demanded position is modulated to achieve the nominal turbine speed. This valve demand is established via a measured rotational speed feedback loop to a programmed proportional-integral controller. For HILS with HyPer, the AtlasPC remains in control of the fuel valve, but the valve demand is now set by the numerical fuel cell model (further details in Section 3.3). A second speed control scheme tested on HyPer with the AtlasPC controller has been speed control by adjusting the variable electrical load. This has applications during HILS simulations, since during a HILS the combustor firing is set by the model. In addition, the AtlasPC has been used to control the hot-air bypass valve to target a setpoint flow through the air plenum.

3.1.4: HyPer Operating Procedure

The operation of HyPer normally requires three personnel. Before each operation, a test plan is documented that describes the objectives of the test and details the procedure. During the test the plan acts as the operational guide. Furthermore, an operational log is kept of each action taken or any noteworthy observation during the test. Presented in Appendix C is a test plan and in Appendix D is a operational log for a HILS experiment with HyPer. Most of the test plans take 2 to 3 hours to complete, while the HILS test can take up to 8 or more hours. The length of time is required to heat the post-combustor vessel before the simulation. The next sections will highlight the basics of operating the HyPer system.

3.1.4.1: Startup Procedure

Before a HyPer startup, a pre-operation inspection of the equipment is completed, and the onsite natural gas compressor is started. To begin a test the bypass valves are positioned as desired, normally all closed, and the control systems' data logs are started. To start a turbine, airflow must be established through the combustor and the turbine must be spun up to a minimum rotational speed. HyPer utilizes the external blower (B-100) for this. For each start, the blower is allowed to come to full speed with the blower block valve (HV-600) closed. The block valve is then opened, forcing flow forward through the air plenum and turbine and backwards through the heat exchangers and compressor. As the blower spins up the turbine, the timed system purge is conducted and a combustor ignition permissive is issued.

At 9,000 rpm an automated ignition is commenced with a 5 % fuel valve position demand to provide fuel flow just sufficient for stable flame retention. Upon ignition, an automated speed program increases the fuel demand at a target rate. The target rate is usually set a to produce a turbine rotational acceleration rate of 500 rpm/s from 9,000 rpm to 40,500 rpm. As the turbine and compressor begin to spin up in rotational speed, compressor back flow diminishes as the compressor engages the air. At approximately 17,000 rpm, the compressor pressure finally exceeds the maximum dead head pressure of the blower, and the blower flow is eliminated by the check valve in front of HV-600. When the turbine reaches its nominal speed, the startup ramp program ends and the controller adjusts the fuel demand to maintain the 40,500 rpm speed. The blower is shutoff, and the system is operated unloaded for several minutes to allow the heat exchanger metal to warm.

3.1.4.2: Normal operation

HyPer operation can vary greatly depending on the test being performed. Specific details on conducting HILS during operation are discussed in Section 3.3. In every test, the process variables must be monitored to ensure that all remain within their respective operating envelopes. If the test plan includes electrical loading of the turbine, the dissipater is activated and its cooling fans are started. Typically, the turbine is loaded in 15 kW increments of electrical power. The bypass valves may also be manipulated. During a transient the HyPer operator must be attentive to the compressor response and must watch for any indication of a compressor surge. In HyPer, if a surge event initiates, the preferred corrective action is to open the cold-air bypass valve to 55 % and attempt a recovery, as opposed to a manual or automatic fuel shutoff leading to ending the test. Opening the cold-air bypass reduces the system pressure loss which promotes the increase of the air mass flow rate through the compressor, thereby moving the operating point away from the surge line.

3.1.4.3: Shutdown

The system shutdown is straightforward for HyPer. First any electrical loading is removed in steps from the turbine and the dissipater is shut off. Second, the normal shutdown procedure sets cold-air bypass to 25% to assist the air plenum in depressurizing during the shutdown. After setting the valve position, the system is allowed to stabilize for several minutes, and then an automated fuel shutdown ramp is initiated. A controlled ramp down is utilized to allow the turbine speed to decrease slowly and provide time for the air plenum to depressurize. If the fuel is just shut off at normal turbine speed and plenum pressure, a compressor surge is probable. Once the ramp down is at 28,000 rpm,

the fuel is manually shut off and the turbine is allowed to coast down. This ends the test and the facility is secured.

3.2: SOFC Stack Subsystem Model

For integration with the HyPer hardware, a natural gas fueled 350 kW SOFC stack with an external reformer was selected as the target for the numerically modeled fuel cell subsystem. In conducting a HILS, the overall goal of the subsystem numerical model is to predict the level of thermal effluent transferred to the airflow from the fuel cell stack and its supporting components. This simulated heat transfer rate, $\dot{Q}_{stack.}$, is calculated as the change in enthalpy between the measured input airflow and the simulated outlet airflow. For this research project, the simulation utilized is a cell level bulk parameter (zero-dimensional) dynamic SOFC model developed in Simulink.

The model subsystem is manipulated by setting user inputs that are adjustable during execution of the model, such as fuel cell current demand and fuel flow rate. With these setpoints and the measured flow conditions, the model then solves for a cell operating voltage and resulting byproduct heat generation. For the HILS testing done in this dissertation, the subsystem model was compiled and executed in real-time first on HyPer's AtlasPC controller and then on the dSPACE system.

As shown in Figure 3.16, the simulated subsystem consists of several components, in addition to the solid oxide fuel cell stack, that contribute to the generated heat predicted by numerical simulation. The heat is a byproduct of the fuel cell's electrochemical reactions and a product of fuel combustion in the subsystem's combustors. The simulated subsystem includes a natural gas pre-combustor (C1) for

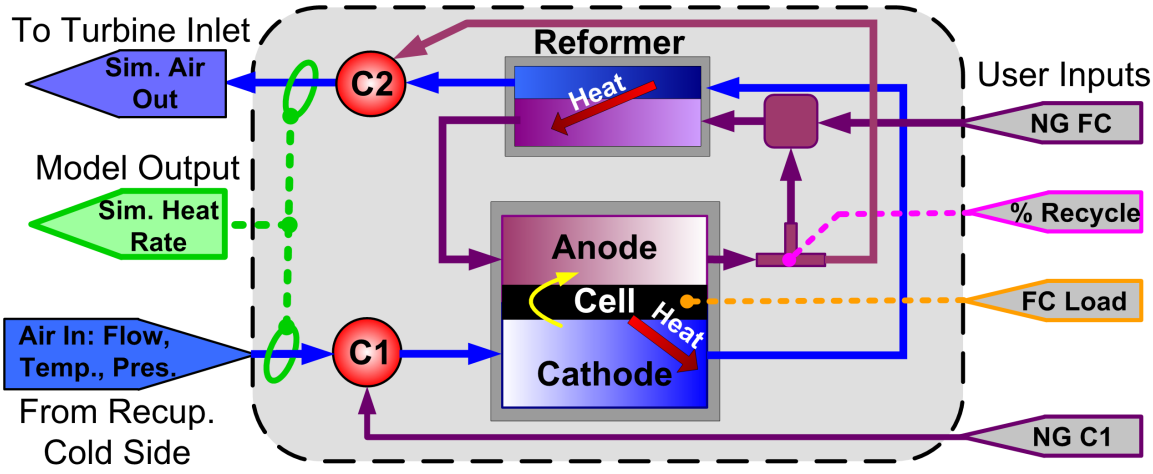

Figure 3.16: Modeled Fuel Cell Stack Subsystem

ensuring a reasonable air temperature at the stack inlet, and a post-combustor (C2) to combust the unutilized fuel that passes through the fuel cell anode unreacted. Also included is an external reformer that accounts for the heat required to reform the natural gas fuel to hydrogen. This layout of simulated components can be modified depending on the stack configuration of interest.

3.2.1: Fuel Cell Model

The modeled stack design used in this study is based on a 20 cm by 20 cm, planar, co-flow, anode-supported solid oxide fuel cell. The number of cells was selected to target approximately 350 kW of electrical power generation at full load. This stack power level matches the thermal input required by the turbine at a 45 kW electrical load. For HyPer HILS the typical number of cells was 1500, but could be varied at the start of a simulation.

3.2.1.1: Selection of the Bulk-Parameter Cell Model

A bulk-parameter approach was used to capture the fuel cell phenomena. The bulk-parameter cell model was created in Simulink by NETL personnel. Further details on its development were published in Liese (2006). In the model, the thermal transients are based on a time-dependent energy balance accounting for the heat capacitance of the cell materials, while the electrochemical calculations are a quasi-steady state formulation. Since the time scales of the electrochemical transients are three orders of magnitude shorter than the thermal time scales, this approach is reasonable. Also, a time-based conservation of mass approach is used to find the concentration of the gas species at the cell exit.

While the bulk-parameter approach does inherently introduce inaccuracy in the results, it was selected as the most fitting solution for the initial HILS with HyPer. Other SOFC models, such as a 1-dimensional model, were evaluated in the development of this work, but did not meet the requirements of the HILS testing. A primary concern was ensuring reliable real-time execution on the AtlasPC controller. Secondary was the ability to integrate the model into Simulink. The selected bulk-parameter model developed by Liese at NETL was available and readily adaptable to the HILS methodology. While the numerical model used in the initial HyPer HILS does provide insightful results, improvements in the HILS accuracy can be made through a more refined and higher-fidelity cell model and through enhanced models for the other components in the subsystem.

3.2.1.2: Modeled Stack and Cell Design

As mentioned, for the HyPer testing the modeled fuel cell stack was typically composed of 1500 cells. However, computationally only a single planar 20 cm by 20 cm cell is simulated. The stack design connects these cells in electrical series and in parallel for the fuel and air streams. In order for the cell model to represent a stack the inlet fuel and air mass flow rate from the rest of the subsystem is scaled down by the number of cells. Conversely, the outlet streams are multiplied by the number of cells factor. Likewise, for the electrical series arrangement, stack power, $\dot{W}_{stack.}$, and stack voltage, $V_{stack.}$, are obtained by multiplying their respective cell values by the number of cells. In this arrangement each cell carries an equal current, I_{cell}.

The cell design, physical parameters, and electrochemical equation formations are based on articles by Aguiar (2004) and Zhao (2005). The thicknesses for the ceramic electrolyte and electrodes are based on the anode-supported button cell tested in Zhao (2005). The stainless steel interconnect and its flow channels were sized to correspond with this cell design. The dimensions for the anode supported planar cells are given in Table 3.1 and diagrammed in Figure 3.17. In the table the single cell mass, m_{cell}, and heat capacitance, $C_{p,cell}$, values are for both the PEN structure and the interconnect combined. To estimate these values, the material properties of a common anode ceramic-metal cermet were used for the PEN and the properties of stainless steel for the interconnect. The interconnect contributes the majority of the heat capacitance at 0.554 kJ/K per cell, while the PEN structure adds 0.108 kJ/K.

Table 3.1: Fuel Cell Modeled Geometry and Physical Parameters

Parameter	Value
Cell length	0.2 m
Cell width	0.2 m
Electrolyte thickness	0.01 mm
Anode thickness, τ_{an}	1 mm
Cathode thickness, τ_{ca}	0.1 mm
Channels/cell	50
Interconnect anode channel width	2 mm
Interconnect anode channel height	1 mm
Interconnect cathode channel width	2 mm
Interconnect cathode channel height	1 mm
Interconnect thickness (total)	3 mm
Anode fuel volume/cell, $\forall_{an}$	0.02 L
Cathode air volume/cell, $\forall_{ca}$	0.02 L
Cell mass, m_{cell}	1.4 kg
Cell heat capacity, $C_{p,cell}$	0.662 kJ/K

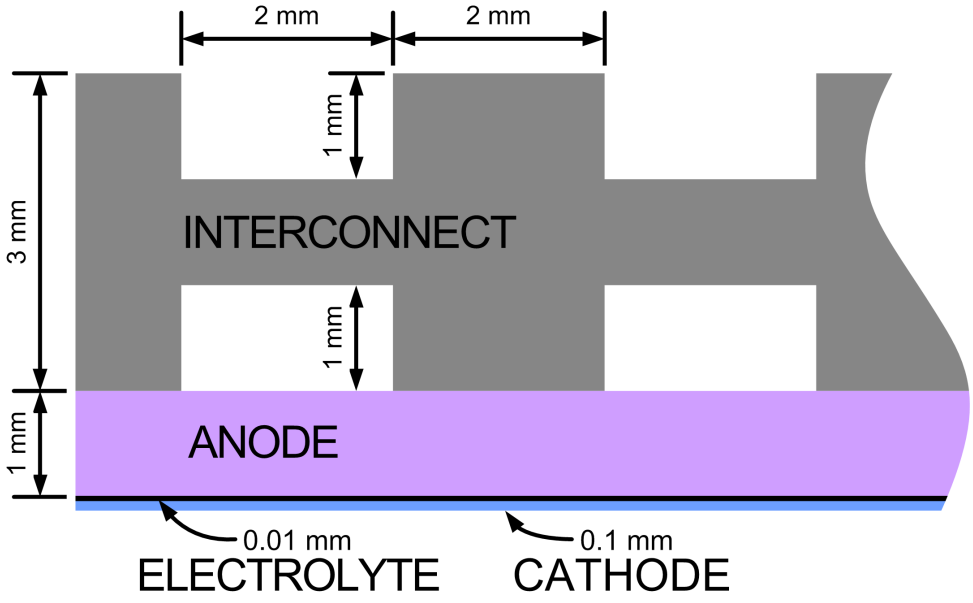

Figure 3.17: Modeled Fuel Cell Dimensions

3.2.1.3: Electrochemical Model Calculation

In the cell model, the primary objective is to calculate the temperature of the air exiting the cathode by calculating the byproduct heat generated, $\dot{Q}_{cell,gen}$, from the electrochemical losses. The generated heat is found by a first law of thermodynamic balance on the cell and fuel stream:

$$\dot{Q}_{cell,gen} = \dot{H}_{fuel,an,in.} - \dot{H}_{fuel,an,out} - \dot{W}_{cell} \quad [3.1]$$

where H terms represent the enthalpy change in the fuel. The $\dot{W}_{cell}$ is electric power generated by the cell, which is simply the operating voltage times the current drawn:

$$\dot{W}_{cell} = V_{cell} I_{cell} \quad [3.2]$$

In this cell model, the primary user setpoint is the current, I_{cell} in amps, drawn from the stack. This sets the current density, i in A/m^2, at which the cell is operating by

$$i = \frac{I_{cell}}{A_{cell}} \quad [3.3]$$

With the current density, the model predicts cell operating voltage by evaluating electrochemical performance of the cell at the operating conditions, such as fuel flow and temperature. The basis for the calculation is

$$V_{cell} = E_{Nernst} - \eta_{conc} - \eta_{act,an} - \eta_{act,ca} - \eta_{ohmic} \quad [3.4]$$

where E_{Nernst} is the Nernst voltage and the polarization losses are the remaining terms. The Nernst voltage is given by

$$E_{Nernst} = E^o + \frac{R_u T_{cell,bulk}}{2F} \ln\left(\frac{p_{H2,an}\sqrt{p_{O2,ca}}}{p_{H2O,an}\sqrt{P^o}} \right) \quad [3.5]$$

where the standard potential is $E°$. For the model, an equation is established for $E°$ as a

function of temperature by fitting an equation to the standard change in Gibbs energy for formation of water reaction. The equation for the standard potential voltage is

$$E^o = 1.2877 - 0.0002904\, T_{cell,\,bulk} \qquad [3.6]$$

The cell temperature, $T_{cell,bulk}$, is in K for this equation, and the model's solution approach for this bulk cell variable is presented in Section 3.2.1.4. The location of the partial pressures, p_x, in this this formation are in the anode fuel and the cathode air stream channels. Furthermore, for the bulk model approach, a global value must be established since a species partial pressure varies spatially as the reactant stream moves through the cell. In this model an average of the inlet and outlet partial pressure for each species is used and their establishment approach is explained in a later section.

To then calculate the operating voltage from the thermodynamic voltage the reaction overpotentials are established. The loss terms in Equation 3.4 all depend on cell current density, as well as other parameters, and are each calculated separately as shown below.

3.2.1.3.1: Concentration Polarization

The electrochemical reaction in a fuel cell occurs at what is called the triple phase boundary (TPB), where an electrode interfaces the electrolyte and the gaseous reaction participants. The reactants must travel from the bulk gas stream through the electrodes to the TPB for the reaction to occur. In an anode supported cell the anode electrode is relatively thick and inhibits mass transport to the TPB. The mass transport restriction leads to a lower concentration of hydrogen at the TPB than the bulk concentration in the fuel channel. Conversely, the water concentration will be high at the TPB since it is being formed there. The cathode layer also inhibits oxygen flow but the effect is less

since it is thinner. The concentration losses are essentially the difference in the Nernst potential in the gas channels and a predicted Nernst at the TPB due to the change in species concentration. Thus the equation is

$$\eta_{conc} = \frac{R_u T_{cell,bulk}}{z F}\left[\ln\left(\frac{p_{H2,an}}{p_{H2,TPB}}\frac{p_{H2O,TPB}}{p_{H2O,an}}\right) + \frac{1}{2}\ln\left(\frac{p_{O2,ca}}{p_{O2,TPB}}\right)\right] \quad [3.7]$$

The species partial pressures are an average of the values for the reactant streams. The partial pressures at the TPB are calculated by (Aguiar, 2004)

$$p_{H2,TPB} = p_{H2,an} - \frac{R_u T_{cell,bulk}}{2F}\frac{\tau_{an}}{D_{eff,an}}\, i \quad [3.8]$$

$$p_{H2O,TPB} = p_{H2O,an} + \frac{R_u T_{cell,bulk}}{2F}\frac{\tau_{an}}{D_{eff,an}}\, i \quad [3.9]$$

$$p_{O2,TPB} = P - (P - p_{O2,ca})\exp\left(\frac{R_u T_{cell,bulk}}{4F}\frac{\tau_{ca}}{D_{eff,ca}}\frac{i}{P}\right) \quad [3.10]$$

where i is the current density in A/m^2, τ is electrode thickness, and D_{eff} is the effective diffusivity of the gases in the electrodes. The diffusivity values are adopted from experimental fitted data from button cell testing presented in Zhao (2005). The atmospheric pressure diffusivities, D_{atm}, were derived with cells having a porosity of 48 % in the anode and a porosity of 45 % in the cathode. The atmospheric diffusivity values divided by the respective electrode thickness is shown in Table 3.2. To account for the pressurization of the cell, ordinary gas diffusion behavior is assumed so the effective diffusivity is then inversely proportional to operating pressure:

$$D_{eff} = D_{atm}\frac{P^o}{P} \quad [3.11]$$

Table 3.2: Fuel Cell Electrochemical Loss Parameters

Parameter	**Value**
Atmospheric anode diffusivity term, $D_{atm,an} / \tau_{an}$	0.025 m/s
Atmospheric cathode diffusivity term, $D_{atm,ca} / \tau_{ca}$	0.117 m/s
Anode activation pre-exponential, k_{an}	6.54E11 $\Omega^{-1}\cdot m^{-2}$
Cathode activation pre-exponential, k_{ca}	2.35E11 $\Omega^{-1}\cdot m^{-2}$
Anode electrode activation term, $E_{a,an}$	140 kJ/mol
Cathode electrode activation term, $E_{a,ca}$	137 kJ/mol
Transfer coefficient, α	0.5
Participating electrons, z	2

3.2.1.3.2: Activation Polarization

Establishing activation loss parameters is difficult because they are dependent on the material type, composition and microstructure morphology. In many cases, the cathode and anode activation overpotentials are lumped together in calculating the loss terms. For this model, separate calculation of the anode and cathode activation overpotentials is used to better account for anode performance. This is required since the mass transfer effects on the anode side are comparable to the activation effects. For the anode activation, Aguiar (2004) gives a relationship for the voltage loss using a modified Butler-Volmer equation that includes corrections for partial pressure of the species at the TPB:

$$i = i_{o,an}\left[\frac{p_{H2,TPB}}{p_{H2,an}}\exp\left(\frac{\alpha z F \eta_{act,an}}{R_u T_{cell,bulk}}\right) - \frac{p_{H2O,TPB}}{p_{H2O,an}}\exp\left(\frac{-(1-\alpha) z F \eta_{act,an}}{R_u T_{cell,bulk}}\right)\right] \qquad [3.12]$$

This equation can be recast (if $\alpha = 0.5$ and $z = 2$, as in this case) to give the anode activation overpotential explicitly by using a inverse hyperbolic sine:

$$\eta_{act,an} = \frac{R_u T_{cell,bulk}}{F}\left[\sinh^{-1}\left(\frac{i}{2 i_{o,an}\sqrt{\frac{p_{H2,TPB}\ p_{H2O,TPB}}{p_{H2,an}\ p_{H2O,an}}}}\right) - \frac{1}{2}\ln\left(\frac{p_{H2,TPB}\ p_{H2O,an}}{p_{H2,an}\ p_{H2O,TPB}}\right)\right] \quad [3.13]$$

The partial pressures are the same as in the concentration loss calculation. The exchange current density, i_o, in A/m^2 is based on data given by Aguiar (2004)

$$i_{o,an} = \frac{R_u T_{cell,bulk}}{z F} k_{an} \exp\left(\frac{-E_{a,an}}{R_u T_{cell,bulk}}\right) \quad [3.14]$$

where the values for the electrode activation, k_{an} and $E_{a,an}$, terms are given in Table 3.2.

On the cathode, the mass transfer effects are less significant in finding the activation overpotential, so a simpler approach can be used. For this model, the following formulation is used

$$\eta_{act,ca} = \frac{R_u T_{cell,bulk}}{F} \sinh^{-1}\left(\frac{i}{2 i_{o,ca}}\right) \quad [3.15]$$

The cathode exchange current density is found in a similar fashion as for the anode:

$$i_{o,ca} = \frac{R_u T_{cell,bulk}}{z F} k_{ca} \exp\left(\frac{-E_{a,ca}}{R_u T_{cell,bulk}}\right) \quad [3.16]$$

3.2.1.3.3: Ohmic Polarization

The ohmic losses arise due to the resistance to current flow in the cell materials. In a SOFC the resistance to ionic flow across the electrolyte is the most significant, but the electronic resistance in the electrodes, the interconnect, and the contact resistance between them also contribute. The model's ohmic loss calculation was developed by combining the experimental measurements of Zhao (2005) and Aguiar (2004). Zhao experimentally measured the resistance for the entire PEN cell structure, but without a temperature correction. Aguiar established temperature-dependent ionic conductivity for

only the electrolyte. For this model, the pre-exponential of Aguiar's equation was scaled to match Zhao's PEN data. The entire cell resistance then has a temperature-dependence similar to the electrolyte itself. This may over-emphasize the effect of temperature on cell resistance, but is a reasonable assumption since the electrolyte resistance is the dominant resistance contributer. The equation for area specific resistance, in $\Omega \cdot m^2$, of the PEN, where temperature is in K, is

$$r_{PEN} = 6.78\text{E-}10 \exp\left(\frac{10.3\text{E}3}{T_{cell,bulk}}\right) \quad [3.17]$$

The interconnect modeled here is composed of stainless steel with a ceramic coating on the cathode side to protect against oxidation. In this arrangement, the interconnect's resistance is dominated by the ceramic coating and the contact resistance with the cathode. Dekker (2004) evaluated the area specific resistance for several steel and contact coating combinations. From the data presented by Dekker, a good candidate set of interconnect materials was selected, and a temperature dependent equation for its area specific resistance was fitted to the data:

$$r_{inter} = 0.23174 \exp(-0.0115\ T_{cell,bulk}) \quad [3.18]$$

Then the total ohmic overpotential was then calculated as

$$\eta_{ohmic} = (r_{PEN} + r_{inter})i \quad [3.19]$$

3.2.1.4: Fuel Cell Model Temperature Calculation

As mentioned, the primary goal of the fuel cell model is to predict the exit air temperature, $T_{air,ca,out}$, from the cathode so that it can be used in establishing the overall thermal effluent from the fuel cell subsystem. The exit air temperature is dependent on on the heat transfer characteristics and the level of byproduct heat generation from the

electrochemical reaction. The electrochemical equations outlined in the previous section establish the level of the cell's heat generation at each time step. This section outlines the bulk parameter approach used to calculate at each time step the representative cell operating temperature and the air exit temperature. Further details on the steps taken in developing the approach used by this fuel cell model in predicting the cell and air exit temperatures are presented in Liese (2006).

3.2.1.4.1: Heat Transfer Considerations

The primary heat transfer of interest is the convection of heat to cathode-side airflow from the cell. This transfer takes place within the 1 mm by 2 mm air channels on the cathode side of the interconnect. The Nusselt number is 4.123, assuming a constant heat flux in a channel with an aspect ratio of 2 and laminar flow. The Reynolds number for the airflow in the channels is approximately 250. In the model, the air thermal conductivity is assumed constant, 0.0732 W/(m·K), and the heat transfer coefficient, h_{HT}, of 302 W/(m^2·K) was used in the model. Each cathode air channel has a surface perimeter of 6 mm. In each cell there are 50 channels of 20 cm length, giving a total heat transfer surface area, A_{HT}, of 0.06 m^2. The single cell heat capacity, $C_{p,cell}$, is 0.662 kJ/K and h_{HT} is 302 W/(m^2·K), leading to the ratio of the gas heat conductance to the bulk material thermal capacitance ($h_{HT}A_{HT}/C_p$) is 0.0274 s^{-1}.

As a further simplification, in the bulk-parameter model the cell and the interconnect are assumed to be at a uniform temperature. Furthermore, for the cell temperature calculations, the cell and the interconnect are treated as one solid body in respect to the thermal capacitance. In doing this, any transient that affects the cell's heat

generation could underpredict the cell temperature transient since the heat capacity of the interconnect is lumped with the cell.

3.2.1.4.2: Temperature Equations

In modeling the cell temperatures, the first step is to track the bulk cell temperature, $T_{cell,bulk}$, with an energy equation including the heat generation and convection to the cathode air:

$$\Gamma C_{p,cell} \frac{\partial T_{cell,bulk}}{\partial t} = \dot{Q}_{cell,gen} - h_{HT} A_{HT} (T_{cell,bulk} - T_{air,ave}) \quad [3.20]$$

The heat capacity scalar, Γ, is a numerical device to assist in setting up a HILS test and is explained below. The heat generation term was previously identified in Equation 3.1:

$$\dot{Q}_{cell,gen} = \dot{H}_{fuel,in.} - \dot{H}_{fuel,an,out} - \dot{W}_{cell} \quad [3.1]$$

In 3.1, the inlet fuel enthalpy is set by the conditions entering the cell. The exit enthalpy is calculated by accounting for the composition change as the reaction proceeds (as detailed in the next section) and by assuming the exit fuel temperature equals the exit air temperature, $T_{air,ca,out}$. In Equation 3.20, the average air temperature, $T_{air,ave}$, is the average of the inlet and outlet temperatures:

$$T_{air,ave} = \frac{T_{air,ca,out} + T_{air,ca,in.}}{2} \quad [3.21]$$

The inlet temperature is set by the conditions, but the exit temperature needs to be established. Assuming quasi-steady air temperatures, since the heat capacitance of the air is much less than for the cell material, the exit air temperature can be found by a simple energy balance on the airflow:

$$\dot{m}_{air,ca} c_{p,air} (T_{air,ca,out} - T_{air,ca,in.}) = h_{HT} A_{HT} (T_{cell,bulk} - T_{air,ave}) \quad [3.22]$$

where $\dot{m}_{air,ca}$ is the air mass flow rate and $c_{p,air}$ is the average specific heat capacity for the temperature range. However, while this bulk-parameter approach gives the proper steady-state exit air temperature, it does not exhibit the proper dynamic behavior. Further details on the nonphysical behavior of this original bulk-parameter approach are given by Liese (2006).

Thus, to compute the exit temperature a modified method that employs additive temperature terms is used to avoid nonphysical behavior. This approach was adapted from a bulk parameter heat exchanger model presented in Smith (1998). The first step in this approach is to recast Equation 3.22, so that $T_{air,ca,out}$ is explicitly a function of the cell temperature, heat generation, air heat capacity, and convection terms. This is accomplished by substituting in $T_{air,ca,in}$ from Equation 3.21 and $T_{air,ave}$ from the steady-state form of equation 3.20. The resulting equation is

$$T_{air,out,ss} = \left(\frac{h_{HT} A_{HT} - 2\dot{m}_{air,ca} c_{p,air}}{2\dot{m}_{air,ca} c_{p,air} h_{HT} A_{HT}} \right) \dot{Q}_{cell,gen} + T_{cell,bulk} \qquad [3.23]$$

This formulation gives a quasi-steady outlet air temperature based on the cell operating temperature, but does not capture the dynamic characteristic of the outlet air temperature. Instead, this equation establishes a target outlet air temperature, $T_{air,out,ss}$, for the actual model output air temperature, $T_{air,ca,out}$, to approach dynamically. This is accomplished by recognizing the first term on the right-hand side of Equation 3.23 as an additive variable. The next step is then to define this term as the steady-state additive temperature:

$$T_{add,ss} = \left(\frac{h_{HT} A_{HT} - 2\dot{m}_{air,ca} c_{p,air}}{2\dot{m}_{air,ca} c_{p,air} h_{HT} A_{HT}} \right) \dot{Q}_{cell,gen} \qquad [3.24]$$

However, the objective is to predict a dynamic temperature response. Therefore, to add the dynamic characteristic, a first order differential equation is introduced with a temperature time constant similar to the cell material:

$$\frac{\partial T_{add,dyn}}{\partial t} = \frac{h_{HT} A_{HT}}{C_{p,cell}} (T_{add,ss} - T_{add,dyn}) \quad [3.25]$$

This differential equation establish the dynamic additive term, $T_{air,dyn}$, that will always over time approach the steady-state additive, $T_{add,ss}$. Finally, the exit air temperature, $T_{air,ca,out}$, is calculated by substituting the dynamic additive term for the first term on the right-hand side of Equation 3.23 to create Equation 3.26:

$$T_{air,ca,out} = T_{add,dyn} + T_{cell,bulk} \quad [3.26]$$

This bulk-parameter approach creates a computationally non-intensive method to reasonably capture the dynamic responses of the cell temperature , $T_{cell,bulk}$, and the exit air temperature, $T_{air,ca,out}$. In this approach, the cell temperature is established by the time dependent temperature differential in Equation 3.20. The cell temperature responds to changes in cell heat generation, $\dot{Q}_{cell,gen}$, or average air temperature, $T_{air,ave}$. The average air temperature depends on inlet and outlet air temperatures. The outlet air temperature is established through the differential in Equation 3.25. For this equation and at each time step, a steady-state additive temperature term, $T_{add,ss}$, is calculated by Equation 3.24. This steady-state additive term may change at each time step; depends on the cell heat generation; and acts as the "target" for the dynamic additive term, $T_{air,dyn}$. The time dependent dynamic additive term is then established by Equation 3.25 and added to the cell temperature in Equation 3.26 to calculate the outlet air temperature, $T_{air,ca,out}$. From these calculations the resulting cell temperature is passed to the electrochemical equations for their calculation in the next time step, and the resulting outlet air

temperature is passed from the stack model to the next component model in the subsystem.

3.2.1.4.3: Cell Heat Capacity Scalar

In addition to the other input parameters that represent physical values, the subsystem model has one nonphysical input that is used to facilitate the HILS experiments. In conducting HILS experimentation, normally a series of different tests are conducted in succession, and each test consists of perturbing a steady condition. Therefore, before the initiation of each test the cell temperature must reach its equilibrium value for the given airflow and loading conditions. Reaching this equilibrium may require a signification amount of time with the full simulated thermal capacitance of the stack. This is undesirable due to the operating costs of HyPer testing and limited personnel time. Therefore, to significantly reducing the time between tests, a scalar term is introduced that is multiplied by the cell's heat capacity, $C_{p,cell}$.

In Equation 3.20, the heat capacity scalar, Γ, can be used to reduce the numerical thermal capacitance of the cell between HILS tests while the model is executing. The scalar can be set to any value in the range between 0.1 and 1. During a HILS test where data is being recorded for analysis it is always set to 1, so that the model's thermal response is correct. However, before a test the cell temperature could be far from an equilibrium and unsteady. This is an undesirable point to initiate a transient because it complicates analysis and reduces experimental reproducibility. To swiftly remedy this condition, the heat capacity scalar is reduced to 0.1 to allow the simulated cell temperature to quickly reach an equilibrium. Once a satisfactory steady-state condition has been reached, the scalar is set back to 1 and the next transient test is initiated.

The benefit of including the heat capacity scalar term in the model is to reduce the time between transit tests. This saves time while the equipment is operating, allowing for a greater number of HILS tests to be conducted. Furthermore, it assists in ensuring that multiple experiments can be initiated at a similar operating point to increase the repeatability of a certain transient test.

3.2.1.5: Outlet Gas Composition Calculation

As mentioned, for the electrochemical calculation the average species partial pressures are used. The inlet partial pressures are set by the conditions as specified by the reactant stream parameters: mass flow rates, pressure, and species mole fraction. The fuel cell model, as well as the subsystem, tracks the mole fractions of seven species: O_2, N_2, CO_2, CO, H_2O, H_2, and CH_4. Non-reacting species do not participate in the model calculations, but do affect the predicted cell performance by lowering the partial pressures of the active species.

The exit partial pressures are dependent on the consumption rate of hydrogen and oxygen. For an electrochemical reaction the reactant consumption rate is directly proportional to the current drawn. The resultant exit partial pressures are resolved via a bulk volume formation:

$$\frac{\partial p_{H2,an,out}}{\partial t} = \frac{T_{cell,bulk} R_u}{\forall_{an}} \left(\dot{x}_{H2,an,in.} - \dot{x}_{H2,an,out} - \frac{i}{2F} \right) \qquad [3.27]$$

$$\frac{\partial p_{O2,ca,out}}{\partial t} = \frac{T_{cell,bulk} R_u}{\forall_{ca}} \left(\dot{x}_{O2,ca,in.} - \dot{x}_{O2,ca,out} - \frac{i}{4F} \right) \qquad [3.28]$$

The steam exit partial pressure, $p_{H2O,an,out}$, in the anode is found by subtracting the H_2 and remaining species species mole fractions from unity, and then multiplying the difference by the total pressure.

3.2.1.6: Bulk-Parameter Fuel Cell Model Evaluation

Before the SOFC bulk cell model could be used in a HILS it had to be evaluated to ensure the model was performing as intended. For the HyPer HILS methodology, the primary objective is to predict the dynamic temperature of the airflow exiting the cathode. Specifically, the dynamic bulk-parameter model had to capture the relative changes in exit air temperature during a transient. Second, the model predicts the quasi-steady electrochemical performance of the cell. Since these two domains are coupled together through the cell heat generation and cell temperature, it is essential that both domains of the model perform sufficiently. A third important concern in developing this model was to design a computationally non-intensive approach so that the real-time requirement could be achieved.

In a fuel cell, spatial distribution of both the cell temperature and reactant molar fractions are present and significant to the heat transfer and electrochemistry. With the relatively low computational power of the AtlasPC controller, the real-time constraint required the use of a zero-dimensional approach. Therefore, a single representative cell temperature and a single partial pressure for each reactant is used. This bulk-parameter simplification does reduce the accuracy of the cell model, however the comparison with the 1-dimensional cell model shown below indicates that the bulk-parameter model performed sufficiently in capturing the dynamic characteristics of the cell exit air temperature.

3.2.1.6.1: Verification of Fuel Cell Model Code

Model verification is required to ensure that it programing produced results as expected. Since the SOFC model is used in a direct-hybrid configuration, the effect of

pressurization was evaluated. Table 3.3 lists the input conditions and resulting performance for two cathode air pressures, at atmospheric pressure and at 360 kPaa (absolute). The model internally sets the fuel pressure to 1.1 times the cathode air pressure. This assumption for the fuel pressure is based from fuel cell stack operational observations. The desired operating point was at a current density of 0.85 A/cm^2, and the fuel flow rate was set to target 50 % per pass fuel utilization. The inlet fuel composition is representative of an external reformer outlet composition for a 75 % recycle of the anode-off gas (λ = 75). The results show that the cell voltage increased by 3.5 % for a pressure increase of 3 times, primarily due to an increase in the Nernst potential. Additionally, the outlet cathode air temperature decrease as expected at the higher pressure since the cell is operating more efficiently.

3.2.1.6.2: Validation Against 1-Dimensional SOFC Model

The electrochemical portion SOFC bulk cell model was validated by benchmarking it against a 1-dimensional (1-D) planar, co-flow model of 20 nodes. The 1-D co-flow model, also developed at NETL, had previously been corroborated with measured data from laboratory SOFC button cell tests (Gemmen, 2004). The 20 nodes in the 1-D cell model are distributed along the direction of flow for a single set of the reactant stream channels. The 1-D model differs from the bulk model in its formulation of the electrochemical equations, and is primarily being used in this work to compare the dynamic thermal response. Additionally, the 1-D cell model does not capture the concentration loss effects, so comparisons are not applicable at high current densities. Table 3.4 shows the steady-state comparison between the bulk and 1-D models. For both models, the inlet parameters match those for the 360 kPaa case, given in Table 3.3. The

Table 3.3: Cell Model Atmospheric and Pressurized Performance

Input Parameters	**Value**	
Air mass flow rate, $\dot{m}_{air\ ,ca}$	1.3E-3 kg/s	
Air inlet temperature, $T_{air,\ ca,\ in}$	1073 K	
Fuel mass flow rate, $\dot{m}_{fuel\ ,an\ ,in.}$	0.120E-3 kg/s	
Fuel inlet temperature, $T_{fuel,\ an,\ in}$	1100 K	
H_2 mole fraction fuel in, $x_{H2,\ an,\ in}$	0.5323	
H_2O mole fraction fuel in, $x_{H2O,\ an,\ in}$	0.1344	
CO_2 mole fraction fuel in, $x_{CO2,\ an,\ in}$	0.3333	
Current density, i	0.85 A/cm^2	
Results (Cathode Pressure)	**101 kPaa**	**360 kPaa**
Operating voltage, V_{cell}	0.681 V	0.706 V
Power density	0.58 W/cm^2	0.60 W/cm^2
Cell per pass fuel utilization, $U_{F,pass}$	50.2 %	50.2 %
Stack fuel utilization, $U_{F,stack}$	80.1 %	80.1 %
Oxygen utilization	10.7 %	10.7 %
Stack efficiency (LHV), $\eta_{TH\ ,stack.}$	43.6 %	45.2 %
Nernst potential, E_{Nernst}	0.934 V	0.966 V
Concentration loss, η_{conc}	0.049 V	0.049 V
Activation loss, η_{act}	0.150 V	0.155 V
Ohmic loss, η_{ohmic}	0.055 V	0.056 V
Anode exch. current den., $i_{o\ ,an}$	1.160 A/cm^2	1.106 A/cm^2
Cathode exch. current den., $i_{o\ ,ca}$	0.573 A/cm^2	0.547 A/cm^2
Cell temperature, $T_{cell,bulk}$	1135 K	1131 K
Air outlet temperature, $T_{air,\ ca,\ out}$	1179 K	1173 K

Table 3.4: Comparison of Bulk and 1-D Cell Models at 360 kPaa

Parameter	Bulk	1-D
Current density, i	0.85 A/cm^2	0.85 A/cm^2
Operating voltage, V_{cell}	0.706 V	0.663 V
Power density	0.60 W/cm^2	0.56 W/cm^2
Cell per pass fuel utilization, $U_{F,pass}$	50.2 %	50.2 %
Nernst potential, E	0.966 V	0.963 V
Concentration loss, η_{conc}	0.049 V	0.000 V
Activation loss, η_{act}	0.155 V	0.171 V
Ohmic Loss, η_{ohmic}	0.056 V	0.129 V
Cell temperature (Average), $T_{cell,bulk}$	1131 K	1161 K
Air outlet temperature, $T_{air,\ ca,\ out}$	1173 K	1195 K

bulk cell shows an improved performance of 6.8 % in operating voltage. This is primarily due to a lower ohmic loss for the bulk cell and is expected from the formulation of the models. Figure 3.18 compares the voltage-current curves of the two models at 360 kPaa. A constant fuel utilization of 50 % at each current density was modeled. The plot shows that the bulk cell has lower activation and ohmic loss as formulated. It also shows the importance of including concentration polarization due to the significant effect it has on the power density curve.

As previously stated, the thermal response is the main concern of the bulk model. To test the dynamic response of the bulk model several comparisons of various perturbations were conducted in parallel on both models (Liese, 2006). One example is shown in Figure 3.19, where the inlet air temperature to the cathode is increased from 1073 to 1153 K. The response of the cell and exit air temperature are plotted. For the1-D model, the cell temperature is the average of the 20 nodes. The dynamic responses of the

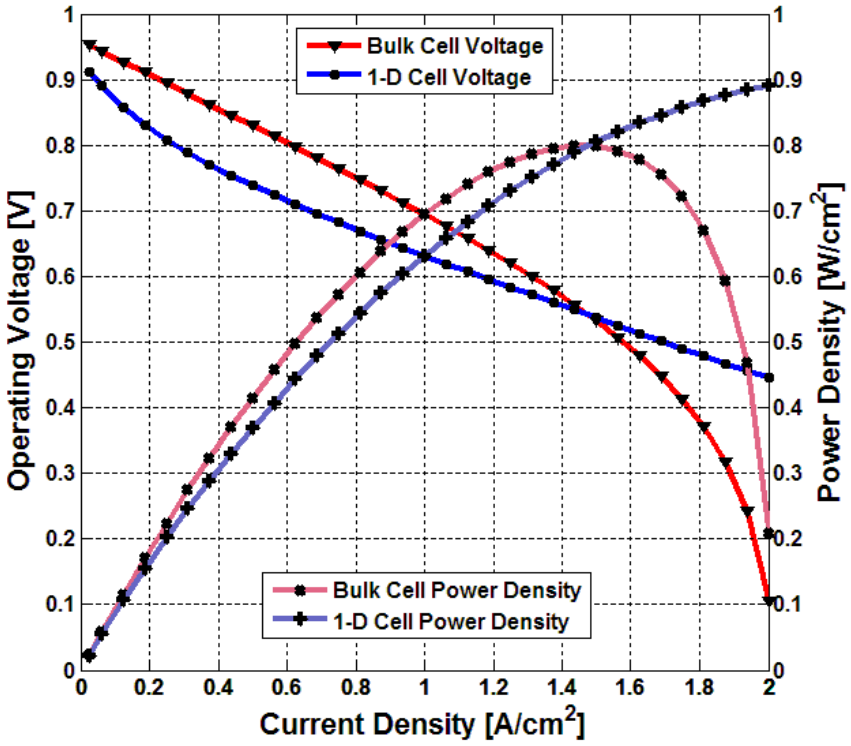

Figure 3.18: Voltage and Power Comparison of Bulk and 1-D Fuel Cell Models

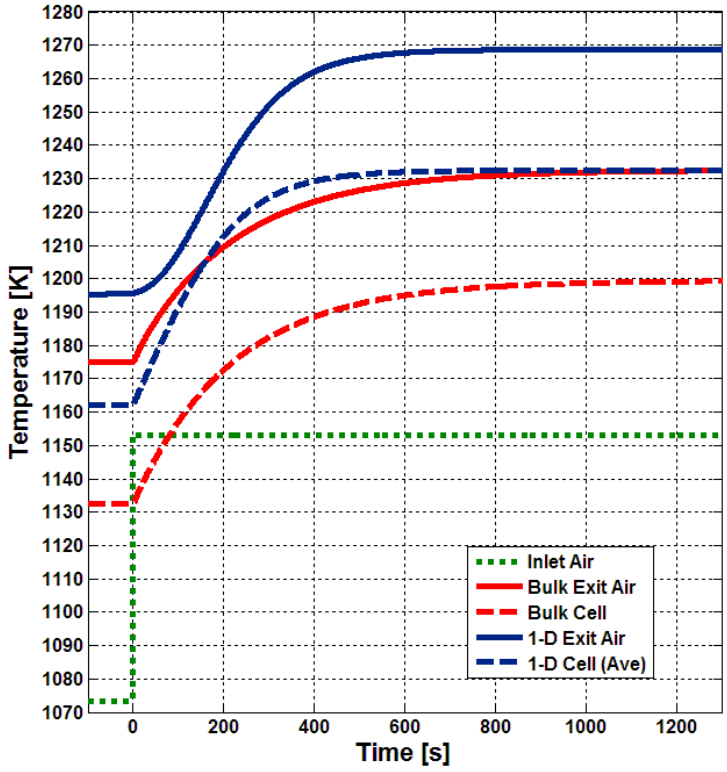

Figure 3.19: Temperature Comparison of Bulk and 1-D Fuel Cell Models

exit air temperatures from the two models are similar, particularly in the length of the responses. A small difference at the inlet air temperature change is that the 1-D model remains continuous in the responses slope, while the numerics of the bulk model give rise to a discontinuity in slope. This is because the first-order equation used in the bulk model cannot capture a second order response, while the multiple nodes of the 1-D model can simulate a continuous first derivative of the exit air temperature in response to the step change in inlet temperature. The two models do display a discrepancy in steady-state exit air temperatures, but the primary concern is the dynamic response. The bulk model has a higher voltage, which relates to a higher efficiency and less heat generation. In part, this explains why the bulk cell's steady-state temperature is lower, but does not seem to resolve the full discrepancy. Overall, the bulk model exhibits reasonable exit air performance and provides the necessary thermal response of the fuel cell model for the HILS with HyPer.

3.2.2: Model Subsystem Layout

The fuel cell stack model is part of a larger numerically modeled subsystem. The other model components exist to support the fuel cell stack, as in a real system. For the HILS tests conducted for this dissertation the subsystem configuration is based on a natural gas fueled SOFC stack. To support the stack, the subsystem includes two combustors and an external reformer, as shown in Figure 3.16. Numerous fuel cell stack configurations may be modeled and used with HyPer, such as a coal syn-gas fed system which would not require a reformer.

The modeled subsystem is manipulated by setting user inputs that are adjustable during execution of the model. As indicated in Figure 3.16 , the user setpoints for this

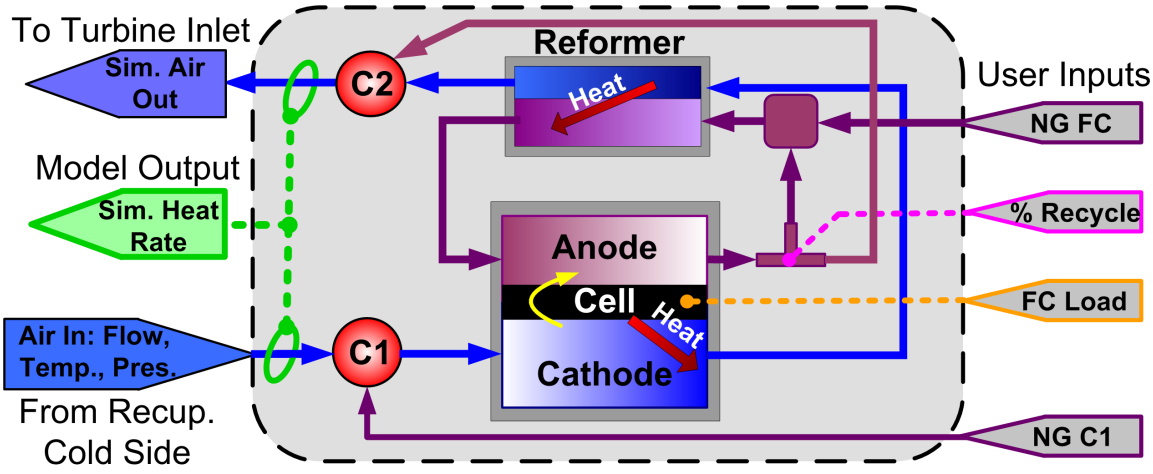

Figure 3.16 (Duplicate): Modeled Fuel Cell Stack Subsystem

model are the following: stack current demand, stack fuel flow rate to reformer, anode-off gas recycle percentage, C1 fuel flow rate. The inlet air variables of mass flow, temperature, and pressure are also fed to the numerical simulation. When the model is executing in a stand-alone setting, these airflow parameters are set by the user. In a HILS, the inlet air conditions are set dynamically by measured HyPer variables.

In the current stack subsystem configuration the inlet air is first preheated by the C1 pre-combustor, a natural gas fueled combustor. The preheating is required to ensure that the inlet air temperature to the stack does not thermally shock the cell leading to crack damage. A sufficient inlet air temperature to avoid damage to the cell is approximately 800 °C. The C1 exit temperature is simulated by the control of the natural gas fuel flow rate to the C1 combustor. The preheated airflow then passes through the cathode side of SOFC stack where it removes the electrochemical reaction by-product heat from the high temperature cells. Next, the fuel cell cathode air exhaust is used as the heat source for the external natural gas reformer. This removes heat from the air to support the endothermic steam-methane reforming reaction. The air stream then goes to

the C2 combustor where unutilized hydrogen from the anode is combusted. The calculated effluent conditions from C2 are the simulated exit air conditions from the fuel cell subsystem.

On the fuel side of the numerical subsystem, the fuel cell stack is fueled by reforming natural gas, which is assumed to be pure methane for the HILS, to produce the hydrogen for the electrochemical reaction. This is done in the simulation by an external reformer utilizing an anode-off gas recycle loop. The recirculation is used to provide the required steam for the reformation reaction. The steam is present in the anode-off gas since it is the product of the electrochemical reaction. The fuel loop process begins by separating a recycled portion of the anode-off gas and mixing it with fresh natural gas (methane) supply. Typically, 75 % of the gas exiting the anode is recycled back to the reformer, and the remaining anode gas is sent to the post-combustor.

In the modeled subsystem used for this dissertation, there is no heat transfer or pressure-flow dynamic associated with the simulated balance of plant components. For instance, there is no thermal lag to the reformer since its thermal capacity is assumed to be negligible. Also note that the anode recycle percentage is an adjustable set-point and is not based on any pressure-flow calculation. In a real system this may not be a trivial parameter to adjust or control.

3.2.2.1: Pre-Combustor

The simulated inlet air is first preheated by the pre-combustor labeled as C1. It is a natural gas fueled combustor. C1 is modeled as a bulk-parameter reactor with fuel and air inlet streams and a single effluent outlet stream. The formulation of the Simulink model assumes complete combustion, ideal gas behavior, and no losses. The model first

does a stoichiometric calculation to find the outlet gas composition for complete oxidation of the methane. Then, it predicts the exit temperature of the effluent by a first law energy balance for the three streams. To account for the change in chemistry, the enthalpy of formation for each species is used. To do the temperature calculation, an iteration loop is required, but it converges quickly to ensure that it can be used in a real-time model. The outlet effluent flow rate, temperature, and pressure are then passed on to the cathode inlet of the fuel cell model.

The C1 exit temperature is manipulated by adjusting the flow rate of the simulated natural gas fuel to the combustor. In the simulation, a programmed proportional-integral controller has been added to modulate the simulated fuel flow to track a target exit temperature. The controller will adjust the simulated C1 fuel flow rate to compensate for changes in the inlet airflow rate and temperature. The C1 controller can be switched off and a set constant fuel flow rate can be simulated to C1. During a HILS, the C1 can switched to either a constant fuel flow rate or to a controlled exit temperature setting.

3.2.2.2: Post-Combustor

The post-combustor, C2, receives process airflow after it passes through the reformer and reacts it with unutilized fuel from the fuel cell anode. The exit stream is the simulated outlet from the model subsystem. The model for C2 is a duplicate of the C1 model. For the post-combustor the complete oxidation of the hydrogen in the anode-off gas is the concern, as opposed to methane in the C1. The simulated anode-off gas composition will be about half water and a quarter hydrogen, with the remaining being carbon dioxide.

3.2.2.3: Reformer

The primary function of the external reformer is to convert the simulated inlet natural gas to hydrogen, thereby establishing the inlet fuel conditions for the cell model. The steam methane reforming reaction used is endothermic, so heat must be supplied. In this model, this is done by removing heat from the process airflow as it passes through the reformer. In the subsystem the reformer receives airflow from the stack's cathode and passes it on to the post-combustor. The reforming reaction also requires steam. The steam is supplied by recovering the bulk of the steam rich anode-off gas stream and mixing it with the inlet natural gas fuel. This mixed fuel stream is then supplied to the reformer. The air and fuel streams do not mix in the reformer.

As with the combustor models, the reformer is a bulk-parameter reactor with negligible thermal capacitance. In the model, the calculation of the fuel stream exit composition is similar to the stoichiometric calculations performed in the combustor models. In this case though, for each methane molecule there are 2 water molecules removed, while 4 hydrogen molecules and a carbon dioxide are produced. This calculation assumes complete steam reformation, including the water-gas shift reaction. An iterative energy balance is then done on the 4 streams to establish the exit temperatures of the process air and fuel streams, which are set to be at an equivalent temperature.

3.2.3: Model Subsystem Nominal Conditions

As described above, the models of the fuel cell and the supporting components were combined into a subsystem stack model. The subsystem model could then be integrated with HyPer for HILS simulations. Before this integration could be carried out,

the proper matching conditions between the operating hardware and numerical model had to be established. This step was required to ensure a smooth transition in and out of model control of the HyPer combustor during a HILS test. In establishing the base conditions, the primary concerns were the airflow conditions entering the air plenum and the thermal input rate required by the turbine. The HyPer operating conditions were selected to be a 45 kW electrical load and 1 kg/s of airflow to the air plenum. HyPer was operated at that targeted load and airflow rate and was allowed to reach a steady condition. This was done by utilizing the cold-air bypass to divert about a third of the compressor flow. The steady-state operating conditions were then denoted, particularly the plenum inlet air temperature and fuel flow rate. The fuel flow rate establishes the rate of thermal effluent that is required for the numerical model.

The observed steady HyPer operating conditions were then used to set the size of the fuel cell stack. The number of cells and the subsystem operating conditions were varied to target the required thermal effluent for HyPer. A stack of 1500 cells matched the desired heat production. The steady-state conditions presented in Table 3.5, and a snapshot of the graphical interface used with the model, is shown in Figure 3.20. At this base condition, the current demand is set at 360 A which results in the stack generating a simulated 396.3 kW. For this condition, the pre-combustor is required to heat the inlet air from 425 to 850°C. This high level of pre-heating has a large effect upon the subsystem's thermal responses. For the established nominal conditions, the simulated exit temperature from the subsystem is 1020 °C. This temperature, along with the inlet air temperature and process airflow rate, is used to calculate the change in enthalpy across

Table 3.5: Nominal Steady-State Subsystem Model Conditions

Input Parameter	**Value**
Inlet air mass flow rate, $\dot{m}_{air\ ,\ sys\ ,\ in.}$	1 kg/s
Inlet air temperature, $T_{air,\ sys,\ in}$	425 °C
Inlet air pressure, $P_{air,\ sys,\ in}$	235 kPag
Stack current demand, I_{cell}	360 A
Fuel flow to reformer, $\dot{m}_{fuel\ ,\ ref}$	14.0 g/s
Fuel flow to C1, $\dot{m}_{fuel\ ,\ C1}$	10.2 g/s
Anode recycle level, λ	75 %
Corresponding Hardware Conditions	
Turbine electric load	45 kW
Turbine rotational speed	40,500 rpm
Cold-air bypass valve	44 % open
Results	
Stack air inlet (C1 exit) temperature, $T_{air,\ ca,\ in}$	850 °C
Stack exit air temperature, $T_{air,\ ca,\ out}$	1012 °C
Reformer exit air temperature	874 °C
C2/subsystem exit air temperature, $T_{air,\ sys,\ out}$	1020 °C
Cell temperature. $T_{cell,bulk}$	938 °C
Cell voltage, V_{cell}	0.734 V
Stack power, $\dot{W}_{stack.}$	396.3 kW
Heat from subsystem, $\dot{Q}_{sys}$	682.1 kW

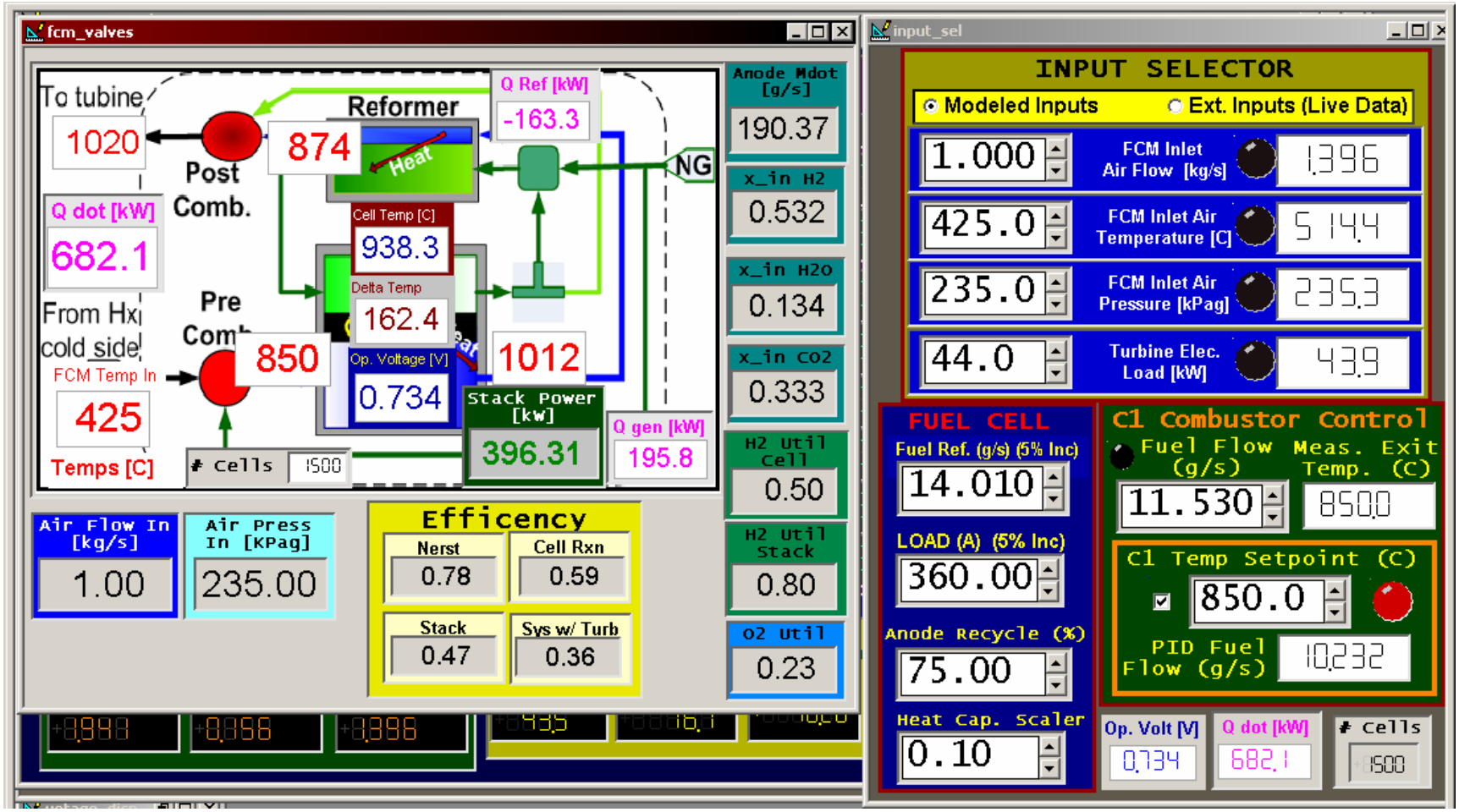

Figure 3.20: Graphical Representation of Nominal Subsystem Conditions

the subsystem. The enthalpy rise in the airflow is the rate of thermal effluent, $\dot{Q}_{sys}$, from the fuel cell subsystem and is 682.1 kW for these conditions. It is this value that is used to control HyPer's fuel valve during a HILS, as described in the next section.

3.3: HILS Methodology Development

As described in the previous section, the numerical simulation predicts the thermal effluent from a fuel cell subsystem that is operating in a hybrid system. In order to conduct HILSs with HyPer and the real-time numeric model, a methodology to couple the two together was required. This included a sensor interface to transfer the measured flow conditions from HyPer to the numerical simulation. The approach must also control the thermal output from a physical heat source in HyPer based on the level of predicted thermal effluent from the subsystem model. Additionally, the HILS approach had to incorporate user inputs and facilitate the storage of data from both the hardware and numerical simulations This was accomplished by the creation of a HILS wrapper program that facilitated the passing of data to and from the subsystem model. As with the subsystem model, the wrapper was also created in Simulink environment. Once created, it was compiled and inserted onto a HyPer control platform.

3.3.1: HyPer HILS Concept

The governing concept behind the HILS design of HyPer is that the air plenums will physically represent the flow impedance and cathode volume of a stack, while the heating by system's combustor will simulate the thermal effluent from a stack. This requires that the combustor's fuel flow rate be dynamically controlled by a fuel cell model that is responding to the changing flow conditions in the air plenum. This is done

by passing live measured flow conditions from process instrumentation to the fuel cell model and returning the thermal effluent dynamics to the HyPer fuel valve controller. This process is depicted in Figure 3.21 by the green dashed lines. When the model is integrated with HyPer's control platform, the measured mass flow (FE-380), temperature (TE-326) and pressure (PT-305) of the process air at the entrance of the plenum (V-301) are passed to the subsystem model. Based on these conditions and the setpoints entered by the operator, the subsystem model predicts the amount of heat that would be imparted to the air flow. This heat rate, $\dot{Q}_{sys}$, is sent to a reverse valve model to establish a demanded fuel valve position. The valve demand is then used to control the fuel flow to the actual hardware combustor (V-302).

This approach transfers one degree-of-freedom back to the hardware from the numerical model: the thermal response of the SOFC subsystem. However, this is sufficient for HILSs of a hybrid with HyPer. The turbine's response to the changing thermal output from the fuel cell stack is a dominating factor in hybrid performance. Furthermore, in an actual SOFC/GT hybrid the stack's flow impedance is set by the design and would not vary significantly during operation once the stack is heated. Finally, the response of the turbomachinery to changes in system pressure losses, either stand-alone or during a fuel cell HILS, can be investigated with the manipulation of HyPer's bypass valves.

The HILS methodology was first implemented on the existing AtlasPC controller. After that was accomplished, the dedicated simulation platform, dSPACE, was added to HyPer's control system. The HILS wrapper program was then adapted for the new platform allowing it to execute a subsystem model during a HILS.

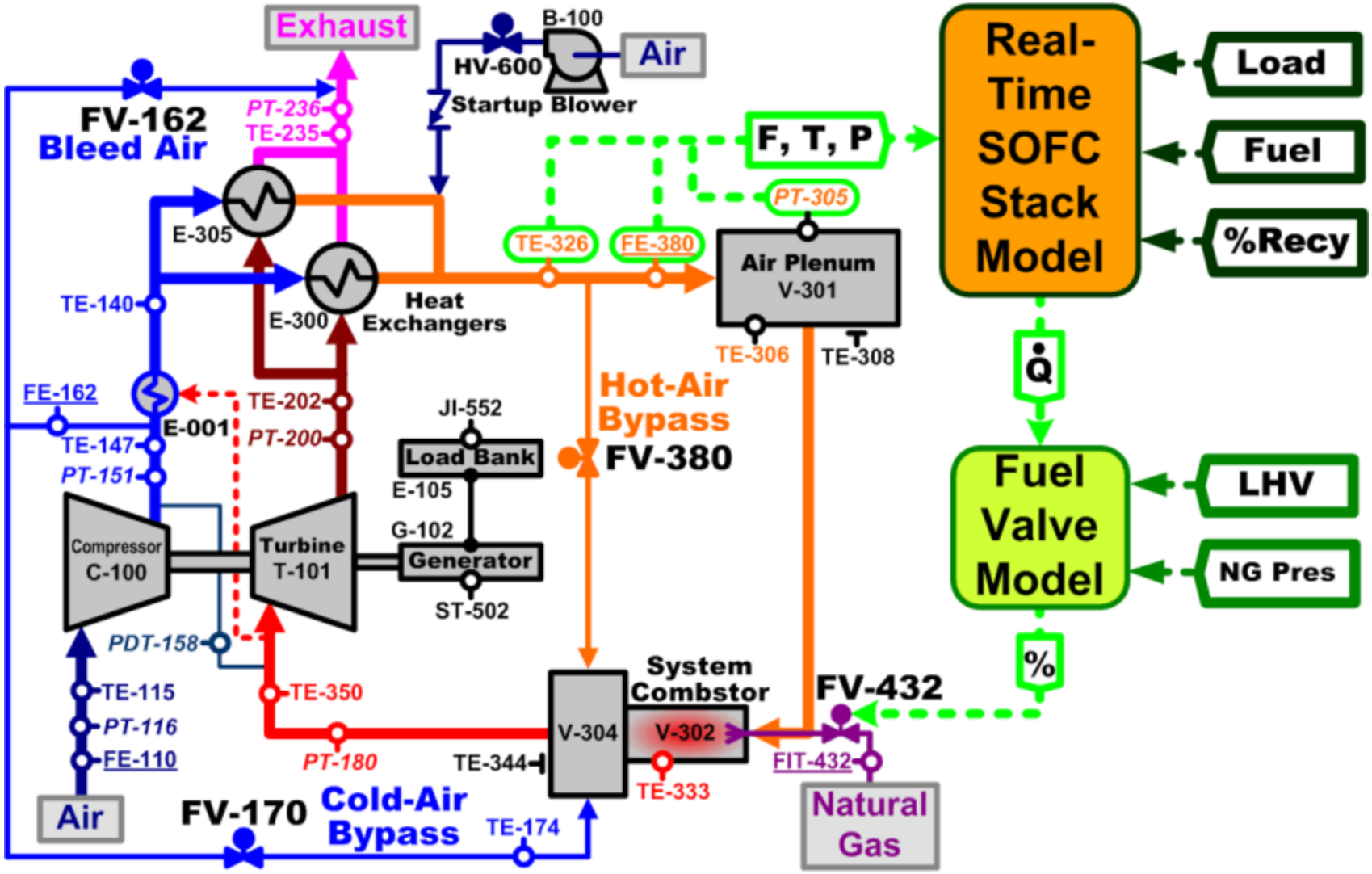

Figure 3.21: HILS Integration with HyPer

3.3.2: Model and Hardware Interfacing Adaptations

Several noteworthy adaptations were included in the HILS wrapper to facilitate the execution of the subsystem model during a HILS. These were primarily pre- and post-simulation modules that were required to condition the data for interfacing with the control system.

3.3.2.1: Measured Air Plenum Flow, Temperature, and Pressure

When the model is integrated with HyPer's control platform, the measured mass flow (FE-380) in kg/s, temperature (TE-326) in °C, and pressure (PT-305) in kPag of the process air at the entrance of the plenum (V-301) are input variables to the subsystem model. On either the AtlasPC controller or the dSPACE platform, the signals from the instrumentation are received by their respective ADC boards and scaled to the proper units. Since the measured data has inherent signal noise that may cause instability in the numerical model, the input data is processed slightly to smooth out large spikes. This is done with an exponential moving average with a time constant of 1 second. In Simulink a first-order transfer function is used on each signal to accomplish this.

An important adaptation for conducting HILS is an input selector switch on these measured HyPer variables. The switch on each signal is used to select between the measured data and a tunable user input. This is required since the execution of the numerical simulation is initiated with the startup of the control platform, before HyPer is operating. When the numerical simulation starts it is supplied the constant inputs so that it will execute in a stable manner. These default flow input parameters are given in Table 3.5. Once the system is operating, a HILS is started by tuning these user inputs to match the actual flow conditions and then switching over the live measured inputs.

3.3.2.2: User Inputs

Along with the plenum airflow conditions there are several user inputs that are used by the numerical simulation. The following input variables are all tunable by the operator during a HILS:

- Stack current demand, I_{cell}, or load in A
- Fuel flow to reformer, $\dot{m}_{fuel,ref}$, in g/s
- Fuel flow to C1, $\dot{m}_{fuel,C1}$, in g/s
- Anode-off gas recycle, λ, in percentage
- Heat capacity scalar, Γ, ranges from 0.1 to 1 (always 1 during a test)

Typical starting values for these parameter are given in Table 3.5.

3.3.2.3: Subsystem Heat Rate

A principal function of the subsystem model is to predict thermal effluent imparted to the simulated airflow. For a HyPer HILS, this is referred to as the heat rate, $\dot{Q}_{sys}$, in kW. This value is the change in enthalpy from the inlet to the exit of the subsystem on a rate basis. Therefore, the subsystem's predicted outlet air condition, as well as the measured inlet condition, is used in the heat rate calculation:

$$\dot{Q}_{sys} = \dot{m}_{air,sys,in.}\left[h(T_{air,sys,out.}) - h(T_{air,sys,in.})\right] \qquad [3.29]$$

The air enthalpy, h, values are tabulated from lookup tables embedded in the model. Ideal gas ideal gas behavior was assumed. This heat rate variable is calculated by a post-simulation module in the HILS wrapper program and is passed to the reverse fuel valve model.

3.3.2.4: Reverse Fuel Valve Model

The heat source in HyPer is the natural gas fueled combustor (V-302). To translate the model's predicted heat rate, $\dot{Q}_{sys}$, to combustion generated heat in HyPer, it must be converted to a fuel valve position. This is done by a reverse fuel valve model that outputs valve position demands that are used to dynamically control the Swift fuel valve in HyPer. In this way, the fuel flow is continually adjusted so that the combustor's heat output reflects the model's thermal effluent prediction.

The reverse fuel valve model is a Simulink module based on the characteristics of the Swift valve (FV-432) and was provided by the manufacturer, the Woodward Governor Company. Based on the inputs, the model utilizes empirical data from operational testing of the Woodward Swift valve to establish the proper valve position as a value between 0 and 100 % open. Along with the heat rate, the valve model requires the pipeline natural gas fuel conditions as input variables:

- Requested heat rate, $\dot{Q}_{sys}$, in kW
- Lower heating value of fuel in kJ/mole
- Molecular weight of the fuel in g/mole
- Temperature of fuel in °C
- Pressure of the fuel in kPag
- Pressure of the combustor's airflow in kPag

The heating value and molecular weight of natural gas fuel regularly varies on the NETL campus and is established by onsite gas analysis. The pressures and temperature are process variables monitored by the AtlasPC controller. The reverse fuel valve model is executed on the AtlasPC at an update rate of 5 ms to control the Swift valve through a

4-20 mA current loop signal. Along with the valve position demand, the reverse fuel valve model calculates the desired fuel flow, in g/s, so that it can be verified with the fuel mass flow meter in HyPer (FIT-432).

3.3.2.5: Turbine Speed Operational Band

During a HILS, the turbine rotational speed is allowed to respond to the fuel cell thermal transients. However, there exist operational limits on the upper and lower turbine speeds. These limits are hardwired into the safety control system and need to be avoided. Therefore, in the AtlasPC controller a "watchdog" program monitors the turbine speed and fuel valve demand during a HILS. If the turbine speed approaches one of the limits, the watchdog program will take over control of the fuel valve and end the HILS. It will then control the fuel demand to smoothly return the turbine speed to its nominal value, 40,500 rpm. In the AtlasPC, the lower operation band limit is set to 38,500 rpm and the upper limit is 43,000 rpm.

3.3.2.6: Model-in-Control Variable

When the fuel cell and reverse fuel valve models are controlling the fuel valve, it is referred to as "model-in-control". In HILS testing on HyPer, starting or ending model control of the fuel valve could be done multiple times. Particularly important to denote is the turbine speed operational watchdog automatically ends a simulation. Therefore, the AtlasPC controller generates a flag variable that is set to true for model control, and it is recored in the data logs.

3.3.2.7: Data Capture

During a HILS, there are both measured process variables and numerically generated model variables. Since different aspects of a simulation are captured in the

physical and virtual portions, the post-analysis of the data requires that data from both be integrated together. The HILS wrapper program was designed to pull the relevant data from the hardware and the model so that it would be captured in data logs in this fashion. Also, included in the wrapper program was the calculation of auxiliary variables that lend insight into the simulation, such as cell fuel utilization and efficiency.

On the AtlasPC system the data capture is limited by the computer's buffer so the logs can only run about 15 minutes. The addition of the dSPACE system allowed for larger data set with continuously streaming logs.

3.3.2.8: Time Pulse Variable

With the multiple control platforms (APACS, AtlasPC, and dSPACE), it is possible to have up to three different data logs recording at once. The analysis of a test may require combining the time series data from separate controllers. To facilitate this, a time pulse variable has been added to the data logs. For this variable, the APACS controller generates a pulse signal every 5 minutes that is recored by all three platforms. Later the pulses may be aligned for the data analysis.

3.3.3: Model Compiling and Control Platform Integration

As described previously, the numerical subsystem model and wrapper programs were created in the Simulink environment. Simulink is a graphical programming environment that was selected for its ease of model creation and for its existing tools for integration with controllers. Additionally, Simulink has the capability to incorporate existing programs via its S-function capability. For HyPer HILSs this will facilitate the inclusion of improved fuel cell models that may be created in languages such as C or Modelica.

The integration onto target computation systems, such as the AtlasPC, is done through the Simulink tool Real-Time Workshop. Once a model is created and tested, Real-Time Workshop is used to convert the graphical model to C code. It then compiles an executable program specifically for the target platform, as dictated by the target configuration file. The target configuration file is normally supplied by the manufacturer of the target platform. The AtlasPC target file, supplied by Woodward, directs Real-Time Workshop to create an executable that is designed to be integrated with the AtlasPC GAP environment. The GAP program is then compiled and uploaded to the AtlasPC controller and preforms the execution in the fuel cell real-time during a HILS. The dSPACE system is similar, but its real-time executable is a stand-alone program and is targeted for its platform, as described in Section 3.4.

When compiling the target executable program in Simulink there are several solver options that must be specified. The Simulink environment has a set of built-in ordinary differential equation solvers that facilitate the simulation of systems. A solver performs the numerical integration to compute the simulation's state variable based on the time derivatives programmed in the model. For example, in the fuel cell model, the cell temperature, $T_{cell,bulk}$, in Equation 3.20 is calculated by Simulink's integration solver. For conducting HILS, the solver must be configured to ensure the required real-time execution of the simulation. This means selecting a continuous fixed-step solver, usually an Euler's first order method since the time step are small. A higher order solver can be used, but it would require more computational loading. A simulation time step size must also be specified. It must be sufficiently small to retain accuracy in the simulation, but must be larger than the processor's turnaround time. For HyPer HILS with the AtlasPC

controller a fixed time-step of 40 ms was specified to match with requirements of the controller's GAP environment. When the subsystem model was complied for execution on the dSPACE platform (described in Section 3.4) the time-step was set at 10 ms.

3.3.4: Conducting HILS with HyPer

A HILS is conducted on HyPer by first starting up the system and operating under normal speed control while the vessels heat up. The protocol for starting the turbomachinery has been discussed previously in Section 3.1.4, and Appendix C presents a test plan from a HyPer HILS test. Additionally, during a HILS test, at startup of the numerical fuel cell model is initiated on either the AtlasPC or dSPACE platform. By default, the fuel cell simulation initiates with constant representative input flow conditions and user inputs that result in nominal operational state for the stack. Once started, the first step towards a HILS is to heat the vessels. This is done while the turbine speed is maintained at the nominal state of 40,500 rpm and 45 kW of electrical load is applied to turbine generator. Compressor bleed air can also be used at this stage to accelerate the heating process of the system vessels. The bleed air is normally closed before a HILS, when the heating process is completed. A target for establishing a steady condition is when the post combustor (V-304) skin temperature (TE-344) approaches 600 °C. The post combustor is the largest mass in the system, and requires the longest period of time to reach a steady state.

After the heating period, the process of transfer to “model-in-control” is begun. The first step is to manipulate the cold-air bypass to achieve the desired plenum airflow of 1 kg/s. A cold-air bypass setting of 27 % open normally provides the desired flow. At this point, the heat capacity scalar is reduced to 0.1 so that the simulated cell temperature

responds quickly. Next, the operator manually adjusts the simulated airflow rate, temperature and pressure to match the measured FE-380, TE-326, and PT-305, respectively. The matching ensures a smooth transition to measured data. Once satisfied with a reasonable match with the flow conditions, the operator then switches the modeled subsystem from the user inputs to the live measured flow conditions. At this point, the model subsystem is responding to changes in HyPer's flow conditions, but the combustor is still being operated with its normal speed controller.

The next step toward model control is to bring the reverse fuel valve model inline with the actual fuel valve position demand. This is accomplished by adjusting a tunable heat rate, $\dot{Q}$, input to the reverse fuel valve model until the model's output matches the actual valve position. This step establishes a target heat rate that is required by the fuel cell subsystem simulation. The model's user inputs, such as stack load or C1 fuel flow, are adjusted until the predicted subsystem heat rate, $\dot{Q}_{sys}$, matches the inputed value to the model. When this is achieved, the reverse fuel valve model input is switched to read the subsystem's $\dot{Q}_{sys}$ output, coupling the fuel cell and reverse fuel valve models.

The HyPer system is now prepared to transfer to model-in-control and to conduct a HILS. The last steps are to return the heat capacity scalar to 1 and to perform final fuel cell model user input adjustments. The adjustments may be required to fine tune the reverse fuel valve model position output to align it with the actual position. This is done to ensure a smooth transition in the combutor's firing level when switching to model control. The final switch toward model-in-control is implemented by the AtlasPC controller by taking the Swift fuel valve out of speed control and into reverse fuel valve model control. Previously, the reverse fuel value was set to receive the heat rate from the

fuel cell subsystem model. At this point, the numerical and physical systems are fully coupled for a HILS: the model is responding to measured flow conditions and the system combustor is firing according model's simulated heat rate.

With the model in control and operating at a near steady condition, the system is ready to conduct a dynamic HILS. Various perturbations, such as a current load change or bypass valve manipulation, can be introduced and the system response is observed over a period of time. After each specific test, the heat capacity scalar is temporarily reduced to quickly steady the cell temperature before the next test. Once the HILS is completed the Swift fuel valve is returned to speed control on the AtlasPC and the system is shutdown as described previously.

3.4: Implementation of Dedicated Simulation Computation Platform

The HyPer HILS methodology was initially developed and implemented by executing the numerical simulation on the AtlasPC controller. However, this approach had inherent issues that limited the HILS capabilities of the HyPer facility. There were three main concerns with utilizing the AtlasPC as the simulation target for HILS testing:

- The modest computational power of the AtlasPC would not accommodate the higher fidelity simulations that were desired.
- The memory buffer approach for data acquisition used by the AtlasPC controller limits the capture of process and simulation variables.
- The execution of an unstable numerical simulation could give rise to a processor “lock-up”. Since the AtlasPC is the fuel valve controller, this creates undesirable operational concerns.

For these reasons the decision was made to supplement HyPer's control system with a fourth system dedicated to handling the numerical simulations. To fulfill this enhancement, a high-speed computational system was identified, purchased, and installed alongside the existing controllers. The platform selected is a modular system manufactured by dSPACE Inc. and built around their DS1006 processor board designed specifically for numerically intensive simulations. Figure 3.22 diagrams the general layout of the HyPer control system and shows how the dSPACE platform relates to the other controllers.

3.4.1: Benefits of a Dedicated Simulation Platform

For HILS, a dedicated simulation platform provides a stand-alone computational system specializing in the execution of the numerical model. At the core of any HILS computational system is a high-speed processor operating a real-time kernel that manages the execution of the simulation. Supporting the processor are input/output components that interface the numerical simulations with the physical world. Additionally, the simulation platform is tied to a host computer via a communication link that provides a user interface for simulation management.

In particular, there are several clearly identifiable benefits to utilizing a dedicated computational platform for conducting HILS:

- Significantly increased capacity to handle complex and computationally intensive simulations, while maintaining the real-time requirement.
- Increased flexibility in the creation and modification of numerical models.
- Increased data acquisition capabilities that facilitate large data sets that record both simulation and process variables.

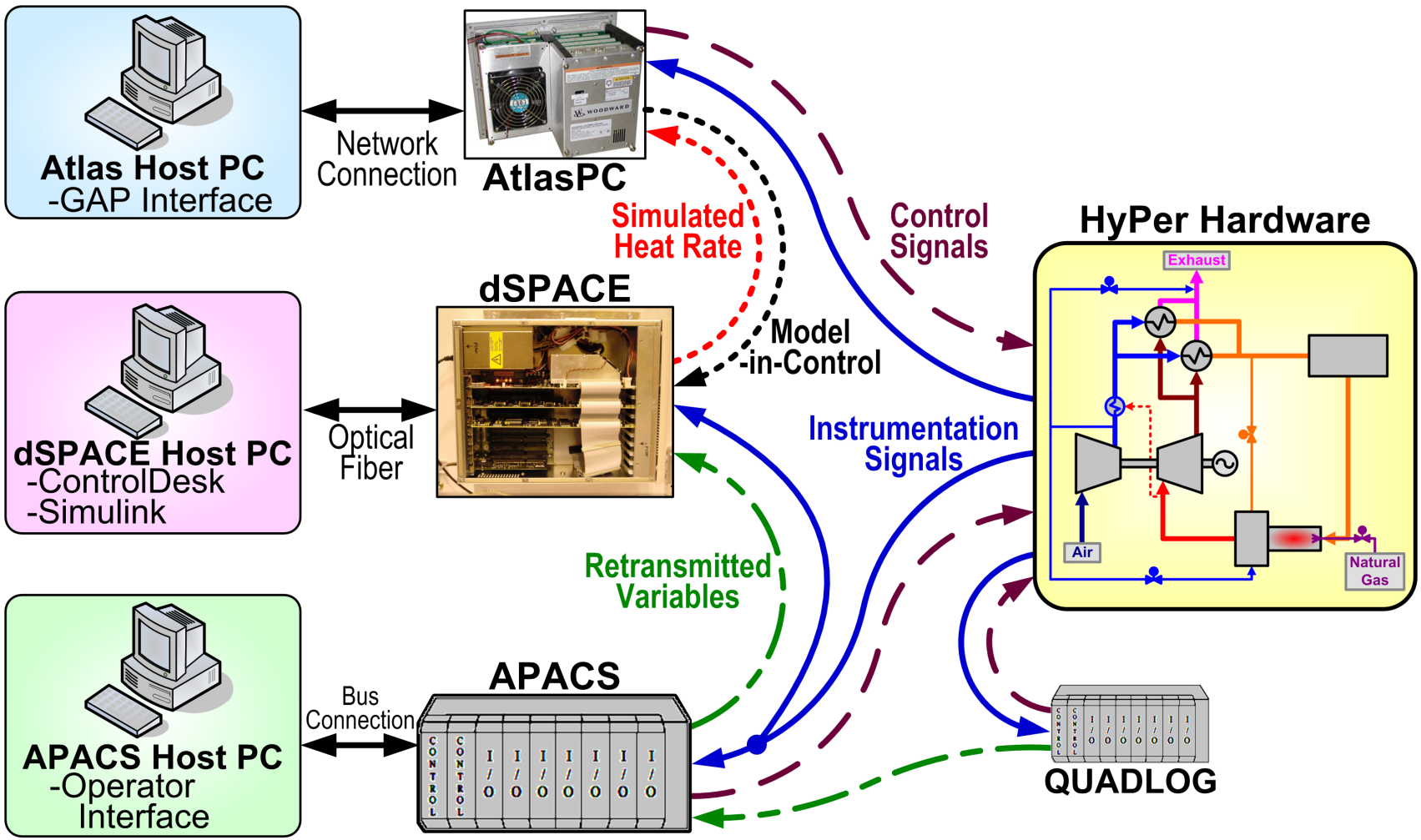

Figure 3.22: General HyPer Controller Layout for HILS

- Independent execution of the model from the hardware controller. This allows the numerical simulation to be stopped and restarted without interruption to the operation of the hardware system.
- More balanced delegation of operator duties while conducting HILS experiments since the PC host interfaces that control the numerical and hardware subsystems are separated.

These benefits provided a strong motivation for implementing a dedicated simulation platform with HyPer, thereby addressing the concerns raised with the AtlasPC HILS approach. Toward that goal, a computational platform had to be selected and a strategy for its integration with the existing hardware had to be designed and implemented.

3.4.2: dSPACE Modular System

After researching various simulation products, a modular system by dSPACE Inc. was identified as the preferred solution for providing HyPer with a computational target for HILSs. dSPACE's module systems are designed to provide optimum scalability and versatility for conducting complex real-time simulations in a laboratory setting. The base of dSPACE's modular system is the processor board model, which can be either part of a single-processor system or networked into a multiprocessor system for parallel computations. The modular approach also includes ADC and DAC boards to manage connections to external instrumentation and devices. The boards are encased in an expansion box that provides a backbone chassis and power supply. A link board is then used to connect the modular system with a host PC, which has dSPACE's experimental software installed.

The dSPACE system selected, purchased, and installed at NETL for HyPer is described below in more detail. The expandability of dSPACE's modular platform allows for the efficient implementation of additional capacity in the future. This is a key feature, since tasks assigned to the HyPer project are always evolving.

3.4.2.1: Computation Platform

The primary criteria in selecting the dSPACE platform was that the system must successfully handle the processor-intensive real-time calculations that form complex simulations. Designed specifically for that purpose, dSPACE's high end DS1006 processor board model was selected. To support the processor board, the rest of the platform includes a DS2002 ADC board for signal inputs, a DS2101 DAC board for output signals, and a PX10 modular expansion box to encase the system. Figure 3.23 is a photograph of the dSPACE modular hardware with the boards labeled.

3.4.2.1.1: Processor Board

The DS1006 is dSPACE's premier processor board for high performance simulation of processor intensive numeric models. The board is based on an AMD Opteron CPU operating at 2.2 GHz. The Opteron is the first widely available 64-bit processor, and it has a 1 MB L2 memory cache. The DS1006 board has a 256 MB local memory for executing models, a 128 MB global memory for data exchange with host PC, and a 2 MB flash memory to boot firmware. The board also has a high speed 32-bit bus to connect it with other boards in the system. The gray ribbon cable in Figure 3.23 is the bus cable connecting the DS1006 processor board with the ADC and DAC boards.

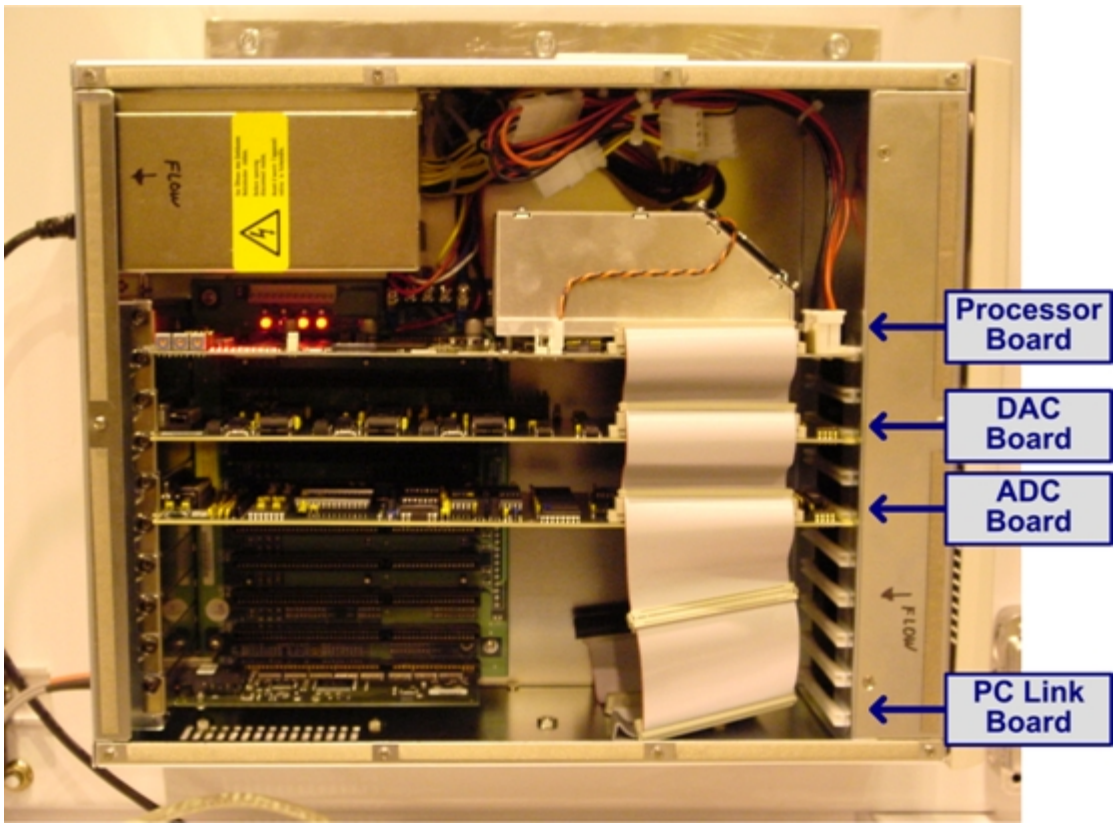

Figure 3.23: dSPACE Hardware

3.4.2.1.2: ADC Input Board

The DS2002 is a multi-channel ADC board that converts analog voltage signals to digital signals and then transmits them to the processor board. The board supports 32 input channels with up to 16-bit resolution. It can be scaled to span voltages from either +/- 5 V or +/- 10 V. The 32 channels share a common ground, instead of differential inputs, which presents challenges when connecting the board to multiple input sources. A 50-pin D-subminiature connector provides the physical access to external instrumentation. As discussed below, dSPACE provides software to configure and access the input signals for utilization during a simulation.

3.4.2.1.3: DAC Output Board

The DS2101 provides five parallel output channels that convert digital parameters to an analog voltage. Each channel drives voltages from +/- 5, +/- 10, or 0-10 V at 12-bit resolution. The 25-pin D-subminiature output connector allows the board to control external devices. As with the input board, the board can be configured and accessed by the numerical model ran on the processor.

3.4.2.1.4: Expansion Case and Host PC Link

The processor and input/output boards are supported and housed in a PX10 modular expansion case. The case contains the platform's power supply and cooling fans. The case's chassis provides 10 full-size 16-bit ISA slots to power and control the boards. Each slot supports a single board. To provide communication with host PC, a DS814 link board is included with the case. Correspondingly, the host PC is supplied with a DS817 PCI link board. A fiber-optic cable then connects the two link boards. The dedicated connection provides two-way 100 Mbit/s data transfer. This high-speed connection is key to streaming numerical data during an experiment from the dSPACE system to the PC for storage.

3.4.2.2: Simulation Design and Management Software

To support the DS1006 platform, dSPACE provides a suite of experiment software tools, referred to as ControlDesk and Real-Time Interface. Installed on the host PC, the dSPACE software works in conjunctions with Simulink in creating, compiling, and uploading the model to the target processor. During a simulation the program manages and interfaces with the execution of the model on the target processor. It also facilitates the storage of simulation data during a test.

3.4.2.2.1: ControlDesk

ControlDesk is a Windows based graphical user interface for managing simulations on the dSPACE platform. Through ControlDesk the operator uploads compiled models to the processor board, initiates and stops the simulation's execution, and interfaces with the model. The ControlDesk environment also has an editor for creating graphical layouts to interface with simulations. Figure 3.24 shows an example of an interface that was created to display the HyPer process variables that were tied into the dSPACE platform. The interface design function has a wide range of virtual instruments, to include numerical displays, control buttons, and input fields. The virtual instruments can be associated with any of the variables in a compiled Simulink model. To access the variables ControlDesk generates a variable index that corresponds with the structure and signals in the original Simulink model. The index is then viewed in a variable browser, shown at the bottom of Figure 3.24. ControlDesk also has the capability to plot live data from the simulation. Furthermore, it administers the storage of simulation data during testing.

3.4.2.2.2: Real Time Interface for Simulink

Real-Time Interface is a Simulink toolbox that supports the generation of simulation executables for the the target processor from Simulink models. Real-Time Interface handles the implementation and integration issues, allowing the programmer to focus on the formulation of the model. In Simulink, it provides the block representations of all the input and output boards. These blocks then handle the configuration and signal flow to provide a seamless interface with the physical world via the input/output boards. Once a model is created, the dSPACE software augments Simulink's Real-Time

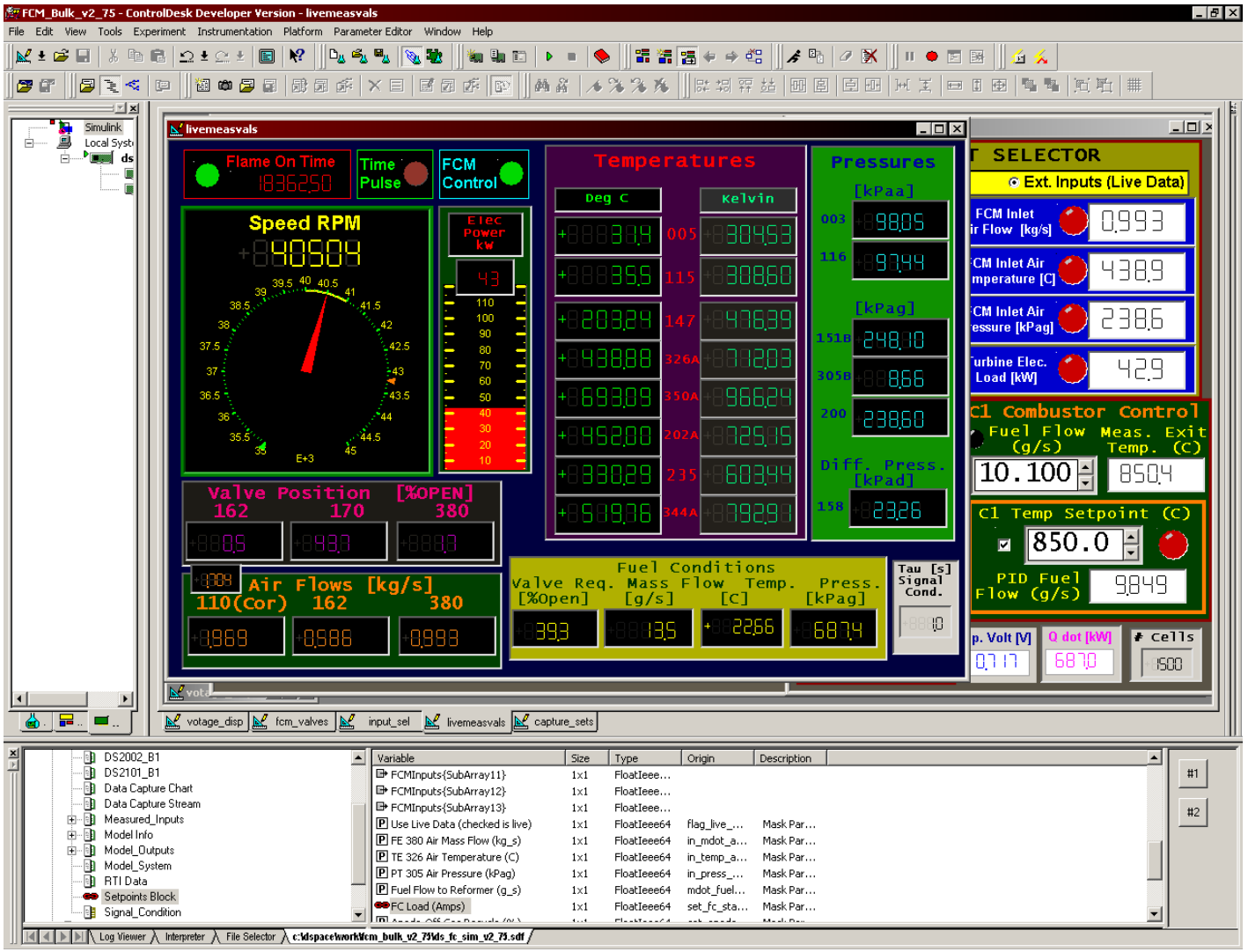

Figure 3.24: Graphical Interface Created in ControlDesk

Workshop to convert the graphical model to a target executable for the DS1006 board. Real-Time Workshop first generates C code and then initiates the compiler. To compile the code into an executable, a GNU C Complier is used that has been tailored for the DS1006 board. Last, the resulting simulation executable is transferred to ControlDesk where it is uploaded to the DS1006 target.

3.4.3: Integration of a dSPACE Platform with HyPer

Once acquired, the dSPACE platform required integration into the existing HyPer hardware and control systems. This included physically installing the system, but the primary concern was connecting the input and output boards to HyPer's existing controllers and instrumentation.

3.4.3.1: Installation of Computational System

The module expansion case was mounted into a signal cabinet located next to the turbine hardware. The cabinet houses the AtlasPC controller and the APACS input/output terminals. Electrical AC power to supply the dSPACE system was also added to the cabinet. To facilitate the connection of HyPer signal wires, two terminal blocks were mounted next to the dSPACE platform. The terminal blocks connect to the dSPACE ADC and DAC boards with D-subminiature cables. A host PC loaded with MATLAB/Simulink was added to the HyPer control room, and the ControlDesk suite was installed on it. The fiber optical cable was also strung to connect the two computers.

3.4.3.2: Interfacing with HyPer Controls and Instrumentation

The most challenging task in integrating the dSPACE platform with the existing HyPer control system was to properly design the wiring scheme. As previously

discussed, the existing APACS and AtlasPC controllers monitor more than 100 instrument signals, such as thermocouples. The dSPACE platform was connected to a subset of the existing instrumentation and required no new instrumentation. Instead, the computational platform was tied in to the existing framework for the APACS and AtlasPC controllers. The majority of the input connections to the dSPACE ADC board were accomplished two ways: by paralleling the existing instrumentation wire loop or by a retransmit of a process variable from APACS. Figure 3.22 diagrams the general layout of the HyPer control system and shows how the dSPACE platform relates to the other controllers. Additionally, the dSPACE system was configured with a single analog output to transmit the heat rate variable to the AtlasPC controller. This connection facilitates model control of the fuel valve during a HILS.

3.4.3.2.1: dSPACE Input and Ouput Variables

In total the dSPACE ADC board receives 29 input variables. Table 3.6 lists all the variables with details about the connection type and settings. The bulk of the inputs are temperatures, pressures, and flows. These process variables were selected to provide the thermodynamic conditions of the cycle. This includes the essential HILS inputs to the fuel cell model: the air plenum flow (FE-380), temperature (TE-326) and pressure (PT-305). To provide information HyPer's operating conditions the subset also includes turbine speed, electrical load, and valve positions. Additionally, to assist in managing the dSPACE data, the platform monitors the time pulse, flame indicator, and model-in-control flags. Listed last in Table 3.6 is the single output connection for the heat rate variable.

Table 3.6: HyPer dSPACE I/O Connections: Inputs to DS2002 ADC and Outputs from DS2101 DAC

Ch. #	Variable	Label	Units	Range	Signal	Connection method
In 1	Time pulse	T-pulse	Binary	0 or 1	0-5 V	APACS output: 0.8 s pulse every 5 min.
In 2	Flame indicator	BSS-450	Binary	0 or 1	0-5 V	APACS retransmits as analog output
In 3	Model-in-control of FV-432	YY-50	Binary	0 or 1	0-5 V	ATLAS analog output
In 4	Turbine speed	ST-502	rpm	0 - 50,000	0-5 V	APACS retransmits as analog output
In 5	Electrical load	JI-552	kW	0-120	0-5 V	APACS retransmits as analog output
In 6	Indicated BA position	ZC-162	%	0-100	1-5 V	Parallel 4-20 mA APACS input via 250 Ω
In 7	Indicated CAB position	ZC-170	%	0-100	1-5 V	Parallel 4-20 mA APACS input via 250 Ω
In 8	Indicated HAB position	ZC-380	%	0-100	1-5 V	Parallel 4-20 mA APACS input via 250 Ω
In 9	Inlet air flow	FT 110	kg/s	0-3	1-5 V	Parallel 4-20 mA APACS input via 250 Ω
In 10	Bypass air flow	FT 162	kg/s	0-1.5	1-5 V	Parallel 4-20 mA APACS input via 250 Ω
In 11	**Plenum air flow**	**FT-380**	kg/s	0-3	0-5 V	APACS retransmits as analog output
In 12	Fuel flow	FIT-432	g/min	0-1800	1-5 V	Parallel APACS input voltage
In 13	Fuel valve demand position	FV-432	%	0-100	1-5 V	ATLAS analog output via loop isolator
In 17	System pressure differential	PDT-158	kPad	0-70	1-5 V	Parallel 4-20 mA APACS input via 250 Ω
In 18	Ambient pressure	PT-003	kPaa	0-120	1-5 V	Parallel 4-20 mA APACS input via 250 Ω
In 19	Compressor inlet pressure	PT-116	kPaa	40-120	1-5 V	Parallel 4-20 mA APACS input via 250 Ω
In 20	Compressor outlet pressure	PT-151	kPag	0-400	1-5 V	Parallel 4-20 mA APACS input via 250 Ω
In 21	**Plenum pressure**	**PT-305**	kPag	0-400	1-5 V	Parallel 4-20 mA APACS input via 250 Ω
In 22	Turbine exit pressure	PT-200	kPag	0-20	1-5 V	Parallel 4-20 mA APACS input via 250 Ω
In 23	Fuel pressure	PT-436	kPag	0-1200	1-5 V	Parallel 4-20 mA APACS input via 250 Ω
In 24	Ambient temperature	TE-005	°C	0-100	0-5 V	APACS retransmits as analog output
In 25	Compressor outlet temperature	TE-147	°C	0-1100	0-5 V	APACS retransmits as analog output
In 26	**Plenum temperature**	**TE-326**	°C	0-1100	1-5 V	Parallel 4-20 mA APACS input via 250 Ω
In 27	Turbine inlet temperature	TE-350	°C	0-1100	0-5 V	APACS retransmits as analog output
In 28	Turbine exit temperature	TE-202	°C	0-1100	0-5 V	APACS retransmits as analog output
In 29	HEX hot side exit temperature	TE-235	°C	0-1100	0-5 V	APACS retransmits as analog output
In 30	Post-combustor temperature	TE-344	°C	0-1100	0-5 V	APACS retransmits as analog output
In 31	Fuel temperature	TE-422	°C	0-100	0-5 V	APACS retransmits as analog output
In 32	Compressor inlet temperature	TE-115	°C	0-200	0-5 V	APACS retransmits as analog output
Out 1	Simulated heat rate	Q-dot	kW	0-1000	0-5 V	Analog signal out to ATLAS

3.4.3.2.2: Input Connection Methods

In HyPer, as is common in industrial controls, the instrumentation utilizes 4-20 mA current loops for analog signaling. The current loops are used for their reliability and immunity to electrical noise. However, the dSPACE ADC board requires voltage analog inputs. Therefore, for each dSPACE input a 250 Ω resistor was used to generate a voltage signal that is properly ranged for dSPACE. In this arrangement, each input channel of the terminal block is wired to measure the voltage drop across the resistor. For an input signal that was configured to parallel the existing instrumentation wire loop the resistor was placed in series with the instrument at the input terminal of APACS, as diagrammed in Figure 3.25. This results in a 1-5V signal to the ADC board which corresponds with the 4-20 mA instrument signal. A second approach was to have a process variable retransmitted from APACS to dSPACE, In this case the resistor was placed across the terminals of an APACS channel for a 0-5 V signal, as diagrammed in Figure 3.26. After the dSPACE ADC board resolved the analog voltages to digital values, the simulation then scaled them into engineering units by the appropriate conversion.

Two connections utilizing loop isolators were installed to transfer signals from the AtlasPC to dSPACE. These were to transmit the demanded fuel valve position and model-in-control flag. The loop isolator was necessary to electrically separate the two controllers. The isolators were powered by the APACS system and connected to dSPACE by the paralleling resistor configuration. Additionally, for the single simulation output, the dSPACE DAC board was directly connected to an analog input channel on the AtlasPC.

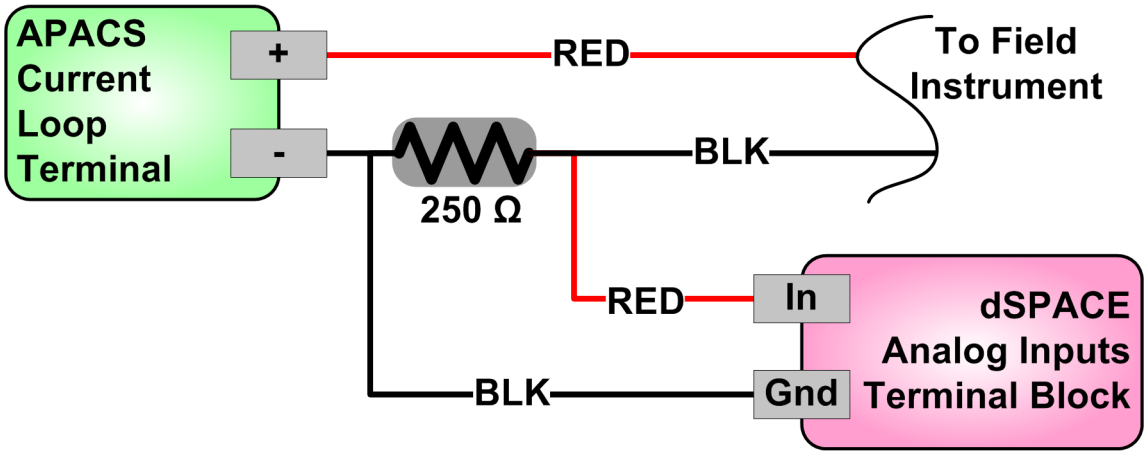

Figure 3.25: General Wiring Diagram for dSPACE Paralleling a Signal

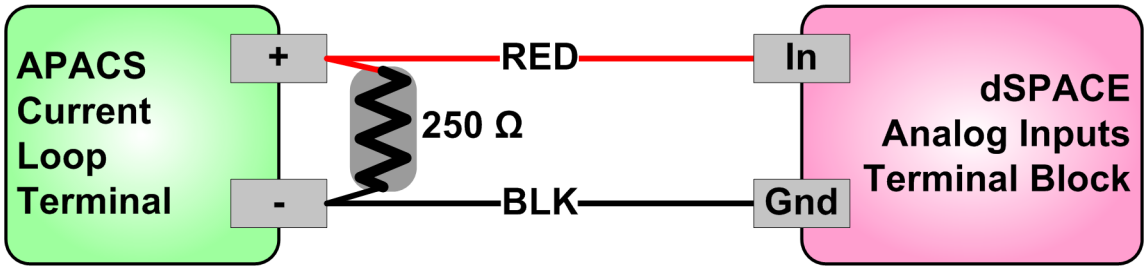

Figure 3.26: General Wiring Diagram for dSPACE with APACS Retransmit

3.4.3.2.3: Input Signal Noise Issue

The high resolution voltage inputs of the dSPACE ADC board are sensitive to signal noise. Unfortunately, the environment of the HyPer controller cabinet has a high level of background electrical noise. Furthermore, a second source of noise is generated by the APACS platform. It overlays a digital signal on the current loops for additional communications with instrumentation. Both of these factors created a noticeable level of signal noise on the dSPACE inputs. To counter the noise, software filters were employed to smooth the data for this project. Nevertheless, a more thorough solution would have been to install a low-pass hardware filter to reduce the noise.

3.4.4: Bulk-Parameter Model Implementation on dSPACE

After installation, the dSPACE system was tested to ensure that the process variables were correctly transmitted to and accessed by a numerical simulation. Also, sample simulations were conducted to gain familiarity with the computational capabilities of the system and its ControlDesk software. The platform was then ready to fulfill its role as the dedicated simulation target for HILS with HyPer.

For initial HILS testing with dSPACE, the bulk-parameter fuel cell model developed for the AtlasPC controller was used. Adapting the original Simulink fuel cell subsystem model to the new platform was fairly straightforward. It entailed modifying the input and output of the model to accommodate the dSPACE method. This included the insertion of the programming blocks for the dSPACE ADC and DAC boards. Additionally, programming was done to handle the added dSPACE signal inputs. Next, a ControlDesk graphical interface was created, as seen in Figure 3.20, to control the numerical simulation during a HILS test. Finally, HILS experiments were performed

with dSPACE executing the numerical simulation and interfacing with the other HyPer controllers. Results from these experiments are presented in the next chapter. Their successful completion demonstrates the utility of the dedicated simulation target approach with HyPer. Furthermore, it completed the goal of expanding HyPer capabilities for conducting more complex numerical simulations.

3.5: HILS Testing of Hybrid Systems

As described in this chapter, implementing HILSs of a SOFC/GT hybrid with the HyPer facility was a multi-faceted endeavor, involving collaboration from a number of individuals. The HyPer facility was initially developed with around a Garrett Series 85 APU gas turbine and pressure vessels to simulate the volume of a SOFC stack. The control platforms and instrumentation outlined in this chapter are essential for HyPer operation and carrying out experimental testing with it. Toward conducting HILSs, a numerical model of a SOFC subsystem was customized for execution on the turbine control system. The model calculates the thermal responses of a SOFC stack based on the flow conditions in the operating hardware. The physical and computational components interact in real-time to realistic model dynamic system behavior. Finally, descriptions of HILS methodology implemented with HyPer and the installation of the dSPACE computer as a dedicated simulation platform represent a substantial step towards higher fidelity and more insightful hybrid simulations.

The next chapter will focus on the experimental results from several HyPer tests conducted to demonstrate the efficacy and value of HILS for evaluating SOFC/GT hybrid performance.

CHAPTER 4: RESULTS

Several sets of experiments were performed to demonstrate the functionality of the HyPer facility in evaluating SOFC/GT hybrid systems through HILSs. The HILS approach of combining turbine hardware with computational fuel cell models to simulate a hybrid system was validated by conducting and evaluating transient experiments. The imposed transients represent conditions that would commonly occur in the operation of a hybrid system. All tests presented here utilized the bulk-parameter fuel cell subsystem model and the HyPer procedures outlined in the previous chapter. In the first set of experiments the numerical simulation was executed on the AtlasPC controller. The first set of tests evaluated the response of the hybrid system to fuel cell load demand changes. In a second set of tests, the dSPACE platform was employed as the simulation target. This test demonstrated the increased HILS functionality the dSPACE system brings to the HyPer facility. In the dSPACE experiment, fuel cell load transients were tested, as in the first test, with additional variations in the test conditions. This chapter presents the results from these sets of HILS experiments.

4.1: Fuel Cell Stack Load Change Simulation with AtlasPC Controller

The initial HILS experiment with HyPer was to validate the developed simulation methodology. Beyond demonstrating HILS with HyPer, this test also evaluated the impact of the fuel cell load change on a hybrid system. In the test, the simulated current

drawn from the numerical stack model was altered by approximately 5 %. During the testing the combined responses of the hardware and numerical simulations were observed. For this experiment, the bulk parameter dynamic SOFC subsystem model described in the previous chapter was executed on HyPer's AtlasPC controller. During the transients numerous physical measurements and numerical variables were recorded with the AtlasPC. Analysis of these experimental results illustrates how HyPer HILS experiments can be used in evaluating SOFC/GT hybrid dynamics and performance. This results discussed in this section were previously presented in Smith (2006).

4.1.1: AtlasPC HILS Test Conditions

The HyPer hardware was started and heated as described in Section 3.1.4. Before the startup, the AtlasPC controller was loaded with a control program that included the fuel cell subsystem model outlined in Section 3.2. For this experiment, the number of cells was set at 1500, which established the cell heat capacitance, shown in Table 4.1. The turbine was loaded with 45 kW of electrical power and a turbine speed of 40,500 rpm was maintained by the controller before the HILS portion of test began. A cold-air bypass valve setting of 27 % open was used to give the 1.23 kg/s of plenum airflow, and this valve position was held for the remainder of this study. The hot-air bypass and bleed air valves were closed during the testing. After the post combustor was

Table 4.1: Fuel Cell Stack Physical Parameters for Load Change Test

Parameter	Value
Number of cells (connected in series)	1500
Total stack mass, m_{stack}	2100 kg
Heat capacity of stack, $C_{p,stack}$	993 kJ/K

heated to a near steady condition, the inputs to the fuel cell simulation were switched from constant values to live measured flow conditions. To initiate the HILS configuration, the system's combustor was placed in model-in-control mode; the turbine's rotational speed was then in an open-loop scenario, meaning it was able to float within safety limits. This allowed the speed to react to any variations in turbine inlet temperature that resulted from thermal changes in the fuel cell subsystem.

Before the initiation of a transient, the numerical simulation and the hardware were at steady operation. The approximate conditions of the fuel cell model during the tests are specified in Table 4.2. These represent the initial conditions, since many of the parameters change significantly during imposed transients. The simulation was started with a simulated current demand of 307 A on the fuel cell at approximately 0.75 V. This

Table 4.2: Fuel Cell Model Approximate Initial Values for Load Change Test

Parameter	**Value**
Fuel flow to reformer (CH_4), $\dot{m}_{fuel,ref}$	11 g/s
Load current, I_{cell}	307 A
Anode off-gas recycle level, λ	70 %
Cell voltage, V_{cell}	0.75 V
Stack power, $\dot{W}_{stack.}$	345 kW
Stack fuel utilization, $U_{F,stack}$	87 %
Cell per pass fuel utilization, $U_{F,pass}$	67 %
Stack oxygen utilization	13 %
Stack efficiency (LHV), $\eta_{TH,stack.}$	62.5 %
Cell reaction efficiency (LHV), $\eta_{TH,rxn}$	59.8 %
Cell temperature, $T_{cell,bulk}$	872 °C
Stack air inlet temperature, $T_{air,ca,in}$	800 °C
Stack air exit temperature, $T_{air,ca,out}$	929 °C

results in 345 kW of simulated fuel cell power and an actual 45 kW electrical load on the gas turbine.

In this experiment, a steady-state operating condition was perturbed by decreasing the current drawn from the stack by approximately 5 % from 307 to 292 A. A 5 % change was selected since it caused a sufficient disturbance in the system while the uncontrolled turbine speed remained within the operating band. All other control parameters were held constant. Most notably, the simulated level of fuel input to the reformer was maintained, and therefore the heating value of the reformed fuel passed to the fuel cell remained essentially unchanged. Additionally, the C1 pre-combustor was simulated with a constant exit temperature setpoint. This maintained a cathode air inlet temperature of 800 °C throughout the test.

After the current demand perturbation, the system was operated at the new current demand for 800 s. This allowed for the thermal responses to approach a new steady condition following the load change. Then the current demand was stepped back up, and the system was allowed to respond over an equivalent amount of time. Last, the simulation was terminated by implementing a turbine speed control recovery procedure.

4.1.2: Current Demand Decrease by 5 % with Constant C1 Temperature

As depicted in Figure 4.1, at time equal to zero the stack current was decreased by 15 A from 307 A. The voltage swiftly rose in response to the lower current density. As the transient progressed, the voltage drifts down slightly due to modest decreases in cell temperature and air pressure. Since these current demands were near the broad peak of the cell power curve, the total stack electrical power did not change significantly, as shown in Figure 4.2, and remained just under 350 kW. However, at the lower current a

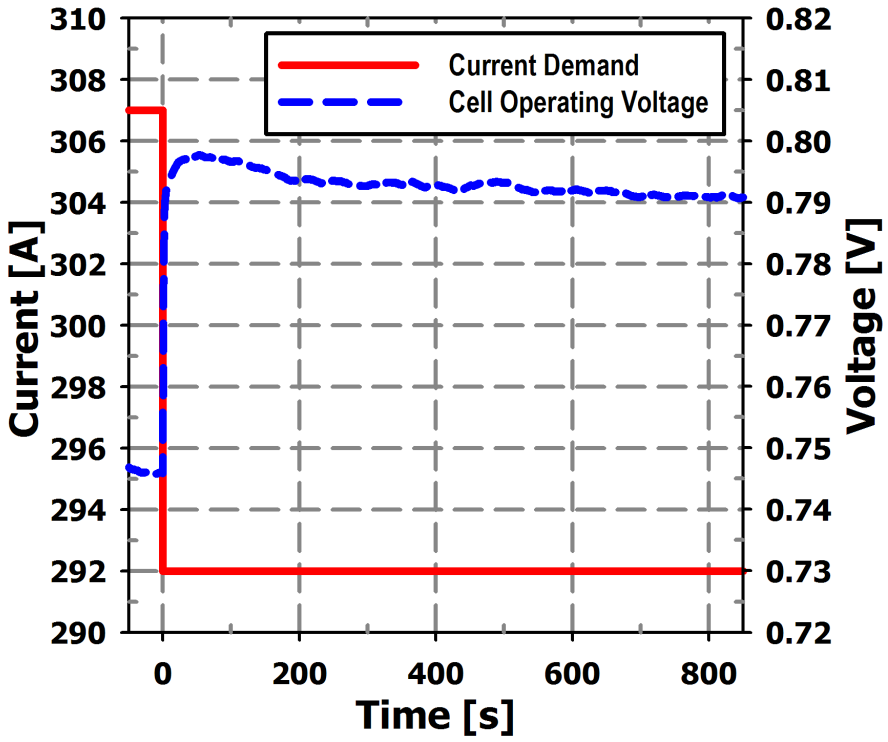

Figure 4.1: Cell Voltage Response to a Current Decrease with Constant C1 Temperature

lower percentage of fuel was being utilized, therefore the per-pass fuel utilization was lowered; this is depicted as the fuel cell H_2 utilization in Figure 4.3. Furthermore, since the level of anode off-gas recycle and fresh fuel flow to the reformer remained constant, the overall stack fuel utilization decreased from 87 % to 82.7 %. This increased the heating value in the anode off-gas being supplied to the simulated C2 post-combustor, thereby increasing the air temperature rise across it. In addition, the temperature difference between the cell and air that establishes the heat transfer rate is slow to change. This is due to the large thermal capacitance of the stack that resists changes to the cell temperature. The compound result was a swift increase in the predicted level of thermal effluent from the numerical subsystem, as shown by Figure 4.2. This level of thermal

effluent is the heat rate, $\dot{Q}_{sys}$,that is replicated by the firing level of the physical combustor.

In order to reflect this change in simulated exit air temperature, the AtlasPC controller then demanded an increase in fuel supplied to the turbine's combustor, resulting in a higher turbine inlet temperature, as shown in Figure 4.4. The turbine responded with a quick increase in rotational speed, and an increase in air mass flow through the system was observed, as shown in Figure 4.5. System pressures were shown to be highly correlated to turbine speed as indicated in Figure 4.6.

After this initial transient, a thermal response on the order of 800 s took place. With decreased stack byproduct heat generation at the lower current, the fuel cell started to cool, as shown in Figure 4.7. While the level of stack heat generation was decreased immediately with the current change (see Figure 4.2) the large thermal capacitance of the stack dampens the change in the heat transfer rate from the cell to air. During this transient, the stack was releasing stored sensible heat as it reached a new equilibrium temperature. Stack cooling was initially compounded by the increased plenum air flow from the initial increase in turbine speed. As the stack cooled there was a corresponding reduction in turbine inlet temperature, reversing the initial turbine speed transient, and the system came to equilibrium close to the initial conditions.

The return to initial turbine operating conditions arose from simulating the fuel cell at its power curve peak. When operating near the broad maximum of the stack power curve, a change in current demand has little effect on fuel cell power output. While the increase in operating voltage indicates an increase in electrochemical reaction efficiency, the voltage gain is offset by the reduced fuel utilization. In this case, the

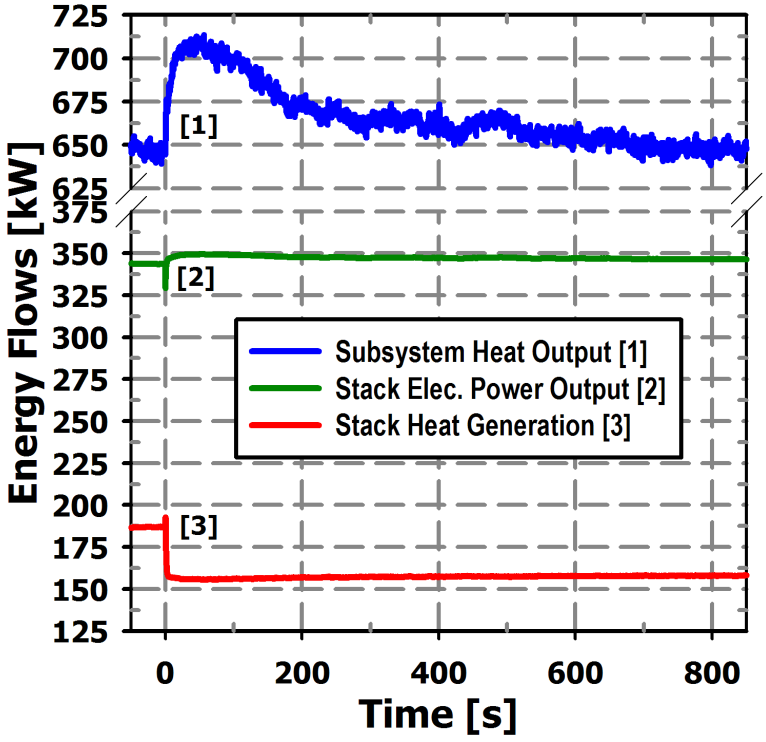

Figure 4.2: Energy Output of Subsystem in Response to Current Decrease with Constant C1 Temperature

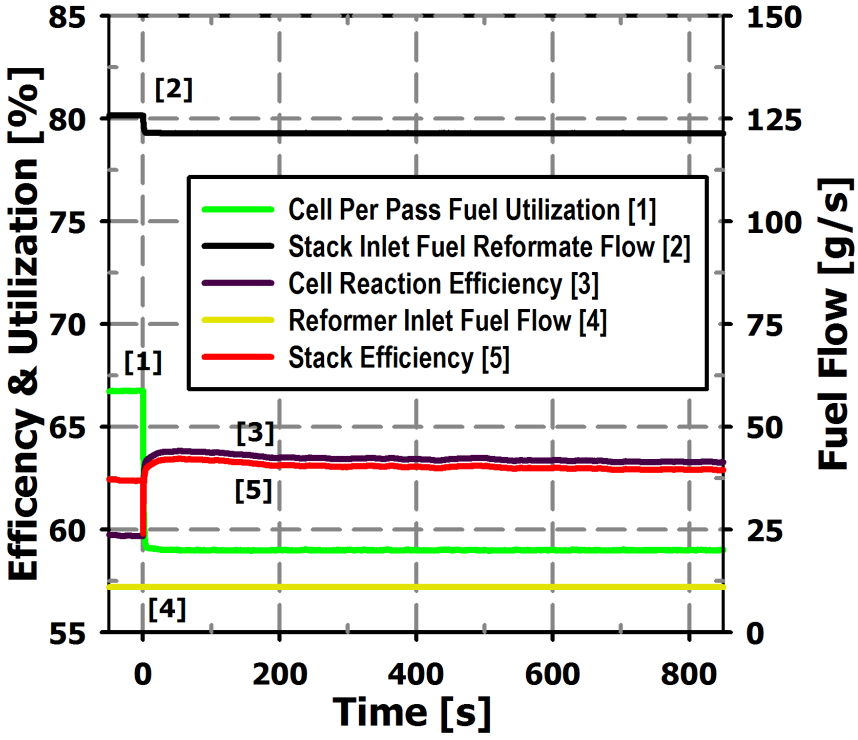

Figure 4.3: Stack and Fuel Conditions in Response to Current Decrease with Constant C1 Temperature

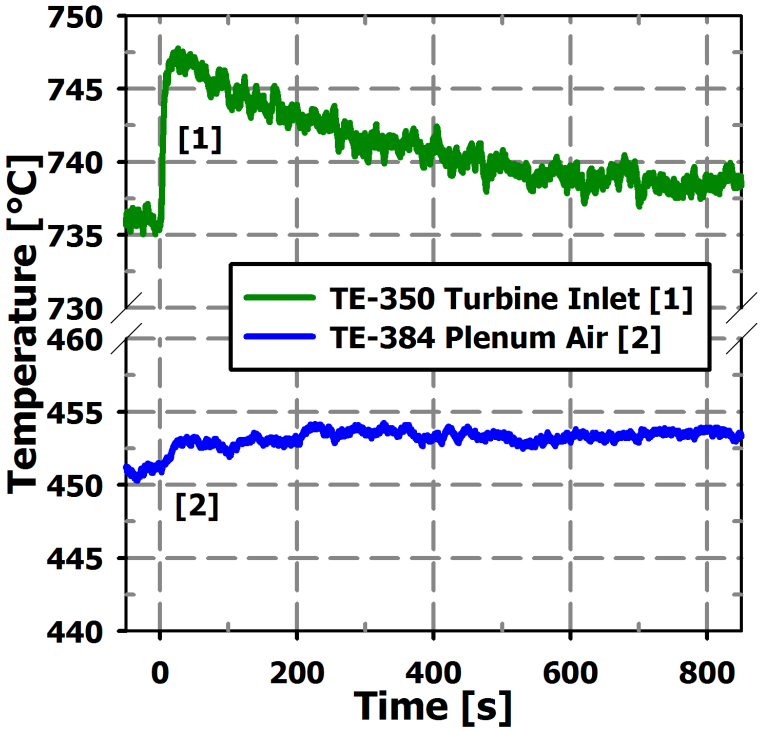

Figure 4.4: Air Temperature Response to Current Decrease with Constant C1 Temperature

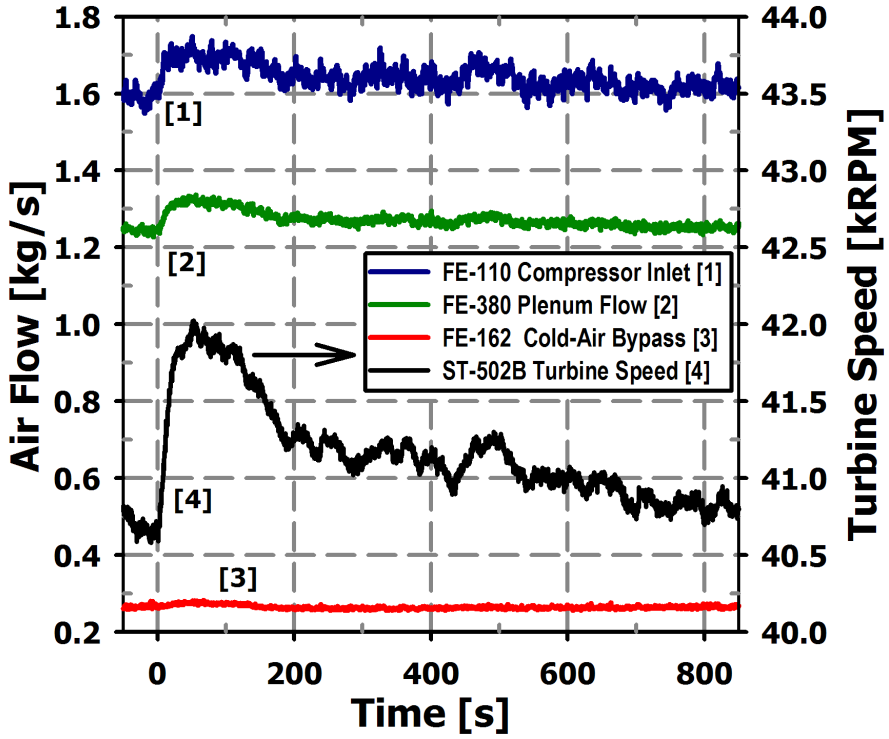

Figure 4.5: Airflow and Turbine Response to Current Decrease with Constant C1 Temperature

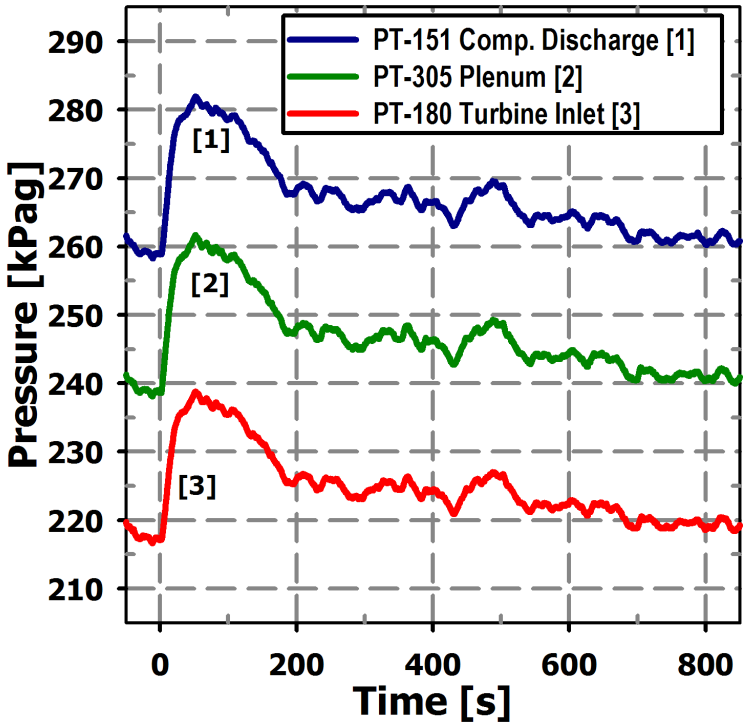

Figure 4.6: Air Pressure Response to Current Decrease with Constant C1 Temperature

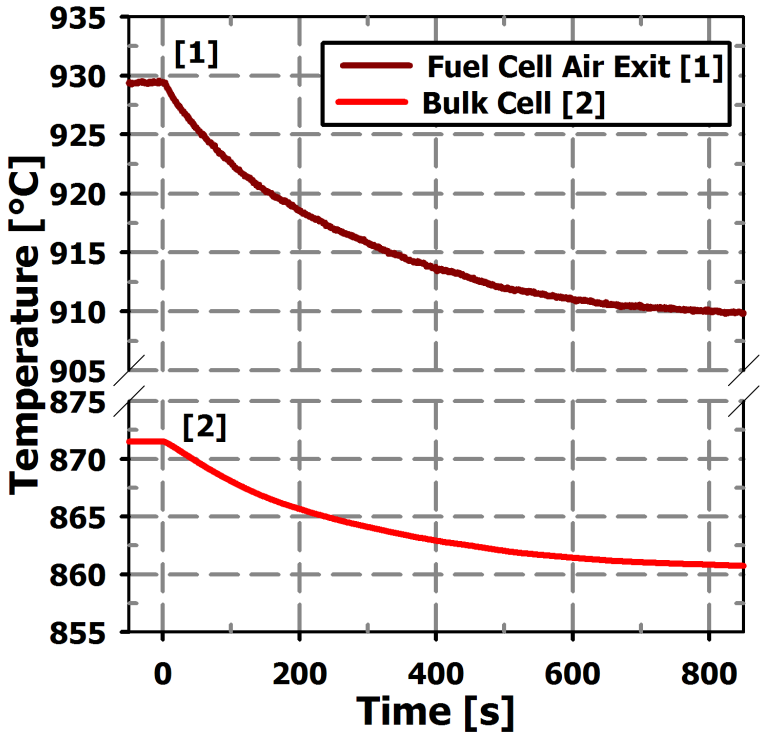

Figure 4.7: Cell Temperature Response to Current Decrease with Constant C1 Temperature

overall stack efficiency, which is a function of both voltage and fuel utilization, is approximately 62.5 % before and only slightly higher after the current change. Therefore, with a sufficient amount of time the thermal input to the turbine from the simulated fuel cell subsystem will return to near its initial level.

4.1.3: Current Demand Increase by 5 % with Constant C1 Temperature

The complementary test to the load decrease is a 5 % load increase. In this experiment, the steady operating condition was perturbed by increasing the current drawn from the stack from 292 to 307 A. This was done at time equal to zero in Figure 4.8. All other control parameters were held constant. The voltage trend almost mirrors that observed in Figure 4.1. First it dropped quickly from 0.79 V to 0.74 V, and then slightly recovered as the cell temperature rises and the plenum air pressure rises. Again, the

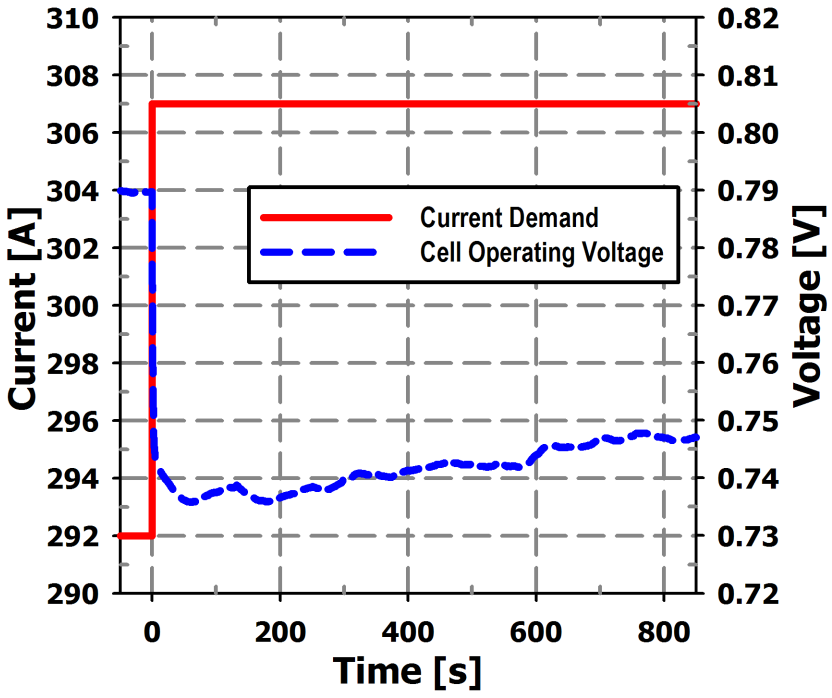

Figure 4.8: Cell Voltage Response to a Current Increase with Constant C1 Temperature

current demands were near the broad peak of the cell power curve, so the total stack electrical power did not change significantly and remained just under 350 kW, as shown in Figure 4.9. However, at the higher current an increase in the fuel utilization was observed as shown in Figure 4.10. Therefore, the anode-off gas has a lower heating value, reducing the energy input into the simulated C2 post-combustor. The result was a swift decrease in the predicted level of thermal effluent from the numerical fuel cell subsystem. In order to reflect this thermal change, the AtlasPC controller then commanded a decrease in the fuel valve position, resulting in a lower level of combustion, thereby reducing the turbine inlet temperature. Less fuel was then available to the C2 post-combustor, and turbine inlet temperature was deceased, as illustrated in Figure 4.11. The turbomachinery responded with an expected decrease in rotational speed as shown in Figure 4.12. This figure also shows that the compressor inlet flow followed the turbine speed and decreased. The system pressures were again highly correlated with turbine speed, as shown in Figure 4.13.

After this initial transient, the fuel cell temperature begins to rise with increased stack byproduct heat generation, as shown in Figure 4.14. As expected, stack heating was initially compounded by the decreased compressor air flow, but since the air flow reduction was less significant, the cell temperature leveled off more quickly (almost 200 s earlier) than for the current demand decrease. In the case of a current demand increase, the turbine inlet temperature, and associated speed and compressor flow, reached or exceeded the initial conditions. These trends indicate that a steady condition was not fully achieved in the first 800 s as was observed in the previous transient.

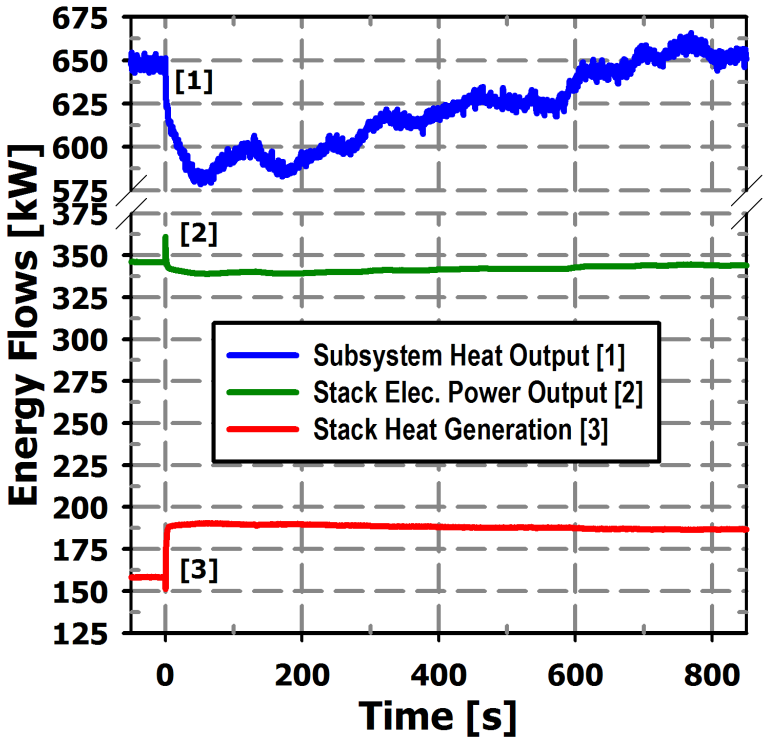

Figure 4.9: Energy Output of Subsystem in Response to Current Increase with Constant C1 Temperature

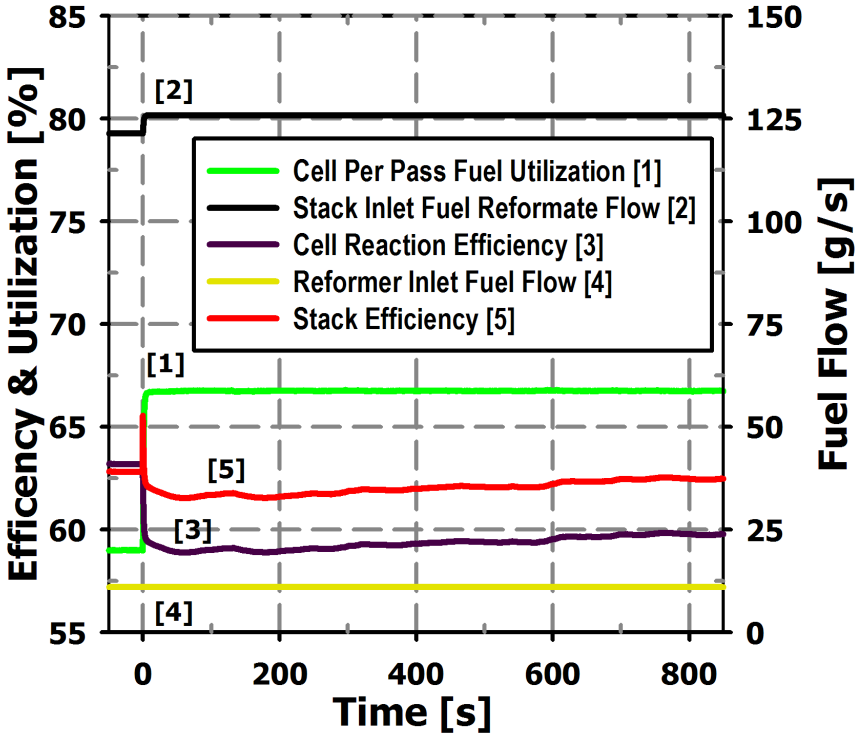

Figure 4.10: Stack and Fuel Conditions in Response to Current Increase with Constant C1 Temperature

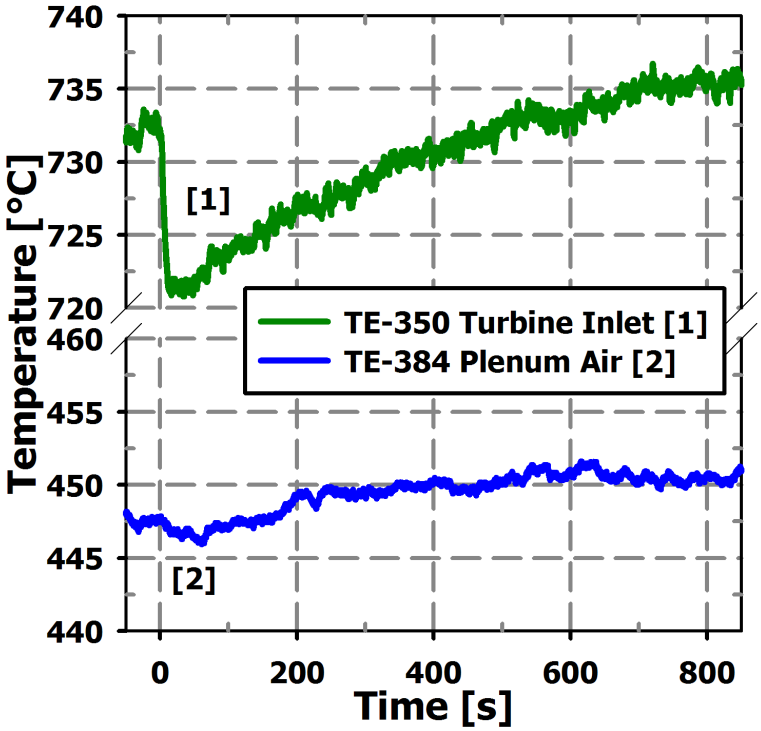

Figure 4.11: Air Temperature Response to Current Increase with Constant C1 Temperature

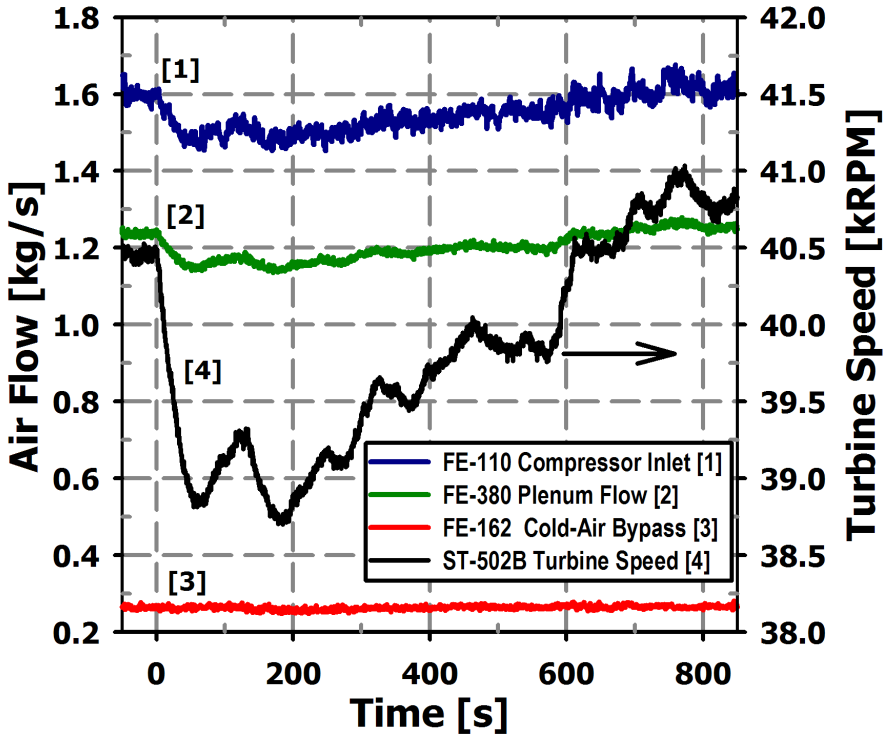

Figure 4.12: Airflow and Turbine Response to Current Increase with Constant C1 Temperature

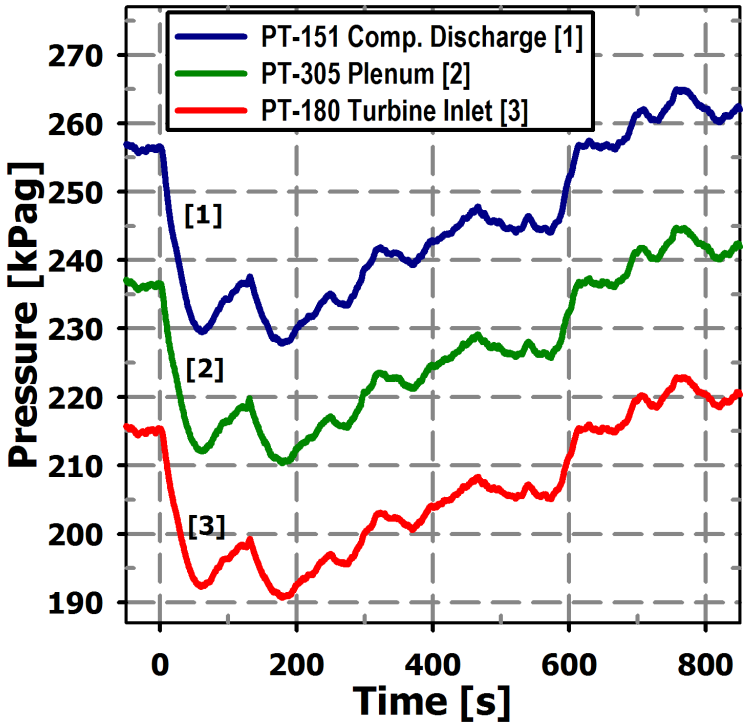

Figure 4.13: Air Pressure Response to Current Increase with Constant C1 Temperature

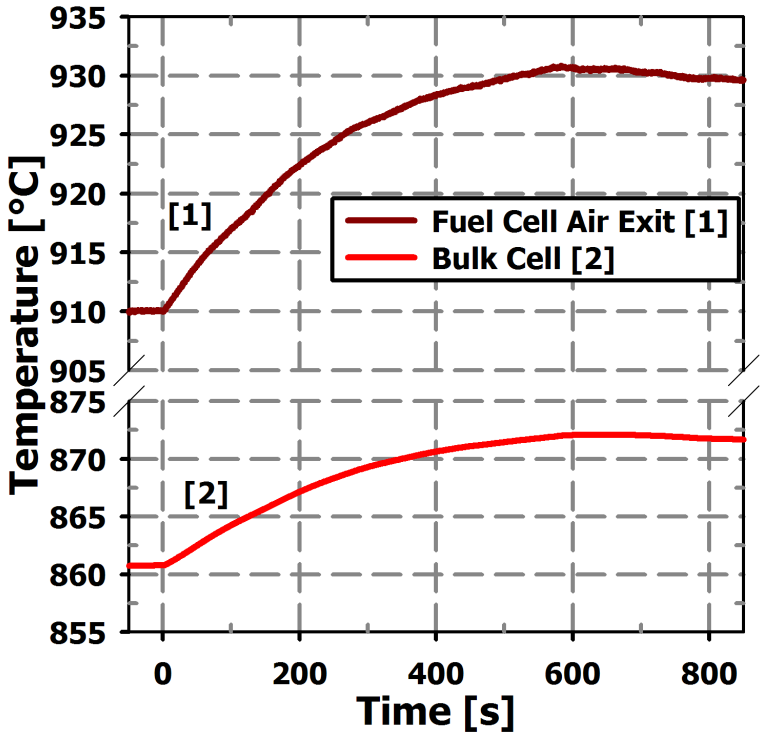

Figure 4.14: Cell Temperature Response to Current Increase with Constant C1 Temperature

4.1.4: Stack Load Change Transient Observations

The observed results of these HILS experiments showed the successful coupling and interaction between the gas turbine hardware and the numerical subsystem model. This initial experiment demonstrated that the HyPer system combustor can be controlled by a numerical model that responds to flow conditions in the hardware. Furthermore, several insights into SOFC/GT hybrid operation were gained by conducting this set of stack load change experiments.

4.1.4.1: Performance of the HILS Approach

A primary goal of these tests was to demonstrate that the computational model responds to the real-time data from the hardware and then properly commands the turbine's fuel value based on the simulated thermal output of the model. The fuel cell load transient perturbations showed that gas turbine hardware will respond to a simulated fuel cell subsystem though control of the system's fuel valve. This was seen by the rapid change in turbine inlet temperature and turbine rotational speed. The alteration in turbine speed effects the airflow rate through the compressor which supplies the process air to the system. This results in the physical turbine response being feedback to the numerical fuel cell through the changes in the plenum flow conditions.

To evaluate the numerical simulation's control of the combustion heat generation in HyPer, the relative change in several parameters was investigated. Figure 4.15 shows the relative response of the parameters from their initial values. The initial values were taken as a 40 s average (500 samples) before the transit initiating event. The driving variable in this plot is the heat rate, which is the predicted thermal effluent from the modeled subsystem. It showed a 9 % spike in response to the simulated load change

decrease. For the HILS approach the critical factor is that the relative change and dynamics of the natural gas fuel flow (FIT-432) are similar to the heat rate variable. Figure 4.15 shows a strong correlation between the two. The plot also shows that the valve only has to open slightly more than 6 % to get the desired 9 % change in fuel flow. An additional observation is that at the 45 kW electrical loading, the turbine speed increased only 3 % in response to the 9 % fuel increase; however it did respond quickly to the thermal changes.

Likewise, Figure 4.16 plots the relative change of the same variables for the current increase case. The results show performance similar to the current decrease case. One difference is that the second simulation showed a pronounced oscillation imposed over the 800 s thermal transient. While its source has not been accounted for, this oscillation has been observed in previous non-HILS testing on HyPer.

4.1.4.2: Hybrid Performance Insights

For this set of experiments, several factors were identified as having an impact on SOFC/GT hybrid performance. It was found that a load change in the SOFC stack will initiate a quick change in turbine inlet temperature because of a change in the unutilized fuel going to the fuel cell subsystem anode off gas combustor. The turbine speed will rapidly respond accordingly, and system pressures and flows are in turn highly correlated with the turbine speed. Then, the large thermal capacitance of the fuel cell stack will dominate as the transient continues. Because the fuel cell was operated near its power peak, the overall steady-state energy balance on the simulated subsystem was not changed significantly. This has the effect of returning the system components to their initial conditions.

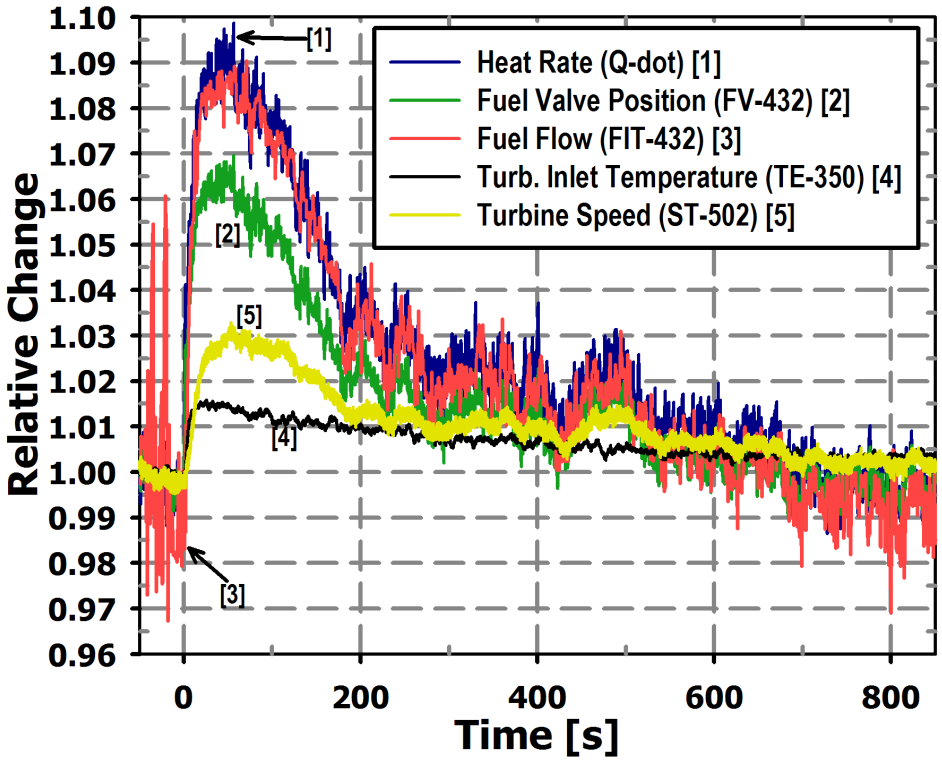

Figure 4.15: Relative Change in Variables in Response to a Current Decrease

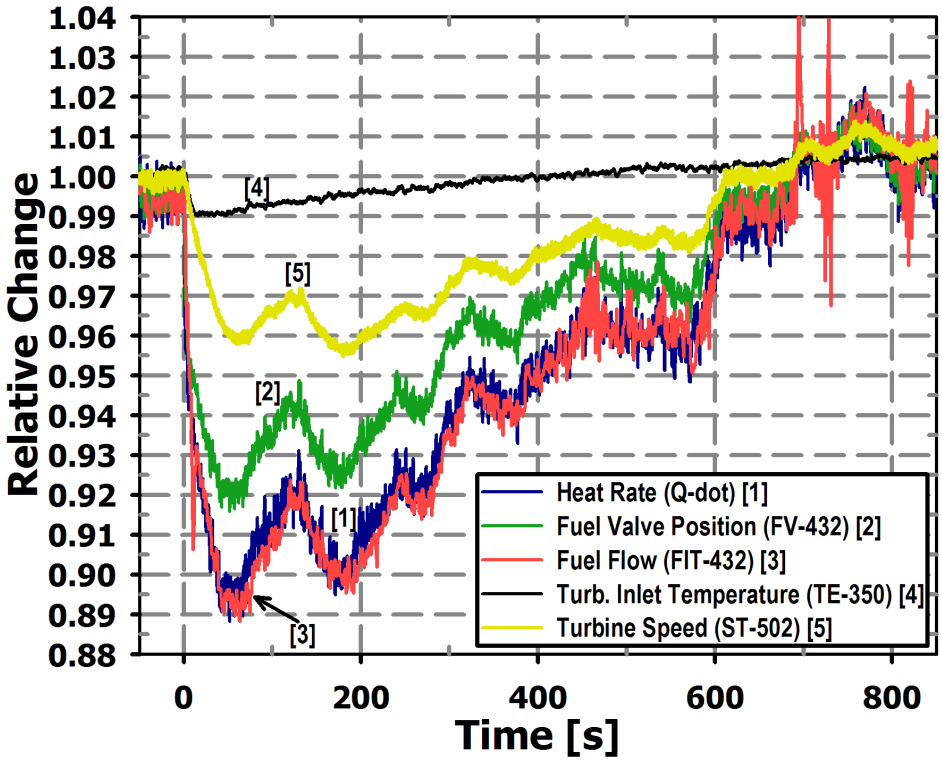

Figure 4.16: Relative Change in Variables in Response to a Current Increase

Although little change in system energy input and output was realized during the current demand transients, significant short-term responses were observed that indicate challenges for hybrid system control. For example, since the cathode air and the anode fuel may be at different pressures, sharp changes in plenum pressure (cathode air) may introduce undesirable stresses in the cell material. Furthermore, if maintaining a constant turbine speed is desired, then secondary speed control methods must be integrated into hybrid system designs.

As this transient event progressed, the fuel cell temperature slowly changed over time. This can be attributed to both the alteration in the airflow supply rate to the stack and the rate of heat generation in the cell due to a change in the level electrochemical losses at a different current. As the stack reached a new steady state temperature, the total predicted thermal output from the simulated section recovered. The corresponding recovery was seen in the turbine inlet temperature and speed. This long term transient is an anticipated characteristic of hybrid systems given the large thermal capacity of a fuel cell stack.

During this set of tests the simulated C1 pre-combustor was set to exit temperature control at the setpoint of 800 °C. This maintained a numerically simulated constant temperature air flow into the fuel cell stack. The model therefore modulated the simulated C1 fuel flow rate to heat the air to the required setpoint. The required heating would depend on the varying rate and temperature of the airflow entering the air plenum. While the C1 fuel flow parameter was not recorded in this set of experiments, it was recognized after the test that it would greatly affect the system, as it accounted for approximately half of the thermal input in the modeled subsystem. Therefore, in future

HILS testing the C1 fuel flow rate was held constant at its initial value throughout a transient to minimize its impact. Nevertheless, this initial set of HyPer HILS experiments illustrated the capabilities of the facility in combining turbine hardware with computational fuel cell models to simulate a hybrid system.

4.2: Fuel Cell Stack Load Change Simulation with dSPACE Platform

With the installation of the dSPACE platform, the HILS approach utilizing a separate computation platform on HyPer required validation. Furthermore, the dSPACE platform facilitates more detailed simulations, improving the evaluation of a fuel cell load change impact on a hybrid system. As with the previous HILS tests where the model was executed on the AtlasPC, a set of fuel cell load change tests were performed to test the dSPACE method. In the three sets of tests, the simulated current drawn from the numerical stack model was reduced by 5 % or 20 %. The first test was similar to the AtlasPC test except that simulated fuel flow to the C1 pre-combustor was held constant during the transient. The second test was also a 5 % current reduction, but in this case stack fuel flow was reduced to maintain a constant fuel utilization. A third test evaluated a more significant 20 % current reduction with the addition of a load-based control scheme to manage the rotational speed of the turbine. This test demonstrated how variable electrical loading on the turbine can be used to maintain a constant rotational speed in a transient.

For this experiment, the bulk parameter dynamic SOFC subsystem model described in the previous chapter was executed on HyPer's dSPACE platform. In this test the dSPACE system successfully received measured data from the other controllers,

executed the numerical subsystem in real-time, and transmitted the thermal heat rate to the AtlasPC controller. During the testing, the combined responses of the hardware and numerical simulations were recorded by the dSPACE system. Analysis of these experimental results illustrates how the dSPACE platform expands HyPer HILS functionality in evaluating SOFC/GT hybrid dynamics and performance.

4.2.1: dSPACE HILS Test Conditions

The HyPer hardware was started and heated as described in Section 3.1.4. Before the startup, the dSPACE platform was loaded with the numerical simulation of the fuel cell subsystem model outlined in Section 3.2. For this experiment, the number of cells was set at 1500, which established the cell heat capacitance, shown in Table 4.1. The numerical time step of the simulation was specified as 0.01 s. The dSPACE system was also set so that the numerical and measured variables were streamed to and recorded by the host PC at a 0.25 s sample rate. Additionally, before system startup, the onsite natural gas was evaluated and found to have a heating value of 845.3 kJ/mol and a molecular weight of 16.97 g/mol. These parameters were entered into the reverse fuel valve model on the AtlasPC.

Once started, the turbine was loaded with 45 kW of electrical power, and a turbine speed of 40,500 rpm was maintained by the controller before the HILS portion. A cold-air bypass valve setting of 44 % open was used to give the 1.01 kg/s of plenum airflow, and this valve position was held for the remainder of this study. The hot-air bypass and bleed air valves were closed during the testing. After the post combustor was heated to a near steady condition, the inputs to the fuel cell simulation on the dSPACE platform were switched from constant values to live measured flow conditions. Next, the AtlasPC was

set to monitor the subsystem model output heat rate, $\dot{Q}_{sys}$, being sent from the dSPACE platform. Then, to initiate the HILS configuration, the system's combustor was placed in model-in-control mode, creating an open-loop scenario for the turbine's rotational speed, which meant it was able to float within safety limits. This allowed the speed to react to variations in turbine inlet temperature that result from thermal changes in the fuel cell subsystem. The various transient tests then could be performed.

Before the initiation of each transient test, the numerical simulation and the hardware were returned to the initial conditions and allowed to reach steady-state operation. The initial conditions of the fuel cell subsystem model are specified in Table 4.3. These values were attained with a 100 s (400 samples) average of the parameters before the first transient test. For these tests, the fuel cell stack was started with a simulated current demand of 390 A to produce 419.7 kW of electrical power. This resulted in 699.1 kW of simulated thermal effluent being produced by the modeled subsystem. This heat rate level was being thermally targeted in the hardware by control of the fuel flow to the combustor. With this level of thermal input and a 45 kW electrical load on the turbine the resulting steady operating conditions are presented in Table 4.4. Under these conditions the compressor was producing 1.96 kg/s of flow at a pressure ratio of 3.56. Through the cold-air bypass 0.58 kg/s of flow was diverted directly to the post combustor, leaving 1.01 kg/s for the air plenum. The discrepancy in the flow values arises from the stab pipe loss of approximately 0.2 kg/s and a suspected under-measurement of the plenum flow by an estimated 0.2 kg/s (see Appendix B). At this operating point, the 200 °C cold-air bypass flow also significantly lowered the turbine inlet temperature. From the predicted 1038.9 °C modeled subsystem output, which the

Table 4.3: Initial Steady-State Numerical Simulation Values for dSPACE Test

User Input Parameter	**Value**
Fuel flow to C1 (CH_4), $\dot{m}_{fuel,C1}$	10.1 g/s
Fuel flow to reformer (CH_4) $\dot{m}_{fuel,ref}$	15.18 g/s
Load current, I_{cell}	390 A
Anode-off gas recycle level, λ	75 %
Hardware Input Parameter	
Inlet air mass flow rate, $\dot{m}_{air,sys,in.}$ (FE-380)	1.01 kg/s
Inlet air temperature, $T_{air,sys,in}$ (TE-326)	434.6 °C
Inlet air pressure, $P_{air,sys,in}$ (PT-305)	242.0 kPag
Model Outputs	
Heat rate from subsystem, $\dot{Q}_{sys}$	699.1 kW
Heat generation rate in stack, $\dot{Q}_{stack.,gen}$	216.9 kW
Cell voltage, V_{cell}	0.718 V
Stack power, $\dot{W}_{stack.}$	419.7 kW
Stack oxygen utilization	25.0 %
Stack fuel utilization, $U_{F,stack}$	80.1 %
Cell per pass fuel utilization, $U_{F,pass}$	50.1 %
Stack fuel flow rate, $\dot{m}_{fuel,an,in.}$	206.2 g/s
H_2 mole fraction fuel in, $x_{H2,in}$	0.532
H_2O mole fraction fuel in, $x_{H2O.in}$	0.134
CO_2 mole fraction fuel in, $x_{CO2.in}$	0.333
Cell temperature, $T_{cell,bulk}$	947.1 °C
Stack air inlet (C1 exit) temperature, $T_{air,ca,in}$	850.7 °C
Stack air exit temperature, $T_{air,ca,out}$	1028.5 °C
Reformer air exit temperature	881.7 °C
Subsystem air exit temperature, $T_{air,sys,out}$	1038.9 °C
Stack efficiency (LHV), $\eta_{TH,stack.}$	55.2 %
Cell reaction efficiency (LHV), $\eta_{TH,rxn}$	57.4 %
Simulated system efficiency (LHV), $\eta_{TH,sys}$	36.6 %

Table 4.4: Initial Steady-State Hardware Conditions for dSPACE Test

User Setting	**Value**
Turbine electric load (JI-552)	45 kW
Cold-air bypass valve (ZC-170)	44 % open
Hot-air bypass valve (ZC-380)	0 % open
Bleed air valve (ZC-162)	0 % open
Model Controlled Setting	
Fuel valve position (FV-432)	39.7 %
Fuel flow to combustor (FIT-432)	13.86 g/s
Measured Parameter	
Turbine rotational speed (ST-502)	40,540 rpm
Compressor flow (FE-110)	1.96 kg/s
Bypass flow (FE-162)	0.58 kg/s
Plenum flow (FE-380)	1.01 kg/s
Compressor discharge pressure (PT-151)	251.5 kPag
Plenum pressure (PT-305)	242.0 kPag
Compressor inlet temperature (TE-115)	30.8 °C
Compressor discharge temperature (TE-147)	200.8 °C
Plenum air temperature (TE-326)	434.6 °C
Turbine inlet temperature (TE-350)	687.1 °C
Turbine exhaust temperature (TE-202)	446.4 °C
Post combustor metal temperature (TE-344)	512.0 °C

system's combustor fuel supply rate was targeting, the measured turbine inlet (TE-350) was 687.1 °C.

Each of the three tests involved perturbing the steady operation with a decrease in the current demanded from the fuel cell stack. After the current demand perturbation, the system was operated at the new current demand for 1000 s. This allowed for the thermal responses to approach a new steady condition following the load change. After completing the testing, the simulation was terminated by implementing a turbine speed control recovery procedure and the system was shutdown.

4.2.2: Current Demand Decrease by 5 % with C1 Fuel Flow Constant

In this experiment, a steady-state operating condition was perturbed by decreasing the current drawn by approximately 5 % from the stack from 390 to 370.5 A, as depicted in Figure 4.17. A 5 % change was selected since it caused a sufficient disturbance in the system while the uncontrolled turbine speed remained within the operating band. In this test, the C1 pre-combustor was set to simulate a constant fuel flow, as opposed to exit temperature control as in the AtlasPC load change test. The simulated level of fuel input to the reformer was maintained at a constant level. Figure 4.18 shows that the electrical power generated by the stack was reduced by 5 kW from the current reduction and voltage decrease as the cell cooled. The small spike in the fuel cell power plot at the instant of the load change is due to the numerics of the model, since it takes a single time step for the voltage to respond to the load change. This figure also plots the turbine electrical loading, which was held constant for this test.

As in the AtlasPC load change test, the response of the subsystem model was to swiftly increase the predicted heat output, $\dot{Q}_{sys}$, as plotted by Line 1 in Figure 4.19. This

figure also plots the heat transfer rates in each component of the modeled subsystem. It shows that total subsystem heat rate (Line 1) is the sum of the heat transfer rates from the C1 pre-combustor (Line 2), the fuel cell stack (Line 3), the reformer (Line 4), and the C2 post-combustor (Line 5). As denoted C1 was set to a constant fuel flow so its heating contribution remains constant during the transient. In steady-state operation the heat transfer from the stack (Line 3) to the air equals the stack heat generation (Line 6). The stack heat generation, $\dot{Q}_{stack.,gen}$, is tied to the current demand and makes a step decrease with it. However, the rate of heat transfer from the stack is driven by the temperature difference between the cell and the air. Therefore, following the initial event the heat transfer from the cell was greater than the heat generation as the cells released sensible heat. Over time, the stack heat transfer rate approached the generation rate as the system reached a new steady-state condition. The heat removed by the reformer (Line 4) remained constant at 175 kW, since the amount of fuel to be reformed did not change. Finally, the C2 post-combustor rate of contribution is traced by Line 5. As with the AtlasPC load change test, the C2 heating showed a step increase as more fuel went unutilized after the current decrease.

The effect from the load change on the gas turbine hardware is shown in Figure 4.20. The turbine rotational speed (Line 4) increased in response to the additional thermal input. The increased speed led to a slight increase in system airflows. While the effect on airflow rate is modest, the performance of the hybrid system is particularly sensitive to changes in process airflow. Additionally, as expected the cell temperature slowly decreased, reducing the heat transfer from the cells and the heat rate from the subsystem. Therefore, over time the turbine speed approached its initial value.

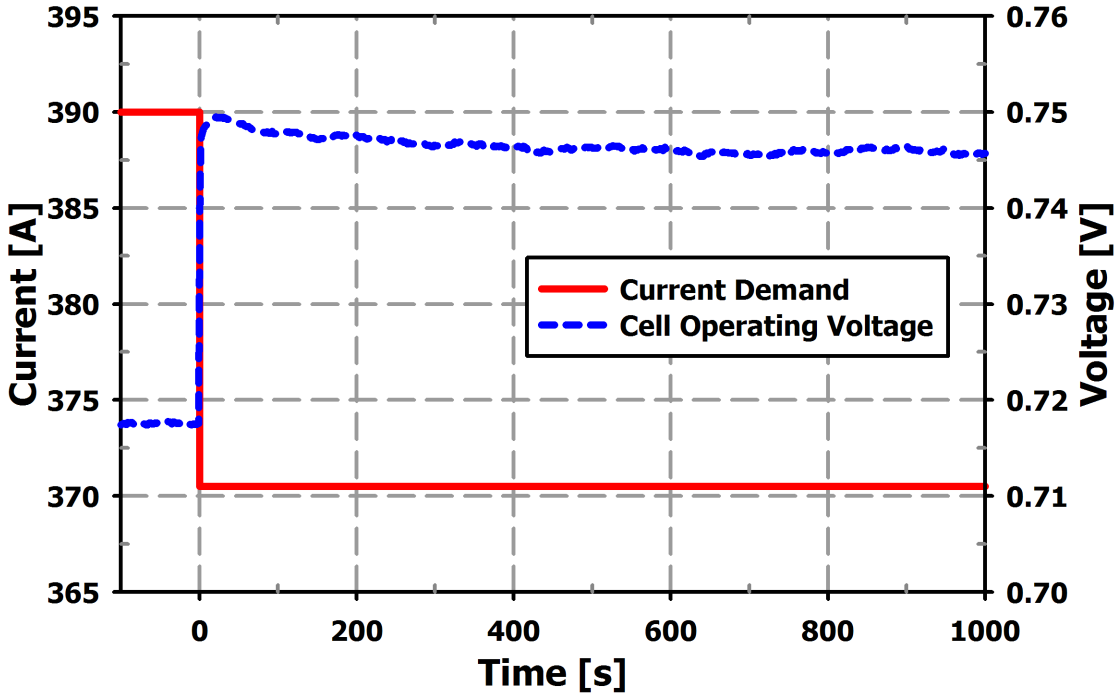

Figure 4.17: Cell Voltage Response to a 5 % Current Decrease with C1 Fuel Flow Constant

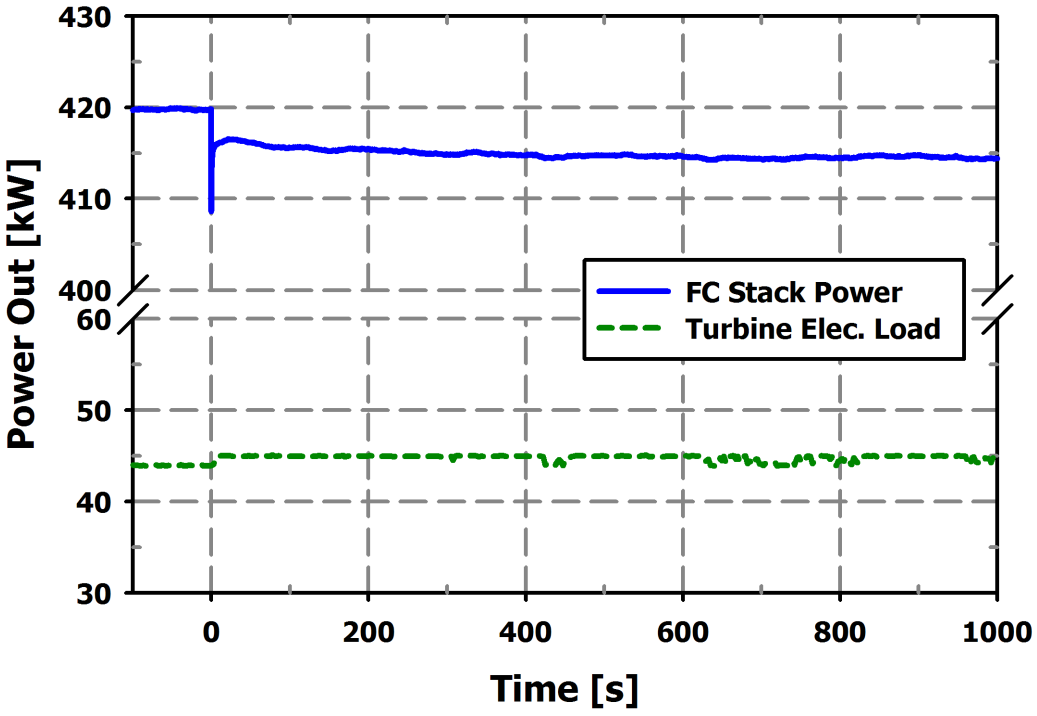

Figure 4.18: Power Response to a 5 % Current Decrease with C1 Fuel Flow Constant

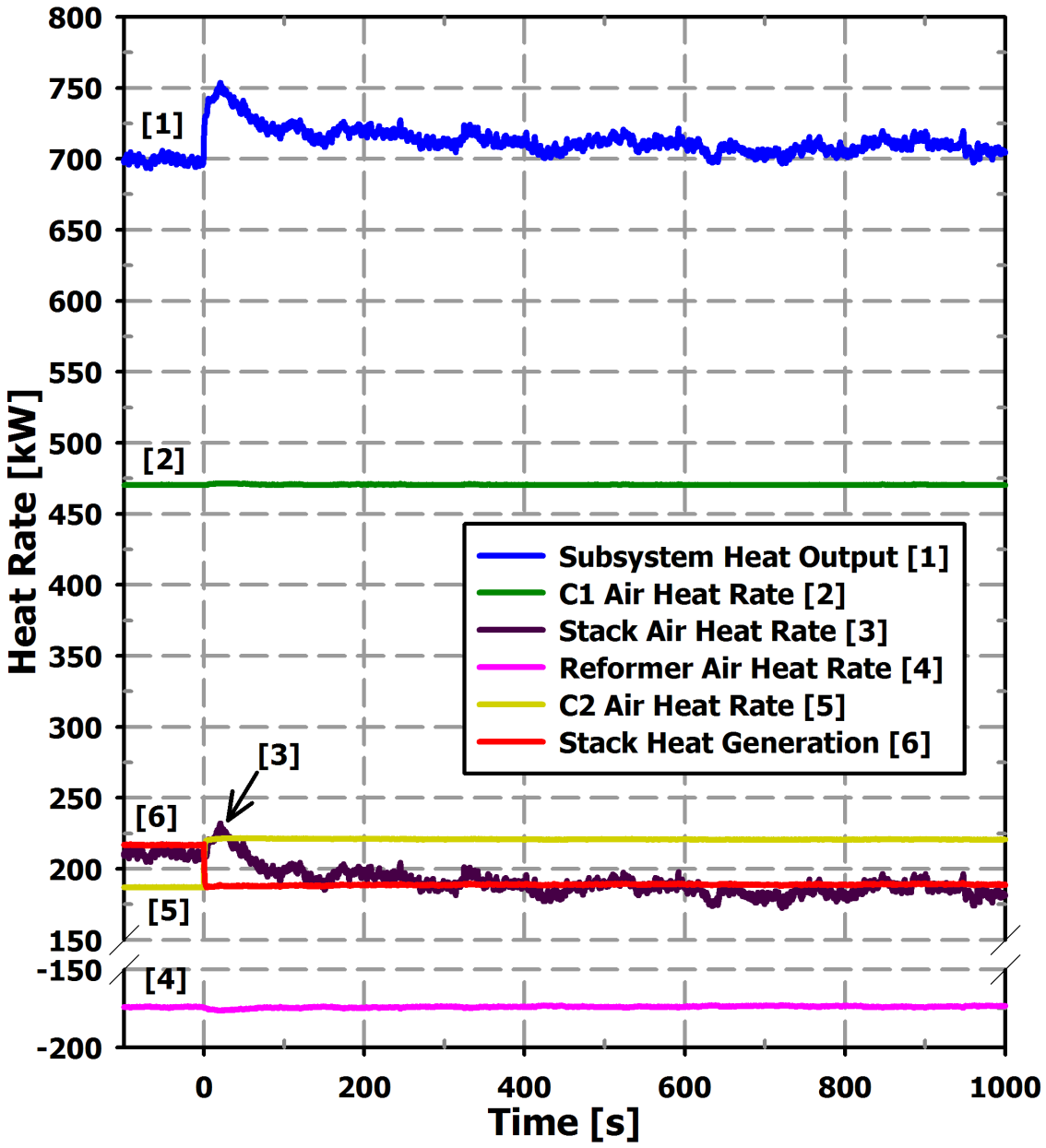

Figure 4.19: Component Heat Response to a 5 % Current Decrease with C1 Fuel Flow Constant

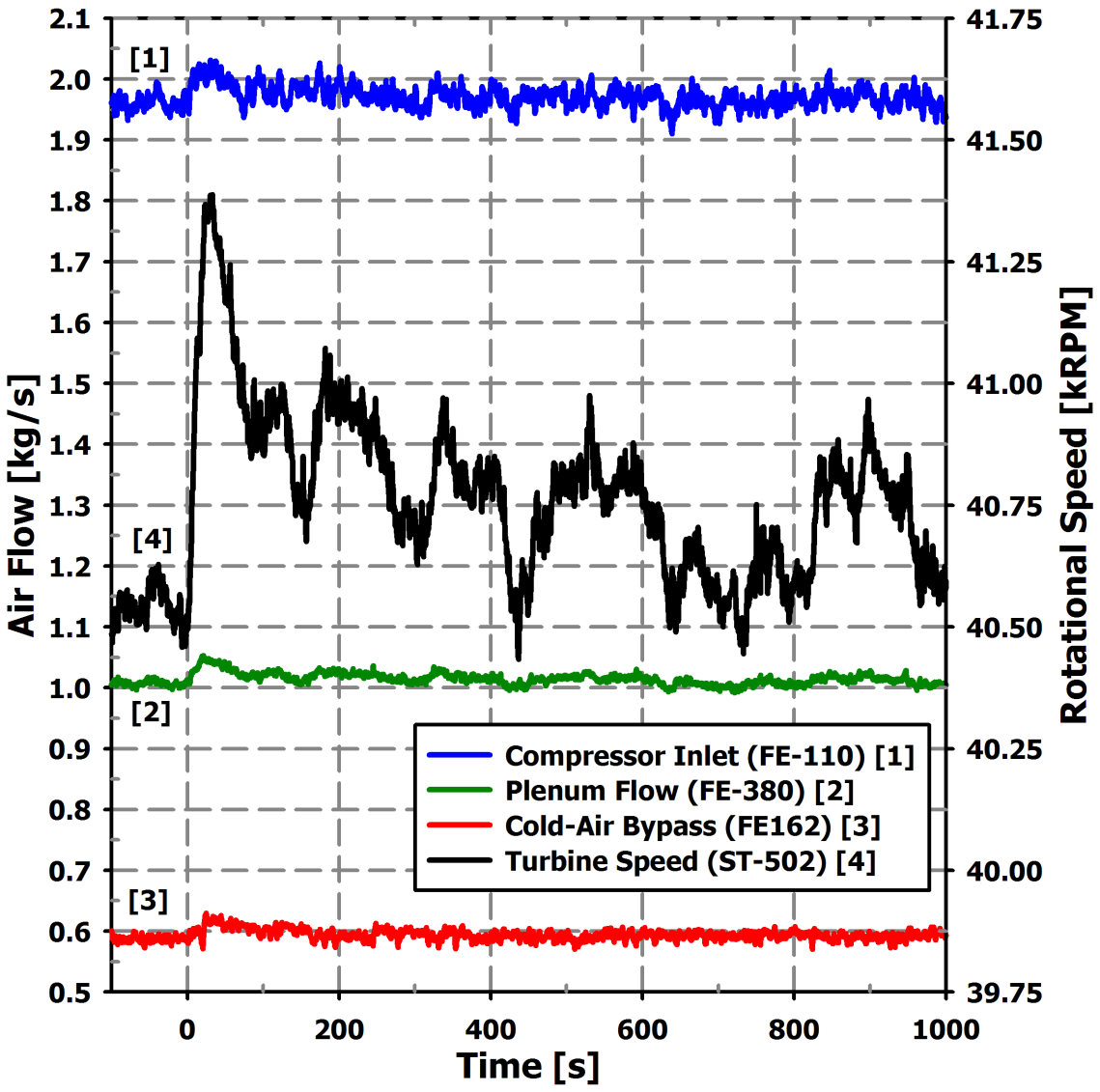

Figure 4.20: Component Heat Response to a 5 % Current Decrease with C1 Fuel Flow Constant

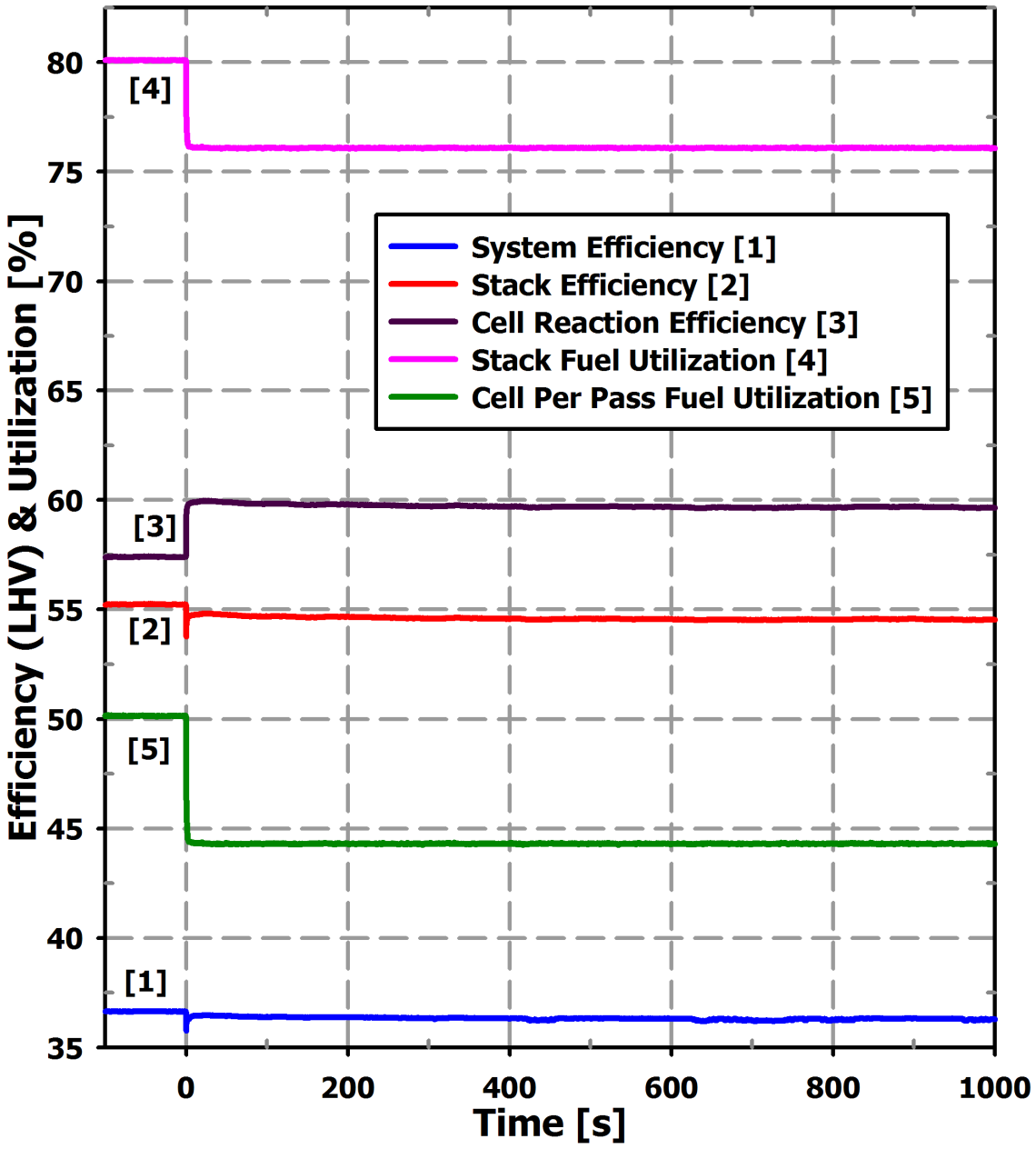

Figure 4.21: Performance Response to a 5 % Current Decrease with C1 Fuel Flow Constant

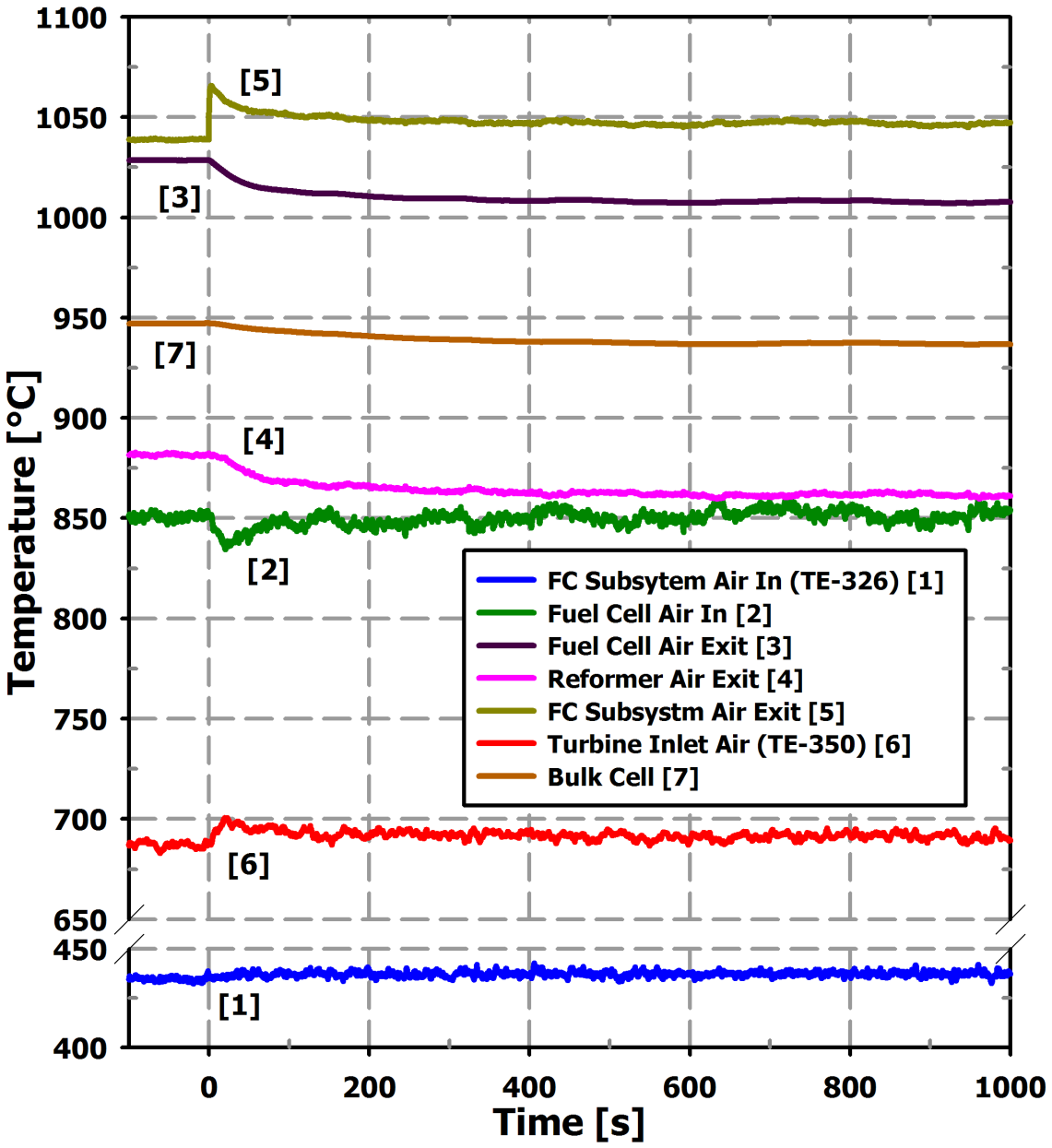

Figure 4.22: Temperature Response to a 5 % Current Decrease with C1 Fuel Flow Constant

Stack performance metrics are presented in Figure 4.21. The equation for calculating these parameters is presented in Appendix A. From the transient, the overall stack efficiency (Line 2) remained nearly constant. This efficiency is the product of the stack fuel utilization (Line 5), which decreased, and the cell reaction efficiency (Line 4). The cell reaction efficiency is proportional to the operating voltage so it increased with the lower current density. Last, Figure 4.22 presents the various temperatures in the subsystem model. Most notable are the subsystem exit temperature (Line 5) and the cell temperature (Line 7). The subsystem exit temperature displayed the expected spike immediately after the transient, and then the showed a slow decline as the the fuel cell stack temperature decreased.

4.2.2.1: dSPACE HILS Performance

A primary goal of this initial dSPACE experiment was to demonstrate the use of a separate computation platform for the execution of the numerical simulation. This load change test successfully showed that the dSPACE platform could execute the simulation on measured inputs and dictate the system's fuel flow. Figure 4.23 shows the relative change of selected parameters during the transients. Their respective initial values were established by a 100 s average (400 samples) before the initiating event. The plot shows that the fuel flow (FIT-432) tracks the predicted subsystem heat rate (Q-dot) as desired. This indicates that the HILS approach is performing as desired.

A secondary goal of the testing was satisfied in that the dSPACE platform facilitated the acquisition of a wider range of variables. This significantly improves the analysis of the experiments. This is best demonstrated by comparing Figure 4.9 from the AtlasPC test and Figure 4.19. These plots trace the heat rates in the subsystem. Due to

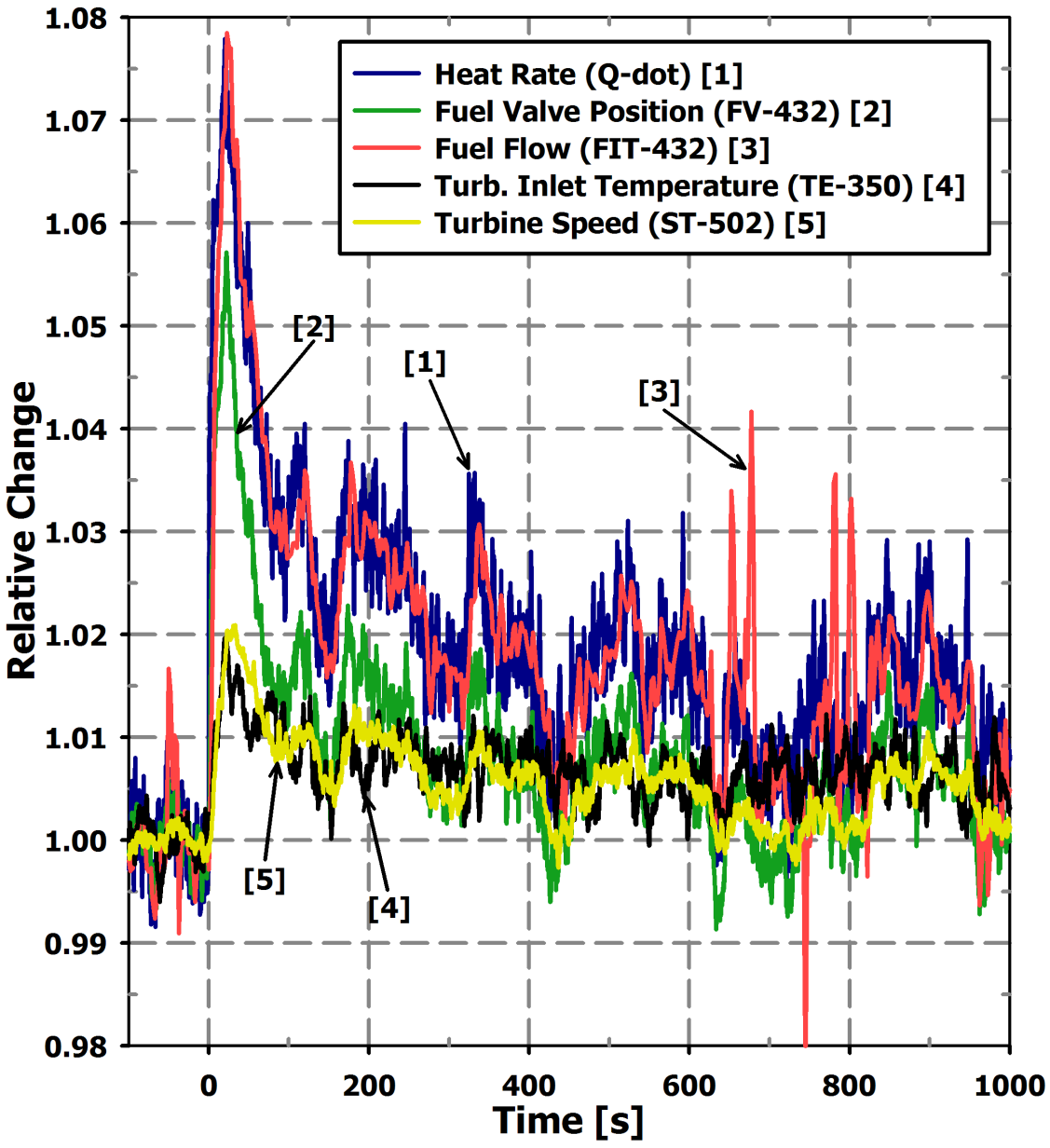

Figure 4.23: dSPACE Relative Response to a 5 % Current Decrease with C1 Fuel Flow Constant

the controller constraints, the AtlasPC only had sufficient capability to record the overall heat rate and stack heat generation terms. In contrast, the dSPACE platform tracked the heat transfer rates of all the subsystem components, providing greater insight into the system dynamics.

4.2.2.2: Hybrid Operation Insights

A significant insight from the larger recorded data set was the delineation of the stack heat generation (Line 6) and stack heat transfer (Line 3) rates in Figure 4.19. Following the initiating event, the heat transfer out of the cell was greater than the heat generation, as the cells released stored thermal energy. This release of sensible heat from the cells supplied the extra thermal energy to the turbine that contributed to the speed increase seen in Figure 4.20. This effect highlights an important difference between the transient behavior of a hybrid system and a stand-alone turbine engine. The large thermal capacitance of the stack will have substantial influence on the thermal energy available to the turbine during a transient.

While the release of sensible heat may lead to a turbine overspeed, the more important concern from an operational standpoint is a transient event with appreciable stack heat absorption that induces a compressor surge. If thermal energy is being absorbed by the stack's thermal capacitance, less is available to the turbine, and a sharp reduction in turbine inlet enthalpy has been known to initiate a compressor surge. While a surge was not observed in the complementary test of a 5 % current demand increase, the absorption of system heat during stack heating was observed. Figures 4.24 and 4.25 present the component heat rates and the turbine speed, respectively, for a current demand increase by 5 % with C1 fuel flow constant test that was also performed during

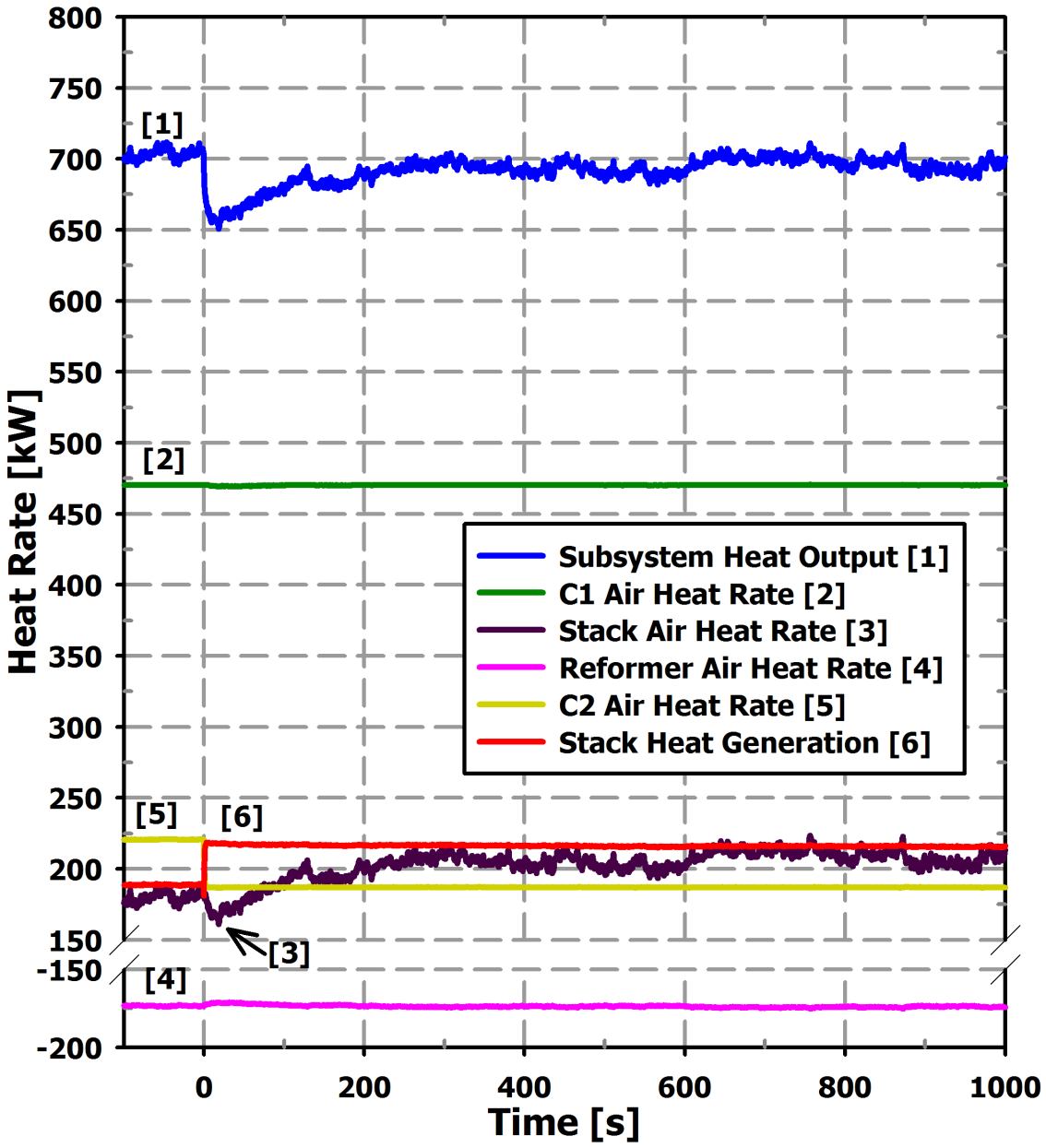

Figure 4.24: Component Heat Response to a 5 % Current Increase with C1 Fuel Flow Constant

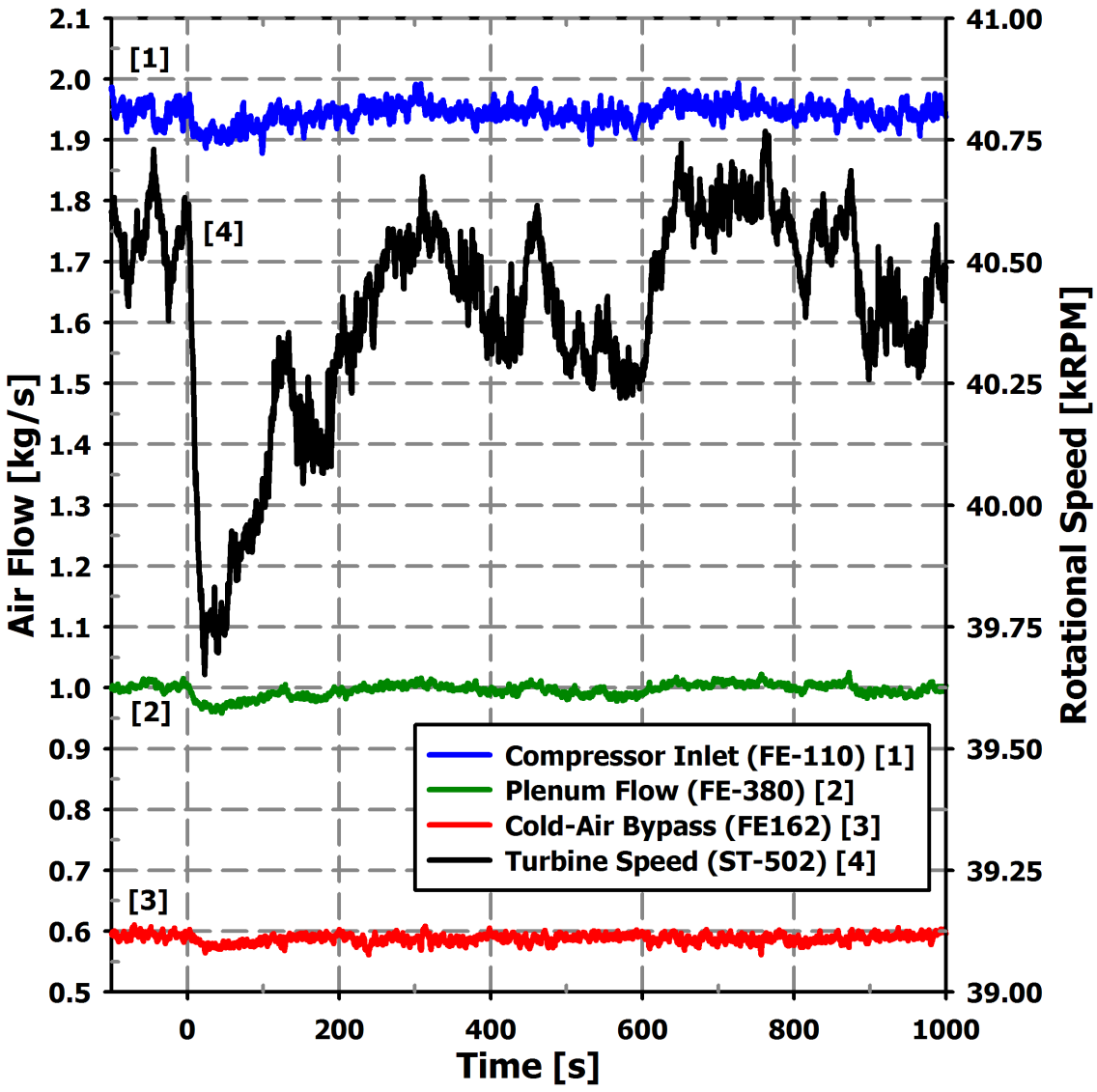

Figure 4.25: Component Heat Response to a 5 % Current Increase with C1 Fuel Flow Constant

this HILS experiment. In this test the turbine speed decreased from the lower simulated post combustion value (Line 5), which led to a reduction in the plenum airflow (Line 2 in Figure 4.25). The lower simulated cathode airflow resulted in a short-term decrease in rate of heat removal by the air from the cell (Line 3 in Figure 4.24), despite the rise in generated heat in the cell (Line 6).

The impact of the stack thermal capacitance has also been observed when the stack current load is held constant and only system airflow is changed. In work related to this dissertation, a HyPer HILS test of a 10 % reduction in cathode airflow by the hot-air bypass change was found to cause a compressor surge (Tucker, 2006b). In this test, even though the stack heat generation remained constant, the lower cathode airflow reduced the heat transfer from the cells while they heated to a higher steady-state temperature. This led to a swift reduction in turbine speed, and the compressor surged as the reduced airflow could not support the pressurized air in the air plenum. This detrimental effect of a bypass flow change was not a readily apparent concern for hybrid operation. The release or absorption of stack sensible energy will present control challenges to hybrid developers, since it is already in the system and cannot be easily regulated.

4.2.2.3: Simulation Design Insights

As shown in Figure 4.19, the C1 pre-combustor contributes a significant portion of the total thermal output of the subsystem. This is not ideal for hybrid operation. Furthermore, this high level of cold-air bypass flow significantly reduces the turbine inlet temperature, limiting the energy available to the turbine. Both of these factors combined resulted in the low projected system efficiency, as plotted by Line 1 in Figure 4.21. To address this concern, the simulated system can be modified. Future designs for the fuel

cell subsystem model corresponding to a different set of turbine nominal operating conditions will be used to reduce or eliminate the required preheating combustion and bypass flow.

4.2.3: Current Demand Decrease by 5 % with Constant Fuel Utilization

In the operation of a SOFC stack a more plausible operating method is to maintain a constant fuel utilization during normal operation. In this method once the target fuel utilization is established, the fuel flow is modulated in proportion to a current demand change. In order to test such a scenario, an experiment was performed with a 5 % reduction in current demand and with a corresponding 5 % reduction in stack fuel flow. The initial steady conditions for the 390 A load were the same as for the previous test, and the C1 pre-combustor was controlled to simulate a constant exit temperature of 850 °C.

As depicted in Figure 4.26, at time equal to zero the stack current was decreased by 5 %. Likewise, the user input for the simulated fuel flow to the reform is stepped down from 15.18 g/s to 14.42 g/s immediately following the load change. The fuel flow rate reduction is indicated by fuel utilization (Line 6 in Figure 4.30) remaining constant during the transient. Reducing the stack loading at a constant fuel utilization led to a 15 kW reduction in electrical power output (shown in Figure 4.27), as opposed to the 5 kW reduction in the previous test where the excess level of fuel flow was maintained. With the constant fuel utilization, the simulated thermal effluent from the modeled subsystem did not result in a sustained rise as in the previous test. This is because the specific heating value of the anode-off gas remained unchanged and its flow rate was

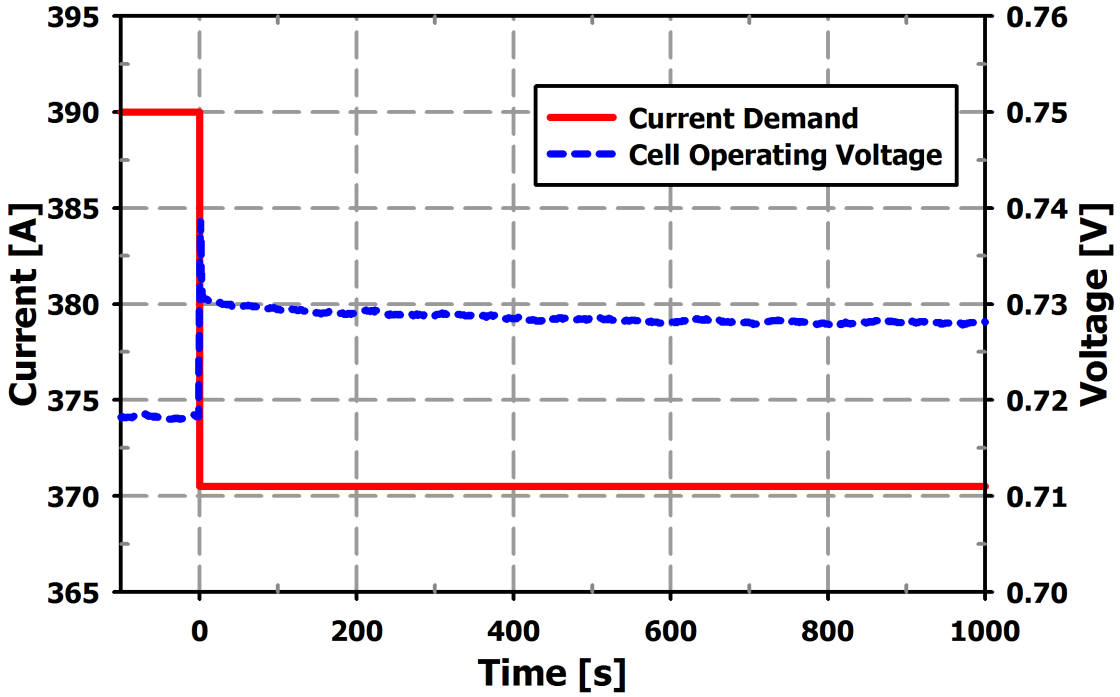

Figure 4.26: Cell Voltage Response to a 5 % Current Decrease with Constant Fuel Utilization

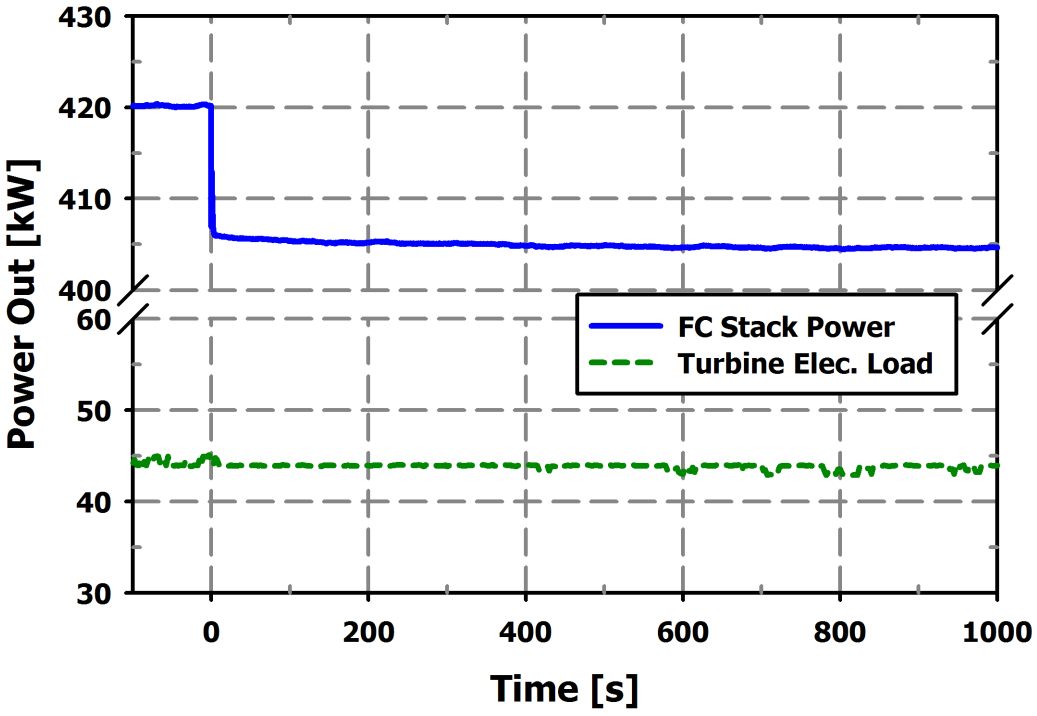

Figure 4.27: Power Response to a 5 % Current Decrease with Constant Fuel Utilization

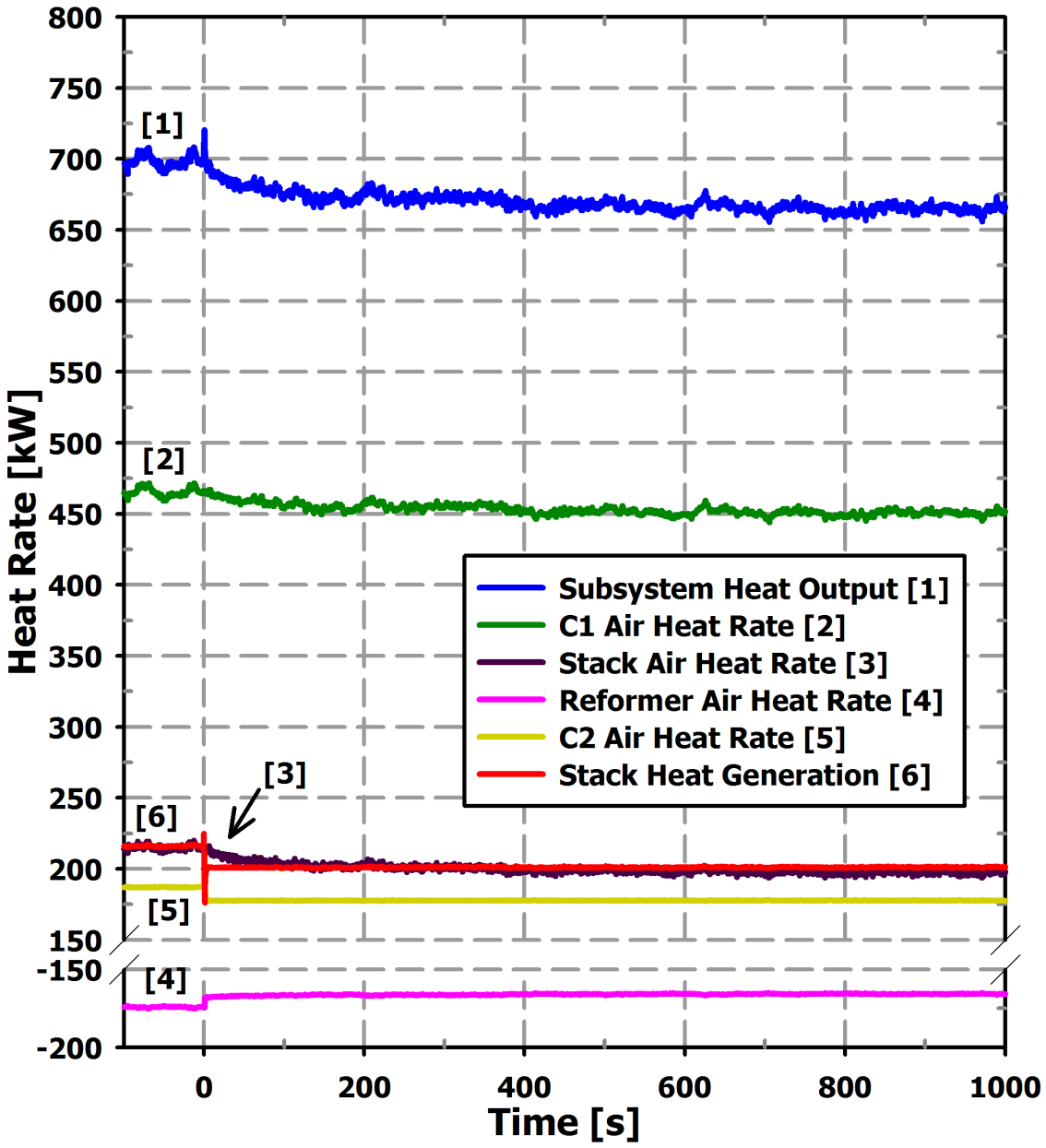

Figure 4.28: Component Heat Response to a 5 % Current Decrease with Constant Fuel Utilization

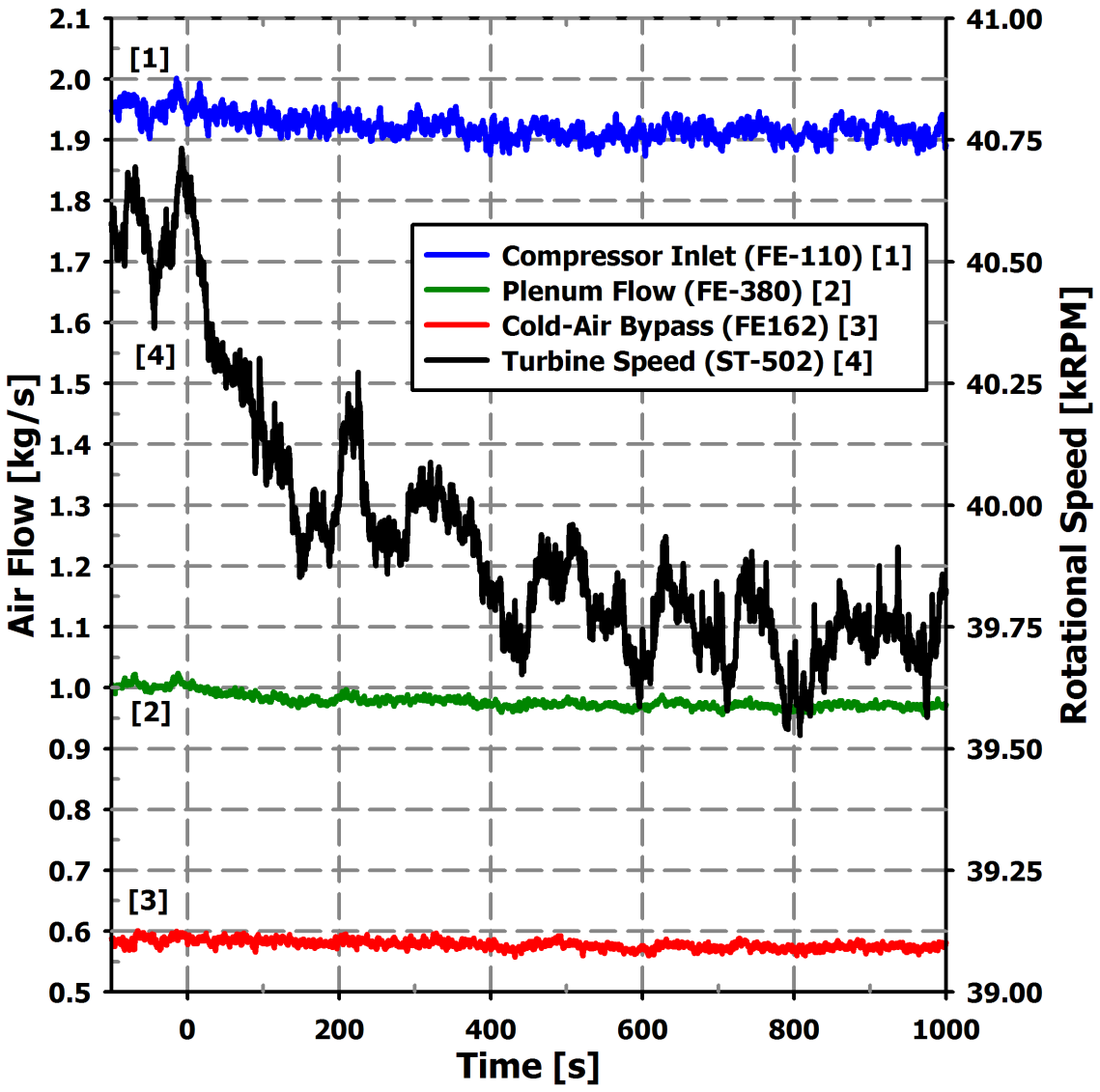

Figure 4.29: Component Heat Response to a 5 % Current Decrease with Constant Fuel Utilization

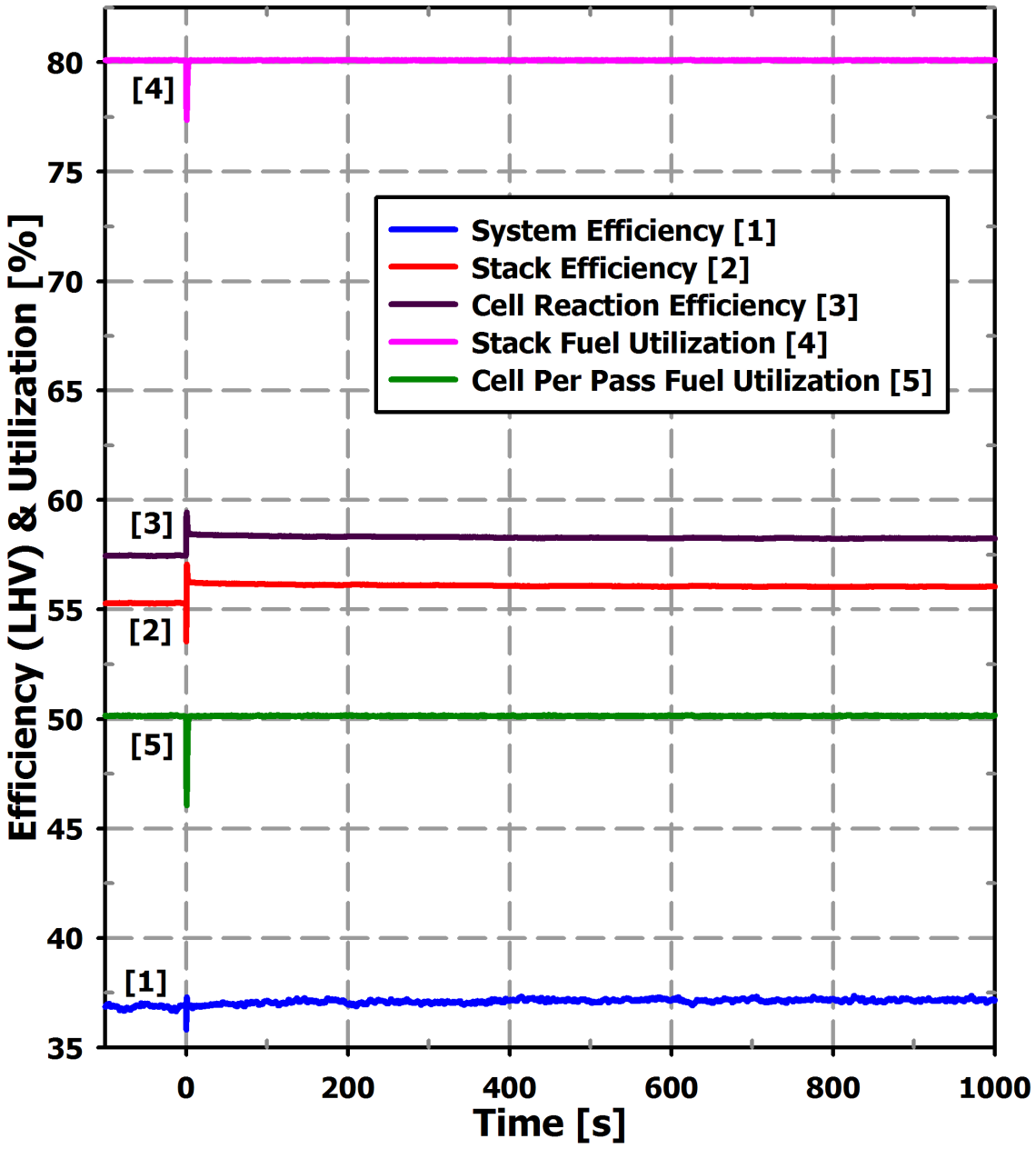

Figure 4.30: Performance Response to a 5 % Current Decrease with Constant Fuel Utilization

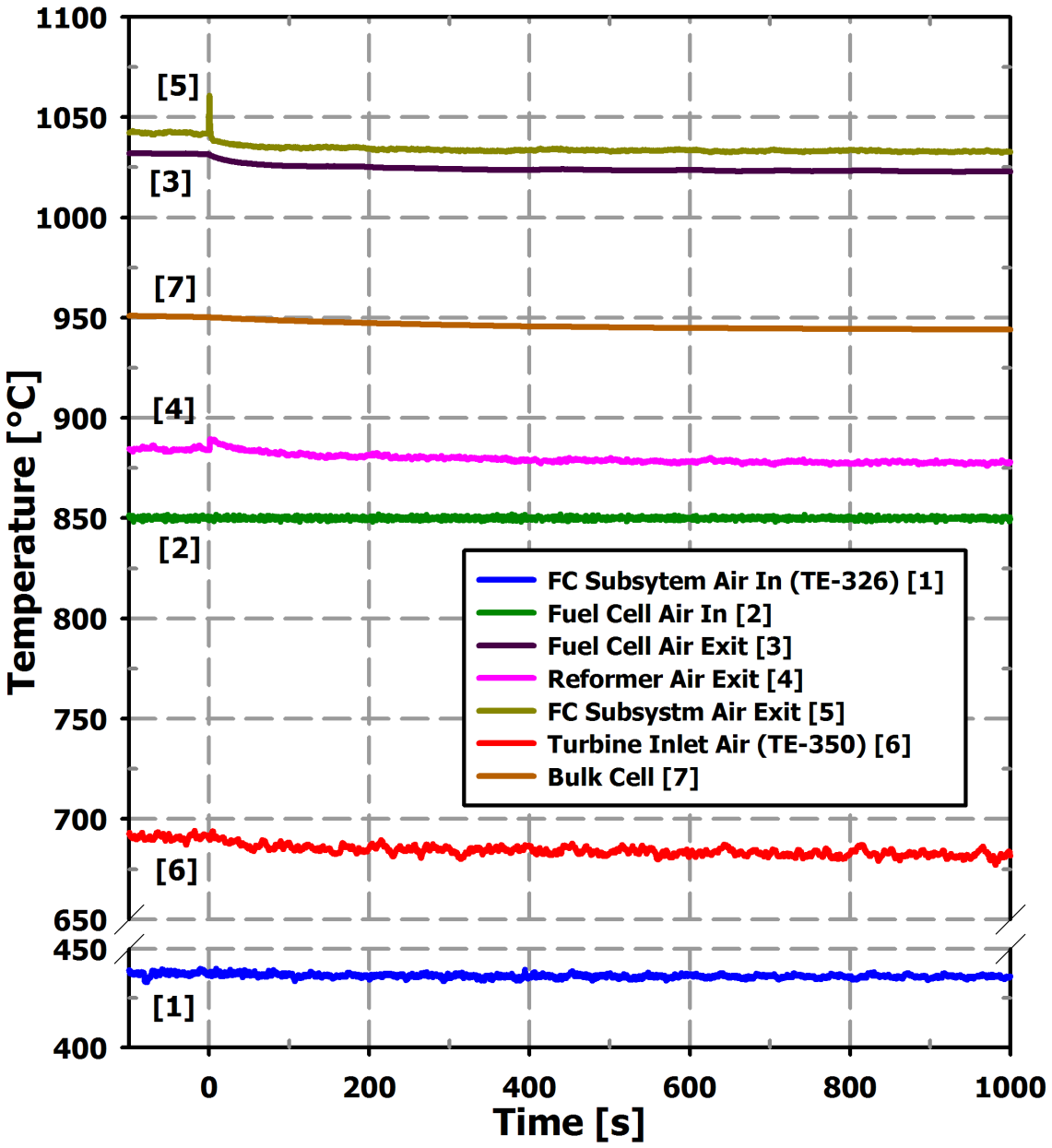

Figure 4.31: Temperature Response to a 5 % Current Decrease with Constant Fuel Utilization

slightly reduced. This resulted in the post-combustor heat rate contribution slightly decreasing (Line 5 in Figure 4.28).

Following the load step-down, the stack heat generation (Line 6) was reduced less than in the previous test since the cells operate at a lower cell efficiency when at a higher fuel utilization. The led to only a slight reduction in the heat transfer rate from the stack (Line 3) over the full transient. However, maintaining the higher overall stack fuel utilization after the transient resulted in higher overall stack efficiency since less unreacted fuel passes through the stack.

As expected, after the initial event the overall heat rate from the subsystem (Line 1 in Figure 4.28) experienced a gradual decline. The turbine speed and airflows responded accordingly to the slow decrease in thermal input (Figure 4.29). Last, as indicated by Figure 4.31, the subsystem temperatures show no significant effects from the load change, with the cell and overall temperatures slowly declining to the new steady condition.

4.2.3.1: Hybrid Operation Insights

As with the previous test, the system's natural gas fuel flow was successfully controlled by the simulation executed on the dSPACE platform. As shown in Figure 4.32, the relative change in the fuel flow correlated well with the predicted subsystem heat rate. The results of the test show that a 5 % reduction in current demand and stack fuel flow had, by the end of the transient, a corresponding 5 % reduction in the subsystem heat output rate. The effect on the turbomachinery was a 2 % reduction in turbine rotational speed with only a 1 % reduction in turbine inlet temperature.

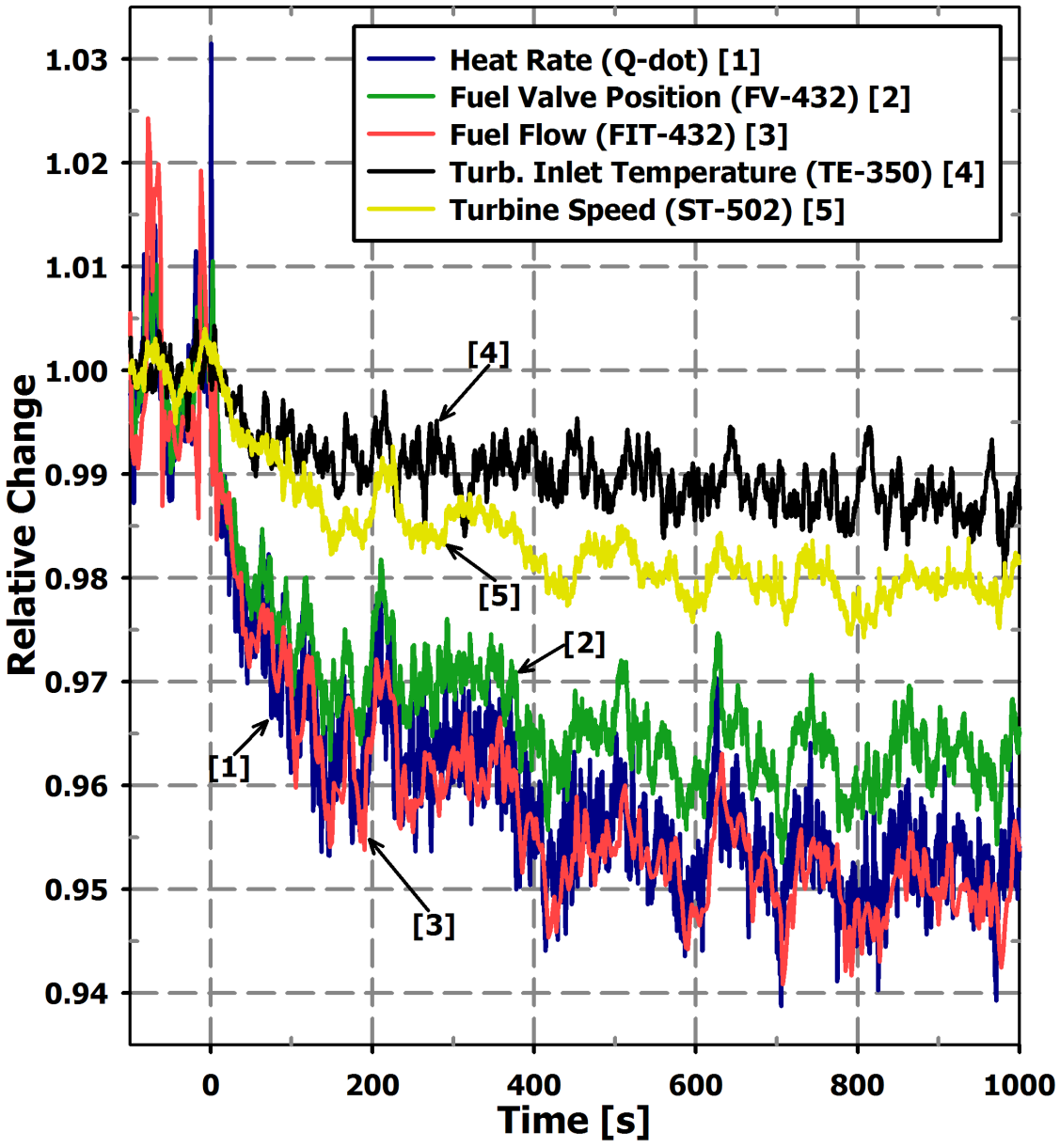

Figure 4.32: dSPACE Relative Response to a 5 % Current Decrease with Constant Fuel Utilization

The overall transient effects of a constant fuel utilization load reduction were minimal on the hybrid system. The gradual transient in turbine speed had leveled by 600 s. However, the cathode airflow was reduced by 2 % by the transient's end (Line 2 on Figure 4.29). If the system's operation required maintaining a target stack airflow rate, then a secondary speed control method may be required.

4.2.4: Current Demand Decrease by 20 % with Load-Based Speed Control

A third HILS experiment with the dSPACE system was to evaluate a more significant fuel cell transient while implementing turbine speed control. This test is a preliminary step to conducting a HILS of a full stack load trip. In a load trip the stack would experience an unexpected event that requires the sudden removal of the electrical load and implementation of measures to smoothly shut down the system. A primary concern for such an event is the combustion of a swift increase in unutilized anode-off gas in the post-combustor. This may result in a large increase in the turbine inlet temperature that may harm the turbomachinery. The scheme utilized in this test to counteract the turbine inlet temperature increase was to vary the turbine electrical loading. Before the test, a feedback controller was programmed into the AtlasPC to adjust the variable electrical load to target a turbine rotational speed setpoint of 40,500 rpm. Furthermore, by implementing a load-based speed control scheme, the HyPer HILS testing domain is expanded by allowing for the evaluation of larger fuel cell transients.

For this HILS experiment, the initial steady conditions for the 390 A stack load and 45 kW turbine load were the same as for the previous tests, the stack fuel flow remained unchanged, and the C1 pre-combustor was controlled to simulate a constant

exit temperature of 850 °C. With the turbine in load base speed control, this transient was initiated by a 20 % reduction in current demand, as depicted in Figure 4.33. This was a change from 390 to 312 A which resulted in a 40 kW decrease in stack power, as shown in Figure 4.34. As expected this resulted in a swift rise in the thermal output from the subsystem. This 160 kW spike is plotted by Line 1 in Figure 4.35. The turbine speed did increase rapidly, as shown in Figure 4.36, causing the speed controller to briefly apply 25 kW of additional load to the turbine. This resulted in a 2 or 3 cycle oscillation in the speed for about 50 s, before the feedback controller leveled out the turbine speed at its nominal level. At the end of the transient, the final turbine electrical load was 52 kW, as plotted in Figure 4.34.

Figure 4.36 also shows that the air flows were maintained throughout the transient by the use of the speed controller. The stack performance plot in Figure 4.37 shows that the 20 % load reduction resulted in a 16 % decrease in overall stack fuel utilization. The resulting predicted fuel cell subsystem outlet temperature, Line 6 in Figure 4.38, was shown to swiftly rise to 745 °C from 690 °C and then settle at 725 °C. An additional noticeable feature was the slow rise in subsystem inlet temperature, Line 1. This temperature is established by the heat recovery in the system's recuperators. After the transient, the turbine exhaust gas temperature rose in accordance with the turbine inlet temperature. The heat exchangers then warmed for approximately 70 s in response to the higher temperature air from the turbine. This resulted in a rise in the air plenum air temperature to 464 °C from 440 °C.

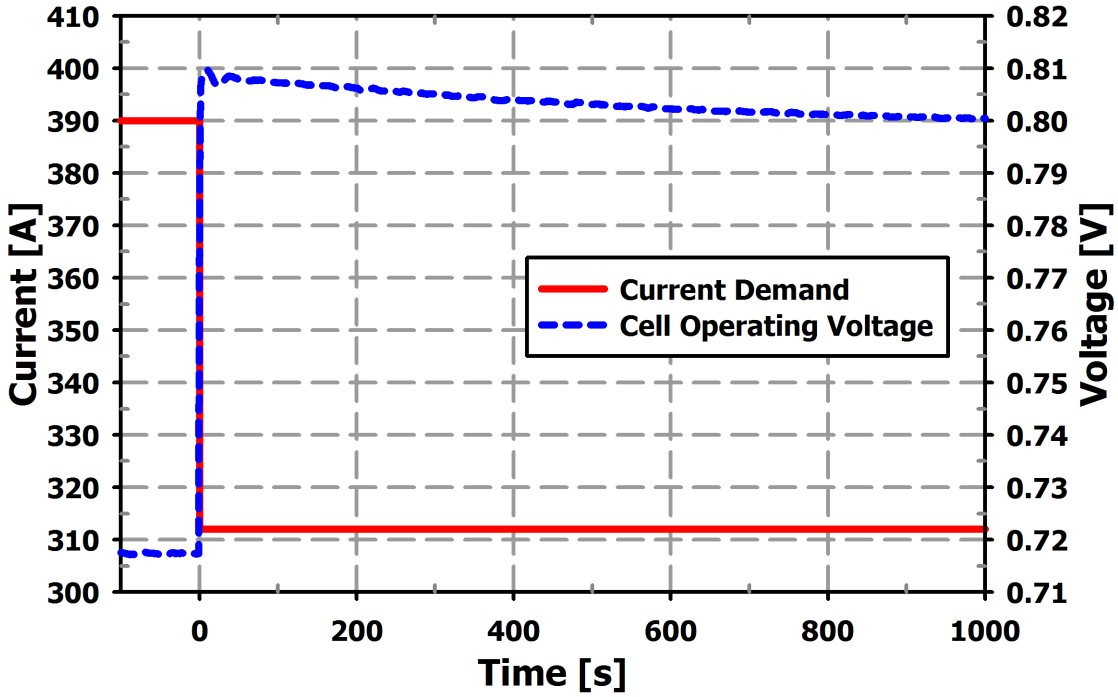

Figure 4.33: Cell Voltage Response to a 20 % Current Decrease with Load-Based Speed Control

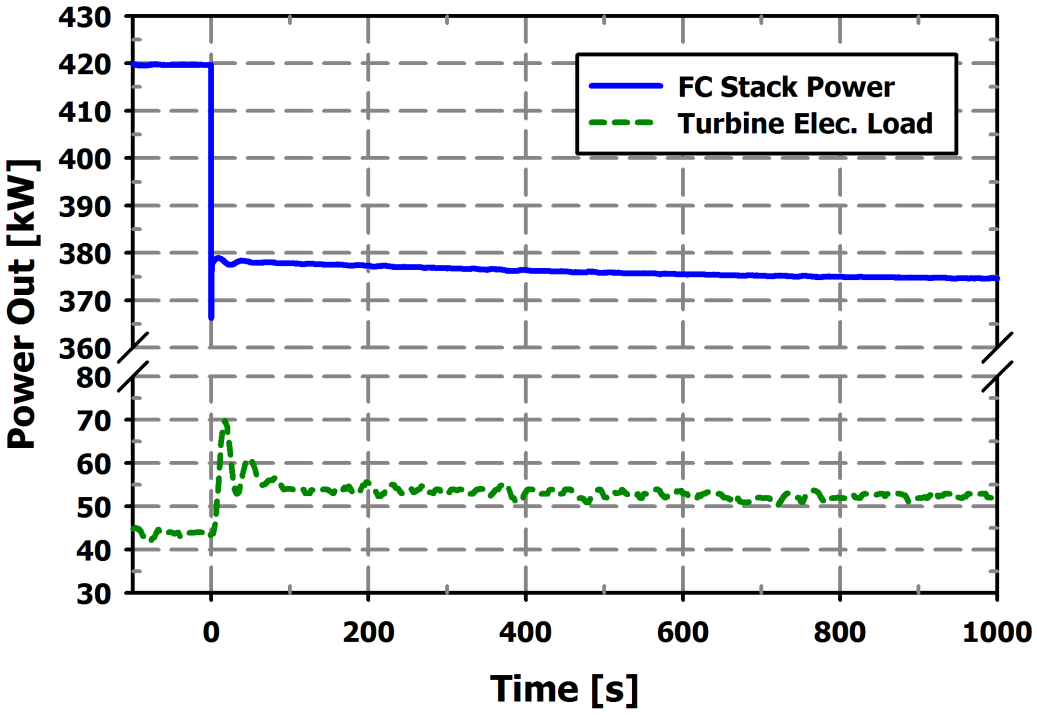

Figure 4.34: Power Response to a 20 % Current Decrease with Load-Based Speed Control

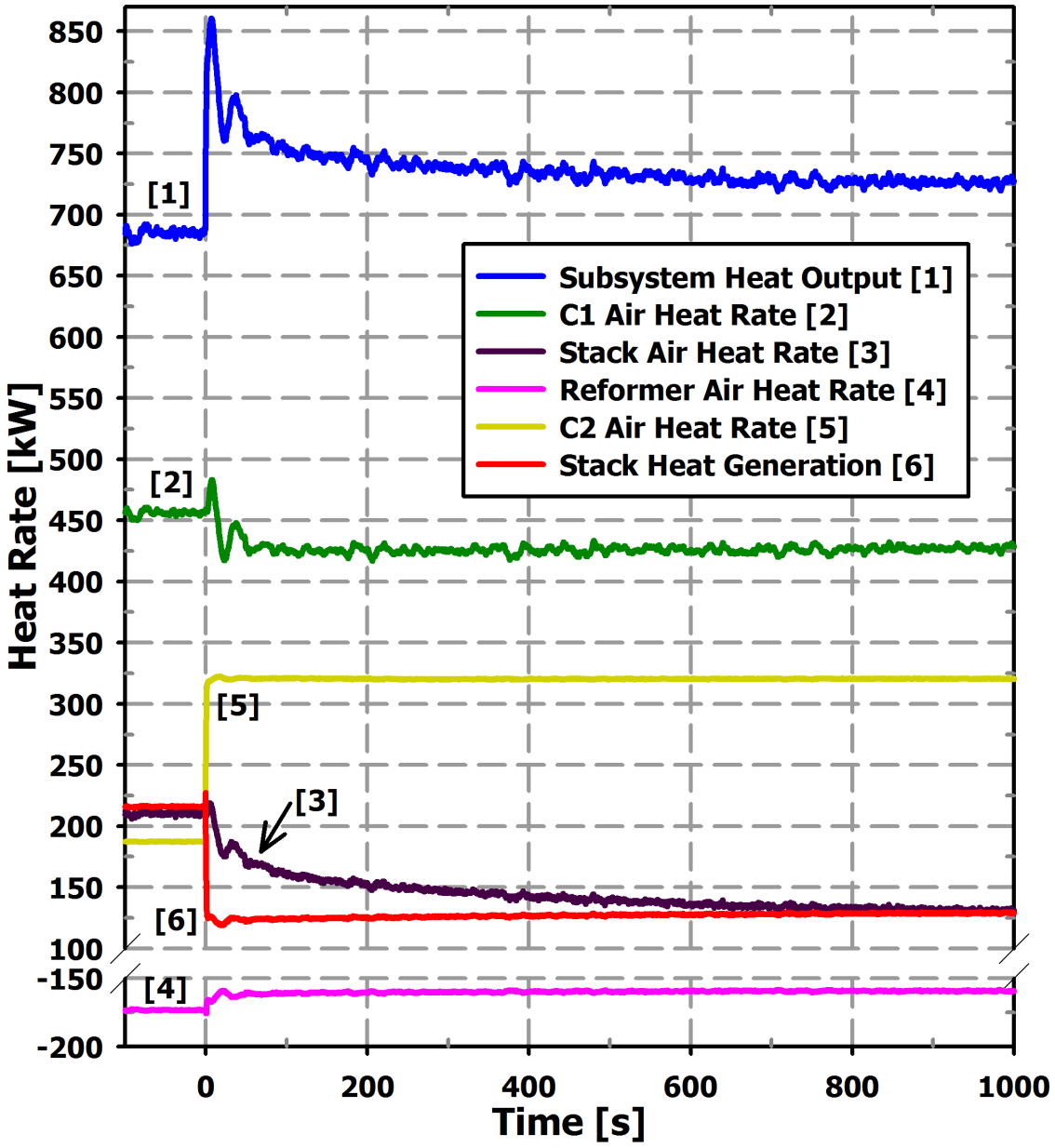

Figure 4.35: Component Heat Response to a 20 % Current Decrease with Load-Based Speed Control

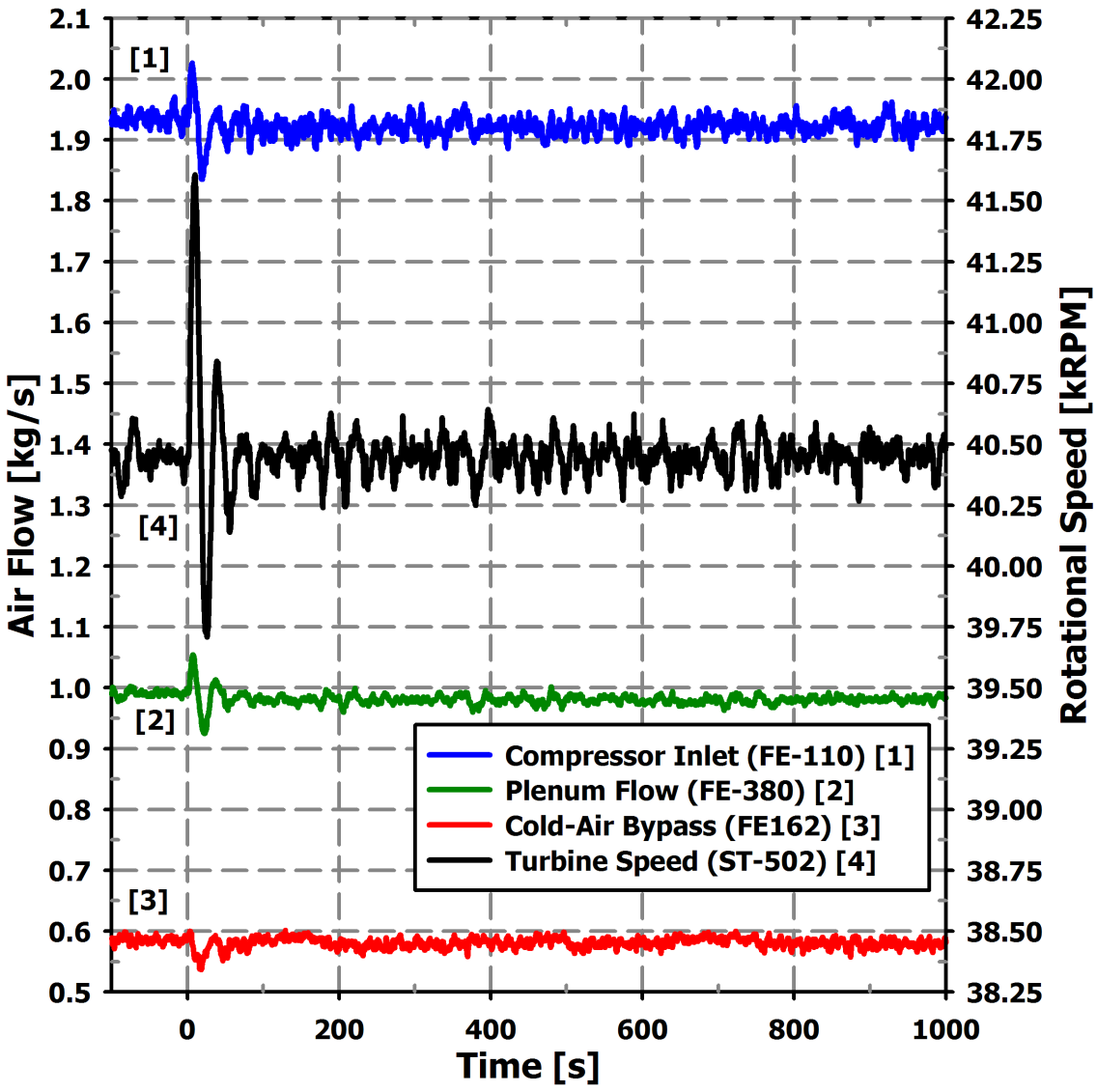

Figure 4.36: Component Heat Response to a 20 % Current Decrease with Load-Based Speed Control

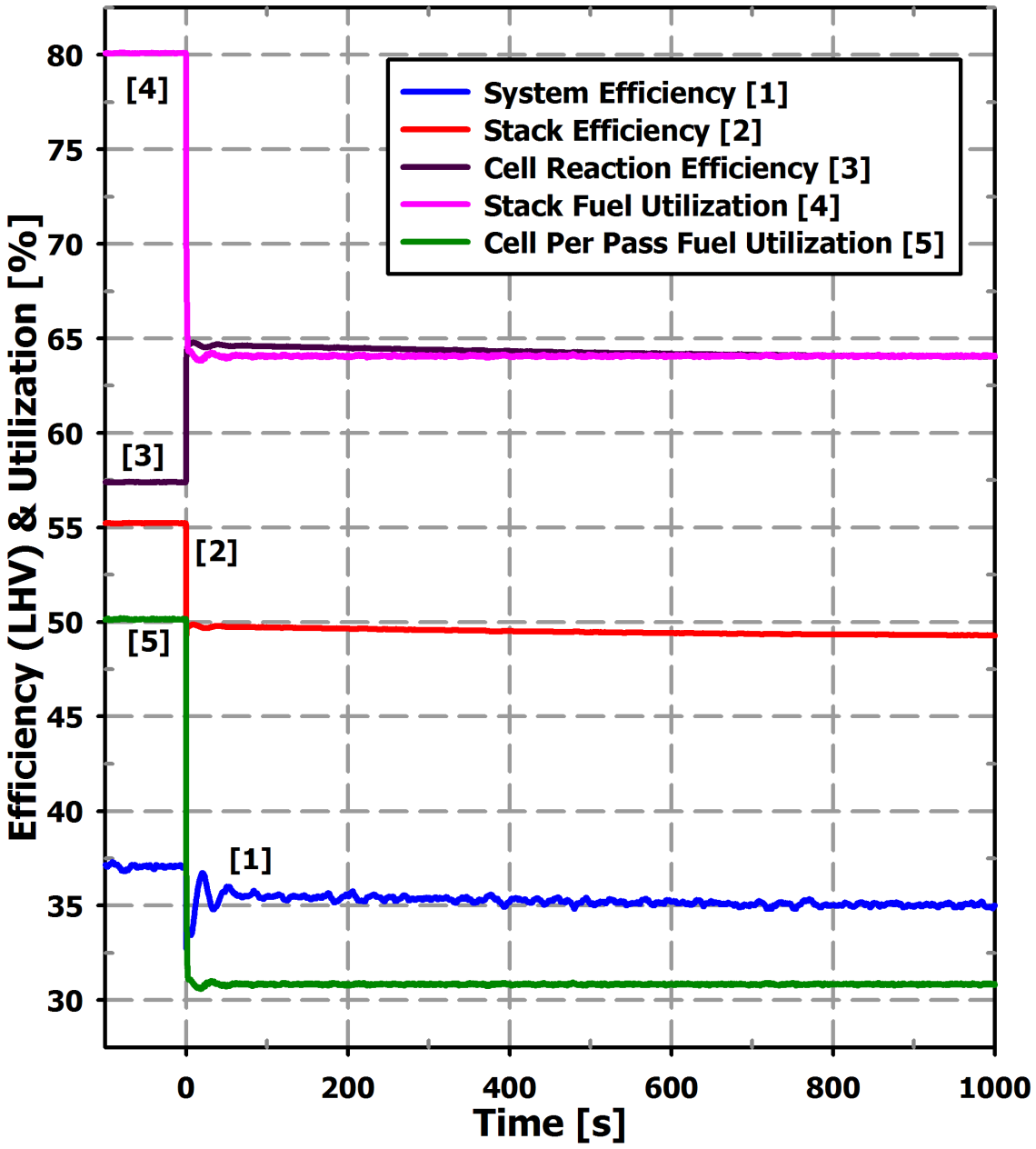

Figure 4.37: Performance Response to a 20 % Current Decrease with Load-Based Speed Control

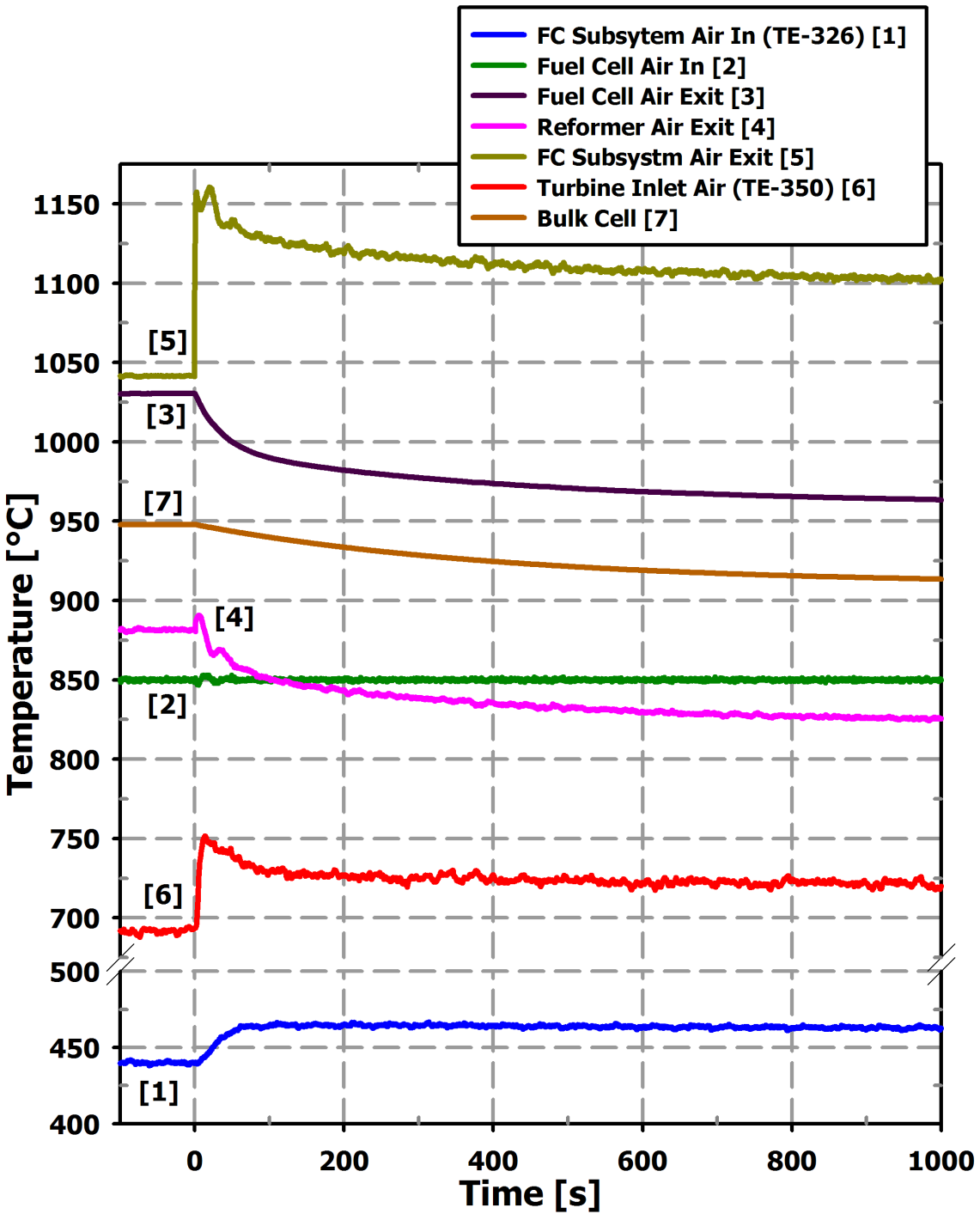

Figure 4.38: Temperature Response to a 20 % Current Decrease with Load-Based Speed Control

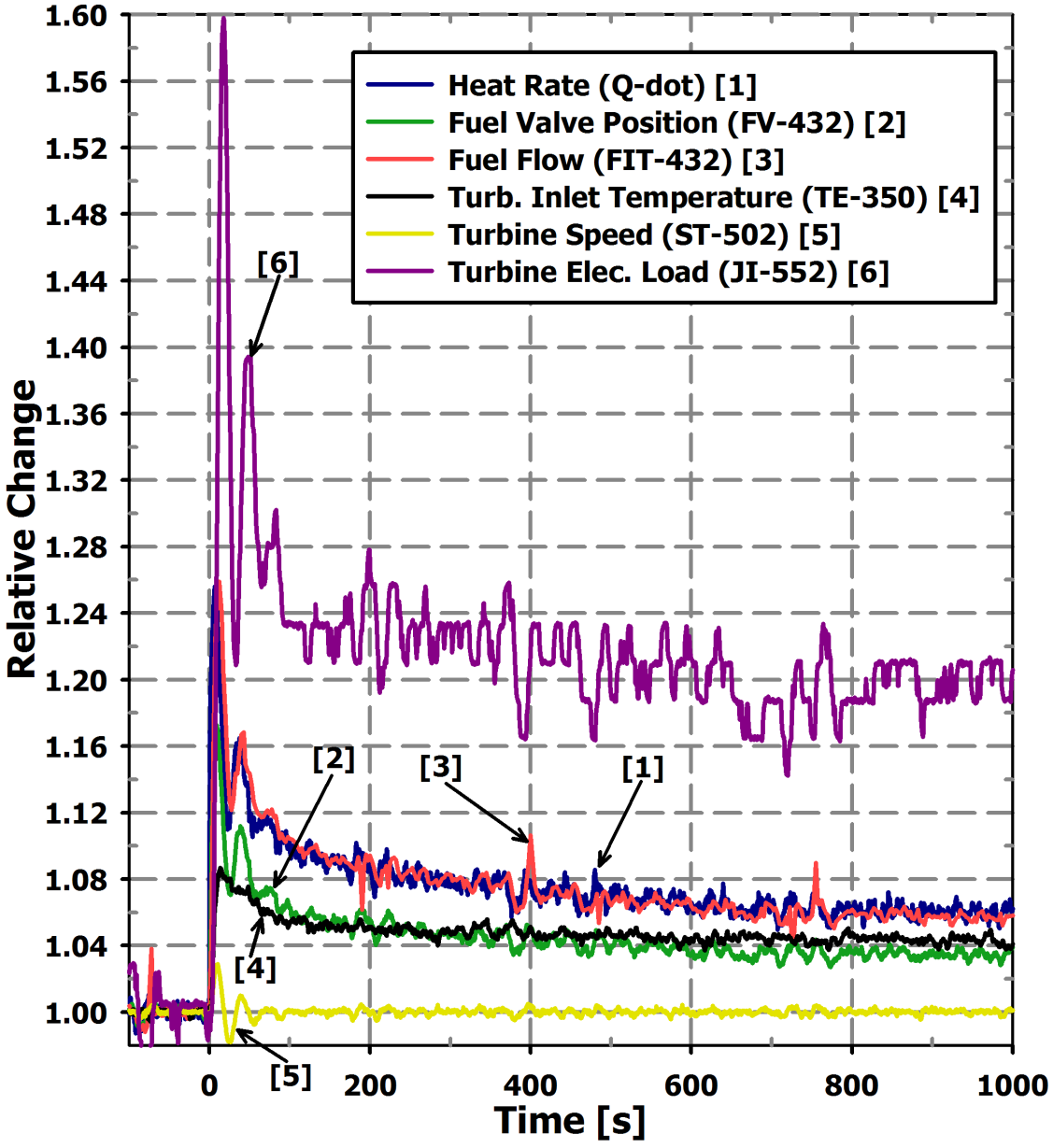

Figure 4.39: dSPACE Relative Response to a 20 % Current Decrease with Load-Based Speed Control

4.2.4.1: Hybrid Operation Insights

A primary goal of the this 20 % stack load reduction with turbine speed control was to evaluate the response of the turbomachinery to a large fuel cell transient. Figure 4.39 plots the relative change of several parameters of interest. In response to the current decrease, the heat output rate from the subsystem spiked to 125 % before settling back to 106% over time. This large increase in the inlet thermal energy to the turbine required a 60 % spike in turbine load to reduce the turbine speed. At the end of transient the turbine's electrical loading had increase by 20 % over its nominal value. These results indicate that a high level of reserve electrical loading would be required if turbine speed control was to be used as a stack load trip response. This may not be practical or it may have a prohibitive cost associated with it. Therefore, other methods of system control must be explored for SOFC/GT hybrid development.

4.3: Performance of the HyPer HILS Methodology

The results presented in this chapter demonstrate the successful coupling of a numerical fuel cell model with gas turbine hardware to simulate a SOFC/GT hybrid system. The results show that the real-time numerical model responded to live inputs measured on the hardware. In response to these signals and user inputs, the model predicted the rate of thermal effluent that would be imposed on the process air. This dynamic heat rate was successfully replicated as generated heat by the hardware combustor. To accomplished this, the numerical heat rate output was set to continuously control the position of fuel supply valve. This successfully regulated the fuel flow rate to fire the combustor at a level reflective of the fuel cell subsystem's simulated thermal

effluent. This accomplishment establishes HyPer's ability to carry out HILSs of SOFC/GT hybrid systems.

This approach was first implemented on the AtlasPC controller that was an exiting component of the HyPer control system. While this validated the HILS approach, the controller's limitations did not allow for more complex simulations, nor did it allow for greater insights into the phenomena. Therefore, a separate computation platform was integrated with the system. This dSPACE platform successfully executed the numerical simulation in HILS testing. The results from the dSPACE testing demonstrate that it expanded capabilities in conducting and evaluating HILS tests by expanding the number of simulation variables that were accessible for analysis. Furthermore, higher fidelity simulation can now be conducted with the HyPer dSPACE platform.

In addition to evaluating the simulation methodology, observations were made that provide insights into the operation of hybrid systems. For example, it was noted that the large thermal capacitance of the fuel cell stack had a prominent affect on system dynamics, and the transient responses were not always intuitive. Even in a case where the long term effect is negligible, there may exist significant short term responses that could have a detrimental effect on the fuel cell stack or turbomachinery. The awareness of these challenges substantiates the need for HyPer HILSs to further the development of SOFC/GT hybrids and their control methods.

CHAPTER 5: CONCLUSIONS

This dissertation effort focused on developing a means to address challenges facing the development of direct-fired SOFC/GT hybrid power generation systems. By successfully integrating a numerical fuel cell model with the gas turbine hardware of the U.S. DOE NETL's HyPer facility a robust platform for conducting HILS investigations of SOFC/GT hybrids was established. The insights gained from HyPer HILS experimentation will assist system designers in integrating a high temperature fuel cell stack and a gas turbine by offering solutions to the numerous system and control challenges that prohibit hybrid commercialization. These solutions will promote the deployment of hybrid systems so that they can fulfill their promise of highly efficient and clean electrical power generation.

5.1: Developments

A method has been developed for the characterization of hybrid system dynamics through HILS experimentation with the HyPer facility. It was accomplished through combining physical and numerical components into a single simulation. Specifically, a physical gas turbine and supporting hardware, such as air plenums and bypass valves, were coupled with a numerical fuel cell model.

The methodology for HILS of hybrids was developed by first examining the existing HyPer hardware system and designing the HILS approach for incorporating a

real-time numerical simulation onto the existing HyPer controller. Next, a bulk-parameter cell model along with supporting component models were combined into a SOFC stack subsystem model. This SOFC stack model was then adapted for execution on HyPer's existing AtlasPC controller. During a HILS, to control the system's combustor, the model predicts the thermal responses of a SOFC subsystem based on the flow conditions measured in the operating hardware. This approach was then evaluated by conducting fuel cell load transient tests. During a simulation the model appropriately responded to measured parameters from the hardware system. In response, the real-time numerical model controlled the fuel flow to the hardware combustor in accordance with the the model's predicted thermal effluent.

The initial HILS testing identified the need for a dedicated simulation platform to provide a stand-alone computational system that specializes in the execution of the numerical model. Therefore, a dSPACE computational platform was selected and integrated with the existing HyPer control system. This robust simulation platform will facilitate higher fidelity numerical models that provide more detailed results leading to greater insights from conducting hybrid HILSs. Following its installation, more in-depth HILSs of a fuel cell load change were performed with the fuel cell subsystem model.

Both the AtlasPC-based and the dSPACE-based HILS operations substantiate HyPer as a hardware simulation tool for investigating SOFC/GT hybrid systems. Furthermore, from the initial testing, insights were developed into transient responses of a SOFC/GT hybrid system.

5.2: Insights

The results from the HILS experiments demonstrated the successful coupling of a numerical fuel cell model with gas turbine hardware to simulate a SOFC/GT hybrid system. In addition, analysis of the transient responses of the simulation provided insights into the operation of hybrid systems.

5.2.1: HILS Approach for SOFC/GT Hybrid Research

A HILS approach was successfully utilized to simulate a SOFC/GT hybrid system. This simulation system can be used to evaluate the dynamic response characteristics of a SOFC/GT hybrid system. Furthermore, it can be adapted and applied to simulate other types of fuel cell systems and advanced power generation systems.

5.2.2: Fuel Cell Stack Thermal Capacitance Impact

The thermal capacitance of a SOFC stack is several magnitudes larger than that of a combustion chamber in a simple gas turbine engine. As expected, in the HyPer HILS testing the stack's thermal capacitance was observed to have a significant impact on the dynamic behavior of a hybrid system. The release of stored sensible heat will provide additional energy to the turbine during certain transients. In contrast, transients that lead to the absorption of heat by the stack will deprive the turbine of thermal input, and thereby increases the risk of a compressor surge.

Furthermore, the stack's thermal capacitance effect upon a transient is not always obvious, particularly when compared to a stand-alone turbine engine. In a turbine engine a change in the combustor airflow is easily mitigated by the fuel controller. However, in a hybrid system, changes in the cathode airflow will affect the heat transfer rate from the

stack to the air. The resulting level of heat recovery from the stack cannot be readily controlled and will impact the rate of enthalpy flow driving the turbine. This will pose challenges to hybrid developers and indicates that novel control methods must be developed for SOFC/GT systems.

5.2.3: Effectiveness of Load-Based Turbine Speed Control

Although variable electrical loading of the AC generator was found to be an effective means of turbine speed control to mitigate the impact of a fuel cell transient, it may not be a compelling control scheme in hybrid operation. To recover the turbine speed following the 20 % reduction in fuel cell load required the momentary application of an additional 60 % of electrical loading was required. Therefore, to handle large transients the turbine's AC generator would require costly oversizing. Moreover, since such transients would be disruptive to the electrical power grid, other means of dissipation would be required, such as a large stand-alone electrical dissipater.

5.3: Recommendations

Interpretations of the HILS testing results indicate a couple of key design recommendations for SOFC/GT hybrids. Furthermore, several improvements to the hardware and computational systems of HyPer are suggested to improve the performance of the HILSs, and the exploration of system transient response from a wider variety of initiating events is recommended.

5.3.1: Hybrid Design and Control Improvements

The stack's airflow is a principle factor in the performance of the fuel cell stack and the overall hybrid system. Management of airflow to the stack is therefore a critical concern in hybrid operation. However, the impact of the fuel cell stack's large thermal capacitance on the transient characteristics complicates airflow control.

5.3.1.1: Stack Precombustor Ineffective for Turbine Control

While the stack's cathode airflow precombustor is effective in and often required for preheating the inlet airflow to the fuel cell, this combustor is not effective for controlling turbine speed. The thermal energy from the preheat combustor has a large influence on the fuel cell operating temperature, but the large thermal capacitance of the stack inhibits any short-term influence on the enthalpy flow to the turbine. For example, the additional energy from increasing precombustor firing will be absorbed by the stack's sensible heating and have only a long-term effect on the energy available to the turbine. Therefore, the modulation of a heat source upstream of the fuel cell system could not be used to effectively manage short-term stack airflow transients. This means other turbine speed control approaches must be developed for SOFC/GT hybrid systems.

5.3.1.2: Operation Analysis Requires Transient Analysis

When transitioning a hybrid system from one steady operation point to another, the HyPer HILS experiments showed that a significant short-term transient may exist, even if there is minimal change between the two steady-state operating points. These significant short-term transient events may be detrimental to hybrid system operation. For example, in the 5 % current demand decrease testing, little change in system energy

input and output was realized during the transient, yet significant short term responses were observed that indicate challenges for hybrid system control.

As mentioned, these short term effects arise from the the stack's large thermal capacitance which can absorb heat from the airflow, meaning this energy is not available to the turbine. To mitigate these short-term responses, hybrid control developers must be able to anticipate and address them. Therefore more transient analysis must be done since these effects are not captured by steady-state hybrid system analysis alone.

5.3.1.3: Hybrid Airflow Control Strategy

Since the turbine supplies additional electrical power that raises the efficiency of the hybrid system, a designer may be temped to maximize the electrical power generation from the turbine. However, this constrains the operating range of the system and limits options for the management of stack airflow. Furthermore, the fuel cell stack performance is highly sensitive to the cathode airflow. Therefore, the hybrid control strategy should be to control the turbine for fuel cell airflow management first and turbine electrical power generation second.

5.3.1.4: Improving Hybrid Operability Through Airflow Bypasses

Including valved process airflow bypasses, such as bleed air, cold-air bypass, and hot-air bypass, adds complexity and cost to the design of a hybrid system. Furthermore, the bypasses can lower system efficiency by increasing the compressor loading or by lowering turbine inlet temperature. However, the inclusion of process air bypasses into a SOFC/GT hybrid design improves overall system operability by permitting independent stack airflow management. This advantageous gain in airflow control is indispensable in

designing an operational hybrid system, despite efficiency cost. Therefore, the benefits and characteristics of valved bypasses should be explored further with HyPer

5.3.2: HyPer HILS Hardware and Instrumentation Refinements

Improvements to several key hardware components or instrumentation would improve the HILS performance the HyPer facility.

5.3.2.1: Low-pass Signal Filter for dSPACE Inputs

The environment of the HyPer facility has numerous electrical devices that generate signal noise. The dSPACE ADC input board is sensitive to the interference. Currently, a software filter is used to reduce the impact of the signal noise. The addition of a low-pass filter system for all the input signals would eliminate most of the high frequency noise and better electrically isolate the dSPCAE platform. This would improve the overall quality of the data acquisition capabilities of the dSPACE platform.

5.3.2.2: Improved Instrumentation for Airflow Measurement

Accurately measuring airflow rates is known to be challenging. However, for HyPer HILS investigations, as well as general HyPer testing, air mass flow rate is a dominating parameter in system and simulation performance. While offering a low pressure loss, the current HyPer annubar flow elements are oversized for HyPer flow rates. Moreover, since typical meters are intended for room temperature operation, additional error arises when measuring airflow rate at elevated temperatures, which is required at the inlet to the air plenum (400 to 500 °C). Identifying and implanting a more accurate flow rate sensor would improve the efficacy of the HyPer HILS investigations.

5.3.2.3: Electric Resistive Heaters for Thermal Transfer System

To replicate the thermal effluent from the fuel cell stack HyPer utilizes a natural gas combustor. This is currently the only heat source in the system, and reproducing stack thermal effluent through combustion has inherent uncertainties, such as variance in the heating value of the fuel. A second solution would be to install a bank of electric resistive heaters into the air plenum. The electrical power supplied to the heaters, and thereby the level of heat dissipation, could then be controlled by the numerical stack model. To accommodate the elevated temperatures, the air plenum would require modification.

The resistive heater approach would improve the accuracy in controlling the thermal input to the system. Additionally, it would create two independent heat sources in the HyPer system. This would allow for the investigation of a wider range of possible hybrid control methods.

5.3.3: Improved Numerical SOFC Subsystem Models

The HyPer HILS methodology developed in this dissertation should be refined further with higher fidelity models and other fuel cell configurations.

5.3.3.1: Refinement to Bulk-Parameter Model

Further developing the existing subsystem model would improve the simulations. This may include adding thermal and mass capacitance to the combustors and reformer. These supporting components can be further improved by introducing incomplete reaction and loss terms to the models. As for the cell model, an important step is to address the oxidation of carbon monoxide in the fuel stream. This could be incorporated

into the model through either direct electrochemical oxidation or the water-gas shift reaction.

A more substantial concern to the HILS dynamics is the refinement of the heat transfer characteristics of the fuel cell model. Evaluation of the results and auditing of the model reveal that effectiveness of the cell-to-air heat transfer may have been over estimated. In this work, a convection heat transfer coefficient, h_{HT}, of 302 W/(m^2·K) was used in the model. However, this is for an hydraulic diameter of 1 mm, when in fact, a hydraulic diameter of 1.33 mm should have been used in developing the model for the rectangle shaped cross section of the cathode airflow channel. This would have resulted in a heat transfer coefficient of 226 W/(m^2·K), but this error was not identified until after the testing. The lower heat transfer coefficient would have lengthened the response time of the cell temperature by approximately 30 %.

A substantial improvement in the bulk-parameter approach could also be achieved by implementing a lumped, non-linear technique for the dynamic model. Zhang (2006) applied this approach to a SOFC cell model by introducing exponential-based spatial distribution functions. The distribution characteristics of the temperature and reactant molar fraction profiles are determined by fitting the exponential-based function's parameter to a detailed numerical simulation. The spatial effects of the temperature and reactant profiles can then be lumped into the dynamic model. While remaining computationally non-intensive, this approach would improve the accuracy in predicting the cathode outlet air temperature by addressing the inherent spatial effects in a fuel cell. However, it would not capture changes in a temperature profile's shape that will arise as the air mass flow changes.

5.3.3.2: Implementation of Higher-Fidelity Models

With the expanded computational power of the dSPACE platform, the obvious next step is the inclusion of high-fidelity SOFC subsystem models into the HILSs. These more complex numerical models will provide more accurate HILSs and offer greater insights into the performance of the SOFC stack. The primary benefit from higher-fidelity models would be the spatially and temporally resolution, of cell variables. The cell model will then predict cell temperature profiles, which is required for investigating the thermally induced stresses in a cell. This is key knowledge in evaluating and understanding the survivability and reliability of SOFC stacks in a hybrid system.

5.3.3.3: Coal Syngas Fueled SOFC Subsystem Model

While this dissertation focused on a natural gas fueled SOFC stack with an external reformer, a benefit of the HILS approach is its ease in accommodating various numerical subsimulations. In HyPer this allows for the testing of numerous SOFC stack configurations. In particular, a SOFC stack fueled by gasified coal is a candidate configuration that is currently garnering attention. A coal syngas fuel stack would not require a natural gas reformer that removes heat from the process airflow, so a higher rate of byproduct heat from the stack would be available to the turbine. This would change the behavior of the hybrid system significantly.

5.3.4: Future HyPer HILS Experiments

The versatility of the HyPer HILS methodology developed in this dissertation can now be utilized to research a wide range of hybrid transients.

5.3.4.1: Bypass Flow Transients and Effectiveness

The HyPer facility has three bypass valves that can be used to modulate the process airflow rates. In HILS testing the effectiveness of each bypass in maintaining targeted cathode airflow rates needs to be established and compared. Furthermore, transients initiated by a flow manipulation alone require evaluation since they pose non-intuitive system responses.

5.3.4.2: Loss of Stack Loading Evaluations

The loss of the fuel cell stack electrical loading presents a substantial challenge to hybrid developers. In both fuel and sensible heat, the fuel cell stack has an appreciable level of stored energy. If an unexpected loss of loading occurs, such as from a power grid failure, this stored energy must be properly dissipated. Current approaches require expensive and bulky backup systems and extra valving that introduce additional system pressure losses. If control schemes for a load trip could incorporate more inherent features of a hybrid system, such as compressor bleed loading, a substantial operational advantage and cost reduction could be achieved by hybrid systems.

5.4: Significance

The application of HILS to a SOFC/GT hybrid system is a novel approach to addressing the complex interactions of an advanced power generation system. As a result of the research efforts detailed in this dissertation, HILS of a hybrid was successfully implemented. This expands the capabilities of HyPer as a tool in researching hybrids. The insights gleaned from HyPer HILS testing will assist in the commercialization of SOFC/GT hybrid generation systems. Therefore, this research effort provides a step

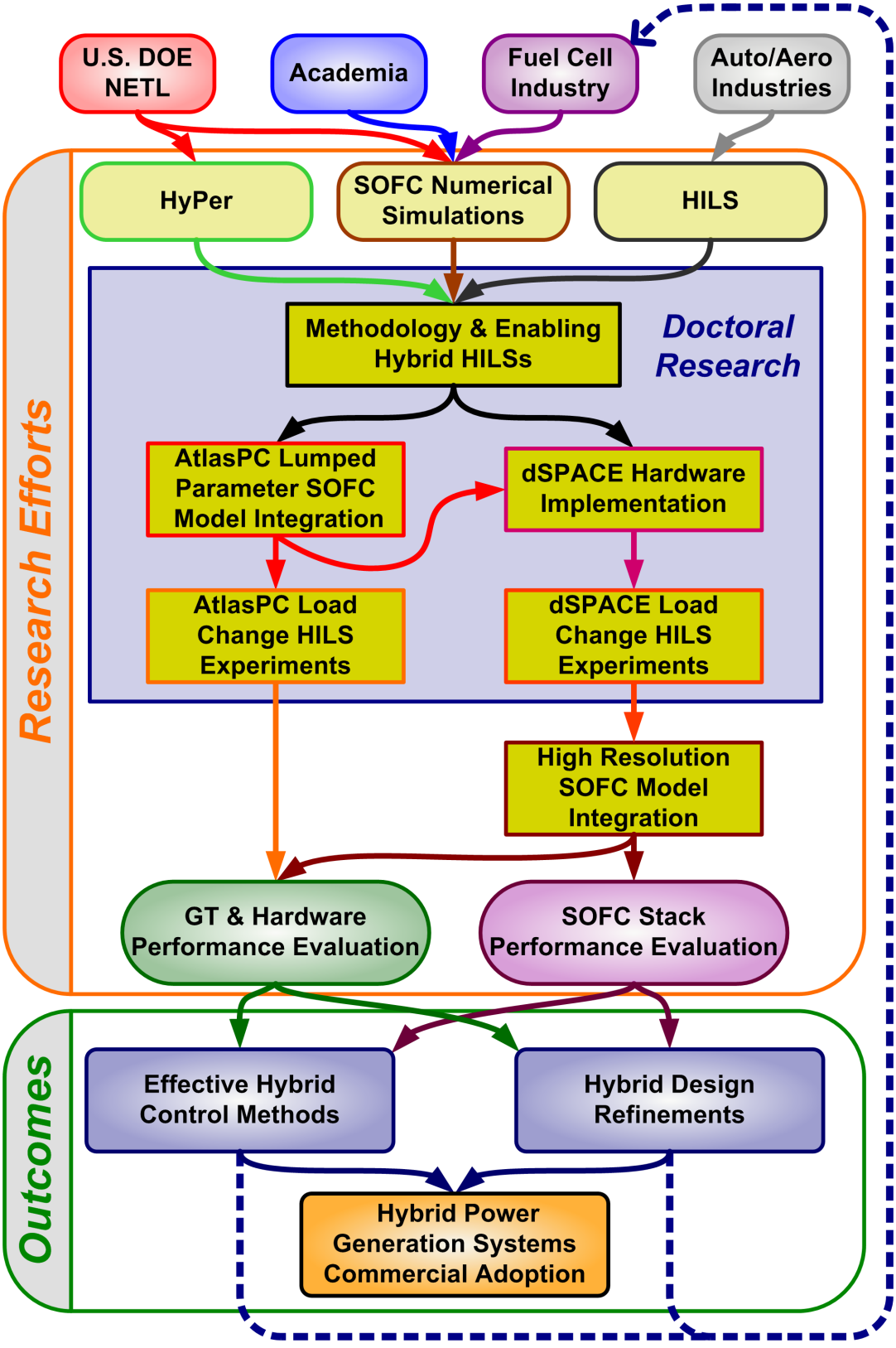

Figure 5.1: Value of Dissertation Research Efforts

toward realizing the SOFC/GT hybrid's potential for efficient, environmentally sound electrical power generation.

Figure 5.1 summarizes how this research effort supports the further development of SOFC/GT hybrids. Partners with a stake in the commercialization of hybrid systems are the U.S DOE NETL and the fuel cell industry. In addition, NETL has contributed with the development of the HyPer facility. By applying the HILS methodology, identified from its use in the automobile and aerospace industries, HyPer was further developed into an effective hybrid research platform. The efforts comprising this dissertation project furnished several key steps: developing the methodology for enabling and conducting hybrid HILS, implementing HILS with a bulk subsystem model, installing a high-speed computation hardware platform, and demonstrating HILS functionality in testing hybrid systems.

Initial HILS tests on HyPer where conducted using an AtlasPC controller. These tests verified the HILS methodology. The addition of the dSPACE platform improved HyPer's computational capabilities to facilitate higher fidelity simulations, allowing for greater insights into gas turbine and SOFC performance and characteristics. The results from HyPer HILS experiments provide insights into system dynamic behaviors. These efforts will thereby provide a tool in developing better control methods and refining hybrid design. In turn, this work will assist fuel cell developers in creating viable hybrid power generation systems, leading to their commercialization and acceptance as reliable suppliers of efficient electrical power.

As demand grows for more environmentally conscious energy systems, hybrids will increasingly be called upon to deliver on this promise. Before that can be realized,

obstacles to hybrid commercialization must overcome. Toward that end, this dissertation effort has produced an innovative application of HILS to hybrid systems, an approach that will enhance the capabilities of researchers in investigating hybrid cycles. In the long term, this work will assist in the implementation of the first generation SOFC/GT hybrids for electrical power generation.

APPENDIX A: EFFICIENCY AND UTILIZATION TERMS

The following pages are used to define the simulated efficiencies and fuel utilization terms used in the previous chapters.

A.1: Cell Per Pass Fuel Utilization

The cell per pass fuel utilization captures the ratio of the rate of fuel reacted in the cell divided by the inlet fuel flow rate to the cell. It is found by using the inlet and outlet molar flow rate of hydrogen:

$$U_{F,\,pass} = 1 - \frac{\dot{n}_{H2,\,an,\,out.}}{\dot{n}_{H2,\,an,\,in.}} \qquad [A.1]$$

A.2: Stack Fuel Utilization

The stack fuel utilization captures the ratio of the fuel utilized in the stack divided by the fuel inlet flow to the reformer. It is found by accounting for the anode fuel recycle and the cell per pass fuel utilization:

$$U_{F,\,stack.} = \frac{U_{F,\,pass}}{1 - \frac{\lambda}{100} + U_{F,\,pass}\frac{\lambda}{100}} \qquad [A.2]$$

A.3: Cell Reaction Efficiency

The cell reaction efficiency captures the ratio of electrical power generated in a cell to the heating value of the hydrogen reacted. It is found by dividing the cell

operating voltage by the ideal lower heating potential of hydrogen, $E_{LHV,H2}$, which equals 1.25 V. The resulting equation is

$$\eta_{TH,rxn} = \frac{V_{cell}}{E_{LHV,H2}} = \frac{V_{cell}}{1.25} \qquad [A.3]$$

A.4: Stack Efficiency

The fuel cell stack efficiency represents the ratio of electrical power generated to the rate of energy input to the stack. It is found by dividing stack power by the lower heating value rate of the methane fuel supplied to the stack's reformer. The equation is

$$\eta_{TH,stack.} = \frac{\dot{W}_{stack.}}{\Delta h_{LHV,CH4}\,\dot{m}_{fuel,ref}} \qquad [A.4]$$

where the lower heating value of the methane fuel is $\Delta h_{LHV,CH4}$ = 50,070 kJ/kg.

A.5: System Efficiency

The system efficiency is the projected operating efficiency of the simulated hybrid system on a lower heating value basis. It is found by summing the simulated stack power and measured turbine power, and then dividing it by the heating value rate of the total simulated methane fuel. The simulated fuel rate is the sum of the C1 precombustor fuel and the stack reformer inlet fuel. The equation is

$$\eta_{TH,sys} = \frac{\dot{W}_{stack.} + (\text{JI-552})}{\Delta h_{LHV,CH4}\left(\dot{m}_{fuel,ref} + \dot{m}_{fuel,C1}\right)} \qquad [A.5]$$

where the lower heating value of the methane fuel is $\Delta h_{LHV,CH4}$ = 50,070 kJ/kg.

APPENDIX B: HYPER INSTRUMENTATION ERROR

The following pages are a brief summary of the measurement error as measured by the APACS control system. The statistics presented in this appendix are from steady-state operation at a 45 kW electrical loading with all bypass valves closed. The reported statistics are for a 200 s sample (501 data points) of continuous operating data.

B.1: Optical Turbine Rotational Speed Sensor

The standard deviation in the rotational speed measurement (ST-502) was 28.8 rpm for a mean speed of 40,500 rpm. This corresponds to 0.07 % relative error in the precision of the measurement.

B.2: Thermocouples

All thermocouples used in the HyPer facility are type K. The manufacturer's stated operating range for these thermocouples is -200 °C to 1250 °C. The indicated standard limits of the error is the greater of 2.2 °C or 0.75 % of the measurement. For the air plenum temperature (TE-326) the standard deviation observed was 0.48 °C at a mean temperature of 473.8 °C. This corresponds to 0.10 % relative error in the precision of the measurement. The relative errors in the precision observed in the other HyPer temperature measurements are similar.

B.3: Pressure Transducers

Numerous types of pressure transducers are used in HyPer, and the information on the manufacturers' indicated error is not readily available. For the air plenum pressure (PT-305) the standard deviation observed was 0.63 kPa at a mean of 234.8 kPag. This corresponds to 0.27 % relative error in the precision of the measurement. The relative errors in the precision observed in the other HyPer pressure measurements are similar.

B.4: Annubar Air Mass Flow Meters

For the annubar meters the manufacturer's stated mass flow accuracy is 0.90%. For the compressor inlet airflow rate (FE-110) the standard deviation observed was 0.017 kg/s at a mean of 1.852 kg/s. This corresponds to 0.93 % relative error in the precision of the measurement. Likewise, for the inlet flow rate into the air plenum (FE-380) the standard deviation observed was 0.0066 kg/s at a mean of 1.426 kg/s. This corresponds to 0.44 % relative error in the precision of the measurement.

In March 2006, the compressor inlet meter (FE-110) was sent off-site for calibration. The results of that calibration indicated that the inlet airflow was being undermeasured by a full scale error of -5 % to -25 %. The calibration results were used to update the FE-110 data acquisition in the APACS control system. However, FE-380 was not calibrated in a similar fashion, and test results indicated that the plenum airflow was also being undermeasured.

Therefore a thermodynamic analysis of numerous HyPer steady-state operating data was used to infer a calculated air plenum inlet flow rate. For this analysis HyPer was operated with all valves closed at various loads and with flow restrictions at the system inlet. This generated a range of compressor and plenum airflow rates. With all

valves closed, the air plenum flow rate should be equal to the compressor rate minus the stab pipe loss. However, the flow rate of the stab pipe loss is unknown, so a balance of the turbine, compressor, and generator power is used to establish the flow rate of the stab pipe loss. This stab loss value is then used to infer a calculated air plenum inlet airflow rate.

Figure B.1 presents the results of the analysis of nine steady-state operating points. In the range that was evaluated, the measured FE-380 is up to 0.2 kg/s less than the calculated value for the air plenum inlet flow.

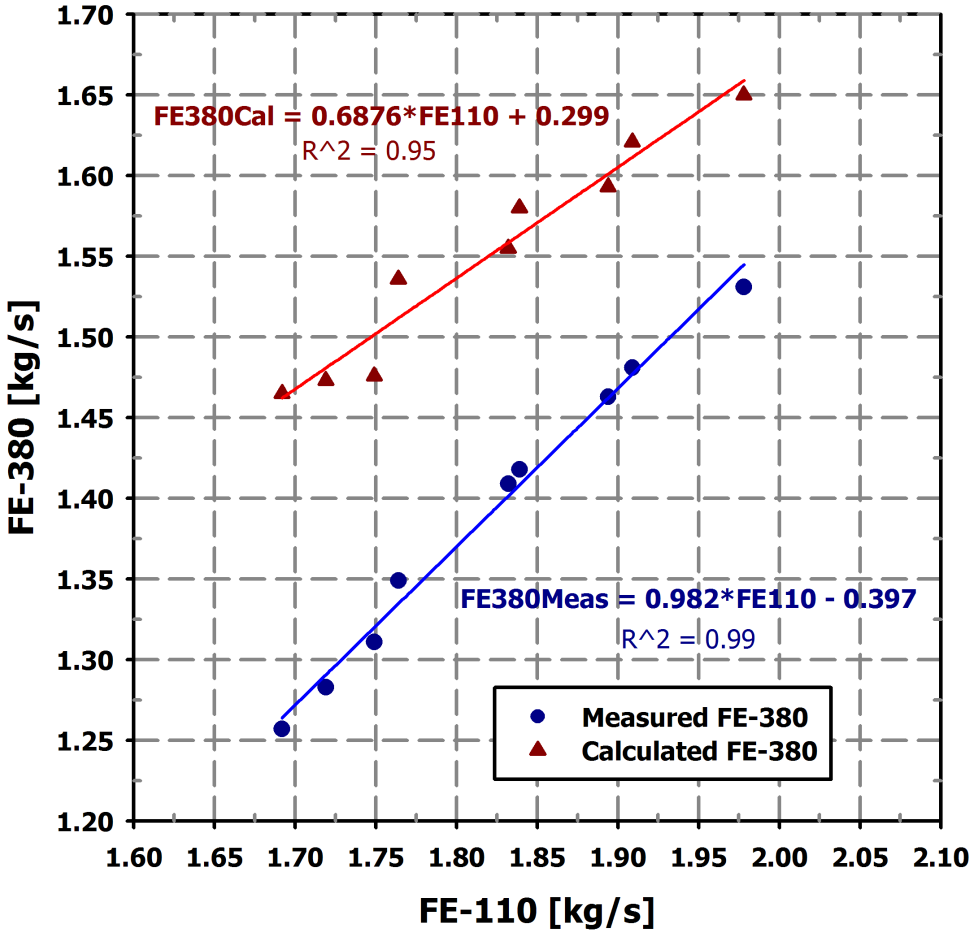

Figure B.1: FE-380 Flow Correction Results

APPENDIX C: HYPER HILS TEST PLAN

The following pages present a test plan for a HyPer HILS operation. This experiment was to evaluate a fuel cell load change under various conditions. The dSPACE system was used for model execution. It was conducted on August 15, 2006.

JVo

Hyper Test Plan and Check List: dSpace FCM Load Change Test
August 15, 2006

Purpose: The purpose of the startup test is to evaluate system performance during a cold start with all bypass valves closed. The remaining control system gains will be set at previously determined default values. Reproducibility of startup and stall will depend on the humidity and ambient pressure.

The purpose of the operational test is to perform five simple fuel cell transients to demonstrate the hardware-in-the-loop simulation process. The dSpace hardware will be used in this test. The test will be performed with a 45 kW load on the turbine. The hot air bypass and bleed air will be closed.

For the fuel cell transients a load **decrease of 5%** from steady state operation will be performed for the first four tests and a load **decrease of 20%** will be done with load based speed control for the last test. Once the new steady state condition is reached the load will be returned to its original set point. During the tests, the simulated fuel flow to the fuel cell reformer will be held constant for test 1, 3, 4, and 5. The simulated C1 pre-combustor fuel flow will be held constant in the first simulation and maintained for an exit temperature control set point for the remainder of the tests. The tests are summarized as follows:

1) A 5% reduction in fuel cell current will be made with a manual **setting of FV-170** for 1.0kg/s as an initial condition. The **C1 combustor will be fired at a constant** fuel mass flow throughout the transient.
2) A 5% reduction in fuel cell current and 5% reduction in reformer fuel flow will be made with a manual setting of FV-170 for 1.0kg/s as an initial condition. The **C1 combustor will be fired to control** temperature set point throughout the transient.
3) A 5% reduction in fuel cell current will be made with **automation of FV-170 for flow** set point of 1.0kg/s throughout the transient. The C1 combustor will be fired at a constant temperature set point throughout the transient.
4) A 5% reduction in fuel cell current will be made with a **manual setting of FV-170** for 1.0kg/s as an initial condition. The C1 combustor will be **fired to control temperature** set point throughout the transient. **Load based speed control** will be used to maintain a constant turbine speed throughout the transient.
5) A 20% reduction in fuel cell current will be made with a **manual setting of FV-170** for 1.0kg/s as an initial condition. The **C1 combustor will be fired to control** temperature set point throughout the transient. **Load based speed control** will be used to maintain a constant turbine speed throughout the transient.

Throughout all testing, the control system will impose both a lower limit and higher limit on the turbine speed to insure that operational constraints are observed. Speed will be limited to 38,500rpm on the low side to avoid a load trip by the 95% speed switch (38,475rpm), and 43,000rpm on the high side to avoid excessive overspeed. A nominal condition of a 40,500rpm turbine speed will be used to initiate each open loop test.

The cold air by-pass will be monitored during the transients, and opened to 55% upon the first indication of stall in an attempt to recover from compressor surge.

Note: Qdot will be calculated based on the same mass air flow at the inlet and outlet of simulation block.

Failed start restart 9:44 AM

Start Procedure of Test 060815FCS

- [x] [x] **DT** Pre-Operational inspection **COMPLETE.** 8:00 A.M. Amb: 19C
- [x] [x] **DT** Watchwindows **OPEN.** At: 29.97 in Hg
- Temp. 22 C
- [x] [x] **LL** APACS and Atlas Clocks **SYNCHONIZED.**
- [x] [x] **LL** Live Engineering Data Spreadsheet **INITIALIZED.**
- [x] [x] **DT** Log Test Conditions
  FC Model Version: DSFCSIMVERSION 2.75 GAP #: HYPER 61
  Note Num. of Cells: 1500 NG LHV for RFV: 845.33 KJ/mol 799 KJ/mol
  ~~16.97 Molar Mass of fuel~~ 16.04 Kg/Kmol
- [x] [x] **TS** Start dSpace System FCM start and **OPERATING ON CONSTANT INPUTS.**

- [x] [x] **DT** Natural Gas Totalizer **RESET.**
- [x] [x] **DT** HV-414, HV-408 and HV-430 **CLOSED.**

- [x] [x] **LL** Set Gas Valve FV-432 Mode to **Auto Ramp (Ramp initiated at 8000rpm)** 7000 rpm
- [x] [x] **LL** Set **All OTHER GAP Gains** to **DEFAULT** settings

- [x] [x] **DT** Set Hot Air By-Pass **FV-380** Mode to **1: Manual, 0% Open**
- [x] [x] **DT** Set Bleed Air **FV-162** Mode to **2: Manual, 100% Closed**
- [x] [x] **DT** Set Cold Air By-Pass **FV-170** Mode to **1: Manual, 0% Open**
- [x] [x] **DT** Blower **ON** (Alt-Tab) 8:41:21 AM
- [x] [x] **DT** APACS Log **START** 9:46:17 8:41:36 AM
- [x] [x] **LL** Data Log **START**
- [x] [x] **TS** dSpace Data Capture **START**

- [x] [x] **DT** HV-600 **OPEN** (Alt-Tab) 8:41:55 AM

- [x] [x] **JV** System Purge **ON**
- [x] [x] **DT** HV-408 and HV-430 **REQUEST OPEN**

- [x] [x] **JV** FE-380 positive flow ≥ 0.10kg/s **CHECK**
- [x] [x] **JV** Purge Complete **CHECK**
- [x] [x] **JV** HS-460C Burner Ignition Automated at 9,000rpm **CHECK** cut off
- [x] [x] **JV** If purge complete over 9,000rpm, HS-460A Manual Ignition **ON**
- [x] [x] **JV** TE-333 shows flame **CHECK** ignition then cut off 9:48:34 AM
- [ ] [x] **JV** ST-502 > 35,000rpm, I-4 enabled **CHECK** New ignition at 9:56:19
  Stop DATA Log at 8:49:20 AM
- [ ] [x] **DT** ST-502 > 41,000rpm, HV-600 **CLOSED**
- [ ] [x] **DT** Blower **OFF**

Preheat System Piping and Vessels

not working switch not on 2L fixed

- ☐ ☑ DT Load Bank Cooling Fan (HS-530) **ON**
- ☐ ☑ DT Interlock 14 **ENABLED** 10:02 AM
- ☐ ☑ DT Load Bank in Manual Mode **CHECK**
- ☐ ☑ DT Set Bleed Air By-Pass **FV-162** Mode to **2: Manual, 85% Closed**
- ☐ ☑ DT Increase load to 45kW 25 KW then 45 KW 10:04:26 AM 10:05:07 AM
- ☐ ☑ JV ST-502 at approximately 40,500rpm **CHECK** 10:05:47 AM
- ☐ ☑ JV Wait until TE-344 is at about 1000°F **CHECK** Stop Data Log at 10:10 10:25:25 IVO
- ☐ ☑ DT 10:28:56 Set Cold Air By-Pass **FV-170** Mode to **1: Manual, 25% Open** using auto mode @ 1 kg/sec
- ☐ ☑ DT 10:29:08 Set Bleed Air By-Pass **FV-162** Mode to **2: Manual, 100% Closed**
- ☐ ☑ DT 10:33:29 Set Cold Air By-Pass **FV-170** Mode to **1: Adjust until FE-380 = 1.00kg/s, Note%:**
- ☑ LL Step change to 1.1 kg/sec Setpoint 10:36:02 back to 1 kg/sec
- ☐ ☐ LL Data Log **STOP, RETRIEVE, RENAME, SAVE and START NEW LOG**

FV-170 44.0 % Open
Stop Time:
Start Time: 11:54:12

- ☐ ☑ JV Wait until TE-344 is constant for 30s (±0.1°C) **CHECK**

- ☐ ☑ DT Set Cold Air By-Pass **FV-170** Mode to **1: Adjust until FE-380 = 1.00kg/s, Note%:** 44.1 % 1.0079 kg/s #198
- ☐ ☑ JV If stall indicated, implement stall recovery.
- ☐ ☑ TS Evaluate FCM and adjust or reload as required.

Prepare for Fuel Cell Simulation

- ☐ ☑ TS 11:56:15 Adjust C1 setpoint temperature to agree with simulated C1 exit temperature. 850 °C 10 9/8
- ☐ ☑ TS Switch to C1 exit temperature control.
- ☐ ☑ TS Verify FC model input conditions are initialized on dSpace.
- ☐ ☑ TS Adjust FC $\dot{m}_{AIR}$ to agree with Hyper FE-380. 1 kg/sec
- ☐ ☑ TS Adjust FC T_{AIR} to agree with Hyper TE-326A. 435 °C
- ☐ ☑ TS Adjust FC P_{AIR} to agree with Hyper PT-305. 240 kPag
- ☐ ☑ TS Adjust Tubine Elec Load to agree with Hyper JI-552A. 44 kW / 45 kW
- ☐ ☑ TS Switch to live measurements.

- ☐ ☑ LL Adjust RFV P_{NG} to agree with Hyper PT-436 and switch to live measurement. 39 % 388 kPa
- ☐ ☑ LL Adjust RFV T_{NG} to agree with Hyper TE-422 and switch to live measurement. 19°C

☐ ☑ **LL** Insure that the LHV = 799 kJ/mol and fuel molar weight = 16.04.

☐ ☑ **LL** Vary $\dot{Q}$ to RFV until predicted fuel flow matches measured fuel flow at FT-432 695 vs 688

☐ ☑ **LL** Adjust RFV Scalar to match FV-432 demand 1.065

☐ ☑ **TS** Adjust Fuel Cell model so predicted $\dot{Q}$ agrees with RFV $\dot{Q}$

☐ ☑ **LL** Switch to RFV(FC $\dot{Q}$) live fuel cell model output from dSpace

Verify Turbine Speed Dead Band Limits

☐ ☑ **LL** Verify Lspeed (SetPoint=38,500)

☐ ☑ **LL** Verify Hspeed (SetPoint=43,000)

☐ ☑ **LL** Verify Lspeed_FC LSS(SEL_1=TRUE from RFV(FC))

☐ ☑ **LL** Verify Hspeed_FC HSS(SEL_2=TRUE from RFV(FC))

Switch to Fuel Cell Model Control

☐ ☑ **LL** Final adjustment of fuel cell model so RFV demand = FV-432 %demand **CHECK** 39.6 39.5

☐ ☑ **LL** Verify fuel cell heat capacity scalar = 1 **CHECK**

☐ ☑ **LL** Data Log **STOP, RETRIEVE, RENAME, SAVE and START NEW LOG**
Time: 12:15:54

☐ ☑ **LL** Select IN_2 FC with DB Speed Split control (Fuel cell model in control) **CHECK**
Time: 12:17:08

☐ ☑ **LL** Watch for drift or oscillations of pv432% or ST-502 **MONITOR**

☐ ☑ **TS** Record FC SS inputs and conditions: Load= 390A FC Fuel= 15.178 gps Recycle% 78
Qdot = 700 KW C1 Fuel= 10.1 gps C1 Setpoint Temp= 850°C

TEST 1: Implement 5% Fuel Cell Transient Load Decrease with C1 set to constant Fuel Flow C1($\dot{m}$)

☐ ☑ **TS** Verify Heat Capacity Scalar = 1.

☐ ☑ **TS** Verify C1 to fire at controlled exit temperature set point and **Note flow:** 10.1 gps

☐ ☑ **TS** Set C1 to fire at manual set point as noted above. 850°F

Stop data log 12:15:54 / Start data log 12:17:08

☐ ☑ **LL** Watch for drift or oscillations of pv432% or ST-502 **MONITOR**
Note Speed ST-502 at End of Transient:
Note Fuel Flow FT-432 at End of Transient:

☐ ☑ **TS** Set FC Load Amps to **95%** current setpoint. Note new Load: 370.5 A Time: 12:18:46

☑ ☐ **LL** Watch for drift or oscillations of pv432% or ST-502 **MONITOR**
Note Speed ST-502 at End of Transient: ST502 = 550rpm DT
Note Fuel Flow FT-432 at End of Transient: 39.8%
waiting on tail end of this test

☑ ☐ **LL** Data Log **STOP, RETRIEVE, RENAME, SAVE and START NEW LOG**
STOP 12:55:25 ~~STOP~~ Time: START 12:57:25 GCF DT

☑ ☐ **TS** Set FC Load Amps to original setpoint. Note new Load: 390A ~~Amps~~ Time: 12:37:33

☑ ☐ **LL** Watch for drift or oscillations of pv432% or ST-502 **MONITOR**
Note Speed ST-502 at End of Transient: 40,550 rpm 12155525 GCF
Note Fuel Flow FT-432 at End of Transient: ~~14.9 g/s~~ 39.8 %

TEST 2: Implement 5% Fuel Cell Transient Load Decrease with Constant Fuel Utilization and C1 set to Exit Temperature Control *C1(T)*

☑ ☐ **TS** Verify C1 to fire at controlled exit temperature set point. **Note C1 StPt:** 850°C Flow to C1 10 g/s
Note FC Load: 390 A **FC Ref Fuel Flow:** 15.17 g/s

☑ ☐ **LL** Watch for drift or oscillations of pv432% or ST-502 **MONITOR**
Note Speed ST-502 at End of Transient: 40,600 GCF
Note Fuel Flow FT-432 at End of Transient: 39.7 % GCF

☑ ☐ **TS** Set FC Load Amps to **95%** current setpoint. Note new Load: 370.5 A Time: 13:01:30
☑ ☐ **TS** Set FC Ref Fuel to **95%** current setpoint. Note new flow: 14.419 g/s GCF

☑ ☐ **LL** Watch for drift or oscillations of pv432% or ST-502 **MONITOR**
Note Speed ST-502 at End of Transient: 39,730 rpm
Note Fuel Flow FT-432 at End of Transient: 38.4 %

☑ ☐ **LL** Data Log **STOP, RETRIEVE, RENAME, SAVE and START NEW LOG**
Stop Time: 13:36
Start 13:38

☑ ☐ **TS** Set FC Load Amps to original setpoint. Note new Load: 390 Amps Time:
☑ ☐ **TS** Set FC Ref Fuel to original setpoint. Note new Load: 15.18 g/s Time: 13:19:03
DT

☐ ☐ **LL** Watch for drift or oscillations of pv432% or ST-502 **MONITOR**
Note Speed ST-502 at End of Transient: 40300 rpm
Note Fuel Flow FT-432 at End of Transient: 39.2 %

TEST 3: Implement 5% Fuel Cell Transient Load Decrease with C1 set to Exit Temperature Control *C1(T)* **and CA Flow Control**

☐ ☑ **TS** Verify C1 to fire at controlled exit temperature set point.

☐ ☑ **DT** Set Cold Air By-Pass **FV-170** Mode to **2: Auto, Set Point = 1.0kg/s**

☐ ☑ **LL** Watch for drift or oscillations of pv432% or ST-502 **MONITOR**
Note Speed ST-502 at End of Transient: 40550
Note Fuel Flow FT-432 at End of Transient: 39.3%

☐ ☑ **TS** Set FC Load Amps to **95%** current setpoint. Note new Load: 370.5A Time: 13:41:42

☐ ☑ **LL** Watch for drift or oscillations of pv432% or ST-502 **MONITOR**
Note Speed ST-502 at End of Transient: 40600
Note Fuel Flow FT-432 at End of Transient: 39.4%

☐ ☑ **LL** Data Log **STOP, RETRIEVE, RENAME, SAVE and START NEW LOG**
Time: 14:16:25

☐ ☑ **TS** Set FC Load Amps to original setpoint. Note new Load: 390.A Time: 14:03:18

☐ ☑ **LL** Watch for drift or oscillations of pv432% or ST-502 **MONITOR**
Note Speed ST-502 at End of Transient: 40,450
Note Fuel Flow FT-432 at End of Transient: 39.2%

TEST 4: Implement 5% Fuel Cell Transient Load Decrease with C1 set to Exit Temperature Control *C1(T)* **and Load Based Speed Control**

☐ ☑ **DT** Set Cold Air By-Pass **FV-170** Mode to **1: Adjust until FE-380 = 1.00kg/s, Note%:** 44.1%

Implement Load Based Speed Control

☐ ☑ **LL** Fuel valve demand **Note%:** 39.5

☐ ☑ **LL** On Atlas Gap sheet 12 match Manual Open Loop Fuel Valve setting to current Valve Demand -0.1%

☐ ☑ **LL** On Atlas Gap sheet 16 Select (2) Dead Band Speed Control

☐ ☑ **LL** On Atlas Gap sheet 13 verify Max Load to 45 kW

☐ ☑ **LL** Verify Min Load to 44 kW

☐ ☑ **LL** Select LBSC Proc variable (2) ST-502A

☐ ☑ **LL** Verify LBSC min=0 and max=95

☐ ☑ **LL** Verify Load-Based Speed Controller Set-Point to 40,500 rpm

☐ ☑ **DT** On Operator's Control Screen confirm Atlas Load Demand at 45kW

- ☐ ☑ **DT** Toggle Load Demand from Manual to Auto (Atlas source Load Demand)
- ☐ ☑ **LL** Observe no change or inadvertent control malfunction
- ☐ ☑ **LL** Observe speed drift with HX heat-up
- ☐ ☑ **LL** Adjust Manual Open Loop Fuel Valve setting down by 0.1% increments to attain nominal 40,500 rpm
- ☐ ☑ **LL** Increase Max Load to 50kW
- ☐ ☑ **LL** Decrease Min Load to 40kW
- ☐ ☑ **LL** Observe anticipated increase in Load Demand to maintain Speed Set-Point
- ☐ ☑ **LL** Reduce Manual Open Loop Fuel valve setting down by 0.2% increments to attain LBSC near nominal 45kW
- ☐ ☑ **LL** Increase Max Load to 60kW
- ☐ ☑ **LL** Decrease Min Load to 30kW

Start Fuel Cell Simulation

- ☐ ☑ **TS** Verify C1 to fire at controlled exit temperature set point.
- ☐ ☑ **LL** Watch for drift or oscillations of pv432% or ST-502 **MONITOR**
  Note Speed ST-502 at End of Transient: 40500
  Note Fuel Flow FT-432 at End of Transient: 39.2
- ☐ ☑ **TS** Set FC Load Amps to **95%** current setpoint. Note new Load: 370.5A Time: 14:27:33
- ☐ ☑ **LL** Watch for drift or oscillations of pv432% or ST-502 **MONITOR**
  Note Speed ST-502 at End of Transient: 40500 rpm
  Note Fuel Flow FT-432 at End of Transient: 39.5 %
- ☐ ☐ **LL** Data Log **STOP, RETRIEVE, RENAME, SAVE and START NEW LOG**
  Time: Stop 15:02:06 DT
  Start 15:04:32
- ☐ ☑ **TS** Set FC Load Amps to original setpoint. Note new Load: 390 A Time: 14:43:40
- ☐ ☑ **LL** Watch for drift or oscillations of pv432% or ST-502 **MONITOR**
  Note Speed ST-502 at End of Transient: 40500 rpm
  Note Fuel Flow FT-432 at End of Transient: 39.4 % 15:02:00

TEST 5: Implement 20% Fuel Cell Transient Load Decrease with C1 set to Exit Temperature Control $C1(T)$ and Load Based Speed Control

- ☐ ☑ **DT** Set Cold Air By-Pass **FV-170** Mode to **1: Adjust until FE-380 = 1.00kg/s, Note%:** 44.1%

Start Fuel Cell Simulation

☑ ☐ **TS** Verify C1 to fire at controlled exit temperature set point. 850°C

☑ ☐ **LL** Watch for drift or oscillations of pv432% or ST-502 **MONITOR**
Note Speed ST-502 at End of Transient: 40,500 rpm 45kW load set
Note Fuel Flow FT-432 at End of Transient: 39.2%

☑ ☐ **TS** Set FC Load Amps to **80%** current setpoint. Note new Load: 312 Amps Time: 15:04:43

☑ ☐ **LL** Watch for drift or oscillations of pv432% or ST-502 **MONITOR**
Note Speed ST-502 at End of Transient: 40,500 rpm 53kw set
Note Fuel Flow FT-432 at End of Transient: 40.5%

☑ ☐ **LL** Data Log **STOP, RETRIEVE, RENAME, SAVE and START NEW LOG**
15:46:00 Time: 15:42:30 ~~SCF~~ start

☑ ☐ **TS** Set FC Load Amps to original setpoint. Note new Load: 390 Amps Time: 15:25:06

☑ ☐ **LL** Watch for drift or oscillations of pv432% or ST-502 **MONITOR**
Note Speed ST-502 at End of Transient: 40,460 rpm 15:42:50
Note Fuel Flow FT-432 at End of Transient: 39.1%

Return to Manual Load Control

☑ ☐ **LL** Adjust Open Loop Fuel Valve setting to get 40,500 rpm at 45kW Load
☑ ☐ **LL** Adjust Max Load to 45 kW
☑ ☐ **LL** Adjust Min Load to 44 kW

☑ ☐ **DT** Verify Manual Load Demand at 45kW
☑ ☐ **DT** Toggle Load Demand from Auto to Manual

Return to Speed Control by Fuel Valve

☑ ☐ **LL** On sheet 16 Select Fuel Valve Demand from Open Loop to (1)=Speed Control
15:46:10 P.M. SCF

System Shutdown

☑ ☐ **DT** Set Cold Air By-Pass **FV-170** Mode to **1: Manual, 25% Open**
☑ ☐ **DT** Insure all load is removed **CHECK** 15:49:14 P.M. SCF Let Heater cool
☑ ☐ **DT** Load Bank Cooling Fan (HS-530) **OFF**

☑ ☐ **DT** Select GAP Speed Sheet- Set Gas Valve Mode to Automated fuel shutdown ramp. Start at 150rpm/s but increase rate at discretion below 38,000 rpm.
15:52:40

☑ ☐ **JV** At stall or 28,000rpm, Fuel **OFF (Control #1)** 15:54:13
☑ ☐ **LL** Data Log **STOP, RETRIEVE, RENAME** save D:\Work\D060815FCSx.log
15:56:02 P.M. JCF

APPENDIX D: HYPER HILS EXPERIMENT LOG

The following pages present relevant pages from the HyPer operation log book for a HILS test. This experiment was to evaluate a fuel cell load change under various conditions. The dSPACE system was used for model execution. It was conducted on August 15, 2006.

0 Continuation	**Hyper Project Test Log**	Date: 8/15/2006

Operators: David Tucker, Larry Lawson, Tom Smith, Chris Ford, JVO

Test Plan File Name: 060815 FCS **By:** DT and TS

APACS File Name(s): A060815 FCS

Atlas Datalog File Name(s): D060815FCSx DS 060815FCSx

Live Data Eng. Spreadsheet Name(s): E 060815 FCS

Post Run:	Totalized Fuel 301,363 g	Failed Start? Yes	Multiple Starts? Y

Objective: FCS w/ CICT), CI(in), LBSC, and ~~EI~~ setpoint and FV-170 cntrl

Intial Valve Conditions: FV380- 0% open FV162- 100% closed FV170- 0% Open

Initials	Log Time	Event Time	Description of the event or action
DT	8:29	8:00	Pre-run check complete Igniter and UV air needle valves initially closed.
DT	8:41:55	—	HV-600 Open Valve Pointing straight down
DT	9:48	—	Start igniter Failed ignition
DT	9:57:33	—	Turbine speed at nominal (40,500rpm)
DT	15:52:40	—	Shutdown initiated (combustor fuel flow lowered)
DT	15:54:13	—	Control #1 activated (fuel flow stopped)
DT	8:31	8:31	DP = 19°C, Alt. = 29.97 "Hg, T = 22°C 16.97 under water
DT	8:31	—	Using Hyper 61, NG LHV = 845.33 KJ/mol from FC GC
			Fuel Cell model ~~FCS~~ FC Sim V2.75
			Using 1500 cells. Igniter @ ½ turn
DT	8:41:38	—	DL Start
DT	8:43:19	—	Failed start - Going to adjust airflow Ign.
DT	8:49:20	—	DL Stop
DT	8:50	—	Asked to ~~stop~~ suspend operations until notice from
			Mike Monahan regarding Plant Air.
DT	9:30:00	—	Test igniter - Failed at ¼ turn
DT	9:38:03	—	Test igniter at ⅛ turn - Showed Flame
DT	9:46:35	—	HV-600 Open
DT	9:46:47	—	Start DL
DT	9:55:30	—	HV 600 Open
DT	9:56:10	—	Igniter On
DT	9:59:30	—	Load Bank Fan will not go on. Larry to check.
DT	10:01:30	—	Load Bank Fan on
DT	10:02:00	—	IA enabled.
DT	10:03:15	—	BA to 85% closed
DT	10:04:23	—	Increasing load to 25 KW
DT	10:05:07	—	Increase Load to 45 KW
DT	Log continued on next page? Yes		By:

1	Continuation	**Hyper Project Test Log**	**Date:** 8/15/2006

Operators:

Test Plan File Name: **By:**

APACS File Name(s):

Atlas Datalog File Name(s):

Live Data Eng. Spreadsheet Name(s):

Post Run:	Totalized Fuel	Failed Start?	Multiple Starts?

Objective:

Intial Valve Conditions: **FV380-** **FV162-** **FV170-**

Initials	Log Time	Event Time	**Description of the event or action**
			Pre-run check complete
			HV-600 Open
			Start Igniter
			Turbine speed at nominal (40,500rpm)
			Shutdown initiated (combustor fuel flow lowered)
			Control #1 activated (fuel flow stopped)
DT	10:10:00 –		Stop DL
DT	10:17:16 –		ϕ = 0.22 TE-333 and TE-202 in alarm
			EGT = 1048°F (564°C) TE-333 = 1624°F (753°C)
DT	10:18:55 –		TE-344 = 819°F
DT	10:25:25 –		TE-344 = 1000°F
DT	10:27:20 –		FV-170 to ~~25%~~ by 1.00 kg/s by Larry
			in Automated mode.
DT	10:29:08 –		when FV-170 25%, FV-162 100% Closed
DT	10:33:33 –		FV-170 to automated 1.80 kg/s ~40%
			Limited between 80% and 20%
DT	10:34:49 –		1107°F
DT	10:36:02 –		Flow set to 1.1 kg/s using FV-170 ~38%
DT	10:37:48 –		TE-344 = 1095°F
DT	10:39	10:38	Flow set to 1.0 kg/s using FV-170 ~ 44%
DT	10:42:45 –		TE-344 = 1077°F
DT	10:48:50 –		TE-344 = 1051°F TE-333 = 1708°F in Alarm
DT	10:57:00 –		TE-344 = 1023°F TE-333 = 1720°F " "
DT	11:08:30 –		TE344 = 996°F TE-333 = 1706°F " "
DT	11:14:00 –		TE344 = 985°F TE-333 = 1704°F " "
			16.97 molar mass of fuel used W/ LHV
DT	11:25:00 –		TE344 = 972°F TE-333 = 1707°F " "
DT	Log continued on next page? Y/N		By:

2	Continuation	**Hyper Project Test Log**	**Date:** 8/15/2005

Operators:			
Test Plan File Name:		**By:**	
APACS File Name(s):			
Atlas Datalog File Name(s):			
Live Data Eng. Spreadsheet Name(s):			
Post Run:	Totalized Fuel	Failed Start?	Multiple Starts?
Objective:			
Intial Valve Conditions:	**FV380-**	**FV162-**	**FV170-**

Initials	Log Time	Event Time	Description of the event or action
			Pre-run check complete
			HV-600 Open
			Start igniter
			Turbine speed at nominal (40,500rpm)
			Shutdown initiated (combustor fuel flow lowered)
			Control #1 activated (fuel flow stopped)
DT	11:26:30	–	Q̇ = 680kW
DT	11:32:00	–	TE344 = 966°F TE333=1711°F CA 44%
DT	11:40:00	–	TE344 = 961°F TE333= 1704°F CA 45%
DT	11:47:50	–	RFV setting 799 kJ/mol 16.04 g/mol FV
DT	11:49:00	–	~~Fuel V.~~ FV-170 clamped to 1% @ 44 to 45
DT	11:50:20	–	FV-170 set to 44.1%
DT	11:51:30	–	TE344 = 957°F TE-333 = 1702°F
DT	11:54:12	–	Start DL TE344 ~ 956°F
DT	11:56:11	–	prepping for FCS
DT	11:58:00	–	Switch to Live measurements on dSpace
DT	12:01:00		Setting Dead Band Limits
DT	12:01:37		FV432 = 39.7%
DT	12:02:28		Change to FC control
DT	12:03:20		Speed dropped to 40,100 rpm FE380= 0.99kg/s
DT	12:05:30		+5 amps load added to FCM · TE344 = 956°F
DT	12:08:38		+5 more amps load added to FCM TE344=956°F
DT	12:11:54	–	ST502C = 40,500 rpm FV432 = 39.6%
DT	12:15:54	–	Stop DL
DT	12:17:08	–	Start DL
DT	12:18:46	–	-5% FC load amps from 390A to 370.5A
DT	12:19:30	–	Speed to 41,300 rpm
DT	Log continued on next page? Yes		By:

3 Continuation	**Hyper Project Test Log**	Date: 8/15/2006

Operators:

Test Plan File Name: **By:**

APACS File Name(s):

Atlas Datalog File Name(s):

Live Data Eng. Spreadsheet Name(s):

Post Run:	Totalized Fuel	Failed Start?	Multiple Starts?

Objective:

Intial Valve Conditions: **FV380-** **FV162-** **FV170-**

Initials	Log Time	Event Time	**Description of the event or action**
			Pre-run check complete
			HV-600 Open
			Start igniter
			Turbine speed at nominal (40,500rpm)
			Shutdown initiated (combustor fuel flow lowered)
			Control #1 activated (fuel flow stopped)
DT	12:28:30 —		TE344 = 958°F FE380 = 1.04, FV432 = 40%
DT	12:36:30 —		ST502 = 550 rpm FV432 = 39.8%
DT	12:37:33 —		+5% Amps to FC from 370.5A to 390A
DT	12:38:00 —		ST502 = 39,700 rpm
DT	12:54:23 —		ST502 = 40,550 rpm FV432 = 39.8
DT	12:55:25 —		Stop DL
DT	12:57:25 —		Start DL 390-370.5
DT	13:01:30 —		-5% Amps and -5% Fuel 15.18 - 14.42%
DT	13:04:20		ST502 = 40,050 rpm FE380 = 0.98 kg/s
DT	13:17:30		ST502 = 39,730 rpm FE380 = 0.97 kg/s
			FV432 = 38.4%
DT	13:19:03		+5% Amps (370.5 - 390A) +5% Fuel to 15.18%
DT	13:21:25		ST502 = 40,300 rpm FE380 = 0.99 kg/s
DT	13:35:39		ST502 = 40,300 rpm FE380 = 0.98 kg/s
DT	13:36:00 —		DL Stop
DT	13:38:00 —		DL Start
DT	13:40:00 —		FV-170 in FE380 Flow Control
DT	13:44:45 —		ST502 = 40,450 FV432 = 39.4% TE344 = 96°F
DT	13:46:42 —		-5% FC Amps (370.5 Amps)
DT	13:54:50		ST502 = 40,680 FV432 = 39.6%
DT	14:02:02		ST502 40,600 rpm FV432 = 39.4%
DT	Log continued on next page? Yes		By:

4	Continuation	**Hyper Project Test Log**	Date: 8/15/2006

Operators:

Test Plan File Name: **By:**

APACS File Name(s):

Atlas Datalog File Name(s):

Live Data Eng. Spreadsheet Name(s):

Post Run:	Totalized Fuel	Failed Start?	Multiple Starts?

Objective:

Intial Valve Conditions: **FV380-** **FV162-** **FV170-**

Initials	Log Time	Event Time	**Description of the event or action**
			Pre-run check complete
			HV-600 Open
			Start igniter
			Turbine speed at nominal (40,500rpm)
			Shutdown initiated (combustor fuel flow lowered)
			Control #1 activated (fuel flow stopped)
DT	14:03:18		+5% Amps (390 Amps)
DT	14:16:25		Stop DL
~~DT~~	~~14:18:4~~		~~Start DL~~ DT
DT	14:19:00		ST502 40,480 FV432 = 39.2%
DT	14:21:00		FV170 = 44.1%
DT	14:21:50		Load to Auto
DT	14:22:20		Max load 94kw
DT	14:22:30		Min load to 0KW
DT	14:23:00		In load Based Speed Control
DT	14:25:00		Start DL
DT	14:27:33		-5% Amps (~~390~~ 370.5 Amps)
DT	14:29:50		Speed upto 51KW down to 47kw
DT	14:43:00		ST502 = 40,500, Load 45kw, FV432 = 39.5%
DT	14:43:40		+5% Amps (390 Amps) ⇒ Indicating 43 KW
DT	15:01:30		40,500rpm, Load 45kw, FV432 = 39.4%
DT	15:02:06		Stop DL
DT	15:04:32		Start DL
DT	15:07:23		-20 Amps (390 Amps to 312 Amps)
DT	15:20:30		TE326A = 464°C TE326B = 465°C
DT	15:23:15		Load Set 53KW, FV432 = 40.5%
DT	15:25:06		+20 Amps (312 Amps to 390 Amps)
DT	Log continued on next page? Yes		By:

5	Continuation	**Hyper Project Test Log**	Date: 8/15/2006

Operators:

Test Plan File Name: **By:**

APACS File Name(s):

Atlas Datalog File Name(s):

Live Data Eng. Spreadsheet Name(s):

Post Run:	Totalized Fuel	Failed Start?	Multiple Starts?

Objective:

Intial Valve Conditions: **FV380-** **FV162-** **FV170-**

Initials	Log Time	Event Time	**Description of the event or action**
			Pre-run check complete
			HV-600 Open
			Start igniter
			Turbine speed at nominal (40,500rpm)
			Shutdown initiated (combustor fuel flow lowered)
			Control #1 activated (fuel flow stopped)
DT	15:31:00		EL 42, FV432 = 38.7%
DT	15:40:50		EL 43, FV432 = 38.9% steady condition End
DT	15:42:00		Stop DL
DT	15:43:30		Start DL
DT	15:44:30		Max and Min load clamped
DT	15:45:30		Manual Load Demand
DT	15:46:10		Speed Controled by FV432 — Model ok.
DT	15:48:30		CA to 25% by clamping CA Auto
DT	15:49:14		EL to 0 kW
DT	15:51:07		Load Bank Fan off
DT	15:52:40		Shut down initiated
PT	15:54:13		Control #1 activated
DT	15:55:03		Turbine Stopped
DT	15:56:30		Stop DL

Log continued on next page? No By:

REFERENCES

Aguiar, P., C. S. Adjiman and N. P. Brandon (2004) "Anode-Supported Intermediate Temperature Direct Internal Reforming Solid Oxide Fuel Cell. I: Model-Based Steady-State Performance" *Journal of Power Sources* **138**(1-2): 120-136.

Al-Hamdan, Q. Z. and M. S. Y. Ebaid (2006) "Modeling and Simulation of a Gas Turbine Engine for Power Generation" *Journal of Engineering for Gas Turbines and Power* **128**(2): 302-311.

Bove, R. and S. Ubertini (2006) "Modeling Solid Oxide Fuel Cell Operation: Approaches, Techniques and Results" *Journal of Power Sources* **159**(1): 543-559.

Box, G. E. P. and N. R. Draper (1987) *Empirical Model-Building and Response Surfaces*, Wiley, John & Sons, Inc, pg. 424.

Brooks, F. J. (2000) *GE Gas Turbine Performance Characteristics*, GE Power Systems, Schenectady, NY, October 2000, Report GER-3567H.

Calise, F., M. Dentice D' Accadia, L. Vanoli and M. R. Von Spakovsky (2006) "Single-Level Optimization of a Hybrid SOFC-GT Power Plant" *Journal of Power Sources* **159**(2): 1169-1185.

Cravotta, R. (2005) "Mixing the Real with the Virtual" *EDN* **50**(11): 57-62.

Cumpsty, N. A. and E. M. Greitzer (2004) "Ideas and Methods of Turbomachinery Aerodynamics: A Historical View" *Journal of Propulsion and Power* **20**(1): 15-26.

Darby, A. P., A. Blakeborough and M. S. Williams (1999) "Real-Time Substructure Tests Using Hydraulic Actuator" *Journal of Engineering Mechanics* **125**(10): 1133-1139.

Dekker, N., B. Rietveld, J. Laatsch and F. Tietz (2004) "Evaluation of Interconnect Alloys and Cathode Contact Coatings for SOFC Stacks" *Proceedings of the 6th European Solid Oxide Fuel Cell Forum*: Lucerne, Switzerland, 28 June - 2 July 2004.

Ferrari, M. L., A. Traverso, L. Magistri and A. F. Massardo (2005) "Influence of the Anodic Recirculation Transient Behaviour on the SOFC Hybrid System Performance" *Journal of Power Sources* **149**: 22-32.

Garrett Turbine Engine Company (1982) *Overhaul Manual GTCP85-91C/-291/-291C,* Phoenix, AZ. Report 49-20-64.

Gemmen, R. S. and C. D. Johnson (2004) "Dynamics of Solid Oxide Fuel Cell Operation" *Second International Conference on Fuel Cell Science, Engineering and Technology*: Rochester, NY, 14-16 June 2004, American Society of Mechanical Engineers, **FUELCELL2004-2475**.

George, R. A. (2000) "Status of Tubular SOFC Field Unit Demonstrations" *Journal of Power Sources* **86**(1-2): 134-139.

Greitzer, E. M. (1976) "Surge and Rotating Stall in Axial Flow Compressors, Part I: Theoretical Compression System Model" *Journal of Engineering for Power, Transactions of ASME* **98**(2): 190-198.

Hamilton, S. (1999) "Fuel Cell-MTG Hybrid: "The Most Exciting Innovation in Power in the Next 10 Years" *1999 IEEE Power Engineering Society Summer Meeting*: Edmonton, Alta., 18-22 July 1999, Institute of Electrical and Electronics Engineers.

Haynes, C. and W. J. Wepfer (2000) "Enhancing Fuel Cell / Gas Turbine Hybrid Power Systems via Reduced Fuel Utilization within Indirect Internally Reforming (IIR) Fuel Cell Stacks" *Proceedings of the ASME Advanced Energy Systems Division American Society at the 2000 ASME International Mechanical Engineering Congress and Exposition*: Orlando, FL, 5-10 November 2000, American Society of Mechanical Engineers.

Hildebrandt, A. and M. Assadi (2005) "Sensitivity Analysis of Transient Compressor Operation Behaviour in SOFC-GT Hybrid Systems" *Proceedings of the ASME Turbo Expo 2005*: Reno-Tahoe, NV, 6-9 June 2005, American Society of Mechanical Engineers, **GT2005-68744**.

Kohl, S. and D. Jegminat (2005) "How to Do Hardware-in-the-Loop Simulation Right" *2005 SAE World Congress*: Detroit, MI, 11-14 April 2005, SAE International, **2005-01-1657**.

Kyrychko, Y. N., K. B. Blyuss, A. Gonzalez-Buelga, S. J. Hogan and D. J. Wagg (2006) "Real-time Dynamic Substructuring in a Coupled Oscillator-Pendulum System" *Proceedings of the Royal Society of London, Series A (Mathematical, Physical and Engineering Sciences)* **462**(2068): 1271-1294.

Layne, A., S. Samuelsen, M. Williams and P. Hoffman (2000) "Hybrid Heat Engines: The Power Generation Systems of the Future" *Proceedings of the ASME Turbo Expo 2000:* Munich, Germany, May 2000, American Society of Mechanical Engineers, **2000-GT-549**.

Leeper, J. D. (1999) "The Hybrid Cycle: Integration of a Fuel Cell with a Gas Turbine"*Proceedings of the ASME Turbo Expo 1999*: Indianaplis, IN, 6-9 June 1999, American Society of Mechanical Engineers, **99-GT-430**.

Lemes, Z., A. Vath, T. Hartkopf and H. Mancher (2006) "Dynamic Fuel Cell Models and Their Application in Hardware in the Loop Simulation" *Journal of Power Sources* **154**(2): 386-393.

Liese, E. A., T. P. Smith, C. Haynes and R. S. Gemmen (2006) "A Dynamic Bulk SOFC Model Used in a Hybrid Turbine Controls Test Facility" *Proceedings of the ASME Turbo Expo 2006*: Barcelona, Spain, 8-11 May 2006, American Society of Mechanical Engineers, **GT2006-90383**.

Litzinger, K. P., L. A. Shockling, S. E. Veyo and W. L. Lundberg (2005) "Comparative Evaluation of SOFC/Gas Turbine Hybrid System Options" *Proceedings of the ASME Turbo Expo 2005*: Reno, NV, 6-9 June 2005, American Society of Mechanical Engineers, **GT2005-68909**.

Maclay, D. (1997) "Simulation Gets into the Loop" *IEE Review* **43**(3): 109-112.

Mansoor, S. P., D. I. Jones, D. A. Bradley, F. C. Aris and G. R. Jones (2003) "Hardware-in-the-Loop Simulation of a Pumped Storage Hydro Station" *International Journal of Power and Energy Systems* **23**(2): 127-133.

Magistri, L., F. Trasino and P. Costamagna (2006) "Transient Analysis of Solid Oxide Fuel Cell Hybrids---Part I: Fuel Cell Models" *Journal of Engineering for Gas Turbines and Power* **128**(2): 288-293.

Massardo, A. F., C. F. McDonald and T. Korakianitis (2002) "Microturbine/Fuel-Cell Coupling for High-Efficiency Electrical-Power Generation" *Journal of Engineering for Gas Turbines and Power* **124**(1): 110-116.

Massardo, A. F. and F. Lubelli (2000) "Internal Reforming Solid Oxide Fuel Cell-Gas Turbine Combined Cycles (IRSOFC-GT): Part A -Cell Model and Cycle Thermodynamic Analysis" *Journal of Engineering for Gas Turbines and Power* **122**(1): 27-35.

McDonald, C. F. and D. G. Wilson (1996) "The Utilization of Recuperated and Regenerated Engine Cycles for High-Efficiency Gas Turbines in the 21st Century" *Applied Thermal Engineering* **16**(8-9): 635-653.

Monti, A., H. Figueroa, S. Lentijo, X. Wu and R. Dougal (2005) "Interface Issues in Hardware-in-the-Loop Simulation" *Electric Ship Technologies Symposium*: 25-27 July 2005, Institute of Electrical and Electronics Engineers.

Ng, E. Y.-K., N. Liu and S. Y. Tan (2004) "Parametric Study of Greitzer's Instability Flow Model through Compressor System Using the Taguchi Method" *International Journal of Rotating Machinery* **10**: 91-97.

Oakes, W. C., P. B. Lawless and S. Fleeter (2004) "High-Speed Centrifugal Compressor Instabilities During Speed Transients" *Journal of Aerospace Engineering* **17**(3): 106-112.

Palma, R. A. and J. M. Fernandes (2005) "Hardware-in-the-Loop Simulation - a Methodology Proposal" *ISA EXPO 2005 Technical Conference -Technical Papers of ISA*: Chicago, IL, 25-27 October 2005, Instrumentation, Systems, and Automation Society.

Roberts, R. A. and J. Brouwer (2006) "Dynamic Simulation of a Pressurized 220 kW Solid Oxide Fuel-Cell / Gas-Turbine Hybrid System: Modeled Performance Compared to Measured Results" *Journal of Fuel Cell Science and Technology* **3**(1): 18-25.

Salem, M., T. Das, X. Chen, S. Akella and S. Sivashankar (2005) "Real Time Simulation for Speed Control of Switched Reluctance Motor Drive Powered by a Fuel Cell System" *Proceedings of the ASME Power Conference 2005*: Chicago, IL, 5-7 April 2005, American Society of Mechanical Engineers, **PWR2005-50090**.

Smith, L. P. (1998) *ProTRAX Programmers Manual - Theory Manual*, Trax Corporation, Forest, VA.

Smith, T. P., D. Tucker, C. L. Haynes, E. A. Liese and W. J. Wepfer (2006) "Hardware-Based Simulation of a Fuel Cell Turbine Hybrid Response To Imposed Fuel Cell Load Transients" *Proceedings of IMECE2006 ASME International Mechanical Engineering Congress and Exposition*: Chicago, IL, 5-10 November 2006, American Society of Mechanical Engineers, **IMCEC2006-13978**.

Stiller, C., B. Thorud and O. Bolland (2006) "Safe Dynamic Operation of a Simple SOFC/GT Hybrid System" *Journal of Engineering for Gas Turbines and Power* **128**(3): 551-559.

Stiller, C., B. Thorud, S. Seljebo, O. Mathisen, H. Karoliussen and O. Bolland (2005) "Finite-Volume Modeling and Hybrid-Cycle Performance of Planar and Tubular Solid Oxide Fuel Cells" *Journal of Power Sources* **141**(2): 227-240.

Taccani, R. and D. Micheli (2006) "Experimental Test Facility for the Analysis of Transient Behavior of High Temperature Fuel Cell/Gas Turbine Hybrid Power Plants" *Journal of Fuel Cell Science and Technology* **3**(3): 234-241.

Traverso, A., R. Scarpellini and A. Massardo (2005) "Experimental Results and Transient Model Validation of an Externally Fired Micro Gas Turbine" *Proceedings of the ASME Turbo Expo 2005*: Reno, NV, 6-9 June 2005, American Society of Mechanical Engineers, **GT2005-68100**.

Tucker, D., T. P. Smith and L. Lawson (2006a) "Characterization of Bypass Control Methods in a Coal-Based Fuel Cell Turbine Hybrid" *Proceedings of ICEPAG2006 International Colloquium on Environmentally Preferred Advanced Power Generation*: Newport Beach, CA, 5-8 September 2006, American Society of Mechanical Engineers, **ICEPAG2006-24008**.

Tucker, D., T. P. Smith, L. Lawson and C. Haynes (2006b) "Evaluation of Cathodic Air Flow Transients in a Hybrid System Using Hardware Simulation" *Proceedings of The Fourth International Conference on Fuel Cell Science, Engineering and Technology*: Irvine, CA, 19-21 June 2006, American Society of Mechanical Engineers, **FUELCELL2006-97107**.

Tucker, D., L. Lawson and R. Gemmen (2005a) "Characterization of Air Flow Management and Control in a Fuel Cell Turbine Hybrid Power System Using Hardware Simulation" *Proceedings of the ASME Power Conference 2005*: Chicago, IL, 5-7 April 2005, American Society of Mechanical Engineers, **PWR2005-50127**.

Tucker, D., L. Lawson, R. Gemmen and R. Dennis (2005b) "Evaluation of Hybrid Fuel Cell Turbine System Startup with Compressor Bleed" *Proceedings of the ASME Turbo Expo 2005*: Reno, NV, 6-9 June 2005, American Society of Mechanical Engineers, **GT2005-68784**.

Tucker, D., E. Liese, J. Vanosdol, L. Lawson and R. S. Gemmen (2002) "Fuel Cell Gas Turbine Hybrid Simulation Facility Design" *2002 ASME International Mechanical Engineering Congress & Exposition*: New Orleans, LA, November 2002, American Society of Mechanical Engineers, **IMECE2002-33207**.

Ungethum, J. (2005) "Fuel Cell System Modeling for Real-time Simulation" *Proceedings of the 4th International Modelica Conference*: Hamburg, Germany, 7-8 March 2005, http://www.Modelica.org/events/Conference2005/.

Veyo, S. E. (2003) "Tubular SOFC Hybrid Power Systems" *Third DOE/UN International Conference and Workshop on Hybrid Power Systems,* http://www.netl.doe.gov/publications/proceedings/03/hybrid/hybrid03.html, accessed on: 25 May 2006.

Veyo, S. E., L. A. Shockling, J. T. Dederer, J. E. Gillett and W. L. Lundberg (2002) "Tubular Solid Oxide Fuel Cell/Gas Turbine Hybrid Cycle Power Systems: Status" *Journal of Engineering for Gas Turbines and Power* **124**(4): 845-849.

Wachter, C., R. Lunderstadt and F. Joos (2006) "Dynamic Model of a Pressurized SOFC/Gas Turbine Hybrid Power Plant for the Development of Control Concepts" *Journal of Fuel Cell Science and Technology* **3**(3): 271-279.

Walsh, P. P. and P. Fletcher (2004) *Gas Turbine Performance (2nd Edition)*, Blackwell Science.

Williams, M. C., J. Strakey and W. Sudoval (2006) "U.S. Doe Fossil Energy Fuel Cells Program" *Journal of Power Sources* **159**(2): 1241-1247.

Winkler, W., P. Nehter, M. C. Williams, D. Tucker and R. Gemmen (2006) "General Fuel Cell Hybrid Synergies and Hybrid System Testing Status" *Journal of Power Sources* **159**(1): 656-666.

Yi, Y., T. P. Smith, J. Brouwer, A. D. Rao and G. S. Samuelsen (2003) "Simulation of a 220 kW Hybrid SOFC Gas Turbine System and Data Comparison" *Proceedings of Eighth International Symposium on Solid Oxide Fuel Cells (SOFC-VIII)*: Paris, France, 27 April - 2 May 2003, The Electrochemical Society.

Zhang, H., M. Su and S. Weng (2005) "Hardware-in-the-Loop Simulation Study on the Fuel Control Strategy of a Gas Turbine Engine" *Journal of Engineering for Gas Turbines and Power* **127**(3): 693-695.

Zhang, X., J. Li, G. Li and Z. Feng (2006) "Development of a Control-Oriented Model for the Solid Oxide Fuel Cell" *Journal of Power Sources* **160**(1): 258-267.

Zhao, F. and A. V. Virkar (2005) "Dependence of Polarization in Anode-Supported Solid Oxide Fuel Cells on Various Cell Parameters" *Journal of Power Sources* **141**(1): 79-95.

VITA

Thomas P. Smith, son of Floyd and Carlen Smith, was born in Sioux City, Iowa on July 24, 1975 and grew up in Storm Lake, Iowa. He received a B.S. in mechanical engineering from Iowa State University and a M.S. degree from the University of California, Irvine. At UCI, he held a research assistantship at the National Fuel Cell Research Center and was an assistant operator of the Siemens Westinghouse Power Corporation 220 kW hybrid system. This power generation system was the world's first hybrid that integrated a pressurized fuel cell with a gas turbine. He then came to Georgia Tech to pursue a doctorate degree in mechanical engineering and to investigate fuel cell gas turbine hybrids. Funding for Thomas' graduate work at Georgia Tech was provided by U.S. Department of Energy, National Energy Technology Laboratory and NASA Glenn Research Center.